Government of Western Australia

Department of **Mines, Industry Regulation and Safety**

REPORT 183

METAMORPHOSED MESOARCHEAN Cu–Mo–Ag MINERALIZATION: EVIDENCE FROM THE CALINGIRI DEPOSITS, SOUTHWEST YILGARN CRATON

by MD Outhwaite

THE UNIVERSITY OF WESTERN AUSTRALIA

John de Laeter Centre

Geological Survey of Western Australia

Government of **Western Australia**
Department of **Mines, Industry Regulation and Safety**

REPORT 183

METAMORPHOSED MESOARCHEAN Cu–Mo–Ag MINERALIZATION: EVIDENCE FROM THE CALINGIRI DEPOSITS, SOUTHWEST YILGARN CRATON

by
MD Outhwaite

Perth 2018

Geological Survey of Western Australia

MINISTER FOR MINES AND PETROLEUM
Hon Bill Johnston MLA

DIRECTOR GENERAL, DEPARTMENT OF MINES, INDUSTRY REGULATION AND SAFETY
David Smith

EXECUTIVE DIRECTOR, GEOLOGICAL SURVEY OF WESTERN AUSTRALIA
Jeff Haworth

REFERENCE
The recommended reference for this publication is:
Outhwaite, MD 2018, Metamorphosed Mesoarchean Cu–Mo–Ag mineralization: Evidence from the Calingiri deposits, southwest Yilgarn Craton: Geological Survey of Western Australia, Report 183, 216p.

ISBN 978-1-74168-791-0
ISSN 1834-2280

A catalogue record for this book is available from the National Library of Australia

Grid references in this publication refer to the Geocentric Datum of Australia 1994 (GDA94). Locations mentioned in the text are referenced using Map Grid Australia (MGA) coordinates, Zone 50. All locations are quoted to at least the nearest 100 m.

About this publication
This Report is a Master of Science thesis researched, written and compiled at The University of Western Australia. Although GSWA collaborated in geochronological analyses for this project, the scientific content of the Report, and the drafting of figures, were the responsibility of the author. No editing has been undertaken by GSWA.

Published 2018 by Geological Survey of Western Australia
This Report is published in digital format (PDF) and is available online at <www.dmp.wa.gov.au/GSWApublications>.

Further details of geological publications and maps produced by the Geological Survey of Western Australia are available from:
Information Centre | Department of Mines, Industry Regulation and Safety | 100 Plain Street | EAST PERTH
WESTERN AUSTRALIA 6004 | Telephone: +61 8 9222 3459 | Facsimile: +61 8 9222 3444
www.dmp.wa.gov.au/GSWApublications

Cover photograph: View southeast over Lake Ninan from the southern tip of the Wongan Hills. The Ninan deposit is in the foreground, with the Bindi, Dasher and Opie deposits lying in the distance beyond the lake (photo by MD Outhwaite)

Metamorphosed Mesoarchean Cu-Mo-Ag mineralization: Evidence from the Calingiri deposits, southwest Yilgarn Craton

Michael David Outhwaite

BSc(Hons) Mineral Exploration and Mining Geology (Curtin)

Supervisors: Prof. Steffen Hagemann (UWA)

Dr. Kevin Cassidy (UWA)

Journal formatting guide: Economic Geology

This thesis is submitted in partial fulfillment of the requirements for a Master of Science

SCIE5722 (Master of Science Thesis)

Faculty of Science – Earth and Environment

The University of Western Australia

May, 2017

Actual word count: 12,462 (limit 12,500)

Faculty of Science Assignment Cover Sheet

THE UNIVERSITY OF WESTERN AUSTRALIA
Achieve International Excellence

School of Earth & Environment

Faculty of Science Assignment Cover Sheet

Name/s and Student Number/s	☒ Individual ☐ Group
1. Michael Outhwaite 21687677	4.
2.	5.
3.	6.

It will be assumed that all group members have equally participated in group assignments, unless other arrangements have been made to notify lecturer of participation levels.

UNIT CODE: SCIE5722	UNIT NAME: MSc thesis (part-time)
UNIT COORDINATOR/LECTURER: Dr. Thea Linke	DAY/TIME DUE: 29/5/2017 5:00pm
TITLE/TOPIC OF ASSIGNMENT: Final research thesis	WORD COUNT: 12462
	OFFICE USE ONLY:

The Faculty of Science adheres to the University Policy on Academic Dishonesty which constitutes misconduct and is dealt with under the University's Statute 17 (http://calendar.publishing.uwa.edu.au/latest/partc/stat17). These guidelines make reference to the following:

- **Cheating** in tests or examinations, e.g., copying from another student, or taking unauthorized materials into the test or examination room.
- **Plagiarism**, i.e., presenting another's work as though it were one's own, for instance quoting or paraphrasing someone else's opinions, arguments or research findings, whether published or unpublished (e.g., from a book or article, an internet site, or another student's assignment), without clear acknowledgement of the source. You may quote material from another source, but if you do so, the quotation must be word perfect and, in addition to citing the source reference in the usual manner, the beginning and end of the quotation must be clearly indicated by quotation marks. E.g. "quotation"
- **Falsifying results** of experiments or research studies.
- **Collusion**, e.g., writing an assignment jointly and submitting it as the work of one individual. Although discussion and co-operation are valuable in the pursuit of knowledge and understanding, any work submitted for assessment must be the individual's own work unless it is clearly designated a group project.
- **Helping someone else to commit any dishonest act** such as those listed above.

The consequences for misconduct can be severe, including exclusion from the university. All students are expected to make themselves aware of the definitions and policies relating to academic misconduct, (http://www.teachingandlearning.uwa.edu.au/staff/policies/conduct), and with any additional requirements or stipulations that may be provided by individual unit co-ordinators.

Late Assignments
There are penalties for late assignments. Refer to the unit outline for more information.

NO ASSIGNMENT WILL BE ACCEPTED UNLESS THE FOLLOWING DECLARATION IS SIGNED AND DATED

DECLARATION

I/We certify that I have read the University guidelines on Academic Misconduct. I/We certify that the assignment submitted online is my own work and that all material drawn from other sources has been fully acknowledged.

I/We certify that I am aware that the work submitted under this declaration is submitted to an online plagiarism detection service for analysis and that the work may be stored in a database either internal or external to the University. I/We have a photocopy or electronic copy of this assignment in my possession.

Sign: MDOuthwaite	Date: 29/5/2017	Sign:	Date:
Sign:	Date:	Sign:	Date:
Sign:	Date:	Sign:	Date:
Submission date: 29/5/2017			

FACULTY OF SCIENCE

Thesis Declaration

I, Michael David Outhwaite, certify that:

This thesis has been substantially accomplished during enrolment in the degree.

This thesis does not contain material which has been accepted for the award of any other degree or diploma in my name, in any university or other tertiary institution.

No part of this work will, in the future, be used in a submission in my name, for any other degree or diploma in any university or other tertiary institution without the prior approval of The University of Western Australia and where applicable, any partner institution responsible for the joint-award of this degree.

This thesis does not contain any material previously published or written by another person, except where due reference has been made in the text.

The work(s) are not in any way a violation or infringement of any copyright, trademark, patent, or other rights whatsoever of any person.

Third party editorial assistance was provided in preparation of the thesis by my supervisors, Prof. Steffen Hagemann and Dr. Kevin Cassidy.

The work described in this thesis was funded by Caravel Minerals Ltd, under UWA project grant number 5000 4400.

Technical assistance was kindly provided by Dick England, who helped with some aspects of petrography at the Ninan deposit.

This thesis does not contain work that I have published, nor work under review for publication.

Signature: 

Date: 29th May 2017

Abstract

The southwest Yilgarn Craton has received little attention from mineral explorers, relative to the eastern part of the craton, due to limited bedrock exposure, private land ownership, and a perceived lack of prospectivity. In 2010, granite-gneiss-hosted, bulk-tonnage Cu-Mo-Ag mineralization was discovered at Calingiri, 120 km north-northwest of Perth, adjacent to a domain boundary in the southwest of the craton. The majority of mineralization is contained within three granite-gneiss-hosted deposits (Bindi, Dasher and Opie), which have a combined Indicated and Inferred Resource of 529 Mt grading 0.27% Cu (1.4 Mt contained Cu), 54 ppm Mo, 1.33 ppm Ag and 0.02 ppm Au. The smaller Ninan deposit is hosted in the ca. 3010 Ma Wongan Hills greenstone belt.

The Dasher mineralization is hosted in a 3010 ± 4 Ma (SHRIMP U-Pb zircon) High-Ca biotite monzogranite that is compositionally banded (S_{BAN}). An early foliation (S_1) in the monzogranite is cut by discrete 3010 ± 4 Ma (SHRIMP U-Pb zircon) syenogranite intrusions that are also affected by S_1. The resultant granite-gneiss (*sensu lato*) was intruded by a pair of ~150 m wide, unmineralized granite (*sensu stricto*) dikes at 2673 ± 5 Ma (SHRIMP U-Pb zircon). D_2 ~east-west compression and ~synchronous upper amphibolite facies metamorphism occurred after ca. 2673 Ma as indicated by: (1) peak metamorphic sillimanite in the S_2 foliation; and (2) trace sillimanite and garnet in the granite dikes. At Dasher, D_2 resulted in west-verging F_2 folds of S_{BAN}, S_1 and the granite dikes. The district-scale, granite-gneiss mineralized corridor (Opie through Dasher to Bindi) was also folded during D_2.

Early, Mo-dominant mineralization at Dasher was synchronous with D_1, as evidenced by quartz-feldspar-molybdenite veins being affected by isoclinal F_1 folds, and Re-Os geochronology on molybdenite in that setting giving an age of ca. 2997-2957 Ma. The main stage of copper-dominant mineralization occurred late- to post-D_1, as evidenced by sulfide stringers and quartz-sulfide stockwork veins that are parallel to, or cross-cut S_1. Mineralization is associated with D_1 high-strain zones, at all scales. All mineralized veins are affected by F_2 folds, confirming implications from geochronology that Cu-Mo-Ag mineralization at Dasher was pre-D_2, and pre-peak metamorphic.

Syn-mineralization hydrothermal alteration assemblages at Dasher were recrystallized during peak metamorphism. A widely developed biotite-garnet-sillimanite-magnetite assemblage represents a plagioclase-destructive hydrothermal alteration (including original sericite-chlorite) that depleted Na and Ca in the granite-gneiss, creating Al-rich to peraluminous bulk compositions. Metamorphic recrystallization produced the observed garnet- and sillimanite-bearing assemblages. A localized granoblastic quartz-microcline-plagioclase-sillimanite assemblage likely represents recrystallized hydrothermal K-feldspar alteration. Metamorphosed hydrothermal alteration assemblages suggest peak metamorphic P-T conditions of ~660°C to 800°C and <10 kbar at Dasher. Dehydration reactions during peak metamorphism may have initiated partial melting, producing pegmatoidal mineralized leucosome veins.

The Calingiri Cu-Mo-Ag deposits have grade-tonnage profiles, metal distributions and hydrothermal alteration characteristics that are comparable to those of Phanerozoic porphyry Cu-Mo deposits. The discovery of the Calingiri mineralization reveals the latent mineralization potential of little-explored Archean granite-gneiss terranes.

Table of Contents

Faculty of Science Assignment Cover Sheet ii

Thesis Declaration iii

Abstract iv

Table of Contents v

Acknowledgements viii

Introduction 1

Regional Geology 3

Geology of the Wongan Hills region 5

Gold and base metal mineralization in the southwest Yilgarn Craton 5

Methodology 6

Calingiri District Structural Geology 9

Geological Setting of the Dasher Cu-Mo-Ag Deposit 10

Lithostratigraphy 10

Dasher granite-gneiss 10

Dasher granite dikes 11

Other lithologies 11

Geochronology 15

Structural setting 16

D_1 structures 16

D_2 structures 17

Other structural features 20

Metamorphism 20

Relative and absolute timing of intrusive, deformation and metamorphic events 21

Mineralization, Hydrothermal Alteration and Modification of the Dasher Cu-Mo-Ag Deposit 22

Mineralization styles 23

Early quartz-feldspar-molybdenite veins 23

Re-Os geochronology 23

Main stage Cu-dominant mineralization 25
Mineralized pegmatite veins 27
Modification of mineralization during D_2 and peak metamorphism 27
Hydrothermal alteration 28
Biotite-garnet-sillimanite-magnetite alteration 28
Granoblastic quartz-microcline-plagioclase-sillimanite alteration 31
Retrograde hydrothermal alteration and remobilization 32
Interpretation of metamorphosed hydrothermal alteration assemblages 32
Other Mineralization in the Calingiri District 37
Geochronology 41
Geochemistry of Calingiri Granitoids 43
Preliminary Descriptive Model for the Calingiri Cu-Mo-Ag Mineralization 45
Discussion 48
Classification of the Calingiri Cu-Mo-Ag mineralization 48
Calingiri in the geological and metallogenic evolution of the southwest Yilgarn Craton 49
Implications for exploration 50
Conclusions 50
References 52

Appendix 1 – Literature review 56
Appendix 2 – Example pages of Economic Geology journal 76
Appendix 3 – Outcrop mapping observations 78
Appendix 4 – Dasher pavement outcrop map 87
Appendix 5 – Drill core sample details 88
Appendix 6 – Drill core structural measurements 90
Appendix 7 – Whole-rock geochemistry 101
Appendix 8 – Caravel Minerals Ltd four-acid digest geochemistry 104
Appendix 9 – SEM data 112
Appendix 10 – SHRIMP U-Pb zircon geochronology data 117
Appendix 11 – Re-Os geochronology data 129
Appendix 12 – Thin-section descriptions 131
Appendix 13 – Drill core graphic log sheets 177

Acknowledgements

I would like to thank Caravel Minerals Ltd for agreeing to fund this research, at a time when conditions for junior mineral explorers were dire. I particularly thank Tony Poustie and Graham Kubale for supporting the project from the moment I cold-called them. It has been a privilege to complete the first formal study on this interesting mineralization.

I studied the Calingiri diamond drill core at the Geological Survey of Western Australia's (GSWA) Perth Core Library, and I thank the staff there for their help. I also thank the Government of Western Australia for enabling good geoscience and mineral exploration by funding the GSWA.

I am grateful that Prof. Steffen Hagemann and Dr. Kevin Cassidy agreed to supervise the project, and gave me the advice and criticism I needed. Dr. Michael Wingate (GSWA) and Dr. Svetlana Tessalina (John de Laeter Centre, Curtin University) are thanked for collaborating on the geochronology. Dick England is thanked for helpful discussions about aspects of the petrography, and Prof. Simon Wilde and Dr. David Mole are thanked for discussions about southwest Yilgarn Craton geology.

My work colleagues at Model Earth and its pre-cursor, Jigsaw Geoscience, are all thanked for many years' worth of shared geological adventures, and for driving me to become better. I particularly thank Jon Standing for investing in me as a young geologist, and teaching me the field geology skills required to properly analyze mineral systems.

My parents, Barbara and Simon, and my siblings, Andrew, Darryl and Sarah, are thanked for being interesting, interested, and inspiring people. Sarah, who passed away during this research project, is remembered with much love.

Finally, I am eternally grateful for the support of my wife, Carlie, and my children, Alby and Lucy. Thanks for looking after me, and helping me to do the things I need to do.

Introduction

The Calingiri Cu-Mo-Ag deposits, 120 km northeast of Perth, Western Australia (Fig. 1), are of a style not recognized elsewhere in the Archean Yilgarn Craton: disseminated, bulk-tonnage mineralization hosted primarily in garnet-bearing granite-gneiss (*sensu lato*). Consolidated Indicated and Inferred Resources for Calingiri currently stand at 529 Mt grading 0.27% Cu (1.4 Mt contained Cu), 54 ppm Mo, 1.33 ppm Ag and 0.02 ppm Au, at 0.15% Cu cut-off (Caravel Minerals Ltd, 2016). The metal associations and tonnage-grade profile are comparable to those of Phanerozoic porphyry Cu-Mo deposits (Fig. 2).

The four deposits that make up Calingiri lie along a corridor extending 20 km south from the Wongan Hills greenstone belt (Fig. 3). Although outcropping Cu mineralization at the greenstone-hosted Ninan deposit has been drilled sporadically since 1975 (Lipple, 1982), the larger granite-gneiss-hosted deposits – Bindi, Dasher and Opie – were only discovered recently. Dominion Mining Ltd intersected primary mineralization at Bindi and Opie (then Bartel and Chapman, respectively) in 2010, when they drilled coincident Cu and Mo soil anomalies initially generated from roadside soil sampling that covered ~120,000 km^2 of the southwest Yilgarn Craton (Dominion Mining Ltd, 2010). The current project owner, Caravel Minerals Ltd, discovered the primary mineralization at Dasher in 2013 (Caravel Minerals Ltd, 2013).

The discovery of the Calingiri deposits, on farming land not previously subject to mineral exploration, illustrates the potential for non-prescriptive exploration, focused on major crustal structures, to produce discoveries that are unusual in both location and style. It also contributes to a recent trend of significant mineral discoveries in high-grade metamorphic terranes, where structural and mineralogical complexity have inhibited previous explorers – e.g. the Tropicana Au deposit (Doyle et al., 2015) and the Nova-Bollinger Ni-Cu deposit (Maier et al., 2016) in the Albany-Fraser Orogen, Western Australia, and the Borden Au deposit in the Kapuskasing Structural Zone, Ontario (Palmer et al., 2015).

The data density (diamond drill holes, outcrop) at Calingiri is sparse, making rigorous spatial analysis of the mineral system difficult. This study therefore focuses on constraining the relative and absolute (where possible) timing of lithological, structural, metamorphic and mineralization events, with an emphasis on the Dasher deposit.

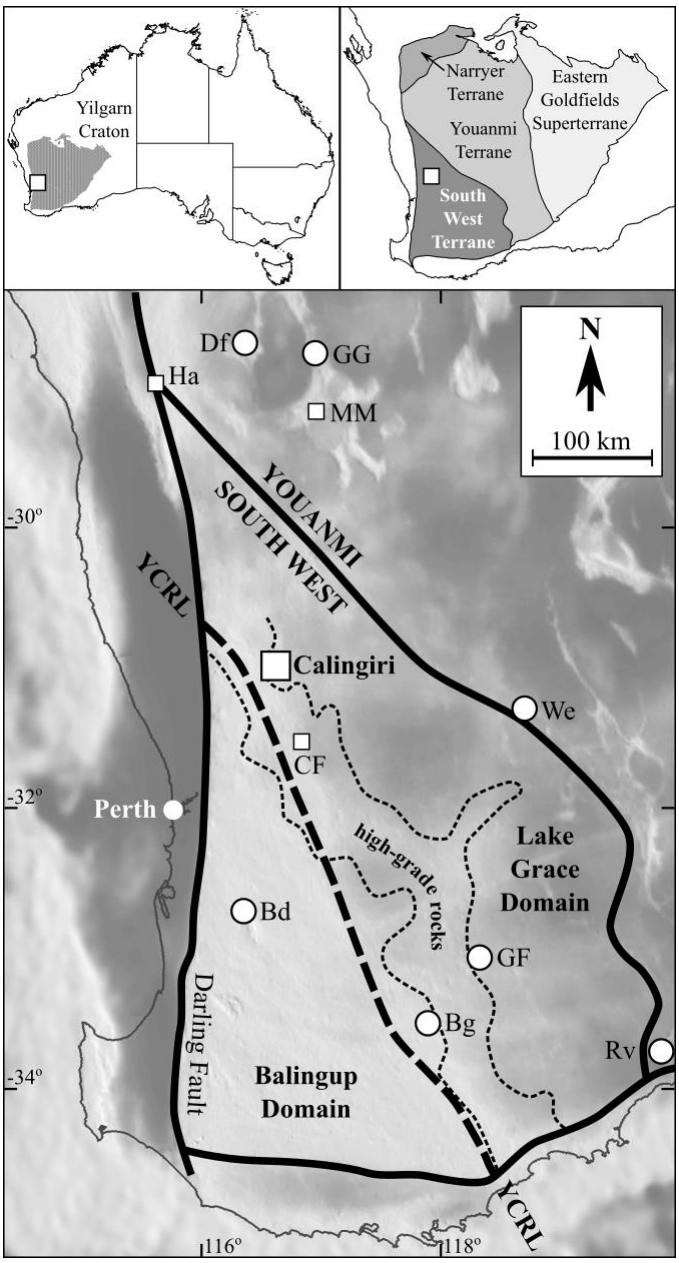

Fig. 1. Bouger gravity image (data from http://www.dmp.wa.gov.au) showing the Calingiri deposits in relation to terrane boundaries (thick solid lines), domain boundaries (thick dashed lines), and high-grade metamorphic rocks (thin dashed lines) in the southwest Yilgarn Craton. Boundaries modified from Wilde et al. (1996), Cassidy et al. (2006) and Mole et al. (2012). YCRL = Yandanooka-Cape Riche Lineament. Gold and/or base metal mineral deposits (white circles) and prospects (white squares) are shown. Bd = Boddington, Bg = Badgebup, CF = Centre Forrest, Df = Deflector, GF = Griffin's Find, GG = Golden Grove, Ha = Harrisons, MM = Mt Mulgine, Rv = Ravensthorpe, We = Westonia.

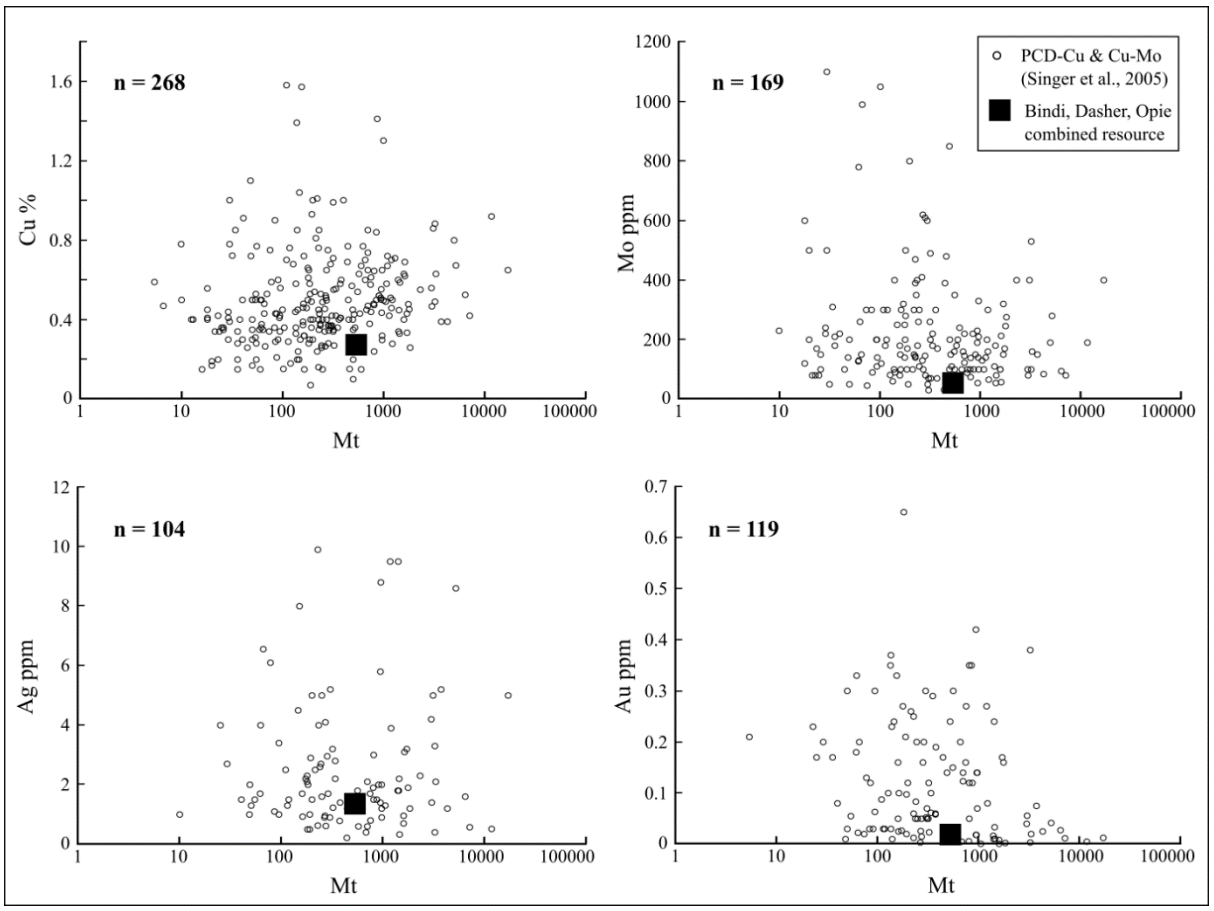

Fig. 2. Tonnage-grade characteristics of the Calingiri resource, against porphyry Cu and porphyry Cu-Mo resource data from Singer et al. (2005). Data from the Au-rich porphyry deposit class is not shown.

Regional Geology

The granitic, volcanic and sedimentary rocks that comprise the Yilgarn Craton formed principally between 3.0 and 2.6 Ga, and have been divided into a number of distinct terranes and domains, based on stratigraphic, structural, geochemical and geochronological constraints (Cassidy et al., 2006). In this paper, the Wongan Hills greenstone belt and the granite-gneiss rocks to its immediate south, are assigned to the Lake Grace Domain of the South West Terrane (Fig. 1), based on terrane boundaries proposed in Cassidy et al. (2006) and domain subdivisions proposed by Mole et al. (2012). The study area is immediately east of the Yandanoooka-Cape Riche Lineament (YCRL) (Dentith and Featherstone, 2003), a major north-northwest-trending, east-dipping geological (Wilde et al., 1996) and geophysical feature (Middleton et al., 1995; Dentith et al., 2000), most clearly defined by a sharp fall in regional Bouger values, going west to east (Fig. 1). Based on spatial analysis of SHRIMP U-Pb zircon ages of southwest Yilgarn granites, Mole et al. (2012) proposed that their Balingup and Lake Grace domains were amalgamated across the YCRL at ca. 2650-2640 Ma, but also noted evidence that the YCRL had been a significant tectonic boundary at several times ca. 3200 Ma. Nemchin et al. (1994)

proposed that the YCRL marked the western limit of a parallel belt of high-T, low-P granulite facies metamorphism (Fig. 1) that occurred at ca. 2649-2640 Ma, based on conventional U-Pb analysis of metamorphic zircons in mafic granulites.

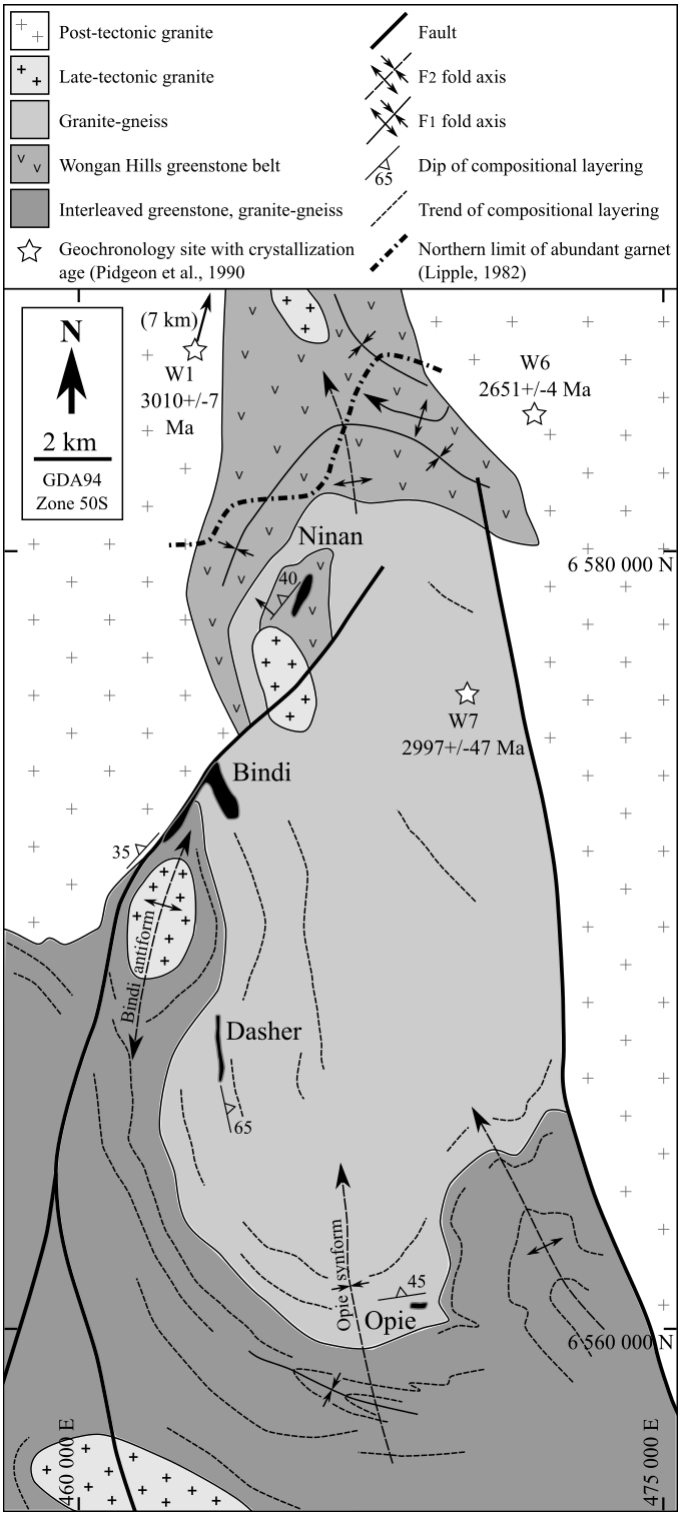

Fig. 3. Schematic lithological and structural interpretation of the Calingiri mineralized district, based on outcrop mapping and drill hole analysis completed in this study, and the interpretation of Lipple (1982).

Geology of the Wongan Hills region

The Wongan Hills greenstone belt (Fig. 3), host to the Ninan deposit, comprises mafic to felsic volcanic and volcaniclastic rocks, intercalated with metasedimentary rocks, including banded iron formation (BIF) (Lipple, 1982). A minimum age of 3010 ± 7 Ma is estimated for greenstone deposition, based on SHRIMP and conventional U-Pb zircon analysis of a felsic porphyry that intrudes the sequence (Fig. 3; sample 'W1' of Pidgeon et al., 1990). Peak metamorphic P-T conditions of ~660°C and ~2 kbar (Blight, 1977) are estimated to have affected the highest-grade southern end of the belt, where garnet is most abundant (Fig. 3; Lipple, 1982). There are no geochronological constraints on the absolute age of this peak metamorphic event. Greenschist facies retrogression has been dated at 2646 ± 11 Ma, based on conventional U-Pb analyses of cogenetic titanite (Pidgeon et al., 1990). Limited work on the structural evolution of the Wongan Hills greenstone belt suggests that an early phase of isoclinal folding, transposition and shearing, has been refolded by north-trending open folds (Fig. 3; Carter and Lipple, 1982; Lipple, 1982). The absolute ages of these deformation events are unconstrained.

The granite-gneiss rocks south of the Wongan Hills greenstone belt (Fig. 3), are poorly exposed, and have not been subject to any detailed studies. Regional 1:250,000 scale mapping (Carter and Lipple, 1982) describes variation between even-grained, porphyritic and K-feldspar megacrystic variants of biotite- (primarily) and hornblende-bearing granites in this region. SHRIMP U-Pb zircon geochronology on a granite-gneiss 5 km northeast of the Bindi deposit (then undiscovered) resulted in an interpretation of igneous crystallization at 2997 ± 47 Ma, followed by partial anatexis and gneiss formation at 2800 ± 9 Ma (Fig. 3; sample 'W7' of Pidgeon et al., 1990). A 2651 ± 4 Ma post-tectonic granite intrusion (SHRIMP U-Pb zircon; sample 'W6' of Pidgeon et al., 1990) forms the eastern margin of the Wongan Hills greenstone belt and the granite-gneiss rocks to its south (Fig. 3).

Gold and base metal mineralization in the southwest Yilgarn Craton

In the southwest Yilgarn Craton (Fig. 1), there are no known mineral deposits that are directly analogous to Calingiri, in terms of metal association, tonnage-grade profile and host-rock characteristics (Table 1). However, elements of the Calingiri mineralization are observed in other deposits in the region – e.g. high grade metamorphic host rocks, and deposits with significant Cu and/or Mo content (Table 1). Mineralization genetically linked to ca. 3.0 Ga host rocks is present in the western Youanmi Terrane (Fig. 1), at the Ravensthorpe Cu-Au-Ag-Pb-

Zn deposits (Witt, 1998), and at the Golden Grove Cu-Zn-Pb-Ag-Au VMS deposits (Sharpe and Gemmell, 2002).

High-grade metamorphic rocks parallel to the YCRL host Au mineralization where the mineralizing event is interpreted to have occurred prior to, or synchronous with, the ca. 2649-2640 Ma metamorphic peak (Fig. 1; Table 1). The Griffin's Find Au deposit was considered the type-example of ~syn-peak, granulite facies, orogenic mineralization in a crustal-continuum model (Barnicoat et al., 1991; Groves, 1993), but several workers have since concluded that it is a lower temperature deposit that has been subjected to granulite facies metamorphism (e.g., Alach, 1997; Tomkins and Grundy, 2009). Felsic granulite-hosted Au mineralization at Badgebup is interpreted to be the result of high-grade metamorphism of existing, lower metamorphic grade mineralization (Blackburn et al., 1990), though detailed studies are lacking. Limited exploration of Au-Cu mineralization at the Centre Forrest prospect shows that it is located in quartz-sulfide veins within mafic granulites, and is of either pre-peak or syn-peak metamorphic origin (Brauhart and Swager, 2003; May, 2006).

Methodology

Outcrop within the ~20 x 3 km Calingiri mineralized trend was mapped onto aerial photo bases at 1:5000 scale, with notes and structural measurements (n = 179) recorded at each locality (Appendix 3). Detailed 1:100 scale mapping was undertaken over a granite-gneiss pavement 1 km south of Dasher (Appendix 4). Caravel Minerals Ltd provided aeromagnetic imagery that enabled solid geology interpretation.

There were only four diamond drill holes into the granite-gneiss mineralization at the time of this study: three from Dasher (12CADD001, 12CADD002 and 14CADD001) and one from Bindi West (14CADD002). These drill holes, along with two historic diamond drill holes from Ninan (08WHDDH001 and DWN4), were graphically logged (Appendix 13). Structural measurements from the core (n = 403; Appendix 6) were recorded using alpha-beta-gamma angles. Selected samples of the different lithologies, hydrothermal alteration zones and mineralization styles were taken from the drill core (details in Appendix 5), and these samples were used for detailed transmitted and reflected light petrography (46 thin-sections, oriented where possible; Appendix 12), whole-rock geochemistry, mineral chemistry and geochronology.

Table 1. Characteristics of mineralization in the southwest Yilgarn Craton (Fig. 1). References are: (1) Cassidy et al. (1998); (2) Barnicoat et al. (1991), Groves (1993), Alach (1997), Tomkins and Grundy (2009); (3) Blackburn et al. (1990); (4) Allibone et al. (1997), Stein et al. (2001); (5) Sharpe and Gemmell (2002); (6) Muhling and Low (1977), Doray Minerals Ltd (2016); (7) Savage et al. (1995), Witt (1998); (8) Duuring et al. (2007); (9) Brauhart and Swager (2003), May (2006); (10) Baxter and Harris (1979).

Locality and status	Host rocks and age	Principal metals	Mineralization style and age (if constrained)	Peak metamorphic grade and age	Timing of mineralization with respect to peak metamorphism	Ref.
MINES						
Westonia (active)	Granitoid, 2808±6 Ma	Au	Orogenic, >ca. 2637 Ma dykes	Upper amphibolite facies, >ca. 2637 Ma dykes	Syn-peak to post-peak	1
Griffin's Find (inactive)	Mafic granulite, <ca. 2790 Ma	Au	Orogenic, ≥ ca. 2627 Ma metamorphism	Granulite facies, 2627±12 Ma	Pre-peak or syn-peak	2
Badgebup (inactive)	Mafic granulite, <ca. 2790 Ma	Au	Orogenic?	Granulite facies, 2629±10 Ma	Pre-peak or syn-peak	3
Boddington (active)	Greenstone, ca. 2714-2675 Ma	Au-Cu-Mo	Orogenic, intrusion-related, early phase at 2726±24 Ma, late phase at 2629±34 Ma	Upper greenschist facies, ca. 2640 Ma	Pre-peak and post-peak (inferred from mineralization and metamorphic ages)	4
Golden Grove (active)	Greenstone, ca. 2960-2941 Ma	Cu-Zn-Pb-Ag-Au	VMS, ca. 2960-2941 Ma	Greenschist facies, <ca. 2941 Ma.	Pre-peak (inferred from VMS origin)	5
Deflector (active)	Greenstone, uncertain age	Au-Cu	Orogenic?	Upper greenschist to lower amphibolite, uncertain age	Uncertain	6
Ravensthorpe (inactive)	Calc-alkaline intrusive/ extrusive, ca. 2950-3000 Ma	Cu-Au-Ag-Pb-Zn	Predominantly syn-volcanic, ca. 2950-3000 Ma	Middle greenschist to upper amphibolite facies, prior to ca. 2650 Ma	Pre-peak	7
PROSPECTS						
Mt Mulgine	Syenogranite, 2767±10 Ma, and adjacent greenstone	Mo-W	Intrusion-related, inferred ca. 2767 Ma with granitoid	Amphibolite facies, uncertain age (syn-intrusion?)	Syn-peak	8
Centre Forrest	Mafic granulite, uncertain age	Au-Cu	Quartz-sulphide veins in mafic granulite, uncertain age	Granulite facies, likely ca. 2649-2640 Ma event	Pre-peak or syn-peak	9
Harrison's	Gneissic greenstone and granite, uncertain age	Cu-Mo	Disseminated and stockwork, uncertain age	Lower amphibolite facies	Post-peak	10

Whole-rock geochemical analysis of 16 samples was completed at ALS Minerals in Perth, in order to constrain the major oxide, trace element and rare earth element (REE) characteristics of type lithologies (Appendix 7). Sample preparation involved crushing and pulverizing to a nominal 85% passing 75 μm. Major element oxides were determined by fused disk XRF, while trace and REE elements were determined by a combination of lithium borate fusion, four acid digest and aqua regia with ICP-MS or ICP-AES finish (ALS Minerals method CCP-PKG03). ALS Minerals conducted QA/QC checks on certified standards and blanks, plus laboratory duplicates of two samples from this study. All analyses returned results within the laboratory's acceptable ranges, defined as "concentration ± (precision expectation of method x concentration)". Caravel Minerals Ltd provided four-acid digest, multi-element geochemistry covering part of the logged diamond drill holes (Appendix 8). Mineral chemistry information from two thin-sections (Appendix 9) was collected on the TESCAN VEGA3 scanning electron microscope (SEM) instrument at the Centre for Microscopy, Characterisation and Analysis (CMCA) at UWA.

SHRIMP U-Pb dating of zircon was completed in collaboration with the Geological Survey of Western Australia (GSWA), on four samples selected by the author (Appendix 10). Geotrack International Pty Ltd completed mineral separation on each 2-3 kg sample, and forwarded the zircons to the GSWA for mounting and imaging. U-Pb zircon analysis was undertaken on the SHRIMP instrument at the John de Laeter Centre (JDLC) at Curtin University, Western Australia. Two molybdenite-rich samples were selected by the author for Re-Os dating at the JDLC (Appendix 11). The Carius tube technique was used, with ^{188}Os-^{190}Os double spike, and mass spectrometry on a TIMS Triton™ instrument.

Mineral abbreviations used in figures within this paper are:

Ab = Albite	Grt = Garnet	Po = Pyrrhotite
Als = Aluminosilicate	Gru = Grunerite	Py = Pyrite
Am = Amphibole	Mc = Microcline	Qtz = Quartz
Bt = Biotite	Mo = Molybdenite	Ser = Sericite
Chl = Chlorite	Ms = Muscovite	Sil = Sillimanite
Cpy = Chalcopyrite	Mt = Magnetite	St = Staurolite
Cpx = Clinopyroxene	Opx = Orthopyroxene	Su = Sulphide
Ep = Epidote	Pl = Plagioclase	

All directions and structural data are relative to GDA94 MGA Zone 50 South. Structural data are given in 'dip/dip direction' format for planar features (e.g., 50/200) and 'plunge→trend' format for linear features (e.g., 50→200).

Calingiri District Structural Geology

The ~20 x 10 km granite-gneiss domain south of the Wongan Hills greenstone belt (Fig. 1) is a >3 km true thickness (estimated) granitoid that is compositionally banded (S_{BAN}) and contains a pervasive biotite-defined foliation (S_1) that is variably gneissic. The Wongan Hills greenstone belt structurally overlies the granite-gneiss domain in the north, based on the northwest dip of layering present in supracrustal rocks near Ninan, and the plan-view trace of the north-plunging, second-generation antiform interpreted by Lipple (1982) (Fig. 3). The southern and eastern margins of the granite-gneiss domain are structurally underlain by a greenstone sequence that is spatially separated from the Wongan Hills greenstone belt (Fig. 3), but is similarly dominated by amphibolitic mafic-ultramafic rocks and BIF horizons. A pervasive foliation developed sub-parallel to layering in all greenstones is correlated here with S_1 in the granite-gneiss domain. The S_1 foliation is axial planar to isoclinal folds in the southeastern greenstone sequence (Fig. 3). Greenstone rocks near Ninan deposit have a well-developed stretching lineation (L_1) on the S_1 fabric.

Fold and deformation fabric relationships observed in the granite-gneiss, the Wongan Hills greenstone belt, and the southeastern greenstone sequence suggest a significant shared structural history between these domains. Compositional layering and S_1 vary in orientation throughout the district (Fig. 4A), due to the modification by north-south-trending, open folds (F_2), which generally plunge to the north (Fig. 4B) and have a weakly developed axial planar foliation (S_2). The southern tip of the granite-gneiss domain is a kilometer-scale moderately north-plunging F_2 synform, here termed the Opie synform (Fig. 3). A double-plunging F_2 dome south of Bindi is here termed the Bindi antiform (Fig. 3). Similar structural features are observed at deposit scale, and these are annotated with the D_1 and D_2 terminology used here.

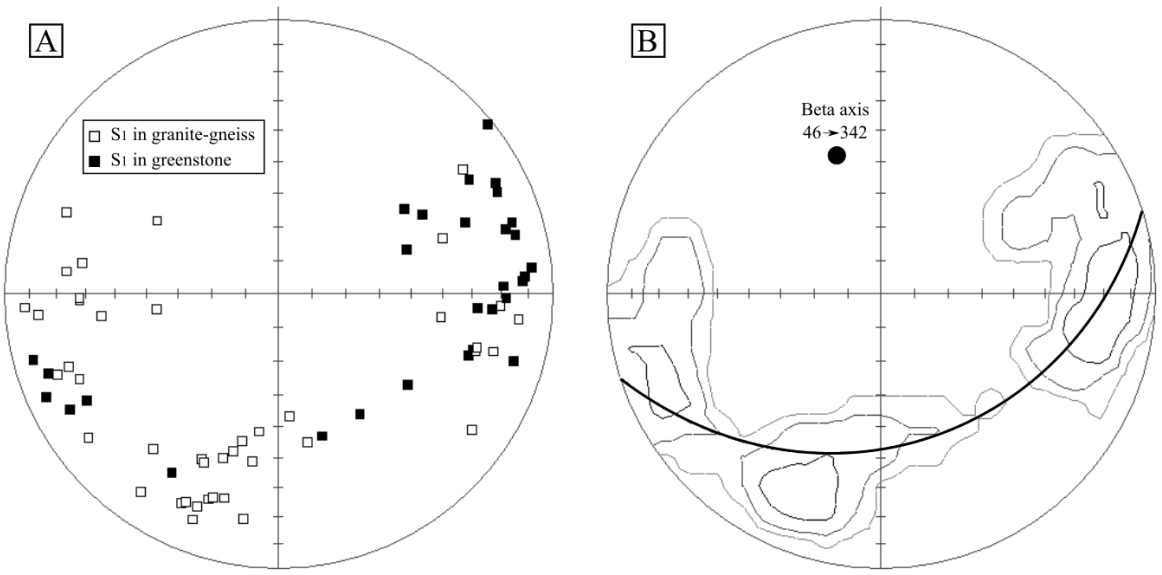

Fig. 4. Stereonets of district-scale outcrop structural data, from this study. (A) Poles to S_1 foliation, showing a fold-related distribution. (B) Contours of the S_1 poles, with a best fit girdle (great circle). The beta axis orientation (pole to the great circle) is an approximation of the plunge of regional F_2 folding.

Geological Setting of the Dasher Cu-Mo-Ag Deposit

The Dasher deposit (Fig. 3) was studied as the type-example of granite-gneiss-hosted Cu-Mo-Ag mineralization at Calingiri. The lithostratigraphic, structural and metamorphic characteristics of Dasher are described separately below, followed by a discussion of the relative timing of these events.

Lithostratigraphy

The Dasher mineralization is hosted by a 100-150 m thick zone of biotite-bearing granite-gneiss (*sensu lato*), which is sharply bound on its hangingwall and footwall sides by moderately east-dipping, biotite granite dikes (*sensu stricto*; Fig. 5). These units are termed the Dasher granite-gneiss and Dasher granite dikes, respectively.

Dasher granite-gneiss: The Dasher granite-gneiss is a compositionally and texturally banded granitoid, which preserves some relict igneous textures. The dominant component of the granite-gneiss is a variably K-feldspar-phyric, biotite-bearing granitoid that ranges between monzogranite and granodiorite composition (Fig. 6), based on modal mineralogy of quartz (10-25 vol%), microcline (15-35 vol%), plagioclase (oligoclase, 30-60 vol%), and biotite (5-15 vol%), with accessory zircon, apatite and monazite. Granoblastic recrystallization is common (Fig. 7A), but relict subhedral, poikilitic K-feldspar phenocrysts up to 10 mm in size remain evident as aggregates of microcline grains. Intervals of the typical K-feldspar-phyric granite-gneiss phase grade in and out of biotite-rich intervals (to 30 vol% biotite), and variably

megacrystic intervals, with K-feldspar phenocrysts up to 30 mm in size. In 12CADD001 and 14CADD001, a distinctive quartz-phyric biotite syenogranite cuts across weak S_1 foliation in the monzogranite (Fig. 7B), and is interpreted to be a younger intrusive phase. The modal mineralogy of the syenogranite (Fig. 6) is quartz (30 vol%), microcline (45 vol%), plagioclase (oligoclase, 20 vol%) and biotite (5 vol%), with accessory zircon, and it is recrystallized to a granoblastic texture. The granite-gneiss commonly contains 5-50 mm wide, coarse-grained, quartz-plagioclase-microcline (biotite-absent) bands (Figs. 7C, 7D). These are most common in foliated and biotite-rich intervals, and are interpreted to be leucosomes derived from partial melting of the granite-gneiss.

Dasher granite dikes: The hangingwall and footwall granite dikes are both constrained to less than ~150 m in thickness, based on drill hole and outcrop observations (Fig. 5), and have sharp, low-strain contacts with the granite-gneiss (Fig. 7E). The dikes vary between syenogranite and monzogranite composition (Fig. 6), based on a modal mineralogy of quartz (25-42 vol%), microcline (35 vol%), plagioclase (oligoclase, 15-32 vol%) and biotite (8 vol%), with accessory zircon and apatite. Granoblastic recrystallization is evident, but poikilitic quartz and microcline grains (to 5 mm) in the dikes are interpreted to be relict igneous phenocrysts. There is no evidence of the compositional banding that is common in the granite-gneiss.

Other lithologies: The Dasher granite-gneiss contains lenses of mafic ortho-amphibolite (Fig. 7F) that are up to 15 m wide, and have a modal mineralogy of hornblende (55 vol%), plagioclase (45 vol%) and minor quartz. These mafic lenses are deformed by the earliest structural events, and may be remnants of the southeastern greenstone belt sequence (Fig. 3) entrained in the granite-gneiss during its intrusion.

Two generations of granitoid dikes cut the granite-gneiss, but are not observed to cut the granite dikes. Sub-horizontal and steeply east-northeast-dipping biotite monzogranite dikes, up to a few meters wide, cut S_{BAN}, S_1 and mineralized veins in the granite-gneiss. Irregular dikes of coarse-grained, biotite-poor granite (*sensu stricto)*, also up to a few meters wide, intrude the granite-gneiss within and outside of the deposit area, commonly migrating across S_{BAN}. These dikes may be leucosomes derived from partial melting of the granite-gneiss, or a separate magmatic event. Subhorizontal, muscovite-bearing pegmatite dikes (up to 3 m wide) are the youngest likely Archean intrusions at Dasher. Dolerite dikes of interpreted Proterozoic age cut all other lithologies, and occur in three principal orientations: (1) sub-vertical, north-striking; (2) sub-vertical, east-striking, and; (3) sub-horizontal.

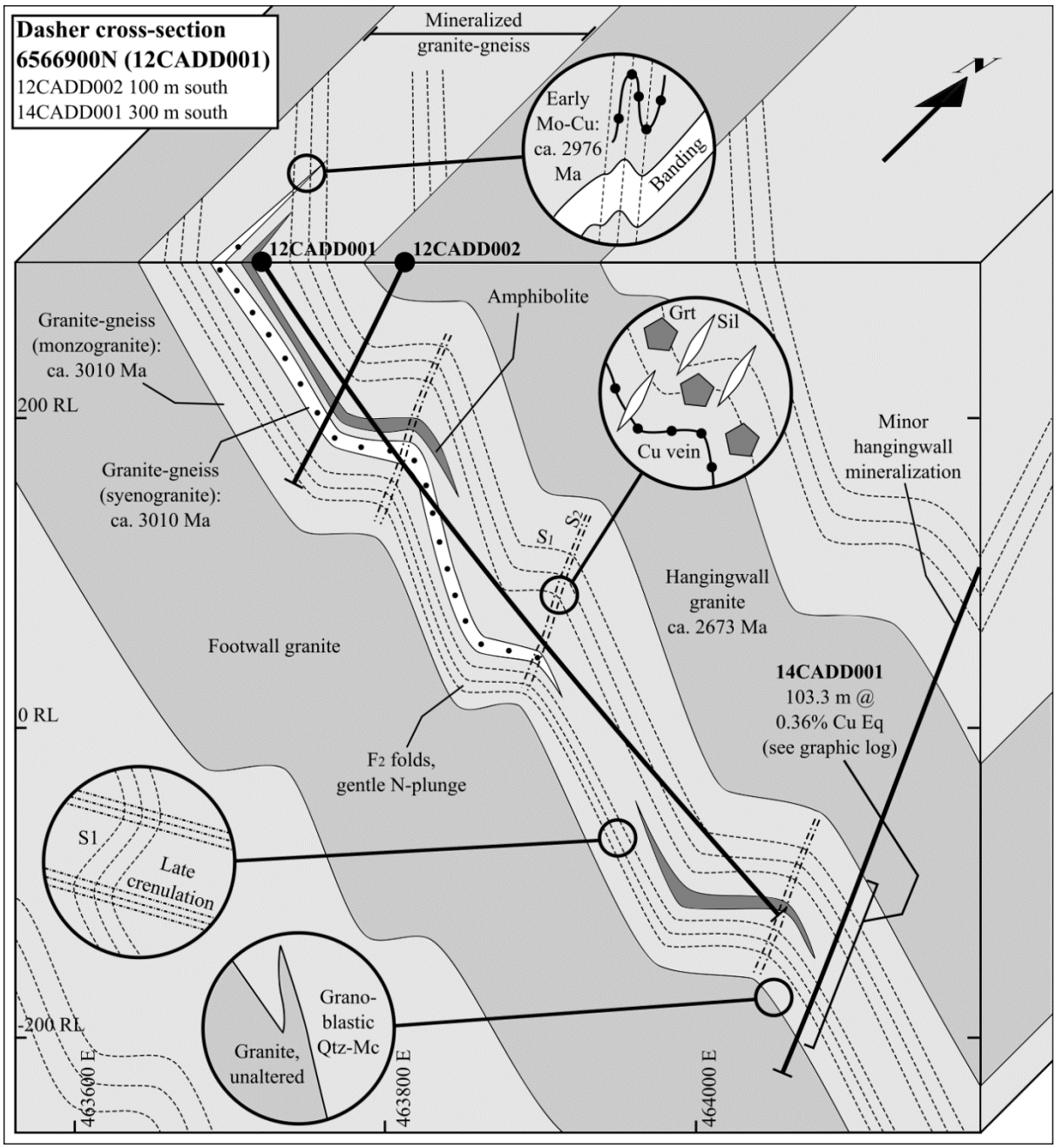

Fig. 5. Block diagram summarizing lithological, structural, metamorphic and mineralization relationships at Dasher, based on a cross-section through 12CADD001. Other holes are projected to the section. Proterozoic dolerite dikes are not shown, for clarity.

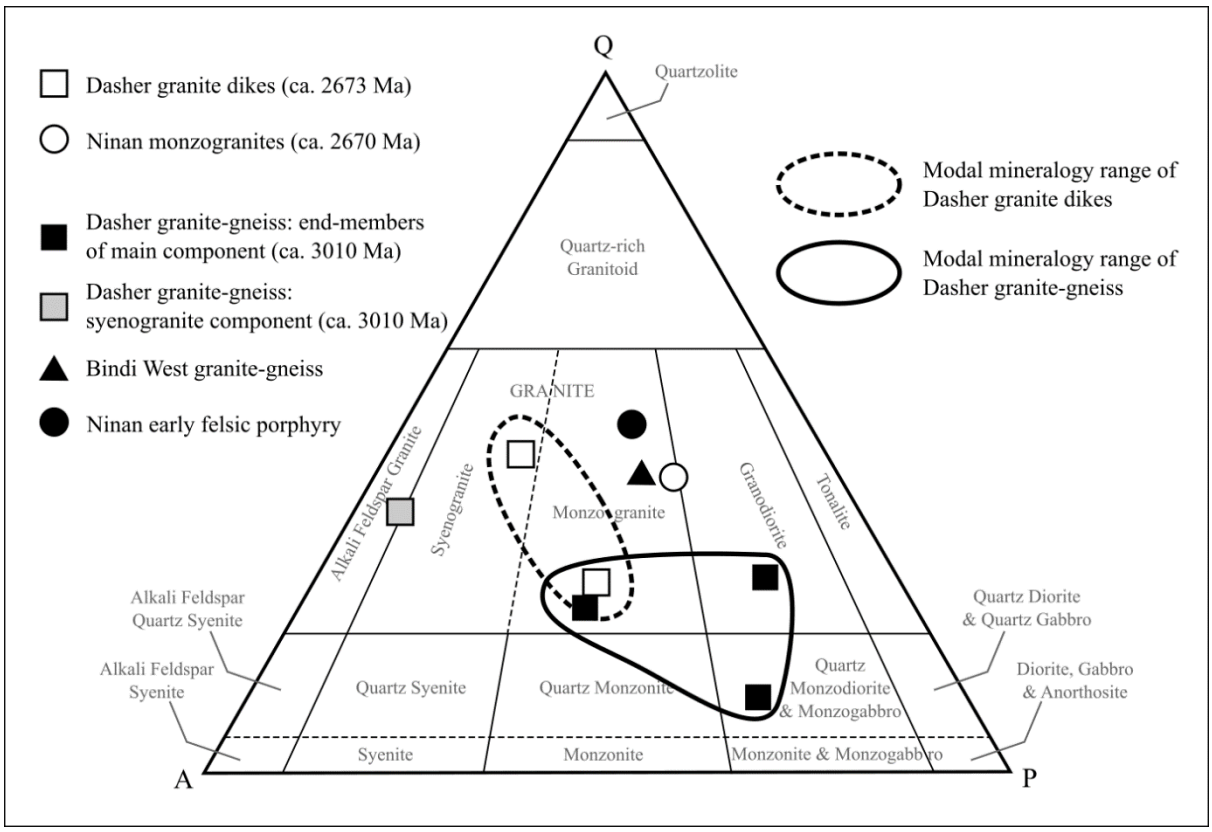

Fig. 6. QAP diagram showing the locations and ranges of least altered granitoid lithologies, based on petrographic estimations of modal mineralogy.

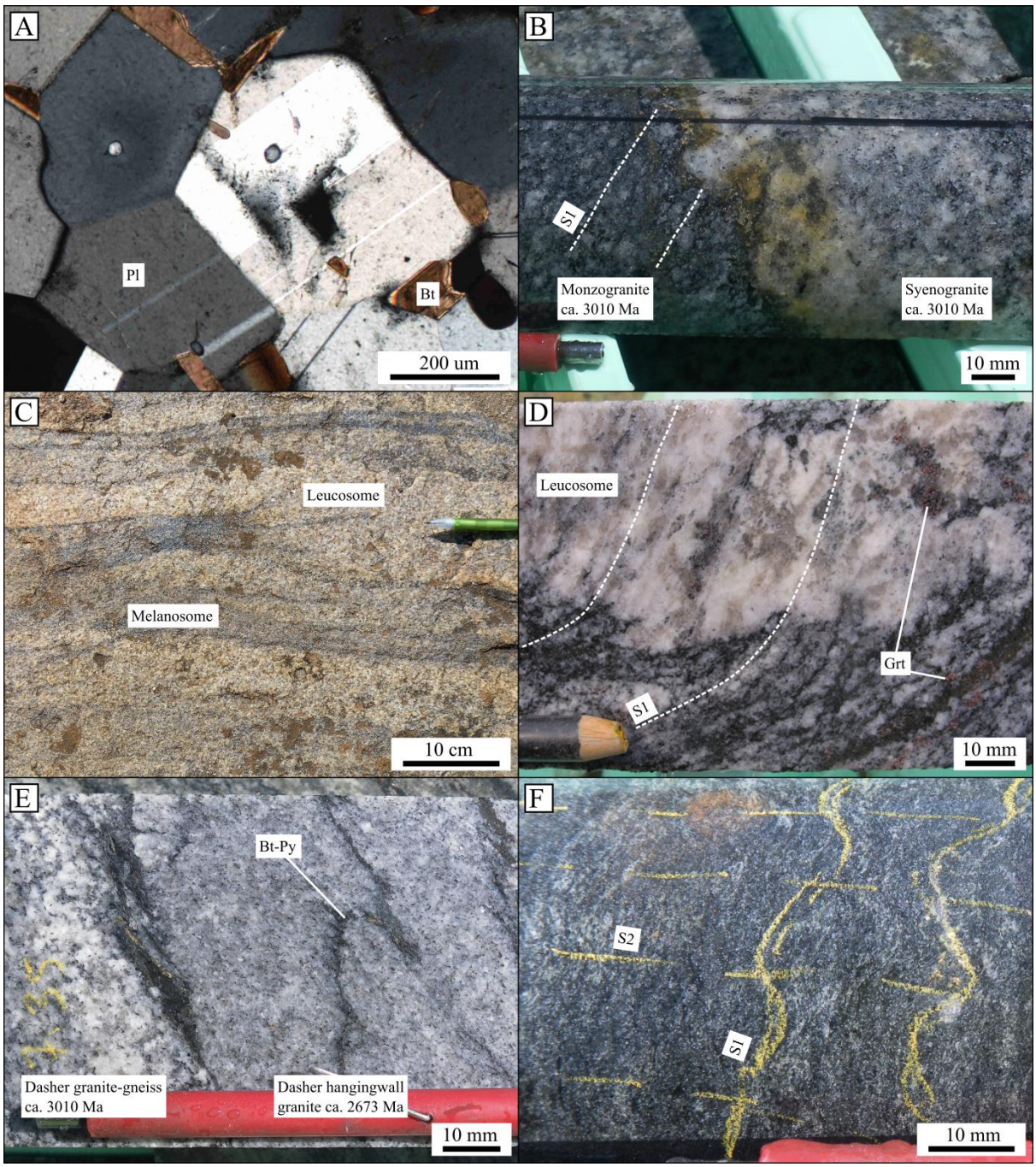

Fig. 7. Dasher host rock features. (A) Photomicrograph (cross-polarized) showing polygonal granoblastic texture of plagioclase, with 120° triple-junctions pinned to biotite grains in places. Sample CAL050. (B) Contact between monzogranite and syenogranite components of the granite-gneiss, with the syenogranite cutting weak S_1 in the monzogranite. SHRIMP U-Pb zircon samples were taken from either side of this contact. 12CADD001, 138.5 m. (C) Leucosome-melanosome bands in granite-gneiss south of Dasher. 6566260N 463980E. (D) Biotite-poor *in situ* leucosome in granite-gneiss, preserving relict S_1 foliation. 12CADD001, 288.0 m. (E) Low strain intrusive contact between the hangingwall granite dike (right) and mineralized granite-gneiss (left). 14CADD001, 437.3 m. (F) Mafic ortho-amphibolite, with S_1 crenulated by S_2. 14CADD001, 445.6 m.

Geochronology

SHRIMP U-Pb geochronology was completed on zircon separates from representative samples of the monzogranite and syenogranite phases of the Dasher granite-gneiss, and the cross-cutting Dasher granite dikes. Unpublished data and interpretations by Wingate and Lu (2016) are in Appendix 10. In all samples, the interpreted igneous zircons have elongate and subhedral-euhedral morphology, and are concentrically zoned. Average $^{232}Th/^{238}U$ ratios (given in brackets for each sample, below), combined with the zircon morphology, are consistent with the zircons being of igneous origin (Hoskin and Schaltegger, 2003).

The monzogranite (sample CAL024, GSWA ID 205930) and syenogranite (sample CAL026, GSWA ID 205931) samples were taken from either side of their observed contact in 12CADD001 (Fig. 7B). Fourteen analyses of 13 zircons from CAL024 yield a weighted mean $^{207}Pb/^{206}Pb$ age of 3010 ± 4 Ma (MWSD = 1.4, average $^{232}Th/^{238}U$ = 0.51), which is interpreted to represent the magmatic crystallization age of the monzogranite (Fig. 8). Twenty analyses of zircons from CAL026 also yield a weighted mean $^{207}Pb/^{206}Pb$ age of 3010 ± 4 Ma (MWSD = 1.5, average $^{232}Th/^{238}U$ = 0.50), which is interpreted to represent the magmatic crystallization age of the apparently younger syenogranite (Fig. 8). The identical ages (within error) of these granitoid phases are consistent with the Dasher granite-gneiss being the product of multiple intrusive events at ca. 3010 Ma. The results also suggest that the Dasher granite-gneiss is part of the same granite-gneiss domain as the quartz-feldspar-biotite gneiss at the 'W7' locality of Pidgeon et al. (1990), although the Dasher granite-gneiss lacks the ca. 2810 Ma zircons attributed to gneiss-formation in 'W7'.

The Dasher granite dike sample was taken from the hangingwall granite in 14CADD001 (sample CAL044, GSWA ID 205932). Nine analyses of seven zircons from CAL044 yield a weighted mean $^{207}Pb/^{206}Pb$ age of 2673 ± 5 Ma (MWSD = 2.4, average $^{232}Th/^{238}U$ = 0.26), which is interpreted to represent the magmatic crystallization age of the granite dike (). Thirty analyses of interpreted older zircon cores from this sample yield inherited ages ranging from 3282-2782 Ma, including significant groups at ca. 3011 Ma (the age of the granite-gneiss) and ca. 2810 Ma. These crystallization and inherited age characteristics are likely applicable to the visually and geochemically similar footwall granite dike.

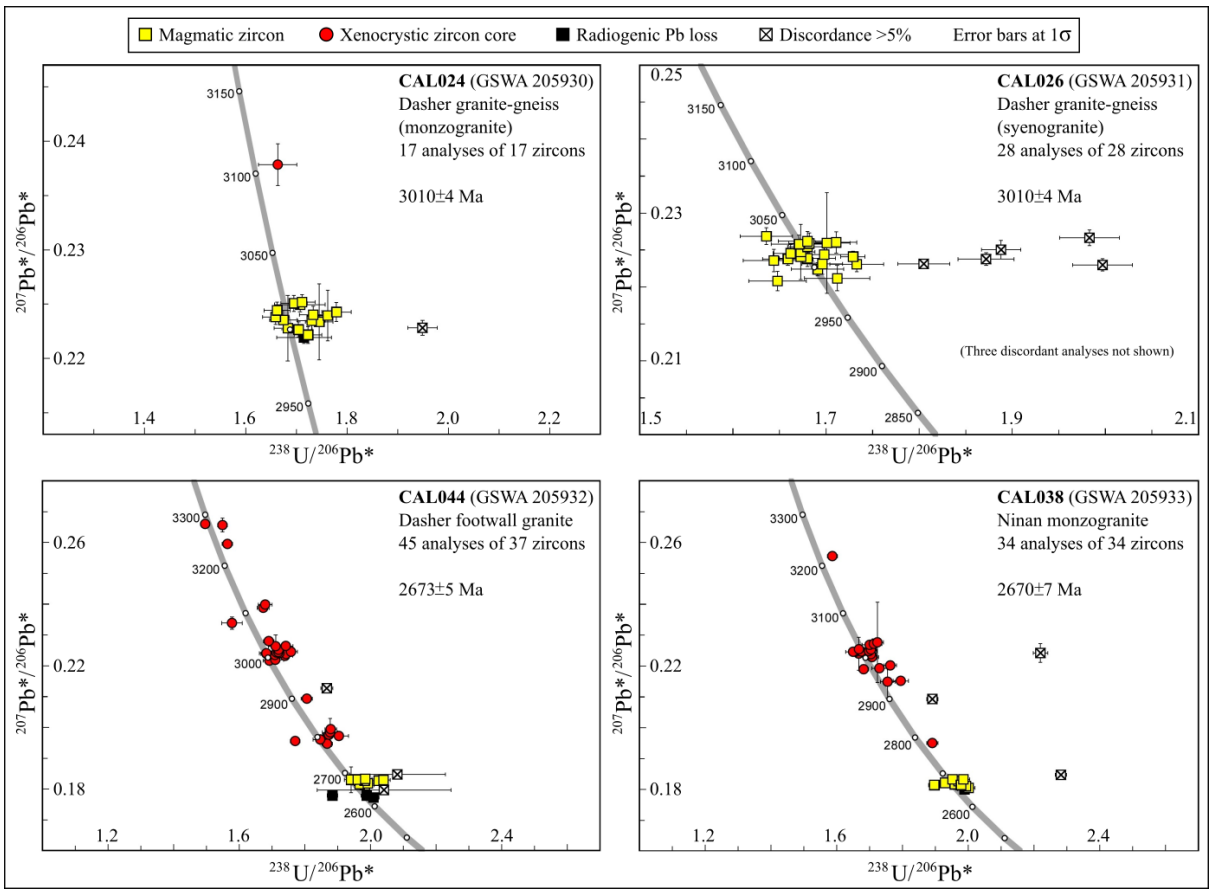

Fig. 8. SHRIMP U-Pb analytical data for zircons from Calingiri granitoid lithologies. Interpreted magmatic crystallization ages are given on each plot. Modified from Wingate and Lu (2016) in Appendix 10.

Structural setting

The preserved geometries of lithological and structural features at Dasher are the product of two significant deformation events, detailed below, and the intrusion of the ca. 2673 Ma granite dikes.

D_1 structures: Internal to the granite-gneiss, S_{BAN} (compositional banding) dips moderately east-northeast, sub-parallel to the orientation of the granite dikes (Figs. 5, 9A). The S_1 foliation, however, is steeper and more northeast-trending than S_{BAN} and the granite dikes, with mean orientation of 65°/061° (Fig. 10A). This relationship, where S_1 is acute to S_{BAN} in a clockwise sense, is also consistently developed in outcrop proximal to Dasher (Fig. 11A). The S_{BAN}-S_1 intersection lineation can be inferred to have a ~steep pitch on the plane of S_{BAN} (Fig. 9B), based on the similar dip, but acute strike, of each element in the Dasher area.

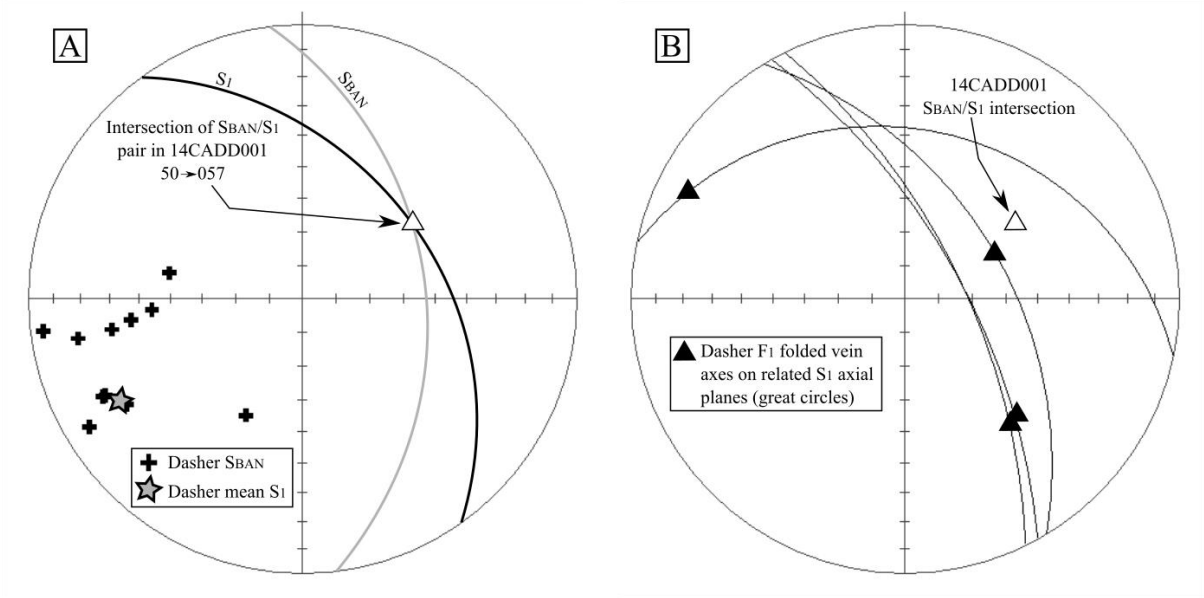

Fig. 9. Stereonets of early structural features at Dasher, from drill core. (A) Poles to S_{BAN}, the pole to mean S_1 from Fig. 10A, and great circles relating to an S_{BAN}/S_1 'pair', along with its intersectional plunge. S_{BAN} is generally more north-striking than S_1. (B) F_1 fold axes from folded early veins, on great circles representing their axial planes. Plunges are variable, but have some similarity to the S_{BAN}/S_1 intersection plunge.

The S_1 foliation is most clearly defined by the alignment of biotite grains in the granite-gneiss. Strain in this deformation phase is heterogeneously developed, with increasing strain characterized by the segregation of biotite-rich bands and quartz-feldspar-rich bands into a gneissic fabric (Fig. 11B). In high-strain zones affecting porphyritic granite-gneiss, biotite deflects around microcline phenocrysts, but there is no clear rotation of the phenocrysts, or asymmetry in the foliation. The L_1 stretching lineation was not observed on S_1 at Dasher.

Early quartz-feldspar ± sulfide veins at Dasher are deformed in tight to isoclinal folds where S_1 is the axial planar foliation, and these are therefore interpreted to be F_1 folds (Fig. 11C). Fold axes of these folded veins show an inconclusive spread of orientations (Fig. 9B) that is the product of the original, unfolded geometry of the veins (unknown) and reorientation by F_2. No significant F_1 folds of granite-gneiss units were recognized. The consistent vergence relationship between SGN and S_1 in core and outcrop around Dasher (e.g. Fig 11A) suggests that, overall, the deposit is located on a single limb of a kilometer-scale F_1 fold.

D_2 structures: At regional scale, Dasher lies on a west-verging F_2 limb, with the Bindi antiform to the west and the Opie synform to the east (Fig. 3). At the deposit scale, this setting is reflected by the development of open, west-verging F_2 folds, which have a significant influence on the preserved geometry of the host rocks (Figs. 5, 11D, 11E). The spread of S_1 foliation orientation away from the mean of 65°/061° occupies a fold-related girdle with a beta-axis orientation of 13°→341° (Fig. 10A). This approximation of the plunge of F_2 folds at Dasher

is consistent with measurements of individual F_2 fold axes, the intersection of the average S_1 and S_2 orientations (Fig. 10C), and the district-scale plunge of F_2 folds (Figs. 3, 4).

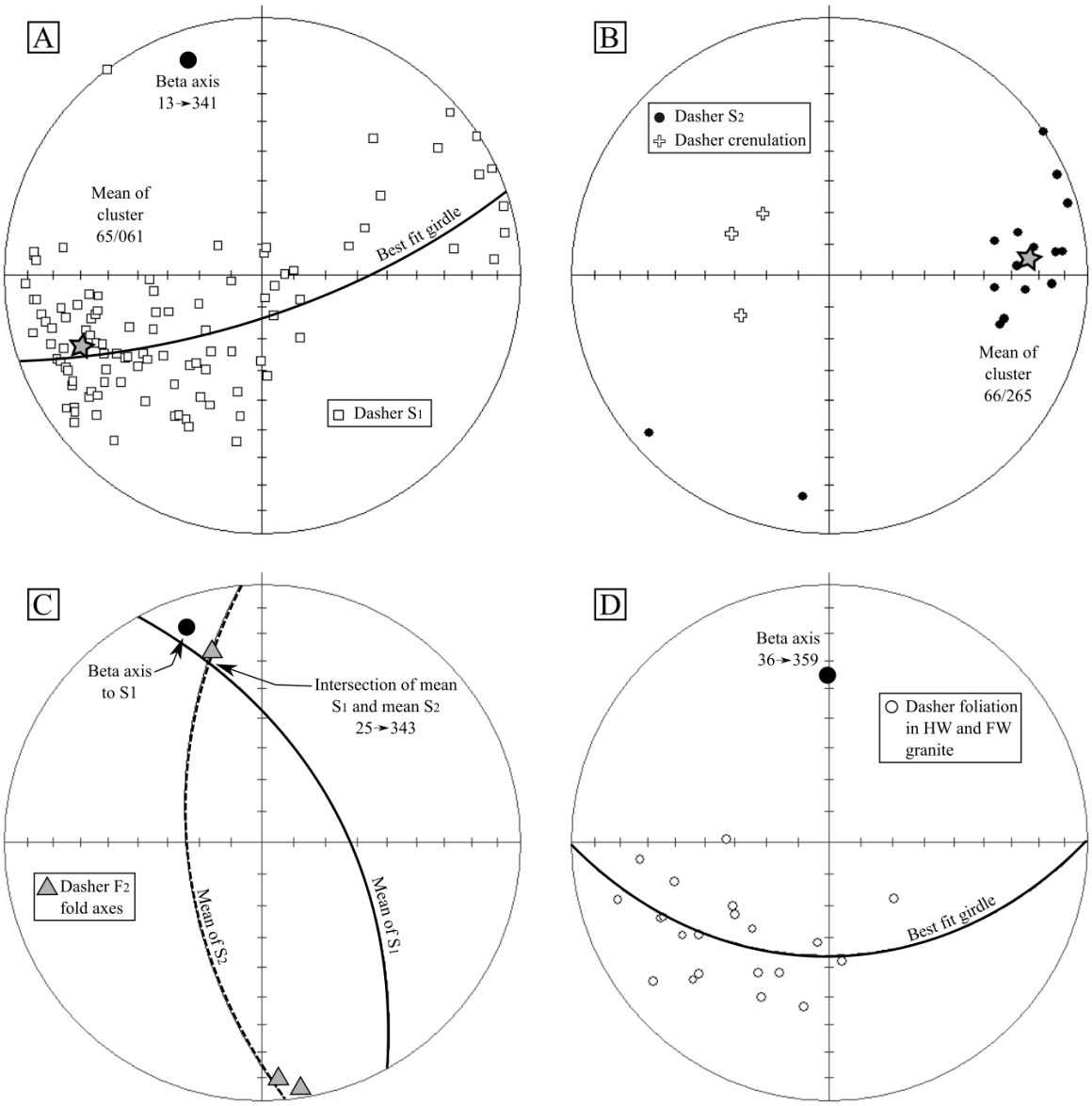

Fig. 10. Stereonets of D_1 and D_2 features at Dasher, from drill core. (A) Poles to S_1, showing a fold-related distribution. The pole to the best fit girdle (beta-axis) approximates the plunge of the folds responsible. (B) Poles to S_2 and a late crenulation cleavage. (C) Measured F_2 fold axes, the beta axis from Fig. 10A, and great circles of mean S_1 and S_2, from Fig. 10A and Fig. 10B, respectively. All data are consistent with north-northeast-trending, gently plunging F_2 folds. (D) Poles to weak foliation in the granite dikes in 14CADD001, showing a fold-related distribution. The pole to the best fit girdle (beta-axis) approximates the plunge of the folds responsible, and suggests an F_2 influence.

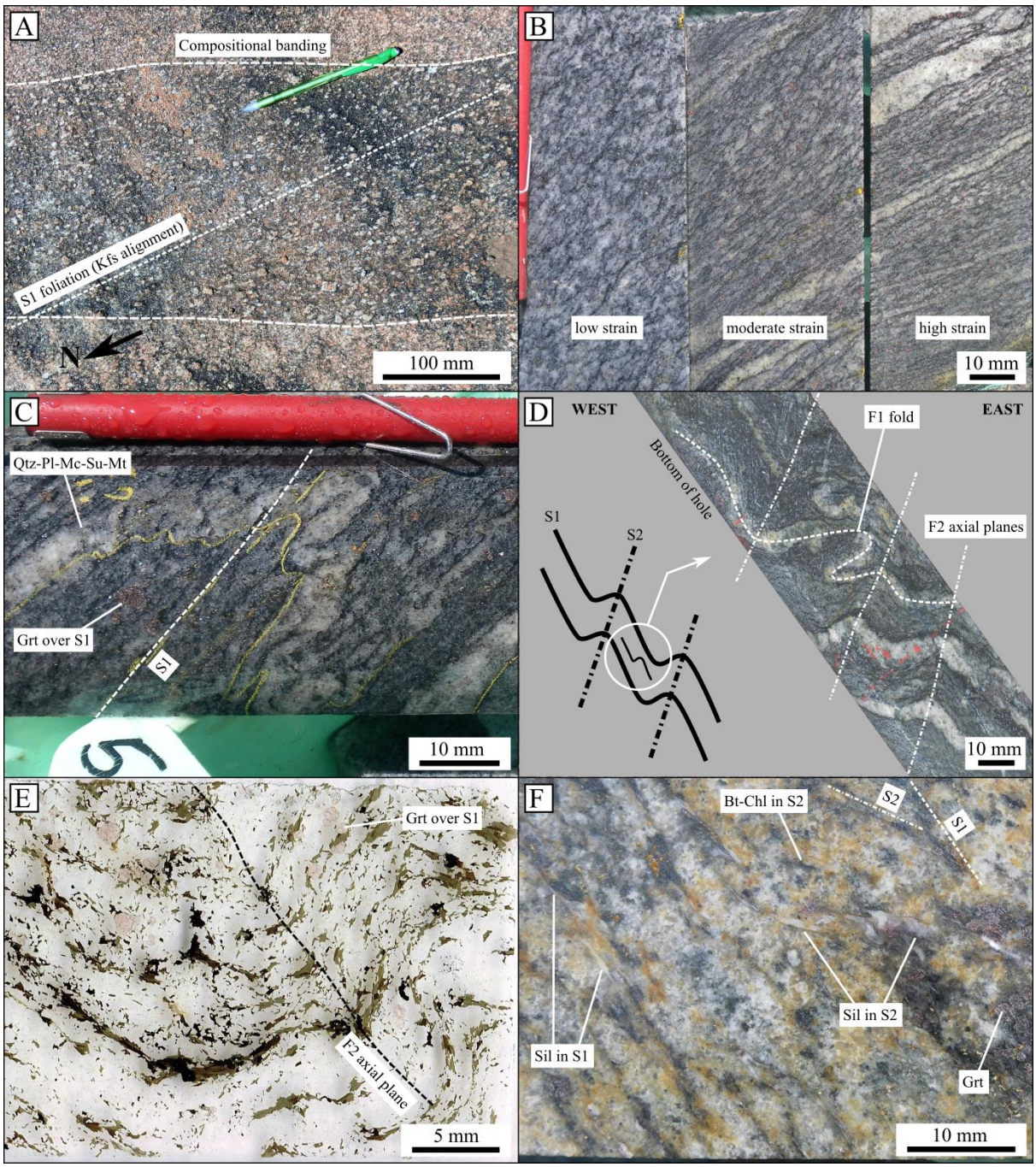

Fig. 11. Dasher structural features. (A) Typical acute relationship between S_{BAN} and S_1, in granite-gneiss outcrop. 6567756N 465187E. (B) Effects of increasing strain on the same granite-gneiss, including development of S_1-parallel leucosomes at high-strain. 14CADD001, around 468.0 m. (C) Early quartz-feldspar-sulfide vein affected by tight-isoclinal, ptygmatic F_1 folding, where S_1 is axial planar. Coarse garnet overgrows S_1. 14CADD001, 449.4 m. (D) View north at west-verging F_2 folds of S_1-parallel pegmatoidal veins in drill core, including refolding of a tight F_1 fold. 12CADD001, 54.8 m. (E) Scanned thin-section showing fine west-verging F_2 folds of S_1-aligned biotite, and light pink garnet overgrowing S_1. Sample CAL022. (F) Biotite-chlorite and sillimanite developed in both the S_1 and S_2 orientations in microcline- and sillimanite-rich granite-gneiss. 12CADD002, 77.6 m.

In detail, F_2 folds at Dasher are open, concentric folds, with moderately to steeply west-dipping axial planes (Figs. 5, 11D, 11E). A weakly developed axial planar foliation, S_2, has an average orientation of 66°/265° (Fig. 10B), and is defined by alignment of biotite and of fibrolitic sillimanite masses, where present (Fig. 11F). 12CADD001 was drilled down the F_2 long-limb orientation, and intercepts a number of ~50 m long F_2 short-limbs, defined by sub-horizontal to gently west-dipping S_1 (Fig. 5). The orientation of F_2 folds and the S_2 foliation are suggestive of ~east-west compression during the D_2 event.

Other structural features: In 14CADD001, S_1 is locally crenulated about ~30° east-dipping axial planes, to create reclined gently-plunging folds (Fig. 5). The relative timing between this crenulation and D_2 is not clear from this study. In 12CADD001, a 2 m wide tectonic breccia, oriented ~80°/330°, cross-cuts the mineralized granite-gneiss, and contains pre-foliated xenoliths of it. The distinctively brittle structural style of this zone, and the associated retrograde chlorite-sericite-epidote mineral assemblage, indicate that this is a late feature.

Metamorphism

The granite dikes, and unmineralized examples of the granite-gneiss at Dasher, are recrystallized and variably granoblastic, as discussed above, but their interpreted primary igneous mineralogy is generally intact (quartz-plagioclase-microcline-biotite). Proximal to mineralization, however, the granite-gneiss has an equilibrium assemblage of quartz-microcline-plagioclase-garnet ± sillimanite (Fig. 12A). This is interpreted to be a metamorphosed hydrothermal alteration assemblage, and is discussed in more detail later in this paper. Nevertheless, the garnet-sillimanite-bearing assemblage provides general constraints on peak metamorphic conditions at Dasher, and is supported by the presence of trace garnet and sillimanite in the unmineralized Dasher granite dikes (Fig. 12B). The presence of sillimanite suggests high-T, low-P (<10 kbar) series metamorphism (Spear, 1995) that reached at least middle amphibolite facies (>500°C). The lack of metamorphic pyroxene in the mafic amphibolite lenses, together with the stability of biotite in the granite-gneiss, suggests that peak T did not exceed ~800°C (Spear, 1995).

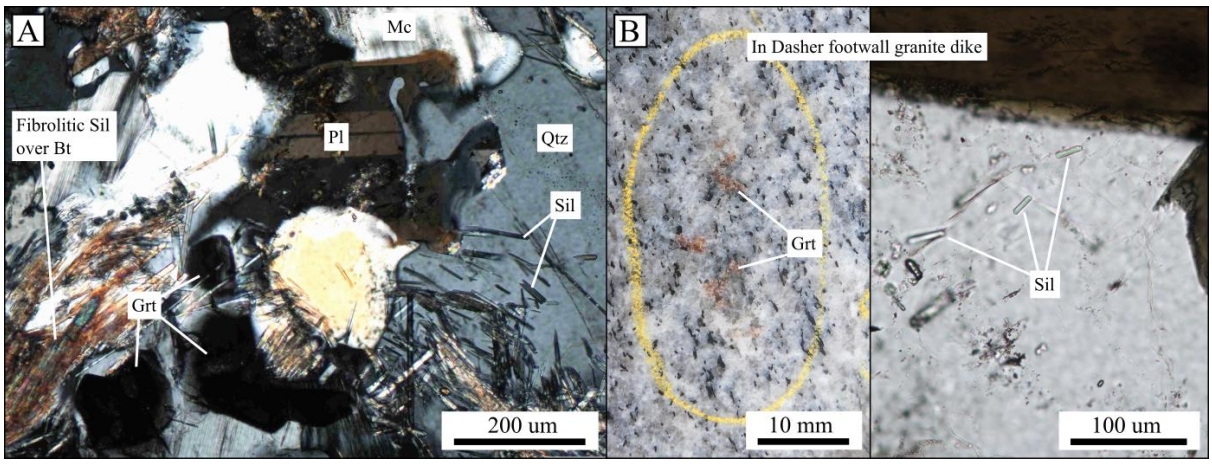

Fig. 12. Dasher metamorphic features. (A) Photomicrograph (cross-polarized) of typical peak metamorphic equilibrium assemblage in granite-gneiss, with sillimanite as fine needles on the margins of quartz and feldspars, but also as fibrolitic pseudomorphs of biotite. Sample CAL019. (B) Garnet and sillimanite in the footwall granite dike. Garnet from 14CADD001, 561.9 m. Sillimanite is a photomicrograph (plane-polarized) from sample CAL045.

Greenschist facies retrograde metamorphism is evident in all Archean lithologies at Dasher, but its intensity is heterogeneous. In least-retrogressed examples of the granite-gneiss, biotite is partly replaced by chlorite-sericite-ilmenite, feldspars are dusted with fine sericite, and garnet (where present) is pristine. More intense retrogression is typically focused around pre-existing or late-tectonic structures, and is characterized by increasing replacement of biotite and feldspars by chlorite-sericite ± epidote ± calcite, and chlorite retrogression of garnet.

Relative and absolute timing of intrusive, deformation and metamorphic events

The D_1 deformation event was likely occurring at ca. 3010 Ma, during the intrusion of the ~monzogranite pre-cursor to the Dasher granite-gneiss. This is indicated by the CAL026 biotite monzogranite (3010 ± 4 Ma; SHRIMP U-Pb zircon) containing foliation that is cut by the CAL024 syenogranite (Fig. 7B), which itself returned the same magmatic crystallization age. The Dasher granite dikes are not affected by S_1, constraining the end of D_1 event to older than ca. 2673 Ma (the age of the dikes; SHRIMP U-Pb zircon). Ubiquitous garnet overgrowth of S_1 (Figs. 11C, 11F) constrains peak metamorphism to a post-D_1 age. Peak metamorphic sillimanite overgrows S_1-aligned biotite, but also occurs in masses aligned to S_2 (Fig. 11F). The critical latter structural-metamorphic texture indicates that sillimanite grew during or after D_2, and provides a temporal link between high-grade metamorphism and D_2 ~east-west compression.

On the present drilling density at Dasher, the relationship between the granite dikes and deposit-scale F_2 folding is equivocal. However, a weak foliation developed inside the dikes has

a spread of orientations that lies on a girdle with a north-plunging beta-axis (Fig. 10D), similar to F_2-related redistribution of S_1 orientations in the granite-gneiss (Fig. 10A). That observation, together with the presence of trace garnet and sillimanite in the dikes, suggests that they are folded, and likely intruded pre- to syn-D_2. On that basis, D_2 deformation and peak metamorphism likely occurred at, or after, ca. 2673 Ma.

Mineralization, Hydrothermal Alteration and Modification of the Dasher Cu-Mo-Ag Deposit

The current Indicated and Inferred resources at Dasher stand at 137 Mt @ 0.30% Cu (0.40 Mt contained Cu), 72 ppm Mo, 1.69 g/t Ag and 0.02 g/t Au, at 0.15% Cu cut-off (Caravel Minerals Ltd, 2016). Copper has a strong positive correlation with Ag and Au, as well as with Bi, Te, and Cd (Table 2; Appendix 8). Molybdenum is poorly correlated with Cu, suggesting a spatial separation between the two elements, internal to the overall mineralized body (Table 2).

Table 2. Metal associations of the Dasher mineralization, based on Caravel Minerals Ltd four-acid digest data from the granite-gneiss portions of 12CADD001 and 14CADD001 (Appendix 8). Elements are in order of their correlation coefficient with Cu in a 0.1-1.0% Cu subset. The expected ranges of the metals in the potassic and deep sericitic zones of porphyry Cu deposits are listed at right, modified from Halley et al., (2015).

	Granite-gneiss			In granite-gneiss with 0.1-1.0% Cu			Range in porphyry Cu Potassic/Deep sericitic	
Element	Median	25th percentile	75th percentile	Correlation with Cu	Minimum	Maximum	Low	High
Ag	1.25	0.80	1.94	0.90	0.35	7.87	0.5	50
Bi	0.95	0.555	1.525	0.75	0.2	7.16	0.05	10
Te	0.31	0.20	0.52	0.72	0.10	2.44	0.1	5
Au	0.024	0.13	0.039	0.67	<0.005	0.223	-	-
Cd	0.06	0.04	0.13	0.52	0.01	0.42	-	-
Zn	23	17	35	0.40	10	90	bkgd	1000
Sn	1.7	1.3	2.1	0.38	0.6	4.7	0.5	30
Mo	26.8	9.3	61.0	0.14	1.25	1480	0.5	ore
Mn	671	444	1395	0.13	105	9000	bkgd	5000
As	0.3	0.2	0.6	0.09	0.1	9.3	bkgd	50
W	0.5	5.7	9.0	0.03	0.1	9.9	bkgd	20
Pb	9.4	5.8	14.5	0.03	3.5	28.3	50	1000
Cs	2.06	1.60	2.49	-0.09	0.51	6.32	bkgd	10
Se	N/A	N/A	N/A	N/A	<1	6	1	20
Sb	N/A	N/A	N/A	N/A	<0.05	4.1	bkgd	3
N/A = insufficient data above detection limit							- = not specified	

The Dasher resource is entirely contained within a ~1500 x ~150 m (true width) tabular zone of granite-gneiss preserved between the hangingwall and footwall granite dikes (Fig. 5). The north-striking, ~50° east-dipping geometry of this zone is controlled by the orientation of the dikes and overprinting F_2 folds, and therefore does not represent the original geometry or extent of mineralization. In the three diamond drill holes studied at Dasher, the entire thickness of the granite-gneiss preserved between the dikes is mineralized, further suggesting that the true limits of the mineralized system have not been observed. The geometries, textures and mineral assemblages preserved internal to the Dasher mineralization are also consistent with them being significantly modified by post-mineralization structural and metamorphic events. The effects of this modification are discussed here, where applicable.

Mineralization styles

The styles of mineralization at Dasher are described here in order from the interpreted oldest to youngest events. The sulfide-oxide species present in each style have some common characteristics that are applicable, unless otherwise stated. The Cu and Mo is hosted within chalcopyrite and molybdenite, respectively, with no other Cu or Mo phases present. In Mo-dominant mineralization (>100 ppm) the molybdenite contains fine inclusions and intergrowths of chalcopyrite-pyrrhotite, suggesting they are cogenetic (Fig. 13A). In Cu-dominant mineralization, the sulfide-oxide equilibrium assemblage is chalcopyrite-pyrrhotite-magnetite, and those three phases have a common anhedral and pitted morphology. Chalcopyrite and pyrrhotite commonly display lamellar intergrowths (Fig. 13B). Pyrite varies from absent up to a ~50:50 split with pyrrhotite as the dominant Fe-sulfide, and generally occurs in a subhedral to euhedral form that appears to overgrow pyrrhotite (Fig. 13B).

Early quartz-feldspar-molybdenite veins: The earliest mineralized veins observed at Dasher, here termed 'V1', are Mo-dominant, granoblastic quartz-microcline ± plagioclase ± garnet ± sillimanite veins containing molybdenite-chalcopyrite-pyrrhotite ± magnetite ± pyrite mineralization (Figs. 13C, 13D). The V1 veins are commonly affected by ptygmatic, tight-isoclinal folds, where S_1 is in the axial plane orientation, constraining them to a pre- to syn-D_1 timing (Fig. 13D).

Re-Os geochronology: Re-Os geochronology was completed on molybdenite from two samples of Mo-dominant mineralization. Unpublished data and interpretations by Tessalina (2016) are in Appendix 11. Sample CAL009 (12CADD002, 66.64-66.74 m) was taken from an S_1-parallel streak of coarse-grained molybdenite through a granoblastic plagioclase-quartz-microcline-sillimanite-garnet unit of the granite-gneiss (Fig. 13C). The molybdenite contains

fine inclusions of cogenetic chalcopyrite and pyrrhotite, and all three sulfides are observed as inclusions inside large garnet grains (Fig. 13A). A single analysis of this sample yielded a model age of 2963 ± 12 Ma. Sample CAL047 (14CADD001, 451.70-451.80 m) was taken from a V1 microcline-quartz-molybdenite vein that is tightly folded, with S_1 as the axial planar foliation (Fig. 13D). The coarse-grained molybdenite contains fine inclusions of cogenetic chalcopyrite, and is intergrown with magnetite and pyrite. Repeat analyses of this sample yielded model ages of 2977 ± 20 Ma and 2975 ± 27 Ma. The structural constraints on the relative timing of the CAL047 vein, and the dual analyses, make its ca. 2976 Ma age (narrowest range of 2997-2957 Ma) the best estimate for the onset of the Cu-Mo-Ag mineralization at Dasher.

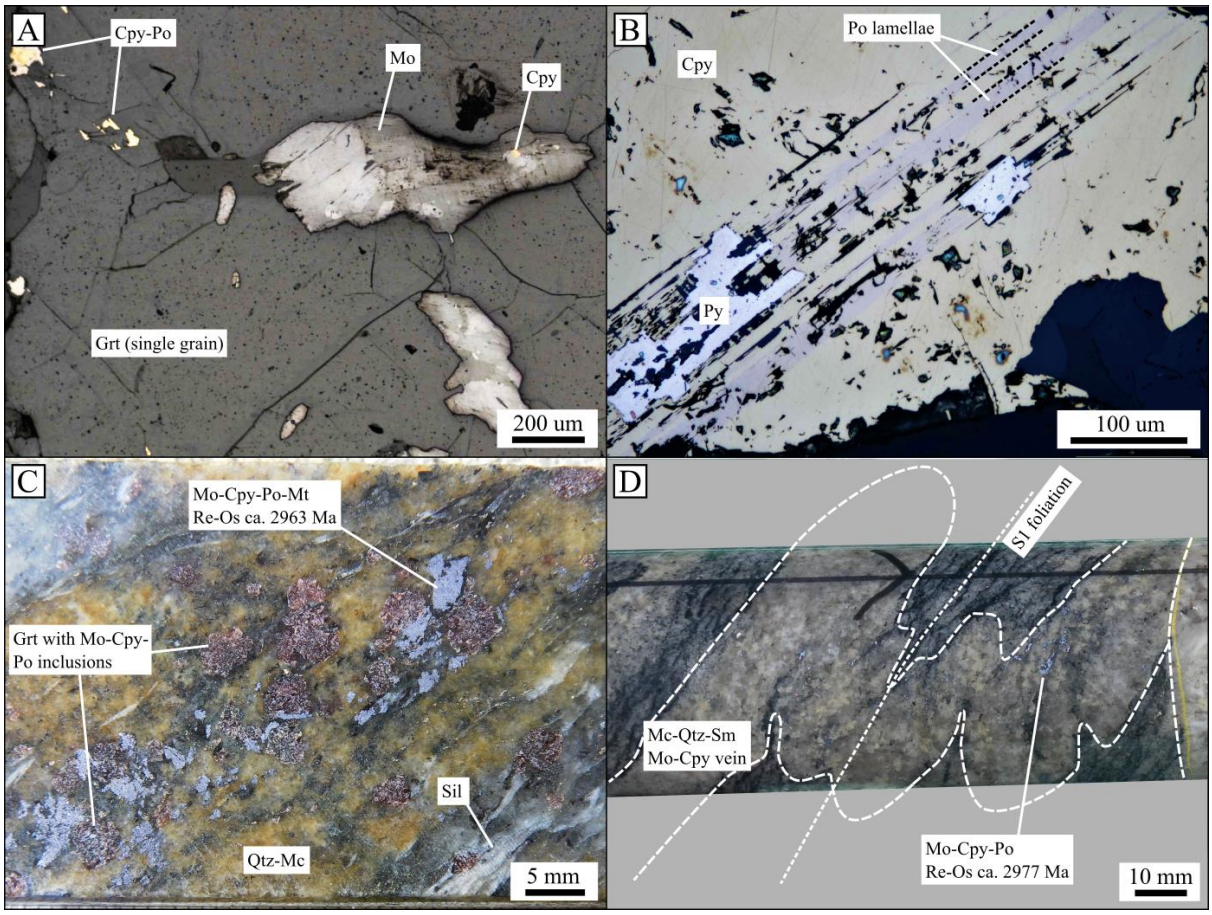

Fig. 13. Dasher mineralization features. (A) Photomicrograph (reflected light) of molybdenite-chalcopyrite-pyrrhotite included in a single large garnet grain. Sample CAL009, also shown in Fig. 13C. (B) Photomicrograph (reflected light) of anhedral lamellar chalcopyrite-pyrrhotite overgrown by subhedral pyrite. Sample CAL048. (C) Re-Os geochronology sample CAL009. An S_1-parallel streak of coarse molybdenite in quartz-microcline-biotite-sillimanite-garnet granite-gneiss. Fig. 13A shows sulfides inside large garnet grains at bottom left. Yellow colouration is weak oxidation. (D) Re-Os geochronology sample CAL047. The mineralized vein is affected by tight-isoclinal F_1 folding, where S_1 is axial planar.

Main stage Cu-dominant mineralization: Chalcopyrite-dominant variants of the V1 veins (although still containing molybdenite) are the earliest form of vein-hosted, Cu-dominant mineralization at Dasher, and are similarly observed to be affected by F_1 folds (Fig. 11C). The main stage of Cu-dominant mineralization at Dasher, however, is dominated by disseminated and stringer sulfide, and quartz-sulfide veins. Disseminated chalcopyrite-pyrrhotite ± pyrite forms up to 2 vol% of typical mineralized granite-gneiss (~0.2-0.5% wt% Cu). Thin (<2 mm) sulfide-rich stringers, here termed 'V2' veins, are either parallel to (most commonly), or cross-cut S_1, and favour development in S_1 foliation zones, at all scales (Fig. 14A). Clumps and streaks of biotite-magnetite associated with V2 veins are composed of biotite grains that overgrow S_1 (Fig. 14A).

The most common quartz-sulfide veins at Dasher are 1-10 mm thick quartz-chalcopyrite-pyrrhotite-magnetite ± pyrite veins, here termed 'V3' veins (Fig. 14B). These occur at a density of up to 3 veins per meter in typical mineralized granite-gneiss (~0.2-0.5% wt% Cu), and are either parallel to, or cross-cut, S_1. Although most V3 veins are narrow, a 2 m wide quartz-garnet-chalcopyrite-pyrrhotite vein in 12CADD001 is interpreted to be part of the same vein event. A brittle stockwork origin for V3 veins is suggested by their unfoliated margins and overall planar geometries, but sharp vein-wallrock contacts are not evident. Instead, bands of evenly sized, rounded quartz grains mark the vein locations, and the vein margins are cuspate-lobate contacts between quartz-sulfide-dominant vein mineralogy and the quartz-feldspar-biotite-dominant wallrock mineralogy (Figs. 14B, 14CFig. 14). Sulfide within V3 veins is interstitial to the quartz, 'mantling' the rounded quartz grains in a texture that is characteristic of this vein style (Fig. 14C). The cuspate-lobate vein margins and sulfide mantling of quartz grains, suggest that V3 veins are recrystallized.

Quartz-magnetite-garnet-biotite-chalcopyrite-pyrrhotite veins, distinctive for their dark green colour and very high magnetite (up to 40 vol%) and garnet (up to 50 vol%) contents, are here termed 'V4' veins (Fig. 14D). These are a minor component of mineralization (<1% of the mineralized volume), but are locally associated with Cu grades of >1.0%. Individual veins range from 5 cm to 2 m in thickness, have sharp contacts with the granite-gneiss wallrock, and were only observed parallel to S_1. The dark green colour of these veins is due to distinctive green biotite (pale brown to pale blue-green pleochroism) not observed in any other setting at Dasher.

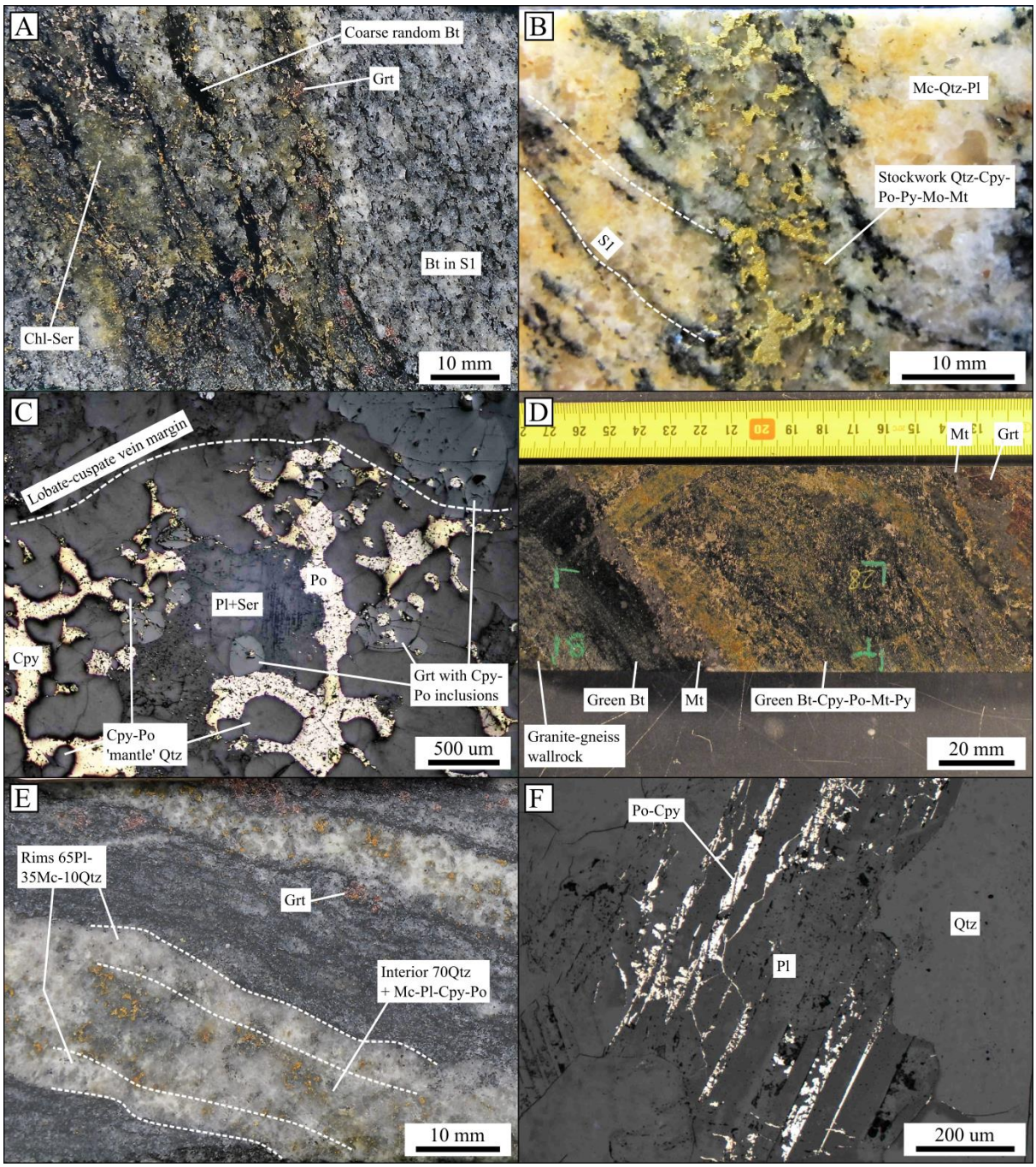

Fig. 14. Dasher mineralization features. (A) Sulfide veinlets and disseminations parallel to S_1, but with selvedges of garnet and clumps of random biotite. Pale green retrograde chlorite-sericite is focused around sulfide grains. 14CADD001, 490.0 m. (B) Quartz-sulfide stockwork vein cuts S_1 foliation, with sulfides 'mantling' quartz. Note the lack of a sharp vein-wallrock contact. Sample CAL011. (C) Photomicrograph (reflected light) of poorly-defined lobate-cuspate margin of a quartz-sulfide stockwork vein. Vein sulfides are interstitial to rounded quartz grains. Sample CAL010. (D) Typical quartz-magnetite-garnet-biotite-chalcopyrite-pyrrhotite vein. Note the mineralogical banding, and sharp contact with the wallrock. Sample CAL028. (E) Pair of mineralized pegmatite veins within high-strain, biotite-rich granite-gneiss Note the preference of sulfide for the quartz-rich portions of the veins. Sample CAL027. (F) Photomicrograph (reflected light) of plagioclase from the mineralized pegmatite vein in Fig. 14E, showing mineralization included in plagioclase twin planes. This suggests it may have been trapped in plagioclase as it crystallized. Sample CAL027.

The Cu-dominant mineralization at Dasher is interpreted to be a progression from the early Mo-rich mineralization, based on the mineralogical (quartz-feldspar-sulfide) and structural (affected by F_1 folds) affinities between Mo- and Cu-dominant versions of V1 veins. However, most of the Cu-rich mineralization is interpreted to be late- to post-D_1, as evidenced by: (1) V2, V3 and V4 veins either parallel to, or cross-cutting, S_1; (2) the focus of mineralization in S_1 high-strain zones; and (3) biotite associated with V2 veins overgrowing S_1. This temporal separation of the Mo-rich and Cu-rich mineralization at Dasher likely explains the poor correlation between Mo and Cu in assay data from the deposit.

Mineralized pegmatite veins: Pegmatoidal quartz-microcline-plagioclase-chalcopyrite-pyrrhotite ± garnet ± biotite veins, ranging from 5 to 40 mm in thickness, are present within some S_1 high-strain zones at Dasher, and locally relate to high Cu grades (>1.0 wt%; Fig. 14E). These veins, here termed 'V5', form irregular bands parallel to S_1, but are not folded or boudinaged in that foliation, indicating that they formed after D_1. Feldspar-rich (generally margins) and quartz-sulfide-rich domains (generally centres) are evident internal to the veins (Fig. 14E). Chalcopyrite-pyrrhotite mineralization in V5 veins is in two forms: (1) anhedral sulfides interstitial to quartz ± feldspar; and (2) fine sulfide inclusions entirely within plagioclase, including selectively along twin planes (Fig. 14F). The latter texture is not observed in typical mineralization at Dasher, and suggests that the sulfides were incorporated into the plagioclase as it crystallized.

The V5 veins are either: (1) external pegmatites, unrelated to mineralization, which have incorporated sulfide mineralization during their passage through the rock; (2) syn-mineralization pegmatoidal veins that are part of the Cu mineralization event; or (3) partial melt leucosomes, derived from mineralized granite-gneiss. The latter origin is supported by the observation that the granite-gneiss hosting V5 veins is generally biotite-rich (i.e., likely a melanosome), relative to surrounding rocks (Fig. 14E).

Modification of mineralization during D_2 and peak metamorphism: The geometry of the mineralization at Dasher is significantly modified by F_2 folding, at all observed scales. At micro- and meso-scale, V1 to V4 veins are folded by overall west-verging F_2 folds, and in places, F_1-affected V1 veins are refolded in F_2 (Fig. 11D). At macro-scale, the entire mineralized body is folded in west-verging F_2 folds (Fig. 5). The deformation of mineralization during the ~syn-peak metamorphic D_2 event, is strong evidence that mineralization was emplaced prior to the metamorphic peak, and provides independent support to the 'old' 2997-2957 Ma Re-Os age. Present evidence suggests negligible mechanical or hydrothermal remobilization of mineralization during D_2 and peak metamorphism: (1) sulfide mineralization

and silicate-oxide hydrothermal alteration reman coincident; (2) sulfide mineralization is retained within veins, even where they are folded or recrystallized (e.g., Figs. 11C, 13D); and (3) there no apparent increase of mineralization in S_2 high-strain zones or F_2 fold hinges, either of which may have indicated syn-D_2 remobilization.

Hydrothermal alteration

Structural, textural and geochronological evidence presented above suggests that the onset of Dasher Cu-Mo mineralization occurred at ca. 2976 Ma, and that minimum middle amphibolite facies metamorphism occurred at or after ca. 2673 Ma. Preserved hydrothermal alteration assemblages described below are, therefore, the metamorphic products of earlier hydrothermal alteration.

Biotite-garnet-sillimanite-magnetite alteration: Increased biotite, garnet, sillimanite and magnetite in the granite-gneiss is the most characteristic distal expression of the Dasher mineralization. The full equilibrium assemblage within granite-gneiss affected by this hydrothermal alteration is quartz-microcline-biotite-plagioclase-garnet-magnetite ± sillimanite (Figs. 12A, 15A). Garnet was observed over the full width of the mineralized granite-gneiss at Dasher, suggesting that the granite dikes likely obscure the true extents of this assemblage. However, garnet was not observed in granite-gneiss outcrops within ~1 km to the east and southeast of the Dasher deposit.

Biotite is elevated (vol%) in the mineralized granite-gneiss (Fig. 16), but does not diagnostically indicate hydrothermal alteration, because it is the principal igneous ferro-magnesian mineral in the granite-gneiss. In the majority of the granite-gneiss, igneous biotite remains evident as fine, dark green-brown grains that are uniformly aligned to the S_1 foliation. Mineralization-related biotite, however, occurs as coarser clusters and streaks of unaligned, subhedral grains with an interlocking, decussate texture, perhaps indicative of metamorphic recrystallization (Fig. 15B; Blatt et al., 2006). This form of biotite also has a distinctive light red-brown colour in thin-section, likely indicating higher TiO_2 content than the green-brown igneous biotite (Hayama, 1959). Preliminary quantitative SEM analyses (Appendix 9) confirm that mineralization-related biotite has higher FeO/FeO+MgO (0.92) and TiO_2 (3.48 wt%, respectively) than the igneous biotite (0.82, and 1.90 wt%, respectively).

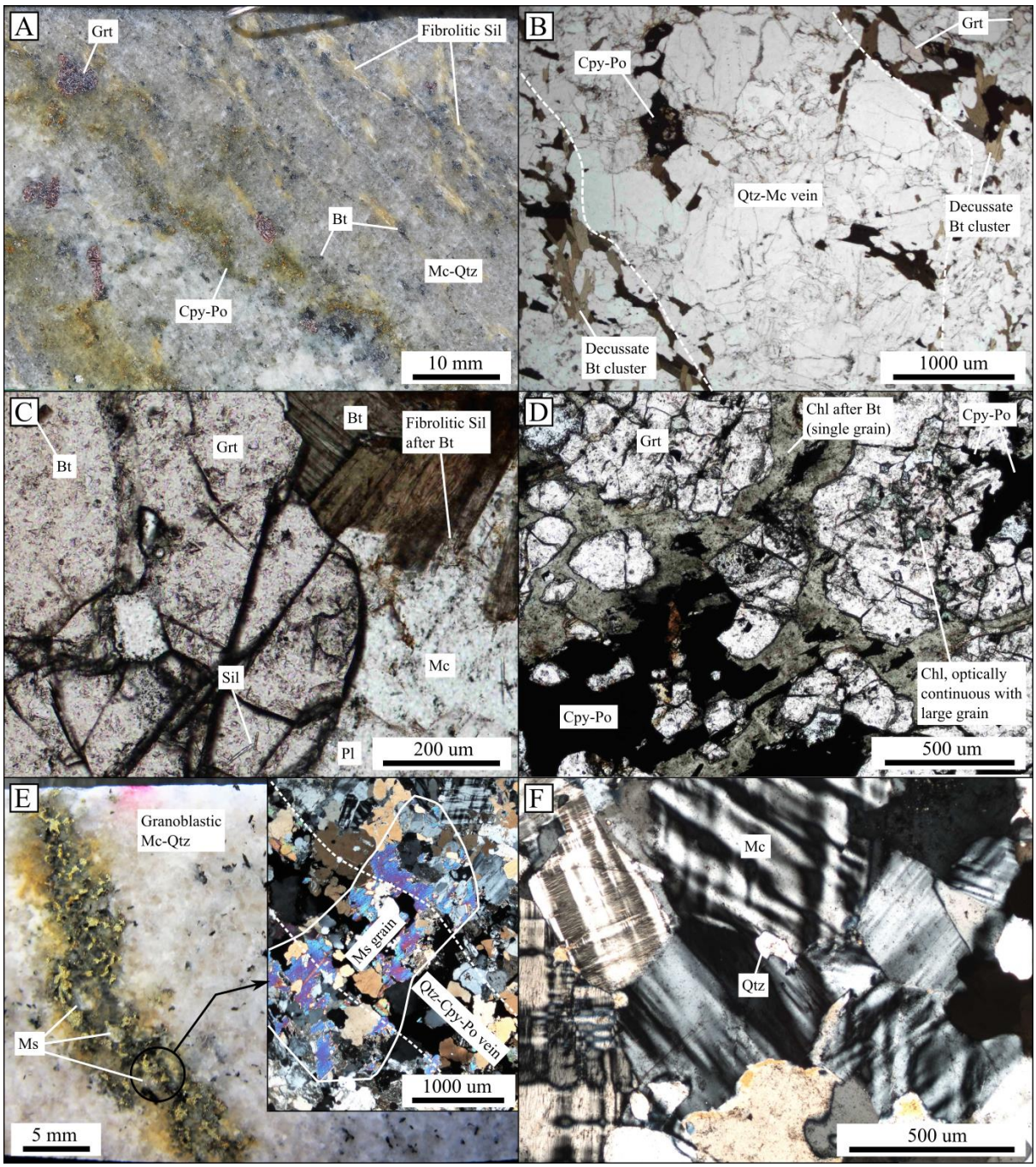

Fig. 15. Dasher hydrothermal alteration features. (A) Granite-gneiss altered to quartz-microcline-sillimanite-garnet-biotite assemblage. Note the near-complete destruction of biotite. 12CADD002, 158.2 m. (B) Photomicrograph (plane-polarized) of mineralized vein with clusters of light brown, subhedral, decussate biotite in its selvedge. Sample CAL048. (C) Photomicrograph (plane-polarized) of quartz-microcline-plagioclase-sillimanite-garnet-biotite assemblage, with fine biotite included in garnet. Sillimanite occurs as fibrolitic pseudomorphs of biotite, and as fine prisms enclosed in garnet. Sample CAL022. (D) Photomicrograph (plane-polarized) showing garnets overgrowing a single chloritized biotite grain and sulfide mineralization. The large garnet at right includes fine chlorite that is optically continuous with the external chlorite, suggesting that it overgrew chlorite. Sample CAL031. (E) Granoblastic quartz-microcline-plagioclase-sillimanite, with characteristic low biotite content. The quartz-sulfide stockwork vein is associated with coarse muscovite that is selectively replaced by quartz-microcline. Sample CAL054. Inset is a photomicrograph (cross-polarized). (F)

Photomicrograph (cross-polarized) of polygonal granoblastic microcline, displaying 120° triple-junctions, within quartz-microcline-plagioclase-sillimanite assemblage. Sample CAL053.

Garnet in this assemblage is pink-red almandine that occurs as subhedral crystals up to 5 mm in size. In typical mineralized granite-gneiss, garnet ranges from 1 to 5 vol% of the rock (Fig. 16). Preliminary quantitative SEM analyses of representative garnets (Appendix 9) show that their chemistry ranges between 72-80 mol% almandine, 10-20 mol% spessartine, 3-6 mol% pyrope and 2-4 mol% grossular. Garnet commonly includes small biotite flakes (Fig. 15C), is generally more abundant in intervals with increased biotite content (Figs. 14A, 16), and overgrows S_1-aligned igneous biotite (Figs. 11C, 11F, 13C). At least some garnet at Dasher has overgrown chlorite, as indicated by a rare texture where clusters of garnet overgrow large chloritized biotite grains (Fig. 15D). This chlorite is unlike the fine retrograde form.

The sillimanite content of this assemblage ranges from trace to 15 vol%. Most of the Dasher granite-gneiss contains fine sillimanite, and trace sillimanite was also observed in the granite dikes (Fig. 12B). Where in trace amounts, sillimanite generally occurs as fine prisms within, or on the margins of, quartz and feldspar grains (Fig. 12A). Discrete intervals (<10 m true width) of pale cream, sillimanite-rich (to 15 vol%) granite-gneiss are developed around well mineralized intervals (~0.5% wt% Cu), but are themselves not well mineralized. Sillimanite in these zones occurs as fibrolitic pseudomorphs of ex-biotite (Figs. 12A, 15A, 15C), and the rock is also abnormally low in plagioclase (<5 vol%). Sillimanite does occur together with garnet, but in the sillimanite-rich granite-gneiss, garnet is volumetrically minor (<2 vol%). Where both minerals are present, garnet commonly includes fine prismatic sillimanite (Fig. 15C).

Disseminated magnetite occurs throughout the mineralized granite-gneiss at Dasher, with a distribution similar to that of garnet, biotite and sulfide mineralization. The occurrence of magnetite in this assemblage, in textural equilibrium with chalcopyrite-pyrrhotite, and in magnetite-rich V4 veins (Fig. 14D), suggests that magnetite is part of the mineralization-related hydrothermal alteration system. Individual magnetite grains are anhedral to weakly octahedral, and have resorbed margins in places. Significant Ti content in the magnetite is indicated by the common exsolution of ilmenite lamellae.

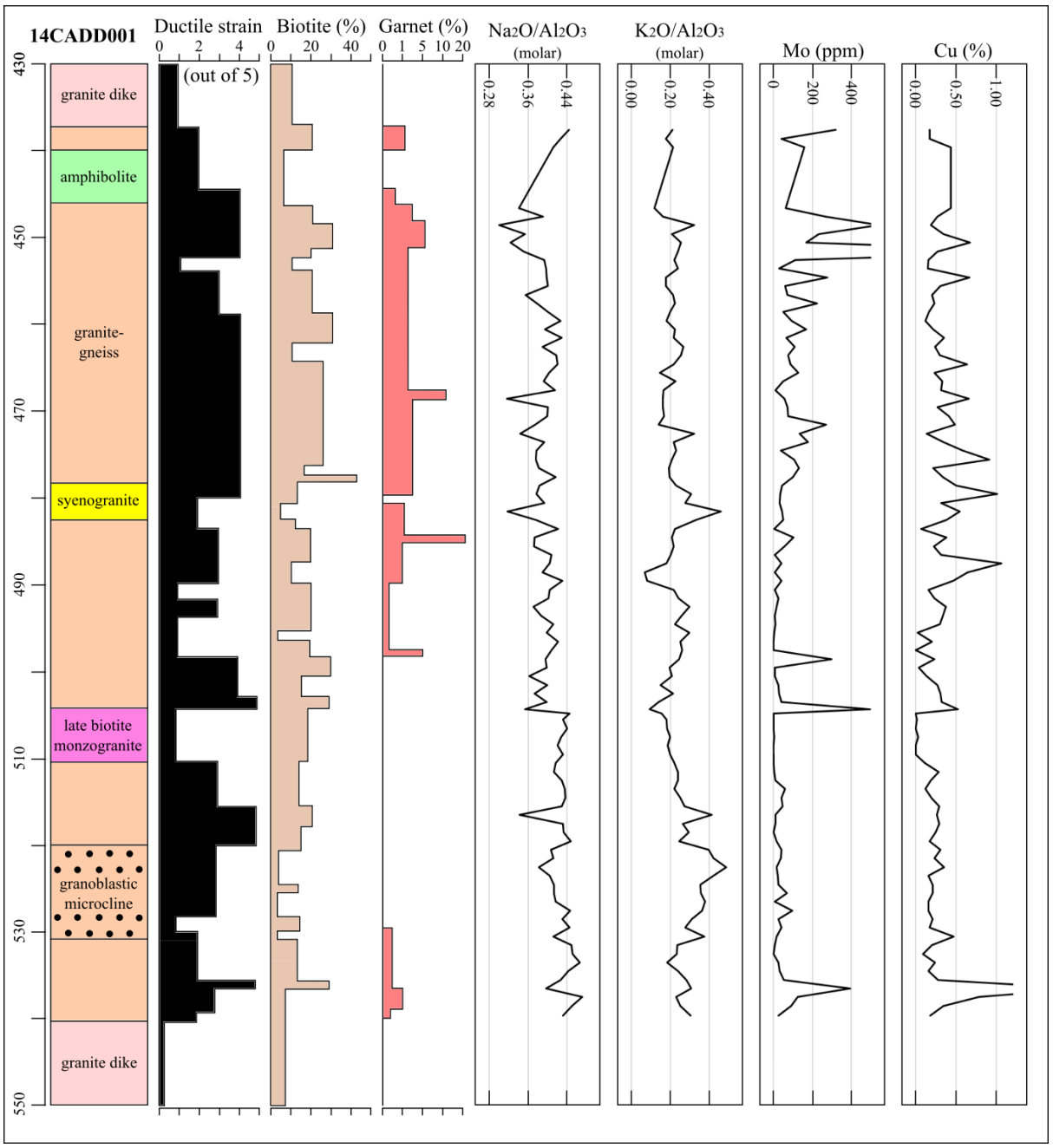

Fig. 16. Graphic log of the granite-gneiss interval of 14CADD001. See Fig. 5 for drill hole location. Ductile strain, garnet abundance, biotite abundance and Na depletion correlate with higher-grade Cu and Mo. Granoblastic microcline zone correlates with K enrichment. Visual logging from this study (Appendix 13). Geochemistry from Caravel Minerals Ltd four-acid digest dataset (Appendix 8).

Granoblastic quartz-microcline-plagioclase-sillimanite alteration: This hydrothermal alteration assemblage was only observed in a low-grade (~0.1 to 0.2% Cu) interval of 14CADD001 (Figs. 15E, 16). The assemblage is expressed as a distinctive 'whitening' of the granite-gneiss, characterized by the absence of garnet and magnetite, and a low biotite content (2-5 vol%). Metamorphic recrystallization of the assemblage is indicated by the ubiquitous polygonal granoblastic texture of quartz and feldspar (Fig. 15F). Microcline makes up 50-90%

of the feldspar component, and the plagioclase is distinctly more sodic (<An20) than plagioclase in least-altered granite-gneiss (~An25-30). Albitic rims on microcline grains suggest that an albite component exsolved out of the microcline, possibly during recrystallization. Sillimanite in this assemblage (<1 vol%) is restricted to fine prisms within, or on the margins of, quartz and feldspar grains.

In 14CADD001, V3-style quartz-chalcopyrite-pyrrhotite stockwork veins within the quartz-microcline-plagioclase-sillimanite assemblage have muscovite grains to 4 mm in their selvedges (Fig. 15E). Optically-continuous grains of this coarse muscovite are partly replaced by quartz-microcline. This form of muscovite was only observed within this assemblage, and is dissimilar in style and timing to the fine-grained retrograde sericitization.

Retrograde hydrothermal alteration and remobilization: The Dasher mineralization is affected by greenschist facies retrograde metamorphism, but is not significantly modified. The most widespread effect is the localization of silicate retrogression adjacent to sulfides, resulting in mm-scale, light green chlorite-sericite haloes around mineralized veins (Fig. 14A) and individual sulfide grains. Retrograde remobilization of sulfide mineralization, with associated chlorite-sericite-epidote ± calcite hydrothermal alteration, has occurred in rare sulfide-rich stringers and breccia zones. The sulfide assemblage in these settings in chalcopyrite-pyrite, with pyrrhotite minor to absent. Remobilized sulfide is a negligible component of the Dasher mineralization.

Interpretation of metamorphosed hydrothermal alteration assemblages

It is difficult to conclusively determine the pre-peak metamorphic hydrothermal alteration assemblages in metamorphosed ore deposits (e.g., Corriveau and Spry, 2014), but textural and geochemical evidence at Dasher allows some of the characteristics of the hydrothermal alteration to be revealed. The garnet- and/or sillimanite-bearing assemblages at Dasher are its most striking proximal mineralogical expression. This association between aluminous metamorphic minerals and mineralization (Fig. 16) suggests that syn-mineralization hydrothermal alteration produced a granite-gneiss composition that was Al-rich, relative to least altered variants. Peraluminous, aluminosilicate-bearing rocks are known to result from the metamorphism of phyllic and argillic hydrothermal alteration assemblages (Corriveau and Spry, 2014).

Molar ratios of Na_2O/Al_2O_3 and K_2O/Al_2O_3 in the Dasher granite-gneiss confirm that relative Al enrichment (Na depletion) is associated with rocks affected by the biotite-garnet-sillimanite-magnetite assemblage (Figs. 16, 17; Appendices 7, 8). Sillimanite-rich granite-

gneiss samples have the lowest Na_2O/Al_2O_3 ratios (Fig. 17), suggesting they are the most altered end-members of this Na-depleted assemblage. Calcium is also depleted in these samples: $CaO+Na_2O$ in the sillimanite-rich granite-gneiss samples ranges from 0.60 to 2.24 wt%, significantly lower than the 4.95 to 6.50 wt% range in least altered granite-gneiss samples (Appendix 7). Together with petrographic observations of abnormally low plagioclase content in the sillimanite-rich granite-gneiss, the Na and Ca depletion is strong evidence that the syn-mineralization hydrothermal alteration was plagioclase destructive. The petrographic observation that microcline remains in the sillimanite-rich granite-gneiss, is supported by K_2O/Al_2O_3 molar ratios that are similar to those in the least altered pre-cursor granite-gneiss (Fig. 17).

In addition to likely plagioclase destruction, sillimanite abundance in the biotite-garnet-sillimanite-magnetite assemblage is also linked to biotite destruction, as evidenced by the low biotite content in sillimanite-rich granite-gneiss, and the fibrolitic sillimanite pseudomorphs after biotite (Figs 12A, 15A). A common link between plagioclase and biotite destruction, and Na and Ca removal, is that all can be caused by muscovite/sericite-producing hydrothermal alteration reactions involving acidic fluids (Jacobs and Parry, 1979; Guilbert and Park, 2007):

$$(1)\quad \text{Albite} + H^+ + K^+ \rightarrow \text{Muscovite} + Na^+ + SiO_2$$

and

$$(2)\quad \text{Phlogopite/Annite} + H^+ \rightarrow \text{Muscovite} + K^+ + Mg^{2+}/Fe^{2+} + H_4SiO_4$$

In Figure 17, the most sillimanite-rich granite-gneiss examples trend towards the muscovite mineral node, suggesting they have a geochemical composition where the presence of sericite would be permissible in a lower temperature assemblage. Sericitization of plagioclase and biotite during syn-mineralization hydrothermal mineralization would enable the production of sillimanite during subsequent peak metamorphism, via the "second sillimanite isograd" reaction (Fig. 18; Spear, 1995):

$$(3)\quad \text{Muscovite (ss)} + \text{Albite (ss)} + \text{Quartz} \rightarrow \text{Sillimanite} + \text{K-feldspar(ss)} + H_2O$$

(ss = solid-solution)

This reaction is consistent with the abnormally low plagioclase content (consumed) and abundant microcline (produced) observed in the most sillimanite-rich granite-gneiss. The formation of sillimanite directly from such a reaction, inside the sillimanite stability field (Fig.

18), is suggested by the absence of andalusite and kyanite at Dasher, either as preserved metamorphic phases or as pseudomorphed pre-cursors to the sillimanite.

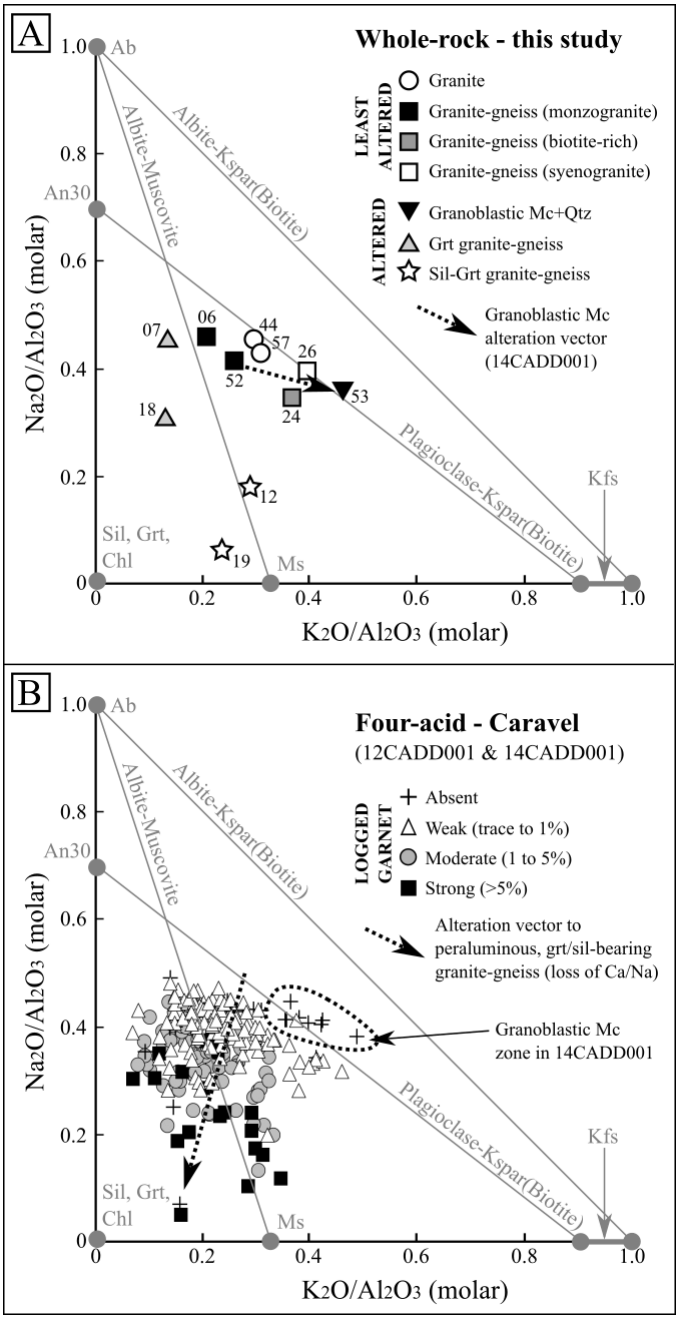

Fig. 17. Molar ratios of Na_2O/Al_2O_3 and K_2O/Al_2O_3 from the Dasher granite-gneiss, on diagrams modified from Davies and Whitehead (2010). Lower Na_2O/Al_2O_3 molar ratios relate to increase intensity of the biotite-garnet-sillimanite-magnetite assemblage, with sillimanite-rich samples having the lowest values. Higher K_2O/Al_2O_3 molar ratios relate to the granoblastic quartz-microcline-plagioclase-sillimanite assemblage. (A) Whole-rock geochemical data (Appendix 7) from least altered and altered samples from this study. (B) Four-acid digest geochemical data (Appendix 8) from the granite-gneiss intervals of 12CADD001 and 14CADD001, with symbols indicating the logged abundance of garnet in the corresponding interval.

The biotite-garnet assemblage observed proximal to V2 sulfide stringers, and in garnet-biotite-rich V4 veins may result from metamorphism of a lower temperature, sericite-chlorite hydrothermal alteration assemblage, via a reaction such as (Blatt et al., 2006):

(4) Chlorite + Muscovite + Quartz → Mg-richer Chlorite + Garnet + Biotite + H_2O

This reaction would proceed until all chlorite is consumed (Blatt et al., 2006). Some pre-peak metamorphic chloritization is suggested by evidence of garnet overgrowing chloritized biotite (Fig. 15D). This may have occurred via a reaction such as (Spear, 1995):

(5) Chlorite + Quartz → Almandine + H_2O

The biotite-garnet-sillimanite-magnetite assemblage, in summary, represents metamorphosed plagioclase-destructive hydrothermal alteration, which may have included sericite (now sillimanite-microcline-rich) and sericite-chlorite (now biotite-garnet-rich) zones. Some of the mineralization-related biotite may also have been an original component of the hydrothermal alteration phase.

Geochemical and petrographic evidence suggests that the granoblastic quartz-microcline-plagioclase-sillimanite assemblage represents a distinct precursor hydrothermal alteration style to the biotite-garnet-sillimanite-magnetite assemblage. On Figure 17, the K_2O/Al_2O_3 molar ratio of this assemblage is higher than in the least altered granite-gneiss, supporting the petrographic observation of abundant microcline (Figs. 15E, 15F). The Na_2O/Al_2O_3 molar ratio remains unchanged from least altered granite-gneiss, suggesting that removal of Na (breakdown of plagioclase) is negligible, and Al-rich bulk compositions have not been produced. This is supported by the trace sillimanite content, absence of garnet, and retention of plagioclase in thin-section. The low biotite content of the granoblastic quartz-microcline-plagioclase-sillimanite assemblage, and the absence of other Fe-bearing (e.g. magnetite) or Mg-bearing minerals, suggests at least localized removal of Fe and Mg. This is supported by whole-rock geochemistry: a sample of this hydrothermal alteration style (CAL053) contained 5.97 wt% K_2O, 0.69 wt% Fe_2O_3, 0.1 wt% MgO, while its adjacent least-altered pre-cursor (CAL052) contained 3.52 wt% K_2O, 3.93 wt% Fe_2O_3 and 0.79 wt% MgO (Appendix 7).

Microcline-rich, granoblastic rocks associated with mineralization at the Hemlo (e.g. Tompkins et al., 2004) and Big Bell (e.g. Phillips and Powell, 2009) Au deposits, are interpreted to be potassic alteration zones, recrystallized during post-mineralization peak metamorphism.

The characteristics of the granoblastic quartz-microcline-plagioclase-sillimanite assemblage at Calingiri suggest a similar origin. Much of the microcline may be hydrothermal K-feldspar alteration that has recrystallized during peak metamorphism, however trace sillimanite in this assemblage suggests that some microcline may have formed by reaction (3) or by (Spear, 1995):

(6) Muscovite + Quartz → K-feldspar + Sillimanite + H_2O

Muscovite observed in V3 stockwork vein selvedges in the granoblastic quartz-microcline-plagioclase-sillimanite assemblage (Fig. 15E) may be a remnant of earlier hydrothermal sericite alteration. The V1 granoblastic quartz-microcline-plagioclase-sillimanite veins (Figs. 11C, 13D) were also possibly quartz-sericite features, metamorphosed to their current form via reactions (3) or (6).

Evidence of partial melting within and around the Dasher deposit (e.g. leucosomes, V5 pegmatoidal veins) suggests that peak P-T was above the "wet granite melting" curve (Fig. 18), which is represented by the reaction (Spear, 1995):

(7) Albite (ss) + K-feldspar (ss) + Quartz + H_2O → Liquid
(ss = solid-solution)

At P-T conditions above this curve, the breakdown of pre-cursor hydrous alteration phases via dehydration reactions (e.g. reactions 3 to 6; Fig. 18), would have resulted in the direct production of melt, rather than H_2O (dehydration melting; Spear, 1995). Any H_2O produced by dehydration reactions below this curve (Fig. 18) may have been retained in the system, and could later have enabled partial melting as P-T conditions increased (e.g. reaction 7). It is not clear which path, or combination of paths, produced partial melt features at Dasher.

In combination, the sillimanite-microcline-producing reaction (3) and the partial melting reaction (7), suggest a minimum temperature of ~660°C for peak metamorphism at Dasher (Fig. 18). A maximum temperature of ~800°C is suggested by the stability of biotite in the granite-gneiss, and the lack of metamorphic pyroxene in the mafic ortho-amphibolites (Fig. 18; Spear, 1995). The upper pressure limit of peak metamorphism can only currently be constrained to less than ~10 kbar, by the upper pressure limit of sillimanite stability within than temperature range.

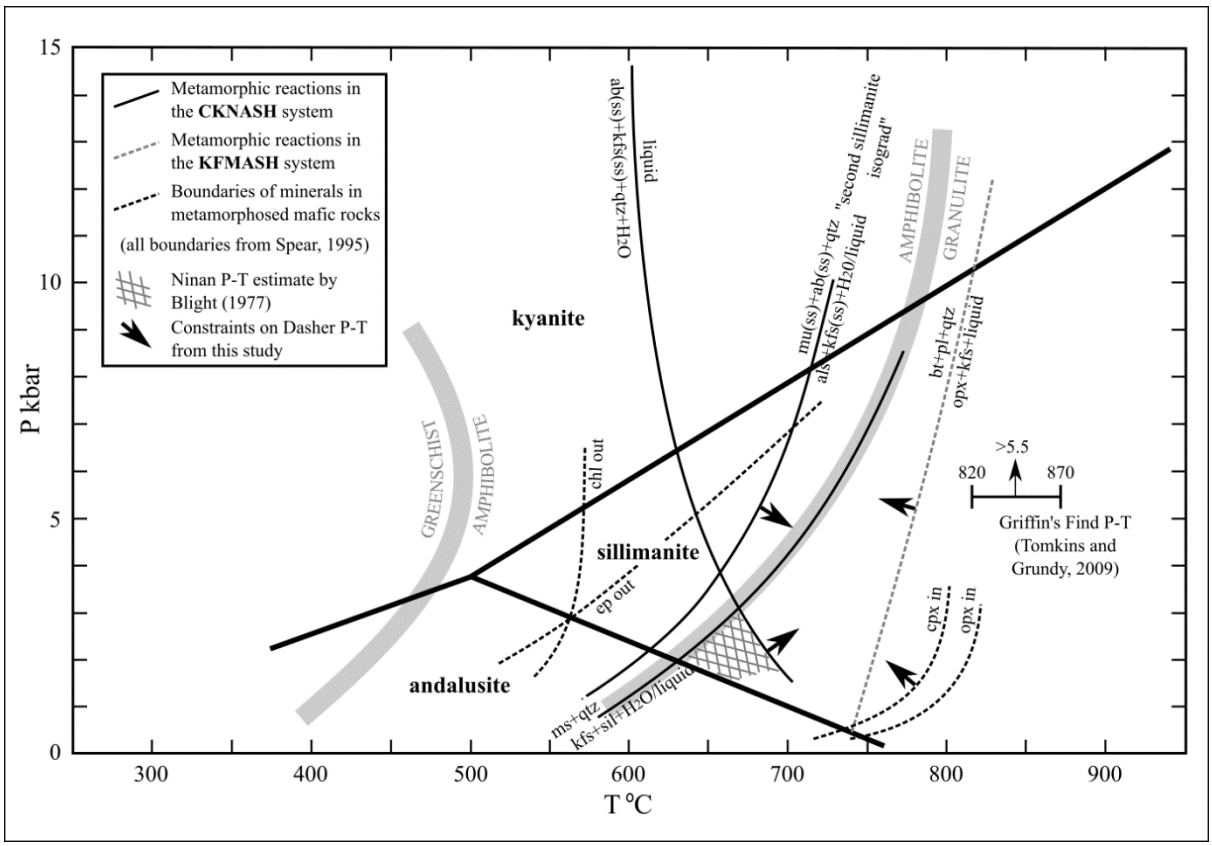

Fig. 18. P-T diagram showing metamorphic boundaries (discussed in text) used to infer peak metamorphic temperatures at Dasher of between 660° and 800°C. Existing P-T estimates for peak metamorphism at Ninan and Griffin's Find are shown for comparison. All references indicated on the diagram.

Other Mineralization in the Calingiri District

Characteristics of the Bindi West and Ninan deposits (Fig. 3) are compared to Dasher in Table 3. There are currently no diamond drill holes into Bindi East or Opie, but at both deposits mineralization is hosted in garnet-bearing granite-gneiss that is visually comparable to the Dasher granite-gneiss (Caravel Minerals Ltd, 2016). The Bindi East mineralization is sub-horizontal, while the Opie mineralization dips ~40° to the north, sub-parallel to S_1 in nearby outcrops.

The Bindi West mineralization is hosted in granite-gneiss (*sensu lato*; Fig. 19A), and is analogous to Dasher in terms of mineralization style and the relative timing of intrusive, structural, metamorphic and mineralization events. The most striking visual difference at Bindi West is the more intense overprint by retrograde chlorite-sericite ± epidote ± carbonate hydrothermal alteration, and associated dominance of pyrite over pyrrhotite as the Fe-sulfide species. The most pervasive retrogression is focused around a ~30 m wide tectonic breccia and vein zone that marks the hangingwall contact of mineralization (Fig. 19B). As observed at Dasher, peak metamorphic sillimanite has grown in the S_2 orientations (Figs. 19C, 20A), which

is axial planar to F_2 folds of S_1 and mineralized veins. The west- to northwest-plunging F_2 folds have Z asymmetry (Figs. 19D, 20B) and northeast vergence, consistent with Bindi West lying on the western limb of the F_2 Bindi antiform (Fig. 3).

The Ninan deposit is dominantly hosted in dacitic (~66% SiO_2) and andesitic (~59% SiO_2) volcanic and volcaniclastic rocks (Fig. 21A). Micro-structures (S-C fabrics, σ-type deformed phenocrysts) show consistent top-to-northwest kinematics on the S_1 foliation, which is associated with a pervasive L_1 lineation, defined by stretching of quartz and feldspar phenocrysts (Figs. 21B, 22A, 22B). North-plunging, east-verging F_2 folds of S_1 and lithological layering (Fig. 21C) are consistent with Ninan lying on the western limb of the kilometer-scale, second generation antiform interpreted by Lipple (1982). Microcline-quartz-biotite-sillimanite-garnet-andalusite schists (Fig. 21D) that were interpreted as meta-sedimentary rocks by Blight (1977), are interpreted to be metamorphosed shear zones in this study, based on their gradational contacts into low strain dacitic volcanic rocks. Post-D_1 peak metamorphism is indicated by the growth of fibrolitic sillimanite and large (>30 mm) microcline porphyroblasts, over S_1-aligned biotite and ex-staurolite (Fig. 21D). An earlier metamorphic event is suggested by garnet grains that are wrapped by the S_1 foliation and/or display multiple growth phases.

Mineralization at Ninan has geometric (tabular, 30-150 m thick), geochemical (Ag-Au association) and mineralogical (garnet-sillimanite-biotite-magnetite) similarities to the granite-gneiss-hosted mineralization (Table 3). A comparable syn- to post-D_1 timing is suggested by weakly mineralized veins deformed in F_1 folds, and main stage actinolite/grunerite-quartz-magnetite-sulfide veins that run parallel to, or cross-cut, S_1 (Fig. 21A). Blight (1977) interpreted grunerite in Ninan samples to be of meta-ultramafic origin, but its association with mineralized veins suggest that it is likely metamorphosed hydrothermal alteration (Fig. 21E).

The Ninan host sequence is intruded by numerous 5-300 cm, plagioclase-phyric, granitoid dikes (Fig. 21F). These are referred to here as the Ninan monzogranite, based on a modal mineralogy of quartz (40 vol%), plagioclase (35 vol%), K-feldspar (20 vol%) and biotite (5 vol%), with accessory zircon. There is trace garnet in some dikes, and plagioclase phenocrysts are zoned from Ca-rich cores to Na-rich rims. The dikes contain abundant xenoliths of foliated and lineated greenstone, constraining them to a post-D_1 age. A body of visually similar biotite monzogranite is exposed in a ~500 x 500 m outcrop centred 1800 m south-southwest of Ninan.

Table 3. Summary of characteristics of the Dasher, Bindi West and Ninan mineralization.

	Dasher	Bindi West	Ninan
Resource (Caravel Minerals Ltd, 2016)	137Mt at 0.30% Cu, 72 ppm Mo, 1.70 g/t Ag, 0.019 ppm Au (0.15% Cu cutoff)	(Bindi total) 317Mt at 0.26% Cu, 49 ppm Mo, 1.14 g/t Ag, 0.018 ppm Au (0.15% Cu cutoff)	Unpublished 2006 oxide Cu resource of 1.27 Mt @ 0.83% Cu (0.25% Cu cutoff)
Data sources	3 x DDH, patchy outcrop	1 x DDH	2 x DDH, patchy outcrop
Host lithologies and geochronology	Granite-gneiss after High-Ca biotite monzogranite and syenogranite (3010 ± 4 Ma, SHRIMP U-Pb zircon)	Granite-gneiss after High-Ca biotite monzogranite	Schistose volcanic and volcaniclastic rocks of dacite to andesite composition
Other lithologies and geochronology	Old mafic ortho-amphbolite; younger granite (2673 ± 5 Ma, SHRIMP U-Pb zircon), pegmatite and Proterozoic dolerite dikes	Old mafic ortho-amphbolite; younger granite, pegmatite and Proterozoic dolerite dikes	Old BIF, mafic ortho-amphibolite and quartz-feldspar-phyric dacitic sills; younger biotite monzogranite (2670 ± 7 Ma, SHRIMP U-Pb zircon) and pegmatite dikes
Structural geometries (dip/dip direction and plunge→trend format)	S1 foliation 65°/061°; L1 stretching absent; S2 foliation 66°/265°; W-verging F2 folds 13°→341°; crenulation ~30°/090°	S1 foliation 36°/309°; L1 stretching absent; S2 foliation 30°/281°; NE-verging F2 asymmetric Z folds 36°→303°	S1 foliation 40°/305° (top to NW); L1 stretching lineation 36°→313°; S2 foliation steep, ~N-striking; E-verging F2 asymmetric Z folds gently ~N-plunging
Metamorphic indicator minerals	Garnet, sillimanite	Garnet, sillimanite	Garnet, sillimanite, andalusite, staurolite
Timing constraints on metamorphism	Possible ~syn-D1 event, peak event syn- to post-D2 (sillimanite in S2 orientation); sillimanite and garnet in granite dikes indicate peak at, or after, ca. 2673 Ma	Possible ~syn-D1 event, peak event syn- to post-D2 (sillimanite in S2 orientation)	Pre- to syn-D1 event (garnet wrapped by S1), post-D1 peak event (sillimanite and metamorphic microcline overgrow S1)
Mineralization geometry	Tabular, ~50°/090° orientation preserved between granite dike, likely S1-parallel internally	Tabular, ~36°/309° (S1-parallel), possibly truncated by late hangingwall fault	Tabular, ~40°/305° (S1-parallel)
Mineralization-related sulfide-oxide assemblage	Chalcopyrite-pyrrhotite-magnetite±molybdenite±pyrite (pyrrhotite dominant Fe-sulfide)	Chalcopyrite-pyrite-magnetite±pyrrhotite±molybdenite (pyrite dominant Fe-sulfide)	Chalcopyrite-pyrrhotite-magnetite±pyrite (no appreciable molybdenite)
Mineralized veins and geochronology	Syn-D1 Mo-dominant quartz-feldspar-sulfide veins; post-D1 Cu-dominant quartz-sulfide-magnetite stockwork veins, quartz-magnetite-garnet-biotite-sulfide veins, stringer and disseminated sulfide; quartz-feldpsar-sulfide±garnet pegmatoidal leucosomes	Quartz-feldspar-chalcopyrite-pyrite±pyrrhotite±molybdenite veins (leucosomes?), stringer and disseminated sulfide	Syn-D1 quartz-hornblende/acitnolite-sulfide (weak); post-D1 quartz-actinolite/grunerite-magnetite-sulfide veins, with biotite-garnet selvedges

Table 3. (continued)

	Dasher	Bindi West	Ninan
Mineralization-related hydrothermal alteration assemblages	Biotite-garnet-sillimanite-magnetite; quartz-microcline-plagioclase-sillimanite	Biotite-garnet-sillimanite-magnetite	Biotite-garnet-sillimanite-magnetite
Mineralization timing and geochronology	Syn- to post-D1, Mo-rich vein folded D1 dated at 2977 ± 20 Ma (Re-Os on molybednite); folded in D2 (pre-peak metamorphism)	Folded in D2 (pre-peak metamorphism)	Syn- to post-D1; folded in D2
Greenschist retrogression	Patchy, weak; moderate around late brittle structures	Pervasive, moderate; intense around late brittle structures	Patchy, weak

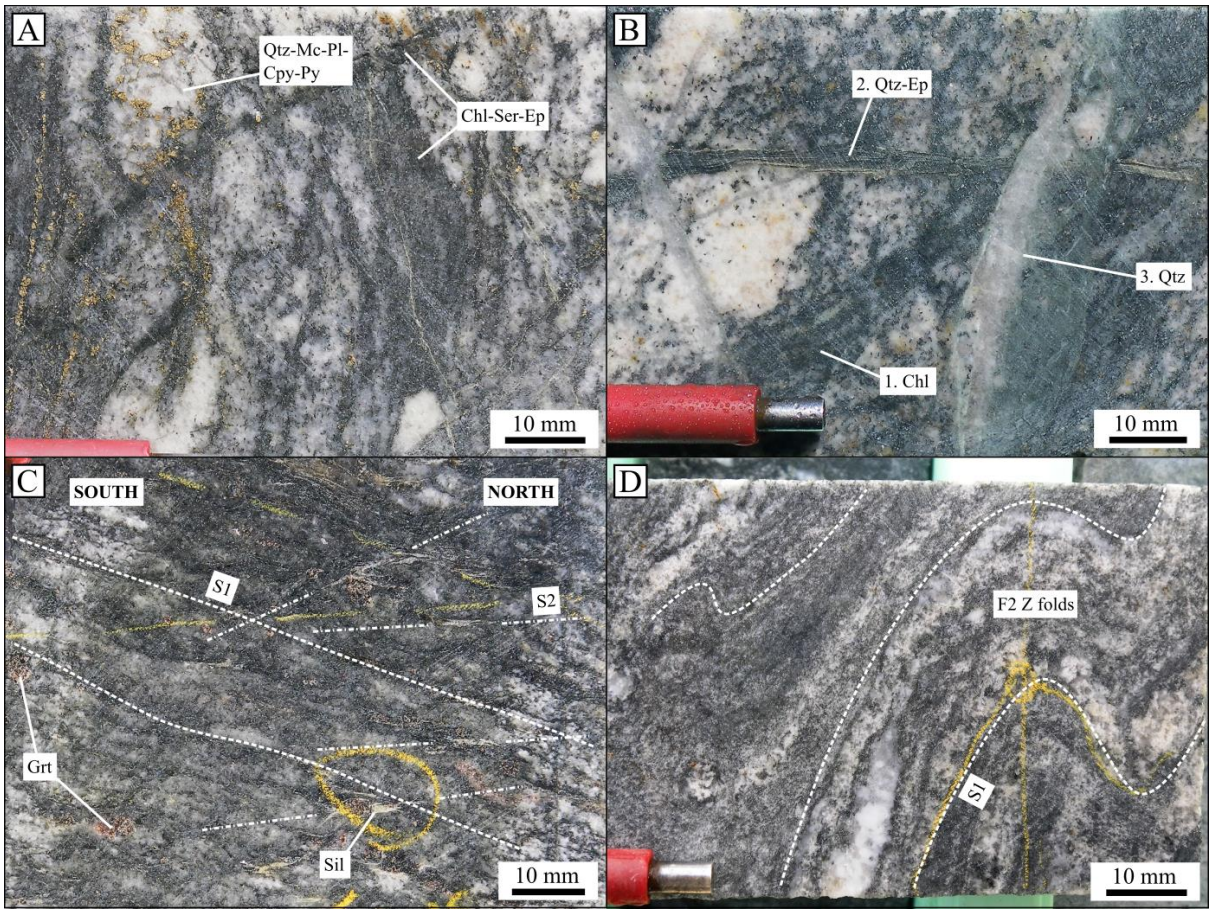

Fig. 19. Bindi West features. (A) Pegmatoidal mineralized vein in granite-gneiss, with near-complete retrogression of biotite. 14CADD002, 123.9 m. (B) Three phases of brecciation, as numbered, associated with the hangingwall fault. Strong retrograde hydrothermal alteration has left no biotite in this granite-gneiss. 14CADD002, 118.0 m. (C) View down to the west of sillimanite masses aligned in the S_1 and S_2 orientations, in granite-gneiss. The vergence is consistent with the observed Z asymmetry of F_2 folds. 14CADD002, 168.7 m. (D) Asymmetric F_2 Z folds of S_{BAN} and S_1 in typical Bindi West granite-gneiss. 14CADD002, 212.0 m.

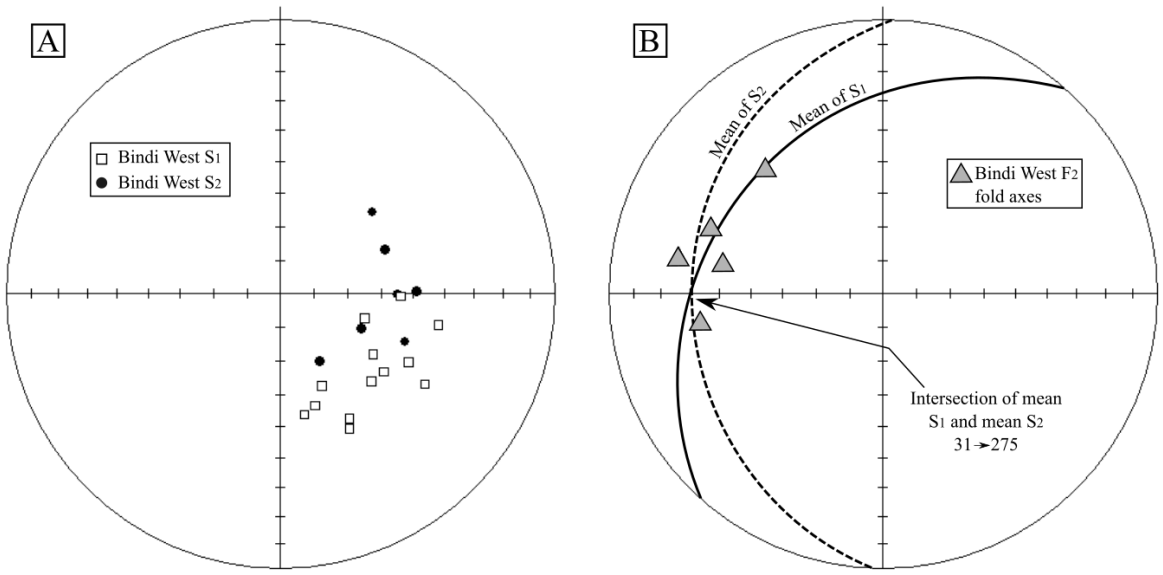

Fig. 20. Stereonets of D_1 and D_2 features at Bindi West, from drill core. (A) Poles to S_1 and S_2, showing the similar dip but more northerly strike of the sillimanite-defined S_2. (B) Measured F_2 fold axes plunge gently west to northwest, similar to the intersection of mean S_1 and S_2 from Fig. 20A.

Geochronology

SHRIMP U-Pb geochronology was completed on zircon separates from a 3 m wide, xenolith-rich Ninan monzogranite dike in 08WHDDH001 (Fig. 21F; sample CAL038, GSWA ID 205933). Unpublished data and interpretations by Wingate and Lu (2016) are in Appendix 10. The interpreted igneous zircons have elongate and subhedral-euhedral morphology, concentrically zonation, and an average $^{232}Th/^{238}U$ ratio of 0.58, which is consistent with them being of igneous origin (Hoskin and Schaltegger, 2003). Nine analyses of zircons from CAL038 yield a weighted mean 207Pb/206Pb age of 2670 ± 7 Ma (MWSD = 1.8), which is interpreted to represent the magmatic crystallization age of the monzogranite (Fig. 8). Twenty analyses of interpreted older zircon cores yielded inherited ages ranging from 3219-2785 Ma, including significant groups at ~3012 Ma and ~2977 Ma. The ~3012 Ma group is comparable to the age of the Dasher granite-gneiss (this study) and the minimum age of the Wongan Hills greenstone belt (Pidgeon et al., 1990). The dated dike contains isolated blebs of chalcopyrite-pyrite (Fig. 21F), some of which is observed as fine inclusions in the Na-rich rims of plagioclase phenocrysts. This mineralization is interpreted to have been entrained in the dike during its intrusion into the mineralized host sequence.

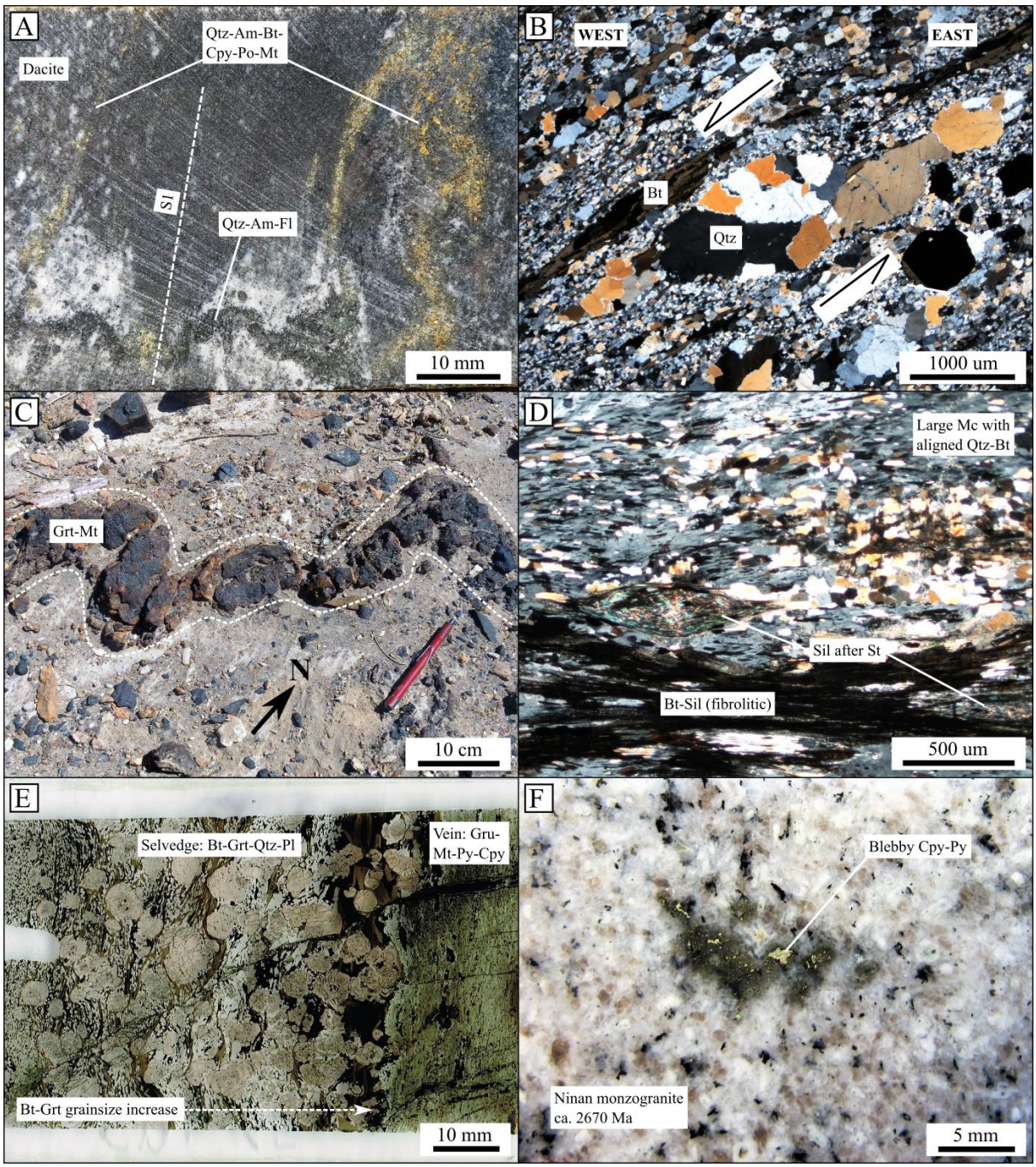

Fig. 21. Ninan features. (A) Typical feldspar-phyric dacitic volcanic rock. An early quartz-feldspar-amphibole vein with a silica-feldspar selvedge is deformed in S_1, and then cut by S_1-parallel sulfide-rich veinlets. 08WHDDH001, 179.1 m. (B) Photomicrograph (cross-polarized) looking north at a porphyritic dacitic intrusion strongly affected by D_1 deformation. Top-to-west kinematics indicated by the asymmetry of a σ-type recrystallized quartz phenocryst. Sample CAL032. (C) East-verging F_2 fold train affecting a mineralization-related garnet-magnetite band in outcrop. 6578819N 465876E. (D) Photomicrograph (cross-polarized) of a large metamorphic microcline that has overgrown S_1-aligned biotite and quartz, and contains abundant fine sillimanite. Sillimanite also occurs as fibrolitic pseudomorphs of former staurolite and foliation-parallel biotite streaks. Sample CAL066. (E) Thin-section scan showing a garnet-biotite selvedge adjacent to a grunerite-magnetite-pyrite-chalcopyrite vein. The grainsize and proportion of biotite in the selvedge increases with proximity to the vein. Sample CAL065. (F)

Dated Ninan monzogranite sample, with entrained sulfide mineralization that localizes greenish chlorite-sericite retrogression. Sample CAL038.

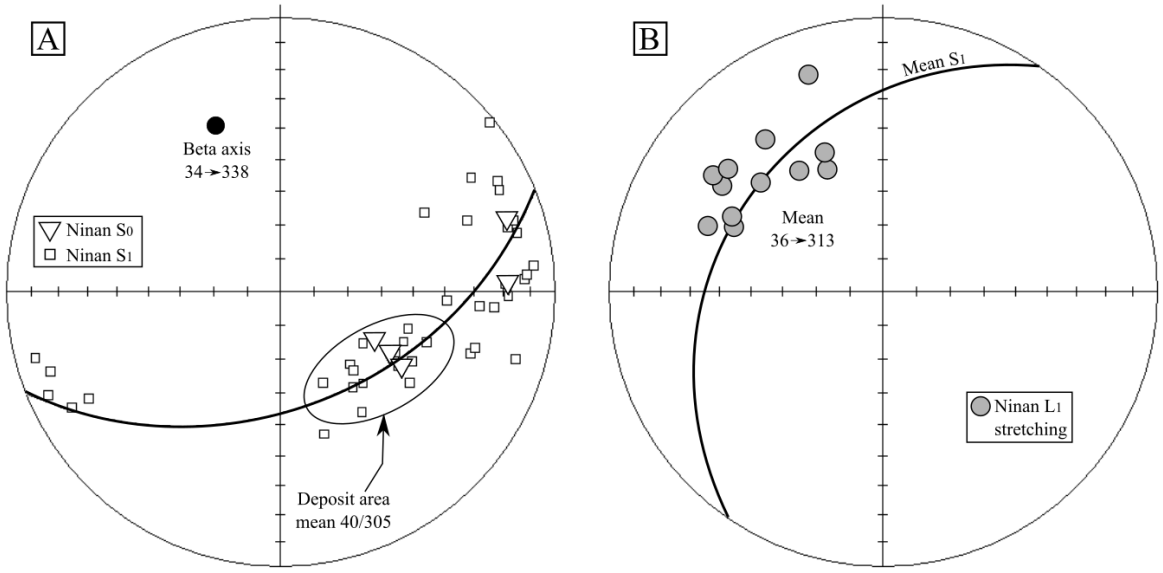

Fig. 22. Stereonets of D_1 features at Ninan, form drill core and outcrop. (A) Poles to S_0 and S_1, showing a fold-related distribution. The pole to the best fit girdle (beta-axis) approximates the plunge of the folds responsible, likely F2. (B) L_1 stretching measurements, in relation to mean S_1 in the deposit area, from Fig. 22A.

Geochemistry of Calingiri Granitoids

The dominant monzogranite to granodiorite (modal mineralogy) component of the granite-gneiss at Dasher and Bindi West ranges from ~67 to 71 wt% SiO_2, while the Dasher syenogranite component contains ~74 wt% SiO_2 (Fig. 23; Appendix 7). All analyzed components of the granite-gneiss show geochemical similarities to the Eastern Goldfields Province High-Ca granite group of Cassidy et al. (2002) (Fig. 23). The ca. 2673 Ma Dasher granite dikes and ca. 2670 Ma Ninan monzogranite dikes contain ~72 wt% SiO_2, and tend towards the high Th and Zr limits of the High-Ca granite group (Fig. 23; Appendix 7). The younger granitoids display a -ve Eu anomaly and flat HREE profile on a chondrite-normalized REE diagram, in contrast to the fractionated LREE to HREE profile of the granite-gneiss (Fig. 24; Appendix 7).

The High-Ca granites in the Yilgarn Craton are interpreted to have from high pressure (>10 kbar) melting of a mostly mafic source, either deep in thickened crust (35-50 km), or from a subducted slab (Cassidy et al., 2002). The higher Th and Zr contents and REE chemistry of the younger granitoids is more consistent with moderate pressure (<10 kbar) melting in a crustal environment (Champion and Sheraton, 1997). This origin for the younger granitoids is consistent with their significant xenocrystic zircon populations (Fig. 8).

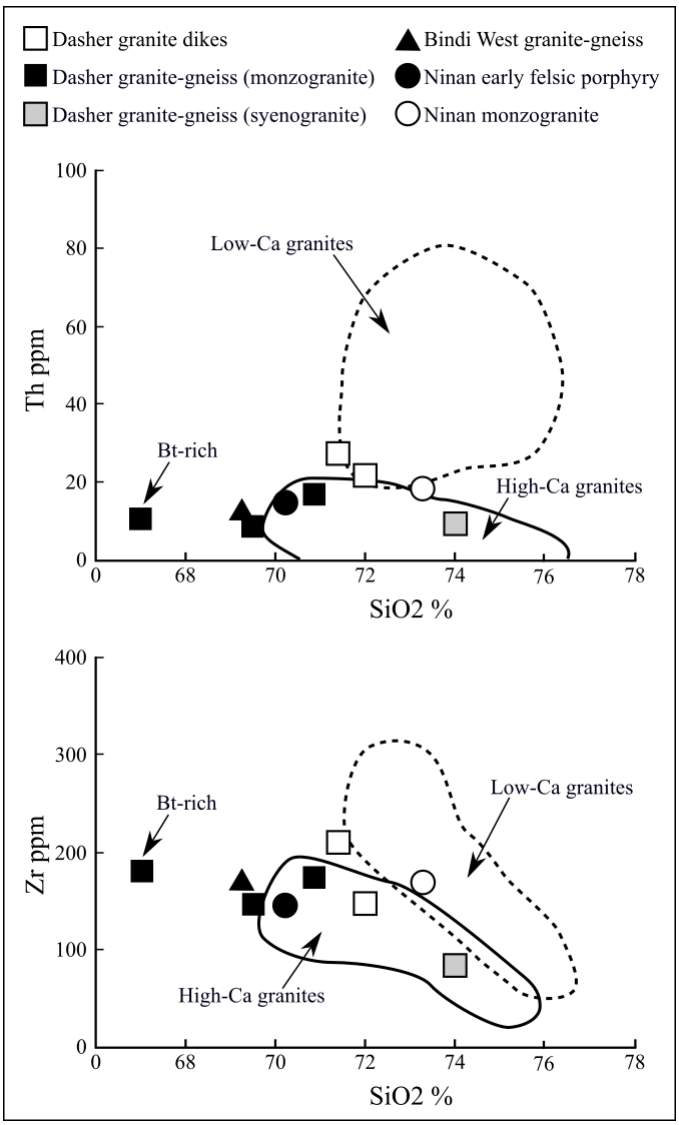

Fig. 23. Geochemistry of Calingiri granitoid lithologies (Appendix 7) in relation to the High-Ca and Low-Ca granite groups from the Eastern Goldfields Province. Outlines are from data in Cassidy et al. (2002).

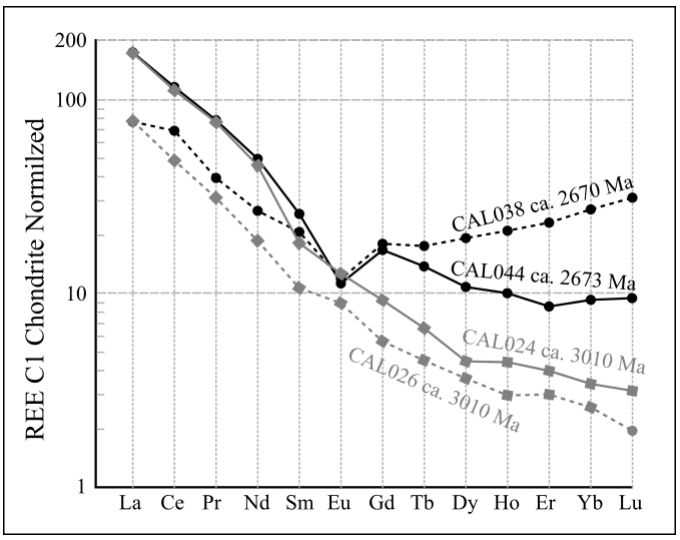

Fig. 24. Chondrite-normalized REE spider diagram of Calingiri granitoids with SHRIMP U-Pb zircon analyses (Appendix 7). The younger granitoids are distinguished by -ve Eu anomalies and enrichment in HREE, relative to the older granite-gneiss samples. Normalization values from Sun and McDonough (1989).

Preliminary Descriptive Model for the Calingiri Cu-Mo-Ag Mineralization

A model for the geological evolution of the Calingiri district is proposed below and summarized in Figure 25, based on the findings of this study, and previous work in the region.

At ca. 3010 Ma (SHRIMP U-Pb zircon; Fig. 8), the Wongan Hills greenstone belt and southern greenstone belt were intruded by multiple pulses of High-Ca monzogranite to syenogranite, which formed a banded, sill-like intrusion of >3 kilometers true thickness (Fig. 25A). The intrusion was synchronous with the onset of D_1 deformation, characterized by the formation of ~layer-parallel foliation (S_1), a stretching lineation (L_1), and isoclinal folds (F_1) (Fig. 25B). The S_1 foliation formed gneissic high-strain domains in the High-Ca intrusion, creating the observed granite-gneiss. An early metamorphic event may have occurred during D_1.

Mineralization in the granite-gneiss-hosted deposits commenced during D_1, favouring a district-scale D_1 high-strain zone developed around the contact of the granite-gneiss with the southern greenstone belt (Fig. 25B). Early Mo-dominant quartz-feldspar veins (V1) within this mineralization corridor were emplaced at ca. 2997-2957 Ma (Re-Os molybdenite; Appendix 11), and progressed to Cu-dominant V1 veins during D_1. The main stage of Cu mineralization was late- to post-D_1 (Fig. 25C), and comprised sulfide stringer (V2), quartz-sulfide stockwork (V3) and garnet-biotite-magnetite-sulfide veins (V4; unlikely the original mineralogy). Mineralization was accompanied by widespread hydrothermal destruction of plagioclase, and related removal of Na and Ca, to create Al-rich to peraluminous bulk rock compositions (Fig. 17). Syn-mineralization hydrothermal alteration assemblages likely included sericite (Fig.

15E), sericite-chlorite (Fig. 15D) and magnetite (Fe addition). Hydrothermal K-feldspar alteration also occurred in separate zones that lack evidence of plagioclase destruction.

Some granitoid magmatism, and possibly further gneiss formation, occurred at ca. 2.8 Ga (Fig. 25D; Pidgeon et al., 1990). At ca. 2673 Ma (SHRIMP U-Pb zircon; Fig. 8) renewed heating generated crustal melts that were emplaced as granite (*sensu stricto*) dikes and stocks (Fig. 25D). These granites cut across D_1 features and mineralized zones, entraining some sulfide. Peak upper-amphibolite facies metamorphism, at ~660°C to 800°C and <10 kbar (Fig. 18), occurred at or after ca. 2673 Ma, based on the presence of garnet and sillimanite in the granite dikes (Figs. 12B, 25E). Peak metamorphism was broadly synchronous with D_2 ~east-west compression, as evidenced by the growth of sillimanite parallel to the north-south striking, moderately west-dipping S_2 foliation (Figs. 11F, 19C). During D_2, pre-existing geological features were folded by open, generally north-plunging F_2 folds. At district-scale, the ~15 km long granite-gneiss mineralization corridor was folded into train of ~30° to 40° north- to northwest-plunging, kilometer-scale F_2 folds (Fig. 3). At the Dasher deposit, west-verging F_2 folds buckled mineralized veins and the mineralized body as a whole (Fig. 5).

During D_2 and peak metamorphism, existing mineralized veins (V1 to V4) and hydrothermal alteration zones in the granite-gneiss were recrystallized into metamorphic equilibrium assemblages. Aluminium-rich to peraluminous zones (e.g. sericite-chlorite) produced biotite-garnet-sillimanite-magnetite assemblages (Figs. 12A, 15A), and hydrothermal K-feldspar zones recrystallized into granoblastic quartz-microcline-plagioclase-sillimanite (Figs. 15E, 15F). Metamorphic dehydration of hydrous alteration phases released H_2O, causing localized partial melting within mineralized areas, and the production of V5 mineralized pegmatite veins (Fig. 14E). Syn-mineralization pyrite may have been converted to pyrrhotite as it heated over ~500°C (Blatt et al., 2006).

The minimum age of D_2 and peak metamorphism is constrained by the intrusion of post-tectonic granitoids at ca. 2651 Ma (SHRIMP U-Pb zircon; Pidgeon et al., 1990). Greenschist facies retrograde metamorphism, accompanied by brittle faulting and hydrothermal chlorite-sericite-epidote-carbonate ± pyrite alteration, followed at ca. ca. 2646 Ma (conventional U-Pb titanite; Pidgeon et al., 1990).

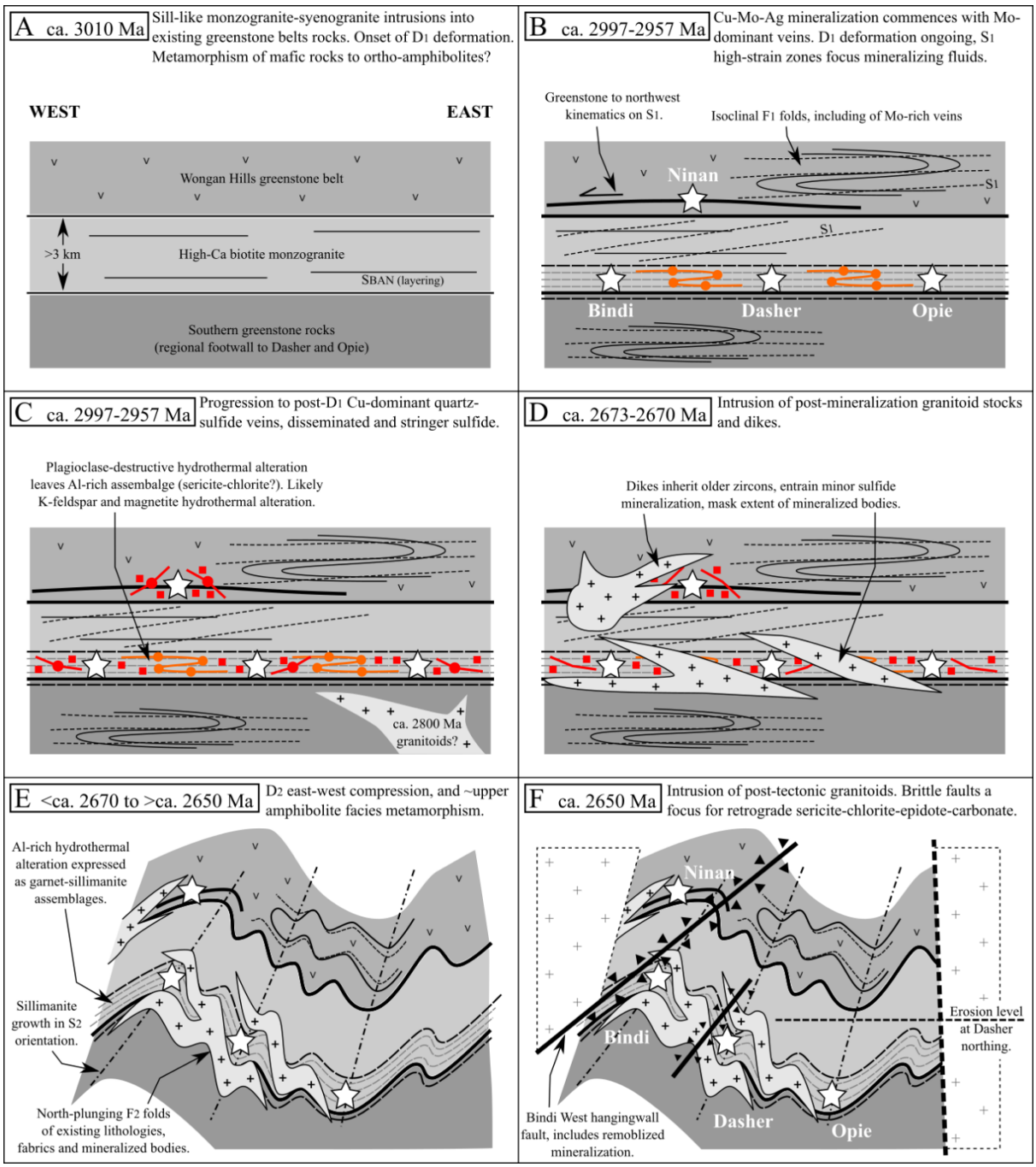

Fig. 25. Schematic east-west cross-section showing the interpreted intrusive, structural, metamorphic and mineralization history of the Calingiri district. Refer to Fig. 3 for plan-view context. The north plunge of F_2 folds (Fig. 25A and Fig. 25B) results in Dasher and Bindi being further north than Opie.

Discussion

There are few analogues to Calingiri Cu-Mo-Ag deposits in the literature: Archean, granite-gneiss-hosted, and Cu-Mo-dominant. The deposits are of interest because their discovery demonstrates latent mineralization potential in poorly-explored granite-gneiss terranes on the Yilgarn Craton, and on other Archean cratons worldwide – e.g. Canada, Brazil. The Calingiri mineralization also provides insights into the geology and metallogeny of the southwest Yilgarn Craton, and is an addition to the class of pre-peak metamorphic, epigenetic mineral deposits (discussed in Appendix 1).

Classification of the Calingiri Cu-Mo-Ag mineralization

Many characteristics of the granite-gneiss-hosted Calingiri mineralization are comparable to Phanerozoic porphyry-style mineral deposits (e.g., Sillitoe, 2010), including: (1) granitoid host rock; (2) Cu-Mo-Ag-(Au) mineralization; (3) bulk-tonnage, with stockwork, stringer and disseminated mineralization styles; (4) separate spatial location of Mo-dominant and Cu-Au-dominant mineralization (Table 2; Fig. 16); and (5) plagioclase-destructive and K-feldspar-magnetite-productive hydrothermal alteration. The Calingiri mineralization is distinguished from the magmatic-hydrothermal iron oxide-copper-gold (IOCG) class of deposits (e.g., Richards and Mumin, 2013) by its lack of: (1) sodic-calcic hydrothermal alteration; (2) U or REE association; and (3) carbonate alteration. Based on this evidence, it is reasonable to describe Calingiri as 'porphyry-style' mineralization. However, it is important to note that this study has not established any genetic link between particular granitoid intrusions and Cu-Mo-Ag mineralization at Calingiri: that is, the ca. 3010 Ma granite-gneiss (SHRIMP U-Pb zircon) should be considered a 'passive' host rock, unless evidence to the contrary emerges.

There are few indisputable examples of Precambrian porphyry mineralization (Richards and Mumin, 2013). Disputed or uncertain Archean to Paleoproterozoic examples include: (1) the Lac Troilus Cu-Au deposit, Superior Province (Fraser, 1993; Rowins, 2000; Goodman et al., 2005); (2) the Boddington Au-Cu-Mo deposit, Yilgarn Craton (Allibone et al., 1998; Stein et al., 1998); and the Malanjkhand Cu-Mo-Au deposit, Central Indian Tectonic Zone (Stein et al., 2004). The difficulty in establishing genetic links between mineralization and the host intrusions – a central tenet of the porphyry model (e.g., Sillitoe, 2010) – is a common hindrance to the definitive classification of these as porphyry, rather than 'porphyry-style' deposits. The Coppin Gap Cu-Mo deposit, Pilbara Craton, is one Archean example where mineralization is interpreted by several workers to be ~synchronous with the ca. 3314 Ma host intrusion (SHRIMP U-Pb zircon) (Williams and Collins, 1990; Huston et al., 2002). The Calingiri

mineralization will remain ‘porphyry-style’ until a genetic relationship between mineralization and a particular intrusive phase can be established from further study.

Calingiri in the geological and metallogenic evolution of the southwest Yilgarn Craton

The discovery of the Calingiri Cu-Mo-Ag mineralization has provided detailed geological information in a little-studied area of the southwest Yilgarn Craton. SHRIMP U-Pb geochronology on the Dasher granite-gneiss (magmatic crystallization 3010 ± 4 Ma) confirms the presence of ca. 3.0 Ga magmatism in this region (Pidgeon et al., 1990; Mole et al., 2012), and locally expands the spatial extent of these granitoids (Fig. 3). This granite-gneiss is part of the oldest suite of granitoid intrusions recognized in the South West Terrane (Mole et al., 2012). The ca. 2670 Ma (SHRIMP U-Pb zircon) post-mineralization granitoid dikes at Dasher and Ninan are part of a 2720-2600 Ma granitoid pulse that includes the majority of preserved southwest Yilgarn Craton granitoids, by volume (Mole et al., 2012). These dikes contain inherited zircons >3.2 Ga, and as old as 3282 ± 3 Ma (CAL044 Dasher granite dike; SHRIMP U-Pb zircon), potentially indicating an older crustal history for the South West Terrane than the ca. 3240 Ma limit suggested by Mole et al. (2012). The ca. 2.8 Ga inherited zircons in the dikes are likely evidence of regional ca. 2.8 Ga granitoid magmatism (Mole et al., 2012) and/or local gneiss formation (Pidgeon et al., 1990).

The onset of D_1 ductile deformation at Calingiri (foliation, isoclinal folding, stretching) has a minimum age of 3010 ± 4 Ma (SHRIMP U-Pb zircon), based on the syenogranite at Dasher cutting an early foliation in adjacent monzogranite (Fig. 7B). This suggests that early deformation was ~synchronous with the deposition of the Wongan Hills greenstone belt (Pidgeon et al., 1990) and High-Ca granitoid magmatism (this study). Early deformation with similar structural characteristics and relative timing is observed in younger granite-greenstone terranes in the eastern Yilgarn Craton (Swager, 1995; Blewett et al., 2010). The timing (ca. 2670 to 2650 Ma), compression direction (~east-west) and metamorphic grade (upper amphibolite facies) of the peak metamorphic event at Calingiri suggest it is likely related to the high-grade metamorphism developed parallel to the YCRL during amalgamation of the Balingup and Lake Grace terranes at ca. 2650-2640 Ma (Nemchin et al., 1994; Wilde et al., 1996; Qiu and Groves, 1999; Mole et al., 2012). The influence of that high-grade metamorphic event is therefore likely to extend further to the northeast than previously known.

This study has shown that the Boddington Au-Cu-Mo deposit (Fig. 1; Table 1), is not comparable to the Calingiri deposits in terms of host rock type, host rock age, or mineralization age (Allibone et al., 1998; Stein et al., 2001). However, the Ravensthorpe Cu-Au-Ag-Pb-Zn

deposits (Savage et al., 1995; Witt, 1999), in the far southwest of the Youanmi Terrane (Fig. 1; Table 1), do have characteristics in common with Calingiri: (1) ca. 3000-2950 Ma intrusive and volcanic host rocks; (2) disseminated, vein-poor, ~syn-volcanic mineralization; (3) potassic hydrothermal alteration accompanied by enrichment of Fe and Mg, and depletion of Ca and Na; and (4) post-mineralization peak metamorphism, at upper greenschist to upper amphibolite facies conditions. Together, Calingiri and Ravensthorpe provide strong evidence for the presence of ca. 3.0 Ga, pre-peak metamorphic, base metal mineralization in the southwest Yilgarn Craton.

Implications for exploration

The Yilgarn Craton has produced >324 Moz Au, predominantly from greenstone belt-hosted deposits (93%), and predominantly from the eastern half of the craton (Witt et al., 2013). This type of mineral deposit has been the focus of much mineral exploration on the craton. The low Au content of Calingiri (0.02 ppm in the resource; Caravel Minerals Ltd, 2016), its location in the southwest of the craton, and its dominantly granite-gneiss host rock, may therefore explain why this vast (~15 x 3 km) mineralized trend was not found earlier, despite sub-cropping on farm land only 120 km from Perth. Additional Calingiri-style mineralization may remain undiscovered in the Yilgarn Craton, and on other Archean cratons where granitoid domains have received relatively little mineral exploration.

Based on the outcomes of this study, criteria for exploration for Calingiri-style mineralization can be proposed: (1) preservation of ca. 3.0 Ga rocks is fundamental, at all scales, because rocks younger than the mineralization are implicitly unprospective; (2) of particular interest are ca. 3.0 Ga High-Ca granite-gneiss domains, and their contacts with ~contemporaneous greenstone belt rocks; (3) within prospective lithological domains, early high-strain zones may act as fluid pathways; and (4) discrete magnetic anomalies may be indicators of hydrothermal magnetite alteration. Recognition of hydrothermal alteration through the masking effects of post-mineralization structural, metamorphic and intrusive events is a particular difficulty at Calingiri, and will likely apply to analogous mineral systems.

Conclusions

This study of the Calingiri Cu-Mo-Ag deposits has placed initial constraints on the relative and absolute (where possible) timing of lithological, structural, metamorphic and mineralization events at Calingiri. The possibility that these deposits represent a new class of Archean, granite-gneiss-hosted mineralization will ensure continuing interest in their

characteristics and controls, from both academia and the mineral exploration industry. Areas of future research on Calingiri should include: (1) detailed geochemical (e.g. mass balance) and fluid-inclusions studies to characterize the mineralizing fluid composition, and its effects of host-rock chemistry; (2) direct dating and P-T estimation (geothermobarometry) on the peak upper-amphibolite facies metamorphic event; (3) characterizing the Bindi East and Opie deposits, when diamond drill core becomes available; (4) SHRIMP U-Pb geochronology on the intermediate volcanic rocks at Ninan, to establish the age of the Wongan Hills greenstone belt, which currently only has a minimum age constraint; and (5) craton-scale investigations into the extent and nature of the ca. 3.0 Ga mineralization represented by Calingiri and Ravensthorpe.

References

Alach, C., 1997, Griffin's Find, Yilgarn Craton, Western Australia: A granulite-facies hosted lode-gold deposit of probable pre-peak metamorphic origin: Unpublished Honours thesis, University of Western Australia, 50 p.

Allibone, A. H., Windh, J., Etheridge, M. A., Burton, D., Anderson, G., Edwards, P. W., Miller, A., Graves, C., Fanning, C. M., and Wysoczanski, R., 1998, Timing relationships and structural controls on the location of Au-Cu mineralization at the Boddington gold mine, Western Australia: Economic Geology, v. 93, p. 245-270.

Barnicoat, A. C., Fare, R. J., Groves, D. I., and McNaughton, N. J., 1991, Synmetamorphic lode-gold deposits in high-grade Archean settings: Geology, v. 19, p. 921-924.

Baxter, J. L., Harris, J. L., 1979, The Darling Fault: Diamond drilling results at Harrison's copper prospect: Geological Survey of Western Australia.

Blackburn, G. V., Fradd, J. F., Mazzuchelli, R. H., and Schupp, J. W., 1990, Badgebup Gold Deposits, in Geology of the Mineral Deposits of Australia and Papua New Guinea: The Australian Institute of Mining and Metallurgy, p. 177-180.

Blatt, H., Tracy, R., and Owens, B., 2006, Petrology: igneous, sedimentary, and metamorphic, Macmillan, 529 p.

Blewett, R., Czarnota, K., and Henson, P., 2010, Structural-event framework for the eastern Yilgarn Craton, Western Australia, and its implications for orogenic gold: Precambrian Research, v. 183, p. 203-229.

Blight, D. F., 1977, Petrological evidence for an unusually high Archean geothermal gradient in the Wongan Hills area, Western Australia: Geological Survey of Western Australia.

Blight, D. F., 1978, Aspects of amphibole chemistry and metamorphic gradient in the Wongan Hills, Western Australia: Geological Survey of Western Australia.

Brauhart, C., and Swager, N., 2003, Second annual report on Exploration Licence E70/2337, Ularring Rock Project, Sipa Exploration NL: Western Australian Department of Mines and Petroleum.

Caravel Minerals Ltd, 2013, Thick new copper-molybdenum intersections point to sigificant emerging discovery at Calingiri, WA: Release to the Australian Stock Exchange, 14th May 2013.

Caravel Minerals Ltd, 2016, Calingiri Scoping Study confirms outstanding WA Copper Project: Release to the Australian Stock Exchange, 28th June 2016.

Carter, J. D., and Lipple, S. L., 1982, Explanatory Notes On The Moora 1:250 000 sheet: Geological Survey of Western Australia.

Cassidy, K.F., Groves, D.I. and McNaughton, N.J., 1998, Late-Archean granitoid-hosted lode-gold deposits, Yilgarn Craton, Western Australia: deposit characteristics, crustal architecture and implications for ore genesis: Ore Geology Reviews, v. 13, p. 65-102.

Cassidy, K., Champion, D., McNaughton, N., Fletcher, I., Whitaker, A., Bastrakova, I., and Budd, A., 2002, Characterisation and metallogenic significance of Archean granitoids of the Yilgarn Craton, Western Australia: Minerals and Energy Research Institute of Western Australia, Report 222.

Cassidy, K. F., Champion, D. C., Krapez, B., Barley, M. E., Brown, S. J. A., Blewett, R. S., Groenewald, P. B., and Tyler, I. M., 2006, A revised geological framework for the Yilgarn Craton, Western Australia: Geological Survey of Western Australia, Record 2006/8.

Champion, D.C. and Sheraton, J.W., 1997, Geochemistry and Nd isotope systematics of Archaean granites of the Eastern Goldfields, Yilgarn Craton, Australia: implications for crustal growth processes: Precambrian Research, v. 83, p. 109-132.

Corriveau, L., and Spry, P. G., 2014, 13.7 - Metamorphosed Hydrothermal Ore Deposits, in Turekian, H. D. H. K., ed., Treatise on Geochemistry (Second Edition): Oxford, Elsevier, p. 175-194.

Dentith, M., Dent, V., and Drummond, B., 2000, Deep crustal structure in the southwestern Yilgarn Craton, Western Australia: Tectonophysics, v. 325, p. 227-255.

Dentith, M., and Featherstone, W., 2003, Controls on intra-plate seismicity in southwestern Australia: Tectonophysics, v. 376, p. 167-184.

Dominion Mining Ltd, 2010, Extensive zones of copper mineralisation intersected in initial reverse circulation drilling programme at Calingiri: Release to the Australian Stock Exchange, 6th July 2010.

Doray Minerals Ltd, 2015, WA Mining Club Presentation: Release to the Australian Stock Exchange, 26th March 2015.

Doyle, M. G., Fletcher, I. R., Foster, J., Large, R. R., Mathur, R., McNaughton, N. J., Meffre, S., Muhling, J. R., Phillips, D., and Rasmussen, B., 2015, Geochronological Constraints on the Tropicana Gold Deposit and Albany-Fraser Orogen, Western Australia: Economic Geology, v. 110, p. 355-386.

Duuring, P., Cassidy, K.F. and Hagemann, S.G., 2007, Granitoid-associated orogenic, intrusion-related, and porphyry style metal deposits in the Archean Yilgarn Craton, Western Australia: Ore Geology Reviews, v. 32, p. 157-186.

Fraser, R. J., 1993, The Lac Troilus gold-copper deposit, northwestern Quebec; a possible Archean porphyry system: Economic Geology, v. 88, p. 1685-1699.

Goodman, S., Williams-Jones, A. E., and Carles, P., 2005, Structural controls on the Archean Troilus gold-copper deposit, Quebec, Canada: Economic Geology, v. 100, p. 577-582.

Groves, D. I., 1993, The crustal continuum model for late-Archaean lode-gold deposits of the Yilgarn Block, Western Australia: Mineralium Deposita, v. 28, p. 366-374.

Guilbert, J. M., and Park, C. F., 2007, The geology of ore deposits, Waveland Press, 985 p.

Halley, S., Dilles, J.H. and Tosdal, R.M., 2015, Footprints: hydrothermal alteration and geochemical dispersion around porphyry copper deposits: Society of Economic Geologists Newsletter, 100, p.12-17.

Hayama, Y., 1959, Some considerations on the color of biotite and its relation to metamorphism: The Journal of the Geological Society of Japan, v. 65, p. 21-30.

Hoskin, P. W., and Schaltegger, U., 2003, The composition of zircon and igneous and metamorphic petrogenesis: Reviews in mineralogy and geochemistry, v. 53, p. 27-62.

Huston, D. L., Sun, S.-S., Blewett, R., Hickman, A. H., Van Kranendonk, M., Phillips, D., Baker, D., and Brauhart, C., 2002, The timing of mineralization in the Archean North Pilbara terrain, Western Australia: Economic Geology, v. 97, p. 733-755.

Jacobs, D., and Parry, W. T., 1979, Geochemistry of biotite in the Santa Rita porphyry copper deposit, New Mexico: Economic Geology, v. 74, p. 860-887.

Lipple, S. L., 1982, Geology of the Wongan Hills: Geological Survey of Western Australia, Record 1982/4.

Maier, W. D., Smithies, R. H., Spaggiari, C. V., Barnes, S. J., Kirkland, C. L., Kiddie, O., and Roberts, M. P., 2016, The evolution of mafic and ultramafic rocks of the Mesoproterozoic Fraser Zone, Albany–Fraser Orogen, and implications for Ni–Cu sulfide potential of the region: Geological Survey of Western Australia, Record 2016/8.

May, R. T., 2006, Annual Technical Report for the Period 01/01/2005 to 31/12/2005, Ularring Rock Project, Sipa Exploration NL: Western Australian Department of Mines and Petroleum.

Middleton, M., Wilde, S., Evans, B., Long, A., Dentith, M., and Morawa, M., 1995, Implications of a geoscientific traverse over the Darling Fault Zone, Western Australia: Australian Journal of Earth Sciences, v. 42, p. 83-93.

Mole, D., Fiorentini, M., Thebaud, N., McCuaig, T., Cassidy, K., Kirkland, C., Wingate, M., Romano, S., Doublier, M., and Belousova, E., 2012, Spatio-temporal constraints on lithospheric development in the southwest–central Yilgarn Craton, Western Australia: Australian Journal of Earth Sciences, v. 59, p. 625-656.

Muhling, P., Low, G., 1977, Explanatory Notes on the Yalgoo 1:250 000 sheet: Geological Survey of Western Australia.

Nemchin, A., Pidgeon, R., and Wilde, S., 1994, Timing of Late Archaean granulite facies metamorphism in the southwestern Yilgarn Craton of Western Australia: evidence from U-Pb ages of zircons fro mafic granulites: Precambrian Research, v. 68, p. 307-321.

Palmer, D., LaFontaine, D., Hill, M., and Allan, S., 2015, The Borden gold deposit: Canada's most unexpected gold discovery [ext. abs.]: NewGenGold Conference 2015, Conference Proceedings, Perth, Western Australia, 16 p.

Pidgeon, R., Wilde, S., Compston, W., and Shield, M., 1990, Archaean evolution of the Wongan Hills Greenstone Belt, Yilgarn Craton, Western Australia: Australian Journal of Earth Sciences, v. 37, p. 279-292.

Qiu, Y., and Groves, D. I., 1999, Late Archean collision and delamination in the Southwest Yilgarn Craton; the driving force for Archean orogenic lode gold mineralization?: Economic Geology, v. 94, p. 115-122.

Richards, J. P., and Mumin, A. H., 2013, Magmatic-hydrothermal processes within an evolving Earth: Iron oxide-copper-gold and porphyry Cu±Mo±Au deposits: Geology, v. 41, p. 767-770.

Rowins, S. M., 2000, Reduced porphyry copper-gold deposits: A new variation on an old theme: Geology, v. 28, p. 491-494.

Savage, M., Barley, M., and McNaughton, N., 1995, SHRIMP U–Pb geochronology of 2.95 to 3.0 Ga felsic igneous rocks at Ravensthorpe, Yellowdine Terrane, Yilgarn Craton: Australian Conference on Geochronology and Isotope Geoscience, Workshop Programme and Abstracts, Perth, Western Australia, p. 30.

Sharpe, R., and Gemmell, J. B., 2002, The Archean Cu-Zn magnetite-rich Gossan Hill volcanic-hosted massive sulfide deposit, Western Australia: genesis of a multistage hydrothermal system: Economic Geology, v. 97, p. 517-539.

Sillitoe, R. H., 2010, Porphyry copper systems: Economic geology, v. 105, p. 3-41.

Singer, D. A., Berger, V. I., and Moring, B. C., 2005, Porphyry copper deposits of the world: database, map, and grade and tonnage models: US Geological Survey, Open-File Report 1060.

Spear, F. S., 1995, Metamorphic phase equilibria and pressure-temperature-time paths, Mineralogical Society of America Washington, 799 p.

Stein, H., Markey, R., Morgan, J., Selby, D., Creaser, R., McCuaig, T., and Behn, M., 2001, Re–Os dating of Boddington molybdenite, SW Yilgarn: two Au mineralization events [ext. abs.]: 4th International Archaean Symposium 2001, Extended Abstracts. AGSO–Geoscience Australia, Record, 2001, p. 469-471.

Stein, H., Sundblad, K., Markey, R., Morgan, J., and Motuza, G., 1998, Re-Os ages for Archean molybdenite and pyrite, Kuittila-Kivisuo, Finland and Proterozoic molybdenite, Kabeliai, Lithuania: testing the chronometer in a metamorphic and metasomatic setting: Mineralium Deposita, v. 33, p. 329-345.

Stein, H. J., Hannah, J. L., Zimmerman, A., Markey, R. J., Sarkar, S. C., and Pal, A. B., 2004, A 2.5 Ga porphyry Cu–Mo–Au deposit at Malanjkhand, central India: implications for Late Archean continental assembly: Precambrian Research, v. 134, p. 189-226.

Sun, S.S. and McDonough, W.S., 1989, Chemical and isotopic systematics of oceanic basalts: implications for mantle composition and processes: Geological Society, London, Special Publications, v. 42, p. 313-345.

Swager, C.P., Griffin, T.J., Witt, W.K., Wyche, S., Ahmat, A.L., Hunter, W.M., McGoldrick, P.J. 1995, Geology of the Archaean Kalgoorlie Terrane: an explanatory note: Geological Survey of Western Australia, Record 1990/12.

Tomkins, A. G., and Grundy, C., 2009, Upper Temperature Limits of Orogenic Gold Deposit Formation: Constraints from the Granulite-Hosted Griffin's Find Deposit, Yilgarn Craton: Economic Geology, v. 104, p. 669-685.

Wilde, S., Middleton, M., and Evans, B., 1996, Terrane accretion in the southwestern Yilgarn Craton: evidence from a deep seismic crustal profile: Precambrian Research, v. 78, p. 179-196.

Williams, I., and Collins, W., 1990, Granite-greenstone terranes in the Pilbara Block, Australia, as coeval volcano-plutonic complexes; evidence from U-Pb zircon dating of the Mount Edgar Batholith: Earth and Planetary Science Letters, v. 97, p. 41-53.

Witt, W. K., 1998, Geology and mineral resources of the Ravensthorpe and Cocanarup 1:100 000 sheets: Geological Survey of Western Australia, Report 54.

Witt, W. K., 1999, The Archaean Ravensthorpe Terrane, Western Australia: synvolcanic Cu–Au mineralization in a deformed island arc complex: Precambrian Research, v. 96, p. 143-181.

Witt, W.K., Ford, A., Hanrahan, B., Mamuse, A., 2013, Regional-scale targeting for gold in the Yilgarn Craton: Part 1 of the Yilgarn Gold Exploration Targeting Atlas: Geological Survey of Western Australia, Report 125.

Appendix 1 – Literature review

Research Proposal and Literature Review (SCIE5590)

Cu-Mo-Ag-Au mineralisation in the Calingiri district: Nature, Controls and Timing

by

Michael David Outhwaite

Word Count: 4564 (Introduction to Methodology, inclusive)

0

Introductory Statement

The recent discovery of bulk-tonnage Cu-Mo-Ag-Au mineralisation in the Calingiri district, 120 km northwest of Perth, has renewed interest in the evolution and mineral potential of the southwest Yilgarn craton. The metal association and tonnage-grade profile of Calingiri, together with its location adjacent to major tectonic boundaries, raise that possibility that it may be a metamorphosed porphyry- or iron oxide-copper-gold (IOCG)-style deposit, formed at an ancient convergent margin. This study will provide the first constraints on the nature, controls and timing of the unusual Calingiri mineralisation, and will link its formation to the evolution of the southwest Yilgarn craton.

Background

In 2013, Caravel Minerals Limited announced the discovery of broad, low-grade Cu-Au-Ag-Au mineralisation at its Calingiri Project, centred 120 km northeast of Perth and 10 km southwest of the town of Wongan Hills (Fig. 1). Since that time, the same style of mineralisation has been defined across several separate prospects, within a curved corridor of approximately 20 km strike length. The main individual prospects are, from north to south, Ninan, Bindi, Dasher and Opie (together, 'the Calingiri mineralisation'). To June 2015, Caravel had defined a combined Exploration Target for the Bindi, Dasher and Opie prospects of 435-460 Mt @ 0.35-0.37% CuEq (0.30-0.32% Cu, 56-63 ppm Mo, 1.6-1.7 ppm Ag, 31-33 ppb Au). This gives a range of 1.0-1.4 Mt of contained CuEq, making it already one of the largest bulk-tonnage Cu deposits in Australia.

The mineralisation is of a style that is not known in the Yilgarn craton, and, due to its recent discovery, no formal studies have been completed on it. This literature review will describe what is currently known about the local geology and mineralisation, and discuss its regional context. The final part of the review focuses on the characteristics of hydrothermal ore deposits that have been subjected to high-grade metamorphism.

Local geology and mineralisation

The Calingiri mineralised trend extends southward from the southern tip of the Wongan Hills Greenstone Belt (host to the Ninan mineralisation), and into an area dominated by granite and granite-gneiss (host to the Bindi, Dasher and Opie mineralisation) (Fig. 1). Existing knowledge on the geology of each area is summarised separately below, followed by an outline of what is known about the mineralisation.

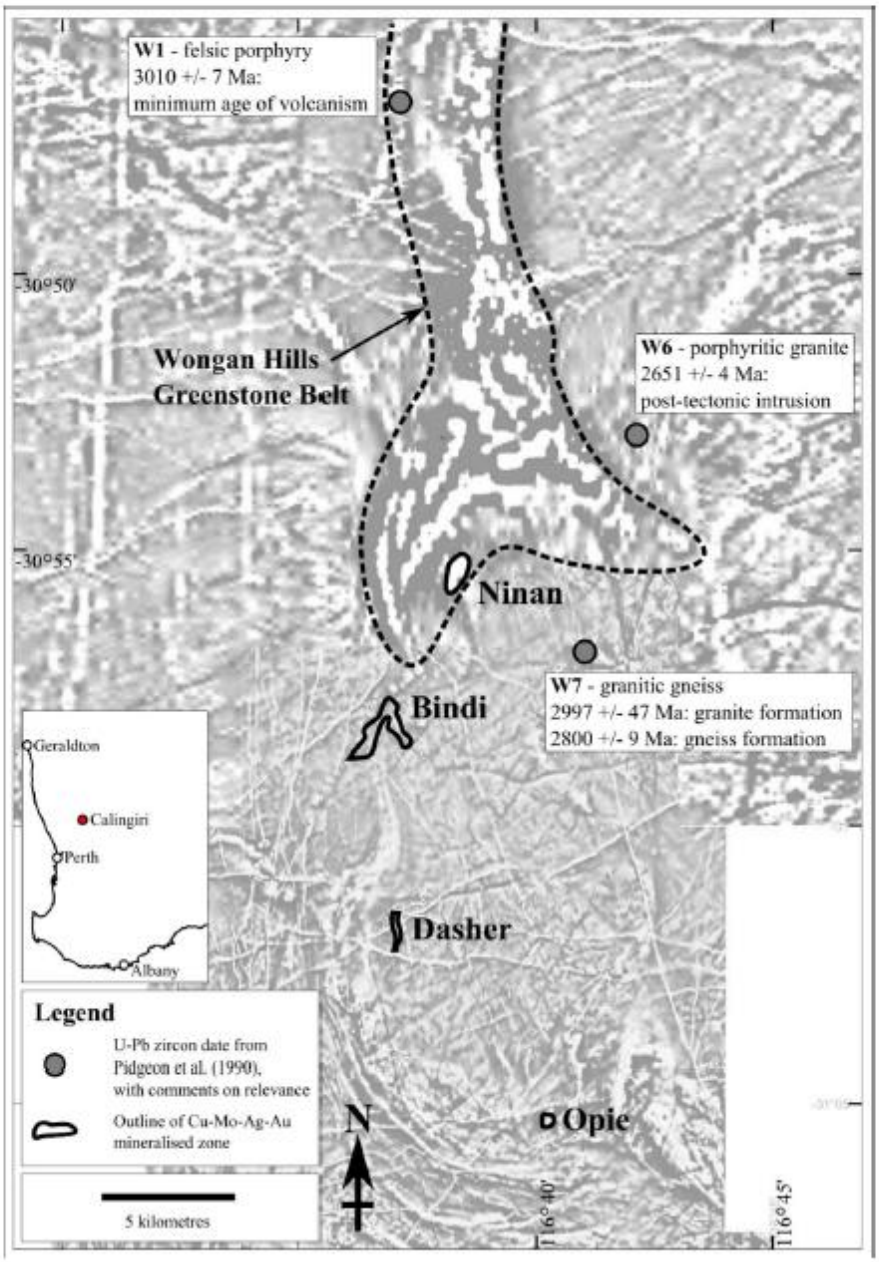

Fig. 1. First vertical derivative, greyscale magnetic image of the study area, showing known mineralised zones, the outline of the Wongan Hills Greenstone Belt, and key geochronology sites from Pidgeon et al. (1990). Location is shown on the inset map.

Wongan Hills Greenstone Belt: The ~30 km long Wongan Hills Greenstone Belt (WHGB) comprises deformed and metamorphosed mafic to felsic volcanic and volcaniclastic rocks, intercalated with metasedimentary rocks, including banded-iron-formation (BIF) (Lipple, 1982). The minimum age of volcanism in the WHGB is estimated at 3010 ± 7 Ma (SHRIMP U-Pb zircon), based on a felsic porphyry (sample 'W1'; Fig. 1) that intrudes the greenstone sequence (Pidgeon et al., 1990). In this document, the WHGB is assigned to the Lake Grace Domain of the South West Terrane (Fig. 2), using the terminology and boundaries of Mole et al. (2012) – see 'Regional context of the Calingiri mineralisation' for further discussion of the regional setting.

The structural history of the WHGB is not well constrained, in comparison to greenstone belts elsewhere in the Yilgarn craton. Carter and Lipple (1982) acknowledge that they were unable to confidently define major fold axes in the WHGB, due to poor exposures. However, outcrop-scale observations suggested that an early phase of isoclinal folding, associated with transposition and shearing, has been refolded by north-trending open folds (Carter and Lipple, 1982; Lipple, 1982). Most identifiable folds plunge to the north, and the dominant late faults in the WHGB are northwest-trending, with variable movement senses.

The rocks of the WHGB have been metamorphosed to mid- to upper-amphibolite facies, with patchy development of greenschist facies retrogression (Lipple, 1982). Blight (1977) estimated pressure-temperature (P-T) conditions of 200 MPa and 700°C for the southern end of the greenstone belt, and noted that this implied an unusually high geothermal gradient of 70°C/km in that area. Blight (1978) suggested that the overall metamorphic grade through the WHGB increases to the south, based on changes in amphibole chemistry and the increasing abundance of garnet, and that this increase was probably controlled by temperature, not pressure. Some of the samples that were used to constrain metamorphic conditions in the south of the WHGB were taken from outcrop and drill core in close proximity to the Ninan mineralisation, the scale of which was not understood at that time. It is possible that unusually high-T conditions and/or the abundance of garnet at the southern end of the WHGB are related to the Calingiri mineral system, rather than regional metamorphic gradients.

Granitic rocks south of the Wongan Hills Greenstone Belt: The granite-gneiss rocks south of the WHGB, which host the bulk of the Calingiri mineralisation, are poorly exposed and there is no detailed work published on them. Mapping of the Moora 1:250,000 map sheet by the Geological Survey of Western Australia (GSWA) describes, in a regional sense, regular textural

variations between even-grained, porphyritic, and K-feldspar megacrystic variants of granite, with no distinct regional distribution pattern (Carter and Lipple, 1982). Biotite is the dominant mafic mineral in the granites, though hornblende is also common. A lack of geochemical data means these granites cannot be described within the Yilgarn craton granite classification scheme of Cassidy et al. (2002).

The only constraint on the age of the granite-gneiss rocks is from Pidgeon et al. (1990) , who studied a quartz-feldspar-biotite gneiss (sample 'W7'; Fig. 1) from approximately 5 km northeast of the Bindi prospect (then undiscovered). These authors interpreted the sample to represent an early granitoid phase in the region, because it is affected by a complex series of structural and metamorphic events. One-quarter of the measured zircons defined an age of 2997 ± 47 Ma (SHRIMP U-Pb zircon), with the remainder defining an age of 2800 ± 9 Ma. Their preferred interpretation is of a ~3.0 Ga age of the granitoid parent, followed by partial anatexis and gneiss formation at ~2.8 Ga. In that scenario, the granitoid parent age would overlap with the minimum age for volcanism in the WHGB (described earlier), suggesting roughly contemporaneous granite and greenstone formation. If the interpretations of greenstone and granite ages Pidgeon et al. (1990) are correct, this may constrain the Calingiri mineralisation to having occurred after ~3.0 Ga.

Characteristics of the Calingiri mineralisation: There are few published studies on the Calingiri mineralisation, due to its relatively recent discovery and the early stage of current exploration. The WHGB-hosted mineralisation at Ninan is the best documented, because is partly exposed at surface has been subject to sporadic investigation by mineral exploration companies since 1975 (Lipple, 1982). The host rocks at Ninan are strongly foliated and lineated schists derived from ultramafic, BIF and aluminous sedimentary rocks, and the aluminous schists include metamorphic indicator minerals such as garnet (almandine), fibrolite (sillimanite), andalusite and cordierite (Blight, 1977; Lipple, 1982). Primary mineralisation at Ninan is associated with thin (<15 cm) bands of chalcopyrite-almandine±magnetite±fibrolite±biotite, best developed in the hinge region of a prospect-scale antiform, which plunges moderately to the north-northwest, parallel to a prominent stretching lineation (Lipple, 1982).

Caravel Minerals Limited's recent releases to the Australian Stock Exchange (ASX) describe the mineralisation at Bindi, Dasher and Opie as being of a common style. The typical mineralisation consists of chalcopyrite±molybdenite±magnetite, disseminated within a coarse-grained, garnet-biotite gneiss, of likely granitic origin. Garnet abundance has a broad spatial

association with mineralisation. The garnet-biotite gneiss, and associated mineralisation, typically forms tabular zones in the order of 50-150 m true thickness (up to 200 m) through the core of the main prospects. The mineralised zones at Dasher and Opie dip moderately to the east and north, respectively, while the Bindi mineralisation is interpreted to be folded (Fig. 1), resulting in the Bindi West (west-dipping) and Bindi East components (dip currently uncertain). Drilling has identified amphibolite lenses at all prospects (possible WHGB equivalents), and some post-mineralisation granite and pegmatite intrusions. Post-mineralisation dolerite dykes of assumed Proterozoic age are common.

A consultant petrologist, Dick England, has described a suite of 11 polished thin-sections taken from two diamond drill holes at the Dasher prospect (England, 2013). The main host rocks are described as low-Ca, high-K biotite monzogranites and granodiorites, though some K-feldspar may be of alteration origin. Mineralisation is dominated by anhedral chalcopyrite, found together with garnet and/or magnetite, with minor pyrite interpreted to be a product of retrogression. In one sample, tabular molybdenite is roughly parallel to a biotite-defined foliation, and in another it contains small chalcopyrite inclusions. England (2013) suggests that the garnet-rich mineralisation may be the product of metamorphosed phyllic alteration, which would imply a pre-peak metamorphic origin for mineralisation.

Regional context of the Calingiri mineralisation

The Calingiri study area is in the southwestern corner of the Archean Yilgarn craton (Fig. 2). The granitic, volcanic and sedimentary rocks that comprise the craton formed principally between 3.02 and 2.62 Ga, and can be divided into a number of distinct terranes and domains, based on stratigraphic, structural, geochemical and geochronological constraints (Cassidy et al., 2006). The following section establishes the location of the study area in relation to those terrane and domain boundaries, reviews the major tectonic events that have affected the area, and summarises the mineralisation styles present in the southwest Yilgarn craton.

Terrane and domain definitions: The study area, using the WHGB as a proxy, is in a complicated location with regards to major tectonic sub-divisions. The WHGB was assigned to the Murchison Terrane by Wilde et al. (1996), based on its age, location (in relation to major geophysical features) and constituent lithologies. It was placed immediately east of the Lake Grace Terrane, the easternmost of the three terranes those authors proposed for the southwest Yilgarn craton (Balingup, Boddington and Lake Grace; Fig. 2). A craton-scale review of Yilgarn tectonic subdivisions conducted by Cassidy et al. (2006) proposed a single South West

Terrane, enveloping the three smaller terranes proposed by Wilde et al. (1996) and tentatively expanding further eastward, although those authors noted the imprecise definition of that eastern boundary. This modification placed the WHGB in the South West Terrane, and not in the Murchison Domain of their Youanmi Terrane (Fig. 2).

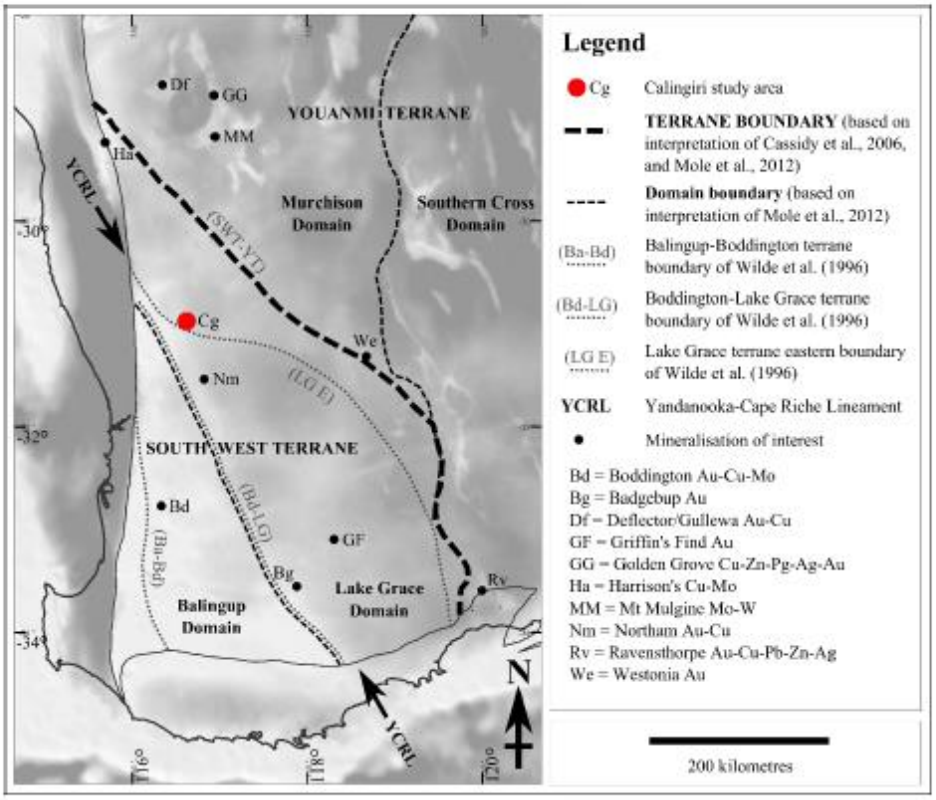

Fig. 2. Greyscale gravity image of the southwest Yilgarn craton, annotated with the location of the study area, proposed tectonic sub-divisions, and mineralisation sites of interest.

More recently, Mole et al. (2012) proposed that the eastern limit of the Lake Grace Terrane, as defined by Wilde et al. (1996), should be extended to the South West Terrane-Youanmi Terrane boundary of Cassidy et al. (2006) (Fig. 2). This refinement was based on analysis of the spatio-temporal distribution of granite emplacement in the southwest Yilgarn craton, and confirmed that the WHGB was part of the South West Terrane. Further, Mole et al. (2012) proposed the sub-division of the South West Terrane into two domains: the Balingup Domain in the west, and the Lake Grace Domain in the east (Fig. 2). These correspond to the Lake Grace Terrane (expanded eastward, as explained above), and the combined Balingup Terrane and Boddington

Terrane of Wilde et al. (1996), respectively. The WHGB, and Calingiri study area, lies within the Lake Grace Domain of the South West Terrane, close to the Balingup Domain boundary. The Mole et al. (2012) definitions are used throughout the remaining discussions, unless otherwise stated.

Significance of the Balingup-Lake Grace domain boundary: The Calingiri study area is adjacent to a significant NNW-trending regional geological feature known as the Yandanooka-Cape Riche Lineament (YCRL; Fig. 2) (Dentith and Featherstone, 2003; Everingham, 1968). The YCRL has been used as the boundary between the Balingup and Lake Grace domains of Mole et al. (2012).

The YCRL is most clearly defined by a sharp fall in regional gravity values (Fig. 2) from the Avon Regional Gravity High to the west, and to the Narembeen Regional Gravity Shelf to the east (Fraser and Pettifer, 1980). In the depth dimension, seismic interpretations indicate that the YCRL is gently dipping to the east, and extends through the entire crust (Dentith et al., 2000; Middleton et al., 1995; Wilde et al., 1996). The interpretation of Dentith et al. (2000) is based on the 'AOB' seismic refraction traverse, which crosses the YCRL approximately 150 km southeast of the Calingiri study area.

In the Archean rocks presently exposed, the YCRL does not have a discrete expression – rather, several different geological features have been used to broadly define the zone. The features include:

- East-dipping shear zones at surface, a change in structural style across the zone from flat-lying nappes (west) to north-plunging upright folds (east), and a concentration of mafic and ultramafic rocks (Wilde et al., 1996)
- The western boundary of 2649-2640 Ma high-T, low-P granulite-facies metamorphism (Nemchin et al., 1994)
- The western extent of 2880-2830 Ma granites and the western extent of charnockitic granites (Mole et al., 2012)

The YCRL is also expressed in modern, intra-plate seismicity, as a first-order control on the South West Seismic Zone, adding weight to its interpretation as a major crustal structure (Dentith and Featherstone, 2003).

Studies of the southwest Yilgarn Craton have consistently identified the YCRL as a major crustal structure and terrane/domain boundary, but there is no definitive view on what it

represents. Wilde et al. (1996) interpreted the YCRL to be an east-dipping thrust, which transported a portion of intermediate crust to surface, such that the flat-lying nappes in the Jimperding Metamorphic Belt in their Boddington Terrane (west of the YCRL) may represent thrust slices that were originally part of the Lake Grace Terrane (east of the YCRL). They suggest that the event must have occurred after ~2640 Ma, because there is no evidence of ~2640 Ma granulite facies metamorphism (which affects the Lake Grace Terrane) in the Boddington Terrane. The larger-scale nature and duration of tectonism at the YCRL was discussed by Qiu and Groves (1999), who proposed that the YCRL is a suture zone marking a continent-continent collision event that occurred from 2690 to 2630 Ma. They further suggest that this event may have triggered lithospheric delamination, melting of the lower crust, and a craton-wide thermal anomaly, coincident with the timing of large-scale Au mineralisation across the Yilgarn Craton. The timing of the last phase of the collisional event across the YCRL is refined to ~2650-2640 Ma by Mole et al. (2012), who invoke the event as the cause of granulite facies metamorphism (Nemchin et al., 1994), and of ~2650 Ma charnockitic granite formation in the Lake Grace Domain.

The possibility that the collision across the YCRL was between continents that were originally separated by oceanic crust is outlined by Dentith et al. (2000), who note the presence of a high-velocity zone coincident with the east-dipping YCRL at depth. They interpret this zone (unexposed at present levels) to be of mafic-ultramafic composition, and suggest that it may represent a sliver of oceanic lithosphere. This geometrical arrangement raises the possibility that the YCRL was an east-dipping subduction zone (terminating in continent-continent collision), rather than an east-dipping thrust. The Calingiri study area is located above (northeast of) the YCRL, within the over-riding block in a subduction scenario. This setting, together with the metal association and tonnage-grade profile of the mineralisation, raises the possibility that Calingiri may be an Archean, subduction-related deposit.

Mineralisation in the southwest Yilgarn craton: There are several styles of mineralisation in the southwest Yilgarn craton, hosting a range of ore metals. These are summarised in Table 1, and their locations are shown in Figure 2. The Calingiri Cu-Mo-Ag-Au mineralisation may have similarities to one or more of these occurrences, as part of a continuum of deposit styles across the region. The variability within the Ravensthorpe area alone (Witt, 1998), with porphyry, VMS, and 'VMS feeder zone' mineralisation interpreted, demonstrates the complexity in the deposit-scale expression of large-scale mineralised districts.

Aspects of the regional metallogeny that are of particular relevance to the Calingiri mineralisation include the presence of:

- Significant Cu- and/or Mo-bearing mineral systems
- Deposit styles associated with convergent margin environments (porphyry, VMS)
- Mineral systems within high-grade metamorphic rocks
- Known or suspected pre-peak metamorphic hydrothermal mineralisation

The hypothesis that the Calingiri Cu-Mo-Ag-Au mineralisation is of porphyry- or IOCG-style, and has been overprinted by high-grade metamorphism, appears to be feasible and worthy of testing, in light of these observations.

Table 1. Summary of mineralisation styles in the southwest Yilgarn craton

Name	Status	Principal metals	Style
Griffin's Find	Mine (inactive)	Au	Metamorphosed orogenic[1]
Badgebup	Mine (inactive)	Au	Metamorphosed orogenic?[2]
Westonia	Mine (active)	Au	Granitoid-associated orogenic[3]
Deflector/Gullewa	Mine (active)	Au-Cu	Shear-hosted, porphyry-related?[4]
Boddington	Mine (active)	Au-Cu-Mo	Intrusion-related[3]
Golden Grove	Mine (active)	Cu-Zn-Pb-Ag-Au	VMS[5]
Ravensthorpe district	Mine (inactive)	Au-Cu-Pb-Zn-Ag	VMS, VMS feeder zones, porphyry[3,6]
Northam	Prospect	Au-Cu	Granulite facies, intrusion-related?[7]
Harrison's	Prospect	Cu-Mo	Unknown, related to Darling Fault[8]
Mt Mulgine	Prospect	Mo-W	Intrusion-related[3]

1 = Tomkins and Grundy (2009), 2 = Blackburn et al. (1990), 3 = Duuring et al. (2007), 4 = Watkins and Hickman (1990), 5 = Hollis et al. (2015), 6 = Witt (1998), 7 = Brauhart and Swager (2003), 8 = Baxter and Harris (1979)

Evidence for pre-peak metamorphic timing of hydrothermal ore deposits

The spatial coincidence of the Calingiri mineralisation with high-grade metamorphic minerals like garnet and sillimanite (Blight, 1977; England, 2013), suggests that mineralisation occurred either synchronous with, or prior to, a high-grade metamorphic event. Differentiating between a syn- and pre-peak origin for Calingiri will influence interpretation of the P-T conditions at the time of mineralisation, interpretation of the overall P-T-time(t) path of the rocks in the local district (with implications for tectonic setting), and the correlation of local events to established regional events.

In metamorphosed syngenetic mineral deposits (e.g. VMS) a pre-peak timing is implicit, but differentiating between pre- and syn-peak timing for epigenetic, hydrothermal mineralisation in high-grade metamorphic rocks is difficult, and conflicting views are common (e.g. Phillips and Powell, 2009). The central problem is that many textures of pre-peak metamorphic deposits can also be explained by a syn-peak origin, and are therefore not diagnostic.

There are a handful of deposits that have been subject to detailed studies in order to resolve the question of pre-peak versus syn-peak timing – in particular, the Griffin's Find Au deposit in the Yilgarn craton, and the Hemlo Au deposit in the Archean Superior province, Ontario. Literature on a selection of these deposits has been reviewed, in order to establish what arguments have been advanced for pre-peak timing. The emphasis is on deposits that are Archean, affected by amphibolite to granulite facies metamorphism, and contain Au±Cu±Mo. The deposits reviewed are listed here, with a recent reference given for each:

- Griffin's Find Au, granulite facies, Archean Yilgarn craton, Western Australia (Tomkins and Mavrogenes, 2002)
- Hemlo Au, middle amphibolite facies, Archean Superior province, Ontario (Heiligmann et al., 2008)
- Big Bell Au, upper amphibolite facies, Archean Yilgarn craton, Western Australia (Phillips and Powell, 2009)
- Challenger Au, granulite facies, Archean Gawler craton, South Australia (Tomkins and Mavrogenes, 2002)
- Troilus Au-Cu, lower amphibolite facies, Archean Superior province, Quebec (Goodman et al., 2005)
- Malandjkhand Cu-Mo-Au, amphibolite facies, Paleoproterozoic Central Indian Tectonic Zone, India (Stein et al., 2004)

The results of the review are summarised in Table 2. Many of these criteria are expected to be relevant at Calingiri, based on present knowledge of the mineralisation.

In addition to the specific criteria outlined in Table 2, some authors (Phillips and Powell, 2009; Tomkins and Grundy, 2009) have more generally questioned whether it is even possible for hydrothermal mineralisation to occur at high temperature, because the addition of hydrothermal fluids at greater than 600-650°C should induce partial melting of the host rock and prevent fluid transfer.

Table 2. Summary of evidence used to argue for a pre-metamorphic origin of ore deposits (continued next page)

Class	Characteristic	Comments	Example deposit(s)
Geochronology	Mineralisation age precedes peak metamorphic age	Difficulties in dating some pre-peak mineralisation, due to resetting	Hemlo[6], Malanjkhand[9]
Structural	Deformed mineralisation	Folded or foliated ore zones, peak metamorphic phases syn- or post-date 'deforming' fabric (e.g. growing in axial planes of folds affecting mineralisation)	Big Bell[1], Challenger[2], Griffin's Find[3], Hemlo[5,8], Malanjkhand[9]
	Ore remobilised into low stress sites that accompany deformation and peak metamorphism	E.g. short limbs of parasitic folds, boudin necks	Challenger[2], Hemlo[7]
Textural	Recrystallised mineralised veins and alteration	Veins lacking original depositional textures, grain triple-junctions, granoblastic K-feldspar, idioblastic muscovite	Big Bell[1], Griffin's Find[3], Hemlo[8]
	Anomalously high partial melting around deposit (leucosomes, pegmatoidal veins)	Breakdown of pre-peak hydrous phases releases H_2O, initiates partial melting in alteration halo	Big Bell[1], Challenger[2], Renco[1]
	Peak metamorphic phases overprint alteration (e.g. garnet over biotite)	Not applicable if alteration phases are recrystallised	Troilus[10]
	Inclusions of ore minerals in peak metamorphic phases	Spherical inclusions most definitive - would be subhedral/euhedral is precipitated at peak conditions	Challenger[2], Griffin's Find[3], Renco[1]

Table 2. (continued)

Class	Characteristic	Comments	Example deposit(s)
Mineralogical	Apparent lack of hydrothermal alteration, or narrow alteration	H_2O lost during metamorphism, anhydrous phases formed, CO_2 lost	Challenger[2]
	Absence of metamorphic index minerals in ore zone	High K activity and S fugacity stabilise other assemblages	Hemlo[8]
	Lower Fe:Mg ratios in garnet and biotite, proximal to sulphide ore	Sulphidation of Fe during mineralisation leaves silicate residue depleted in Fe - reflected in subsequent metamorphic mineralogy	Big Bell[1], Hemlo[8]
	Arsenopyrite-löellingite-pyrrhotite relationships	Löellingite-pyrrhotite 'pairs' indicate metamorphism and breakdown of arsenopyrite - if precipitated at peak, they would not be spatially linked	Challenger[2], Griffin's Find[3,4]
	Stability of quartz-calcite assemblage	Assemblage would form wollastonite in presence of high-T fluid - so peak conditions must have been 'dry', mineralisation was prior	Griffin's Find[4]
	Oxygen isotope exchange between mineralisation-related phases	Indicates if exchange occurred in an 'open' (fluid present) or 'closed' system (fluid absent, mineralisation pre-peak)	Griffin's Find[3]

1 = Phillips and Powell (2009), 2 = Tomkins and Mavrogenes (2002), 3 = Alach (1997), 4 = Tomkins and Grundy (2009), 5 = Lin (2001), 6 = Davis and Lin (2003), 7 = Tomkins et al. (2004), 8 = Heiligmann et al. (2008), 9 = Stein et al. (2004), 10 = Goodman et al. (2005)

Aims

Due to its unusual location and recent discovery, no detailed studies have been completed on the Calingiri mineralisation or its host rocks. The aims of this study are, therefore, to document:

- Host rocks – types, relative timing and geochemistry (magmatic rocks, in particular)
- Structural geology – structural elements and kinematics
- Metamorphism – prograde and retrograde events, facies (P-T conditions), timing relative to structural events and mineralisation
- Hydrothermal alteration and mineralisation – mineralogy, texture, paragenesis, timing in relation to local structural, magmatic and metamorphic events

If suitable rocks and mineral phases are identified, a geochronology study will also be undertaken. This will likely focus on SHRIMP U-Pb zircon dating of host rocks, and direct dating of mineralisation using Re-Os on molybdenite.

Significance and Outcomes

The proposed study will document, and place in context, the newly-discovered Calingiri Cu-Mo-Ag-Au mineralisation. There are few global examples of Archean, bulk-tonnage, Cu-dominant mineralisation, so this study will have significance to academia and the minerals industry.

The potential outcomes of this study for academia are:

- Detailed paragenesis of an unusual type of mineralisation
- Evaluation of whether the mineralisation has affinities to porphyry- or IOCG-styles
- New constraints on the lithological, structural and metamorphic history of the poorly-studied region south of the Wongan Hills Greenstone Belt
- A well constrained locality to use in future revisions of the evolution and mineral potential of the southwest Yilgarn craton

The potential outcomes for the mineral industry are:

- Establish the local controls on mineralisation, leading to more effective exploration at the district-scale
- Provide insights on the regional-scale spatial and temporal controls on Calingiri-style mineralisation, leading to more effective exploration of the southwest Yilgarn craton

- Tentative understanding of the craton-scale controls, which will encourage exploration for Calingiri-style mineralisation within Archean cratons worldwide

Methodology

The methods applied in this study will include:

- Field work, involving drill hole logging and outcrop mapping
- Transmitted and reflect light petrography
- Scanning electron microscopy
- Lithogeochemistry
- Geochronology

The details and goals of each study phase are outlined below.

Field work

The first aspect of the field work will be graphical logging of relevant diamond drill holes. There are currently only four Caravel diamond drill holes into the main Calingiri mineralisation (three from Dasher and one from Bindi West), and each of these will be logged in detail. Historic, unoriented diamond drill holes from Ninan are also available, and a well-mineralised example from that prospect will also be logged. The logging will include detailed observations of lithology, structural elements, hydrothermal alteration and mineralisation. Magnetic susceptibility measurements will also be taken down hole.

The majority of samples for the study are expected to come from the diamond drill holes. These will include 'least-deformed, least-altered' examples of the various host lithologies, deformed variants of the lithologies, and type-examples of different hydrothermal alteration and mineralisation styles. A small subset of the samples will be taken for their potential to be used in geochronological studies. Samples will be photographed, and detailed notes on the location, context, and reason for each sample will be entered into a database. All samples will be oriented, where possible, to enable the preparation of oriented thin-sections and micro-structural analysis.

The second aspect of the field work will be outcrop mapping in the study area, to provide the regional context to core-scale observations. Regional-scale mapping will be completed at 1:5000 scale, and will focus around the mineralised trend. Detailed outcrop features at 'type-localities' will be mapped at 1:500 scale.

Petrography

A selection of samples that will give the best constraints on the nature and paragenesis of the Calingiri mineralisation will be submitted for polished thin-section preparation. This will include all samples that will later be submitted for detailed lithogeochemistry and/or geochronology, to ensure the best possible understanding of those samples. All thin-sections will be described on an optical microscope, using transmitted and reflected light, as appropriate. Particular attention will be paid to identifying mineral phases that may be suitable for geochronology, and mineral assemblages that may be used to constrain P-T conditions.

Scanning electron microscopy

A selection of the polished thin-sections will be chosen for study under the TESCAN scanning electron microscope (SEM), which includes energy dispersive X-ray spectrometry (EDS) capability. The first application of the SEM will be to identify mineral phases that could not be identified on the optical microscope, using the EDS capability. The second application of the SEM will be to capture fine textural detail in mineralised samples, because this may be critical in distinguishing pre- from syn-peak metamorphic origin for the mineralisation. The third application of the SEM will be using the EDS capability to capture mineral chemistry data. Wavelength-dispersive X-ray spectroscopy (WDS) may be employed for detailed mineral chemistry work, such as the study of ion-exchange between mineral assemblages, for P-T estimation (e.g. garnet-biotite thermometry).

Lithogeochemistry

A limited selection of the samples (up to 20) will be sent for lithogeochemical analysis. The main focus will be on characterising different granitic phases, so they can be related to large-scale magmatic events affecting the southwest Yilgarn craton. Some samples from the Wongan Hills Greenstone Belt (Ninan prospect) may also be submitted for analysis, especially if they are candidates for geochronology.

Geochronology

SHRIMP U-Pb zircon geochronology will be undertaken on selected host rocks. This part of the study will be conducted in collaboration with the GSWA, who will perform the analysis on mineral separates provided by the author. To directly date the mineralisation, Re-Os molybdenite analysis will also be undertaken, if suitable samples are identified.

Reference list

Alach, C., 1997, Griffin's Find, Yilgarn Craton, Western Australia: A granulite-facies hosted lode-gold deposit of probable pre-peak metamorphic origin: Unpublished Honours thesis, University of Western Australia, 50 p.

Baxter, J. L., and Harris, J. L., 1979, The Darling Fault: Diamond drilling results at Harrisons copper prospect: Perth, Geological Survey of Western Australia.

Blackburn, G. V., Fradd, J. F., Mazzuchelli, R. H., and Schupp, J. W., 1990, Badgebup Gold Deposits, in Hughes, F.E., ed., Geology of the Mineral Deposits of Australia and Papua New Guinea: Melbourne: The Australian Institute of Mining and Metallurgy, p. 177-180.

Blight, D. F., 1977, Petrological evidence for an unusually high Archean geothermal gradient in the Wongan Hills area, Western Australia: Perth, Geological Survey of Western Australia.

Blight, D. F., 1978, Aspects of amphibole chemistry and metamorphic gradient in the Wongan Hills, Western Australia: Perth, Geological Survey of Western Australia.

Brauhart, C., and Swager, N., 2003, Sipa Exploration NL Second annual report on Exploration Licence E70/2337, Ularring Rock Project: Unpublished WAMEX report A66830, Department of Mines and Petroleum, Western Australia

Carter, J. D., and Lipple, S. L., 1982, Explanatory Notes On The Moora Geological Sheet: Perth, Geological Survey of Western Australia.

Cassidy, K., Champion, D., McNaughton, N., Fletcher, I., Whitaker, A., Bastrakova, I., and Budd, A., 2002, Characterisation and metallogenic significance of Archean granitoids of the Yilgarn Craton, Western Australia: Perth, Minerals and Energy Research Institute of Western Australia, Report 222

Cassidy, K. F., Champion, D. C., Krapez, B., Barley, M. E., Brown, S. J. A., Blewett, R. S., Groenewald, P. B., and Tyler, I. M., 2006, A revised geological framework for the Yilgarn Craton, Western Australia: Perth, Geological Survey of Western Australia.

Davis, D. W., and Lin, S., 2003, Unraveling the Geologic History of the Hemlo Archean Gold Deposit, Superior Province, Canada: A U-Pb Geochronological Study: Economic Geology, v. 98, p. 51-67.

Dentith, M., Dent, V., and Drummond, B., 2000, Deep crustal structure in the southwestern Yilgarn Craton, Western Australia: Tectonophysics, v. 325, p. 227-255.

Dentith, M., and Featherstone, W., 2003, Controls on intra-plate seismicity in southwestern Australia: Tectonophysics, v. 376, p. 167-184.

Duuring, P., Cassidy, K. F., and Hagemann, S. G., 2007, Granitoid-associated orogenic, intrusion-related, and porphyry style metal deposits in the Archean Yilgarn Craton, Western Australia: Ore Geology Reviews, v. 32, p. 157-186.

England, R. N., 2013, Petrographic notes for 11 drill-core samples from 12CAD001 and 12CAD002, Dasher Prospect: Unpublished consulting report, prepared for Caravel Minerals Limited

Everingham, I. B., 1968, Seismicity of Western Australia: Canberra, Bureau of Mineral Resources, Geology and Geophysics.

Fraser, A. R., and Pettifer, G. R., 1980, Reconnaissance gravity surveys in Western Australia and South Australia, 1969-1972: Canberra, Bureau of Mineral Resources, Geology and Geophysics.

Goodman, S., Williams-Jones, A. E., and Carles, P., 2005, Structural controls on the Archean Troilus gold-copper deposit, Quebec, Canada: Economic Geology, v. 100, p. 577-582.

Heiligmann, M., Williams-Jones, A. E., and Clark, J. R., 2008, The Role of Sulfate-Sulfide-Oxide-Silicate Equilibria in the Metamorphism of Hydrothermal Alteration at the Hemlo Gold Deposit, Ontario: Economic Geology, v. 103, p. 335-351.

Hollis, S. P., Yeats, C. J., Wyche, S., Barnes, S. J., Ivanic, T. J., Belford, S. M., Davidson, G. J., Roache, A. J., and Wingate, M. T. D., 2015, A review of volcanic-hosted massive sulfide (VHMS) mineralization in the Archaean Yilgarn Craton, Western Australia: Tectonic, stratigraphic and geochemical associations: Precambrian Research, v. 260, p. 113-135.

Lin, S., 2001, Stratigraphic and Structural Setting of the Hemlo Gold Deposit, Ontario, Canada: Economic Geology, v. 96, p. 477-507.

Lipple, S. L., 1982, Geology of the Wongan Hills: Perth, Geological Survey of Western Australia.

Middleton, M., Wilde, S., Evans, B., Long, A., Dentith, M., and Morawa, M., 1995, Implications of a geoscientific traverse over the Darling Fault Zone, Western Australia: Australian Journal of Earth Sciences, v. 42, p. 83-93.

Mole, D., Fiorentini, M., Thebaud, N., McCuaig, T., Cassidy, K., Kirkland, C., Wingate, M., Romano, S., Doublier, M., and Belousova, E., 2012, Spatio-temporal constraints on lithospheric development in the southwest–central Yilgarn Craton, Western Australia: Australian Journal of Earth Sciences, v. 59, p. 625-656.

Nemchin, A., Pidgeon, R., and Wilde, S., 1994, Timing of Late Archaean granulite facies metamorphism in the southwestern Yilgarn Craton of Western Australia: evidence from U‐Pb ages of zircons fro mafic granulites: Precambrian Research, v. 68, p. 307-321.

Phillips, G. N., and Powell, R., 2009, Formation of gold deposits: review and evaluation of the continuum model: Earth-Science Reviews, v. 94, p. 1-21.

Pidgeon, R., Wilde, S., Compston, W., and Shield, M., 1990, Archaean evolution of the Wongan Hills Greenstone Belt, Yilgarn Craton, Western Australia: Australian Journal of Earth Sciences, v. 37, p. 279-292.

Qiu, Y., and Groves, D. I., 1999, Late Archean collision and delamination in the Southwest Yilgarn Craton; the driving force for Archean orogenic lode gold mineralization?: Economic Geology, v. 94, p. 115-122.

Stein, H. J., Hannah, J. L., Zimmerman, A., Markey, R. J., Sarkar, S. C., and Pal, A. B., 2004, A 2.5 Ga porphyry Cu–Mo–Au deposit at Malanjkhand, central India: implications for Late Archean continental assembly: Precambrian Research, v. 134, p. 189-226.

Tomkins, A. G., and Grundy, C., 2009, Upper Temperature Limits of Orogenic Gold Deposit Formation: Constraints from the Granulite-Hosted Griffin's Find Deposit, Yilgarn Craton: Economic Geology, v. 104, p. 669-685.

Tomkins, A. G., and Mavrogenes, J. A., 2002, Mobilization of Gold as a Polymetallic Melt during Pelite Anatexis at the Challenger Deposit, South Australia: A Metamorphosed Archean Gold Deposit: Economic Geology, v. 97, p. 1249-1271.

Tomkins, A. G., Pattison, D. R. M., and Zaleski, E., 2004, The Hemlo Gold Deposit, Ontario: An Example of Melting and Mobilization of a Precious Metal-Sulfosalt Assemblage during Amphibolite Facies Metamorphism and Deformation: Economic Geology, v. 99, p. 1063-1084.

Watkins, K. P., and Hickman, A. H., 1990, Geological evolution and mineralization of the Murchison Province, Western Australia: Perth, Geological Survey of Western Australia.

Wilde, S., Middleton, M., and Evans, B., 1996, Terrane accretion in the southwestern Yilgarn Craton: evidence from a deep seismic crustal profile: Precambrian Research, v. 78, p. 179-196.

Witt, W. K., 1998, Geology and mineral resources of the Ravensthorpe and Cacanarup 1:100 000 sheets: Perth, Western Australian Geological Survey, p. 152.

Appendix 2 – Example pages of Economic Geology journal

©2017 Society of Economic Geologists, Inc.
Economic Geology, v. 112, pp. 1055–1074

Synextensional Emplacement of Porphyry Cu-Mo and Epithermal Mineralization: The Zijinshan District, Southeastern China

José Piquer,[1, 2, †] David R. Cooke,[1, 3] Jing Chen,[1, 3] and Lejun Zhang[1, 3]

[1] *CODES, University of Tasmania, Private Bag 79, Hobart, Tasmania 7001, Australia*

[2] *Instituto de Ciencias de la Tierra, Universidad Austral de Chile, Edificio Pugín, Av. Eduardo Morales Miranda, Valdivia, Chile*

[3] *Transforming the Mining Value Chain (TMVC), an Australian Research Council Industrial Transformation Research Hub, University of Tasmania, Private Bag 79, Hobart, Tasmania 7001, Australia*

Abstract

The Zijinshan district, Fujian Province, southeastern China, is a major mineral field that contains high- and intermediate-sulfidation epithermal Cu-Au-Ag and porphyry Cu-Mo deposits. This contribution discusses the structural geology and the tectonic regime prevalent during mineralization at Zijinshan. Statistically, the district is dominated by NW-striking fault systems that dip at moderate angles (40°–50°) to the northeast and southwest. They played a first-order role in controlling the emplacement of hydrothermal veins and breccias. Most NW-striking faults were active as oblique normal/strike-slip faults during mineralization, as evidenced by the geometry of syntectonic hydrothermal mineral fibers. NE-striking, steeply dipping faults also controlled the emplacement of hydrothermal veins and breccias, and these faults contain syntectonic mineral fibers indicating predominantly dextral strike-slip movements. The kinematic and dynamic analysis of fault-slip data shows that the predominant tectonic regime during mineralization was extensional, with subvertical σ_1 and NNE- to NNW-trending σ_3. Secondary clusters of subhorizontal σ_1 suggest that short periods of fault reactivation under a strike-slip regime occurred locally. Although the formation of porphyry Cu-Mo systems is commonly thought to be favored by compressive to transpressive tectonic regimes, which lead to a diminution in the rate of volcanic output and to the entrapment of magmas and volatiles in the upper crust, these results show that at least medium-sized porphyry Cu-Mo systems can form under extensional conditions in previously thickened continental crust. This has important exploration implications globally. Based on current geologic knowledge, the district appears to have a high exploration potential at depth, mainly for intermediate-sulfidation epithermal and porphyry-style mineralization.

Introduction

Porphyry deposits are the world's primary source of Cu and Mo, including the largest known economically exploitable accumulations of both elements (Rio Blanco-Los Bronces and El Teniente, central Chile; Sillitoe, 2010). It has long been recognized that most of the giant porphyry deposits, particularly porphyry Cu-Mo deposits, were formed in convergent magmatic arcs under compressional to transpressional conditions, commonly after continental-scale events of crustal thickening, shortening, uplift, and exhumation (e.g., Cooke et al., 2005; Sillitoe, 2010).

This work discusses the district-scale structural geology and explores the tectonic regime prevalent during formation of the Zijinshan mineral district. Zijinshan is a major camp of high- to intermediate-sulfidation epithermal Cu-Au-Ag and porphyry Cu-Mo deposits located in the mountains of Fujian Province, southeastern China, approximately 15 km to the north of the town of Shanghang (Fig. 1). It is the largest epithermal mining district in China (Mao et al., 2007). The district includes the Zijinshan open-pit Cu-Au mine, which exploits a high-sulfidation epithermal system and the Yueyang underground Ag-Cu-Au mine, which exploits intermediate-sulfidation veins about 5 km to the southwest of the Zijinshan open pit (Fig. 1). The Zijinshan Cu-Au deposit is the largest in China, with a total resource of 1.9 Mt Cu and 305 t Au and an annual production of 16 t Au (Jiang et al., 2013). The district also contains porphyry Cu-Mo prospects at Luoboling and Wuziqilong; porphyry to high-sulfidation epithermal prospects at Longjiangting and Ermiaogou; a high-sulfidation prospect at Dajigang; and an intermediate-sulfidation prospect at Gushibei (Fig. 1). The entire Zijinshan district is estimated to contain 2.36 Mt Cu, 323 t Au, 1,554 t Ag, and 4,647 t Mo (Zhong et al., 2014).

Several models have been proposed for the tectonic context of the deposits in the district, including the studies by Feng (1993), So et al. (1998) and Jiang et al. (2015), who concluded that Cretaceous magmatism coeval with hydrothermal activity at Zijinshan occurred in a subduction setting under extensional conditions associated with a steepening subduction angle. Charvret et al. (1994), instead, proposed the existence of a short-lived compressive event coeval with mineralization. Existing geologic maps (e.g., So et al., 1998; Jiang et al., 2013) show two almost orthogonal sets of structures at Zijinshan, with broadly northwest and northeast strikes, and previous studies have highlighted the preferred northwest trend evident in several veins and breccia dikes at Zijinshan (e.g., So et al., 1998). However, no specific studies have been completed regarding the district's structural evolution. Problems such as fault kinematics, stress state during faulting and mineralization, and the detailed relationships between specific structures and hydrothermal fluid flow have not been addressed previously. This study discusses these topics based on kinematic and dynamic analysis of new fault-slip data and the study of syntectonic hydrothermal veins.

† Corresponding author: e-mail, jose.piquer@uach.cl

doi: 10.5382/econgeo.2017.4501
0361-0128/17/1055-20

Submitted: July 28, 2016
Accepted: December 28, 2016

Wu, C., Yano, T., Inomata, M., 1998, Yanshanian orogenies in south China: A relation to Neotethyan evolution: Scientia Geologica Sinica, v. 7, p. 1–10 (in Chinese with English abstract).
Wu, L.Y., Hu, R.Z., Qi, Y.Q., and Zhu, J.J., 2013, Zircon LA-ICP-MS U-Pb ages and geochemical characteristics of quartz syenite porphyry from Jintonghu deposit in Zijinshan ore field, Fujian Province, South China: Acta Petrologica Sinica, v. 29, p. 4151–4166.
Yamaji, A., 2000, The multiple inverse method: A new technique to separate stresses from heterogeneous fault-slip data: Journal of Structural Geology, v. 22, p. 441–452.
Zaw, K., Peters, S.G., Cromie, P., Burrett, C., and Hou, Z., 2007, Nature, diversity of deposit types and metallogenic relations of South China: Ore Geology Reviews, v. 31, p. 3–47.
Zhang, D., Li, D., Feng, C., and Dong, Y., 2001, The temporal and spatial framework of the Mesozoic magmatic system in Zijinshan area and its geological significance: Acta Geologica Sinica, v. 22, p. 403–408.
Zhang, D.Q., Feng, C.Y., Li, D.X., She, H.Q., and Dong, Y.J., 2003, ^{40}Ar–^{39}Ar dating of adularia from Bitian sericite-adularia type epithermal Ag-Au deposit in Fujian Province and its geological significance: Mineral Deposits, v. 22, p. 360–364. (in Chinese with English abstract)
Zhong, J., Chen, Y.-J., Pirajno, F., Chen, J., Li, J., Qi, J.-P., and Li, N., 2014, Geology, geochronology, fluid inclusion and H-O isotope geochemistry of the Luoboling porphyry Cu-Mo deposit, Zijinshan orefield, Fujian Province, China: Ore Geology Reviews, v. 57, p. 61–77.
Zhou, T., Goldfarb, R.J., and Phillips, G.N., 2002, Tectonics and distribution of gold deposits in China—an overview: Mineralium Deposita, v. 37, p. 249–282.
Zhou, X., and Li, W., 2000, Origin of late Mesozoic igneous rocks in southeastern China: Implications for lithosphere subduction and underplating of mafic magmas: Tectonophysics, v. 326, p. 269–287.
Zhou, X., Sun, T., Shen, W., Shu, L., and Niu, Y., 2006, Petrogenesis of Mesozoic granitoids and volcanic rocks in South China: A response to tectonic evolution: Episodes, v. 29, p. 26–33.

Appendix 3 – Outcrop mapping observations

Point	MGA50E	MGA50N	Lithologies	Strain	Feature	Dip	Direction	Comment
MO-001	463564	6567177	Ferruginised granite-gneiss	2				20x20 rubbly patch off side of LAT hill.
MO-002	463516	6567121	Proterozoic dolerite	0				Coarse prot dyke, 5-10% qz.
MO-003	463708	6567009	Proterozoic dolerite	0				North-south, at least 20 m wide.
MO-004	463747	6566989	Biotite monzogranite	0				Fine-med gsz bi monzogranite, with some coarser bi phenocrysts.
MO-005	463793	6567026	Biotite monzogranite	1	Fracture	87	259	South tip of pavement, about 20cm spaced fractures, with some PEGs in same ori.
MO-006	463887	6566972	Biotite monzogranite	1	Fracture	86	281	Spaced fractures, cut by several thin PEGs.
MO-006	463887	6566972	Biotite monzogranite	1	Pegmatite	80	246	Spaced fractures, cut by several thin PEGs.
MO-007	464084	6566683	Laterite, saprolite	0				Pic of typical laterite over saprolite profile.
MO-008	464206	6566615	Ferruginised granite-gneiss, laterite	1				Rubbly ferruginous "gneiss" at tip of laterite hill, close to source?
MO-009	463990	6566274	Migmatised K-feldspar phyric granitoid	2	Banding	57	86	Clearly banded kf-phyric bi monzogranite, with zone of migmatisation - clear bi-rich and qz-fl-rich zones. Dip of banding variable, but always east, and is irregularly wobbled/folded. PEGs with bi-rich selvedge cuts brittle E-W one. Wobbly Z-vergent folds dominate outcrop, ~NW-trending axial planes - or dextral kink bands?
MO-009	463990	6566274	Migmatised K-feldspar phyric granitoid	2	Pegmatite	73	85	Clearly banded kf-phyric bi monzogranite, with zone of migmatisation - clear bi-rich and qz-fl-rich zones. Dip of banding variable, but always east, and is irregularly wobbled/folded. PEGs with bi-rich selvedge cuts brittle E-W one. Wobbly Z-vergent folds dominate outcrop, ~NW-trending axial planes - or dextral kink bands?
MO-010	464044	6566416	K-feldspar-phyric biotite monzogranite	2	Foliation	62	66	Weak ductile foln in GT, with gneiss/migmatite to west. Fol goes across trend of unit?
MO-011	464006	6566481	K-feldspar-phyric biotite monzogranite	1				Intense silica alteration associated with irregular pegmatites in GT.
MO-012	463980	6566478	K-feldspar-phyric biotite monzogranite	1				Coarse bi clots in kf-phyric GT, close to gneiss/migmatite transition.
MO-013	464001	6566404	Migmatised K-feldspar phyric granitoid	2	Banding	75	53	Photo 3510 of typical arrangement of gneissic banding, cut by more NW-trending pegmatites - but both are irregularly folded together. Photo 3511 of definite ductile foliation acute to banding.
MO-013	464001	6566404	Migmatised K-feldspar phyric granitoid	2	Foliation	56	44	Photo 3510 of typical arrangement of gneissic banding, cut by more NW-trending pegmatites - but both are irregularly folded together. Photo 3511 of definite ductile foliation acute to banding.
MO-014	463984	6566582	K-feldspar-phyric biotite monzogranite	1				Very weakly foliated kf-phyric granite, typical texture, abundant phenos to 12mm. About 30% qz in this rock.
MO-015	463769	6566656	Ferruginised granite-gneiss	3	Vein - quartz-sulphide	80	47	Ferruginous (ex sulphide?) PEG and granite, cut by N-S fractures, right at footwall of migmatite/gneiss - likely mineralisation zone.
MO-015	463769	6566656	Ferruginised granite-gneiss	3	Fracture	77	85	Ferruginous (ex sulphide?) PEG and granite, cut by N-S fractures, right at footwall of migmatite/gneiss - likely mineralisation zone.
MO-016	463814	6566874	Biotite monzogranite, K-feldspar-phyric biotite monzogranite	1				Approx contact into ksp-phyric gneiss package. Coarse biotite clots in massive bi mzGT, close to contact, as per previous observations.

MO-038	465187	6567756	Banded, K-feldspar-phyric granitoid	2	Banding	88	101	Banded granite, cut by NW-trending fractures with apparent dextral sense. Hints of NW-trending fabric also (S2?), unclear dip. Recrystallisation in 070-trending dextral kink bands/ax planes. Pic 3542 is of divergent banding and foliation (S1) - can't measure dips, sadly.
MO-038	465187	6567756	Banded, K-feldspar-phyric granitoid	2	Fracture	56	69	Banded granite, cut by NW-trending fractures with apparent dextral sense. Hints of NW-trending fabric also (S2?), unclear dip. Recrystallisation in 070-trending dextral kink bands/ax planes. Pic 3542 is of divergent banding and foliation (S1) - can't measure dips, sadly.
MO-039	465081	6567821	Banded granitoid, amphibolite	2	Banding	81	106	40cm MA band. Highly variable rock with moderate ductile foln, still with Z-vergent or dextral kink bands. Pic 3536 of shallow N-plunging Z-vergent, possible F2 fold?
MO-040	464708	6567794	Banded granitoid	3	S1 foliation	62	88	Quite foliated, with coarseish kf phenos.
MO-041	464964	6567607	Banded granitoid	3	Cleavage	74	219	Start of higher strain banded granite (to east). Note clotting of biotite, and kinking by NE-trending cleavage.
MO-041	464964	6567607	Banded granitoid	3	S1 foliation	72	111	Start of higher strain banded granite (to east). Note clotting of biotite, and kinking by NE-trending cleavage.
MO-042	465000	6567518	Banded granitoid	3	Cleavage	72	331	In pics 3539 and 3541, note that qz-rich GT/PEGs cut S1, but then all is folded - important timing constraint!
MO-042	465000	6567518	Banded granitoid	3	Fold axis	62	53	In pics 3539 and 3541, note that qz-rich GT/PEGs cut S1, but then all is folded - important timing constraint!
MO-042	465000	6567518	Banded granitoid	3	S1 foliation	62	99	In pics 3539 and 3541, note that qz-rich GT/PEGs cut S1, but then all is folded - important timing constraint!
MO-043	464717	6567429	Banded granitoid	2	Banding	64	92	East edge of outcrop, quite massive.
MO-044	464849	6567129	Biotite monzogranite	2	S1 foliation	67	96	Small outcrop, mod foln, no banding.
MO-045	464956	6567127	Biotite monzogranite, banded granitoid	2	S1 foliation	55	83	
MO-046	465118	6567371	K-feldspar-phyric biotite monzogranite	1	S1 foliation	62	89	Very low strain outcrop with rare banding, no PEGs.
MO-047	465327	6567924	Banded granitoid, biotite monzogranite	2	S1 foliation	68	67	Representative S1 from adjacent to massive, coarse bi mzGT. S1 very wobbly near contact, chaotic. Pic 3543 of qz-rich GT dyke cutting banded granite. Paragenesis = Banded granite, then bimzGT, then D1/S1, then late GT - consistent with core obs.
MO-048	465900	6567281	Banded granitoid	2				Kf-megacrystic bimzGT cuts earlier bi-rich bands - consistent with core obs.
MO-049	465943	6567240	Banded granitoid	3	S1 foliation	77	85	Complicated outcrop - fold of bi-rich band (mafic/sed precursor) is possibly F1, and megacrystic unit post-dates it. Fold may be even earlier than "D1". Pic 3548 of coarse bi selvedge on contact between biGT and megacrystic GT.
MO-049	465943	6567240	Banded granitoid	3	Shear	68	129	Complicated outcrop - fold of bi-rich band (mafic/sed precursor) is possibly F1, and megacrystic unit post-dates it. Fold may be even earlier than "D1". Pic 3548 of coarse bi selvedge on contact between biGT and megacrystic GT.
MO-049	465943	6567240	Banded granitoid	3	Vein - quartz-epidote	84	259	Complicated outcrop - fold of bi-rich band (mafic/sed precursor) is possibly F1, and megacrystic unit post-dates it. Fold may be even earlier than "D1". Pic 3548 of coarse bi selvedge on contact between biGT and megacrystic GT.

MO-049	465943	6567240	Banded granitoid	3	Contact	75	289	Complicated outcrop - fold of bi-rich band (mafic/sed precursor) is possibly F1, and megacrystic unit post-dates it. Fold may be even earlier than "D1". Pic 3548 of coarse bi selvedge on contact between biGT and megacrystic GT.
MO-050	465873	6567166	Proterozoic dolerite, K-feldspar megacrystic biotite monzogranite	1	S1 foliation	70	71	At least 10m thick megacrystic granite, very weak foln.
MO-051	463144	6573978	Laterite					Sump.
MO-052	462966	6574597	Proterozoic dolerite	0				Very coarse prot dyke in two patches.
MO-053	463360	6574113	Saprolite	1	Foliation	77	67	Sump. Weak fabric in saprolite.
MO-055	463500	6574113	Saprolite	1	Foliation	82	55	Sump. Weak fabric in saprolite.
MO-056	463662	6574095	Saprolite	0				Sump. Massive SAP clay.
MO-057	463978	6572916	Coarse biotite granitoid	2	S1 foliation	75	70	Cleavage creates vague Z-vergent wobbles of S1. Pic 3561 depicts approx hinge zone in isolated outcrop block. Pic 3563 of definite fold zone, seem steepish plunging.
MO-057	463978	6572916	Coarse biotite granitoid	2	Cleavage	68	231	Cleavage creates vague Z-vergent wobbles of S1. Pic 3561 depicts approx hinge zone in isolated outcrop block. Pic 3563 of definite fold zone, seem steepish plunging.
MO-058	463930	6573041	Coarse biotite granitoid	2	S1 foliation	50	278	Coarse, quite bi-rich GT, similar to stockwork-affected rock at Dasher core. East edge of outcrop, strongly foliated, possibly some west dips?
MO-059	464027	6572870	Coarse biotite granitoid	2	S1 foliation	75	305	Thin fracs/silic zones/veins cut variable foln. Typical 050-trending kinks bands also present.
MO-059	464027	6572870	Coarse biotite granitoid	2	Cleavage	82	84	Thin fracs/silic zones/veins cut variable foln. Typical 050-trending kinks bands also present.
MO-060	463978	6572778	Coarse porphyritic biotite granitoid	2	S1 foliation	70	273	Moderate foln in weakly kf-phyric, coarse granite.
MO-061	463946	6572786	Coarse biotite granitoid	2	S1 foliation	82	87	Some fractures are discrete brittle-ductile zones. Some silic/altd patches here, like MO-059.
MO-061	463946	6572786	Coarse biotite granitoid	2	Fracture	78	208	Some fractures are discrete brittle-ductile zones. Some silic/altd patches here, like MO-059.
MO-062	463910	6572760	Coarse porphyritic biotite granitoid, biotite monzogranite	1	Contact	74	261	Contact between GT types. Coarse kf-phenos right at margin. The coarser biGT seems younger than the fine stuff.
MO-063	463875	6572717	Coarse biotite granitoid	2				Back into coarse unit.
MO-064	463866	6572755	Coarse biotite granitoid	2	S1 foliation	76	53	Small outcrop patch with very different S1 - fold limb?
MO-065	463760	6572616	Granitic saprolite, ferruginised granite-gneiss	4	Fault	51	159	Unusual high strain outcrop, assoc with ferruginisation. Definite granitoid. Rubbly, ferruginous fault measured, pretty accurate.
MO-065	463760	6572616	Granitic saprolite, ferruginised granite-gneiss	4	Foliation	82	89	Unusual high strain outcrop, assoc with ferruginisation. Definite granitoid. Rubbly, ferruginous fault measured, pretty accurate.
MO-066	463565	6572573	Saprolite					Sump.
MO-067	463222	6572577	Saprolite					Sump. Looks foliated, but inaccessible.
MO-068	463044	6572584	Saprolite					Sump. No fabric.
MO-069	462906	6574620	Proterozoic dolerite	1	Fracture	82	171	Clear spaced fracture in gabbroic prot dyke - parallel to dyke ori?

MO-070	471644	6572453	Coarse K-feldspar-phyric granitoid	2	Foliation	55	229	Consistent foln in coarse, true granite? Lots of qz and kf. Kf aligned to strongish foln. Later brit-duct fault and Vqz.
MO-070	471644	6572453	Coarse K-feldspar-phyric granitoid	2	Vein - quartz-epidote	72	273	Consistent foln in coarse, true granite? Lots of qz and kf. Kf aligned to strongish foln. Later brit-duct fault and Vqz.
MO-071	471595	6572638	Proterozoic dolerite					Very thick EW dyke. Some breccia GT rubble to south?
MO-072	473956	6572600	Coarse porphyritic biotite granitoid	1				320-trending foln, consistently foliated (no dip possible), magnetite-bearing, coarse bi granite. Quite a lot of coarse primary (?) magnetite.
MO-073	480455	6575653	Granitoid	1				Coarse qz-kf-pl granite, mica-poor, otherwise similar to MO-073, but without magnetite. Weak foln or mineral alignment.
MO-074	477655	6574828	Biotite granitoid	0				Large, very homogenous outcrop of kf-poor bi GT - very weak fol, no PEGs, no banding.
MO-075	473561	6583554	Biotite granitoid	0				Christmas Rock granite near town, very plain, equigranular, weakly magnetic, bi GT.
MO-076	465439	6578556	Intermediate schist	3	S1 foliation	70	239	Excellent sump with clear S1 and L1, lin defined by feldspars (now clay). Andesitic parent? Fol clearly cut by abundant fracs and ferrug veins (min-stage, post-D1?).
MO-076	465439	6578556	Intermediate schist	3	L1 stretching	31	303	Excellent sump with clear S1 and L1, lin defined by feldspars (now clay). Andesitic parent? Fol clearly cut by abundant fracs and ferrug veins (min-stage, post-D1?).
MO-076	465439	6578556	Intermediate schist	3	Fracture	78	303	Excellent sump with clear S1 and L1, lin defined by feldspars (now clay). Andesitic parent? Fol clearly cut by abundant fracs and ferrug veins (min-stage, post-D1?).
MO-077	465489	6578703	Garnet-sillimanite schist	3	S1 foliation	79	266	Gt-sm-bearing schist. Note ~3cm mt-rich band left of pencil - this is folded with S1?
MO-078	465463	6578748	Sillimanite schist	3	S1 foliation	75	254	Ferrug outcrop.
MO-079	465442	6578842	Sillimanite schist	3	S1 foliation	78	267	Sump. White sm-rich schist, fine gsz, consistent.
MO-080	465435	6579002	Sillimanite schist	3	S1 foliation	78	253	
MO-081	465417	6579046	Sillimanite schist, granitoid, quartz vein	4	S1 foliation	78	286	Red schist in contact with 1m GT dyke (no strain). Sericite-sm rock (?), with rubbly Vqz to west - with old workings? Likely decent fault zone.
MO-082	465547	6579002	Garnetiferous mafic schist	3	S1 foliation	82	264	Finer, mafic (?) rock with bands of garnet.
MO-083	465643	6578990	Sillimanite-mica schist.	4				Sump. Possibly folded sm-mu-rich schist SAP, greasy, glittery SAP. Can't get in sump to measure anything.
MO-084	465778	6578970	Massive hematite-magnetite rock	3	Foliation	23	40	Massive hm-mt rock trends ~330, but is cut by by shallow foln. Hints of S2 and shallow NW-plunging folds just to south?
MO-084	465778	6578970	Massive hematite-magnetite rock	3	S1 foliation	62	249	Massive hm-mt rock trends ~330, but is cut by by shallow foln. Hints of S2 and shallow NW-plunging folds just to south?
MO-084	465778	6578970	Massive hematite-magnetite rock	3	S2 foliation	85	59	Massive hm-mt rock trends ~330, but is cut by by shallow foln. Hints of S2 and shallow NW-plunging folds just to south?
MO-085	465832	6578867	Quartz vein	3	S1 foliation	71	268	5m wide coarse (rex?) Vqz seems ~parallel to S1, cut by brittle fracture set.
MO-085	465832	6578867	Quartz vein	3	Fracture	78	161	5m wide coarse (rex?) Vqz seems ~parallel to S1, cut by brittle fracture set.
MO-086	465876	6578819	Garnet-sillimanite schist	3	Fold axis	36	344	Qz-fe veins folded into NNW-plunging folds - not clear if S1 also folded, these may be F1? No clear evidence that gt predates S1 - probably post?
MO-086	465876	6578819	Garnet-sillimanite schist	3	Vein - quartz	51	293	Qz-fe veins folded into NNW-plunging folds - not clear if S1 also folded, these may be F1? No clear evidence that gt predates S1 - probably post?

MO-086	465876	6578819	Garnet-sillimanite schist	3	Vein - quartz	52	29	Qz-fe veins folded into NNW-plunging folds - not clear if S1 also folded, these may be F1? No clear evidence that gt predates S1 - probably post?
MO-086	465876	6578819	Garnet-sillimanite schist	3	Cleavage	70	268	Qz-fe veins folded into NNW-plunging folds - not clear if S1 also folded, these may be F1? No clear evidence that gt predates S1 - probably post?
MO-087	465866	6578801	Garnet-sillimanite schist	3	S1 foliation	72	271	Qz-fe vein cuts S1. S1 measured nearby, not at pic.
MO-088	465922	6578778	Massive hematite-magnetite rock	1	Bedding	72	269	Massive fmgsz, soft, hm-mt-ch rock, about 3m wide. Low strain. Not sure what this rock is?
MO-089	465869	6578652	Sillimanite schist	3	S1 foliation	45	343	Pic of possible S1/S2 relations. This end of outcrop definitely on a different ori. Vague fold axes measured.
MO-089	465869	6578652	Sillimanite schist	3	L1 stretching	40	311	Pic of possible S1/S2 relations. This end of outcrop definitely on a different ori. Vague fold axes measured.
MO-089	465869	6578652	Sillimanite schist	3	S2 foliation	84	106	Pic of possible S1/S2 relations. This end of outcrop definitely on a different ori. Vague fold axes measured.
MO-089	465869	6578652	Sillimanite schist	3	Fold axis	38	9	Pic of possible S1/S2 relations. This end of outcrop definitely on a different ori. Vague fold axes measured.
MO-090	465846	6578642	Quartz vein, ferruginous schist	3	Vein - quartz-iron	63	293	Ferrug VQ with tarnished sulphides present.
MO-091	465704	6578432	Schist	3	S1 foliation	62	288	No distinctive sm or gt. Vqz rubble at east outcrop edge.
MO-092	465297	6578711	Mafic schist, amphibolite	3	S1 foliation	77	245	Fairly clear mafic (amphibolite) "schist" with S1 running across more N-S bands. Strongish rodding/min lin. No gt or sm - mostly chlorite (?), but some dark porphyroblasts, likely mt (oxidised to hm).
MO-092	465297	6578711	Mafic schist, amphibolite	3	L1 stretching	46	325	Fairly clear mafic (amphibolite) "schist" with S1 running across more N-S bands. Strongish rodding/min lin. No gt or sm - mostly chlorite (?), but some dark porphyroblasts, likely mt (oxidised to hm).
MO-093	465043	6579250	Quartz vein	4	Fracture	65	313	Big patch of qz and silic GT (?), likely fault.
MO-094	464747	6579979	BIF, amphibolite	3	Bedding	32	298	Close-spaced cleavage, forms int lin. S1 and L1 in adjacent wthd MA suggests (together with S0) that F1 synform is to the west.
MO-094	464747	6579979	BIF, amphibolite	3	Cleavage	82	198	Close-spaced cleavage, forms int lin. S1 and L1 in adjacent wthd MA suggests (together with S0) that F1 synform is to the west.
MO-094	464747	6579979	BIF, amphibolite	3	S1 foliation	67	274	Close-spaced cleavage, forms int lin. S1 and L1 in adjacent wthd MA suggests (together with S0) that F1 synform is to the west.
MO-094	464747	6579979	BIF, amphibolite	3	L1 stretching	50	335	Close-spaced cleavage, forms int lin. S1 and L1 in adjacent wthd MA suggests (together with S0) that F1 synform is to the west.
MO-095	465945	6579853	Mafic schist	3	S1 foliation	48	305	Ferrug schist, typical, probable mafic parent.
MO-096	466089	6578890	Saprolite, ferruginous saprolite	2	S1 foliation	63	286	Very ferrug sap (after sed/mafic?) overlies leached sap. Possible GT at east outcrop edge. Quite low strain. Clear later cleavage creates intersection lin. Pic of clearly banded sparolite - layered sequence like 08WHDDH001? Likely same later cleavage as MO-094.

MO-096	466089	6578890	Saprolite, ferruginous saprolite	2	Cleavage	58	228	Very ferrug sap (after sed/mafic?) overlies leached sap. Possible GT at east outcrop edge. Quite low strain. Clear later cleavage creates intersection lin. Pic of clearly banded sparolite - layered sequence like 08WHDDH001? Likely same later cleavage as MO-094.
MO-097	465515	6578022	Amphibolite, granitoid	2	S1 foliation	76	61	Sump. Mafic sap/MA mod foliated, looks chloritic, cut by weathered 5cm GT dyke.
MO-098	465632	6577973	Amphibolite	1				30m wide massive to very weak fol MA trending about 155.
MO-099	465486	6577997	Amphibolite, schist	3	S1 foliation	44	326	Very odd S1 ori with faint, brittle "S2" cleavage. S1 highly variable through outcrop, into NNW-plunging fold of unknown vergence.
MO-099	465486	6577997	Amphibolite, schist	3	Cleavage	82	243	Very odd S1 ori with faint, brittle "S2" cleavage. S1 highly variable through outcrop, into NNW-plunging fold of unknown vergence.
MO-100	465448	6577995	Amphibolite, schist	3	S1 foliation	50	241	Vergence just west of MO-099, indicates synform to west, locally. Later 5mm-spaced cleavage in local zones, similar to observed further north.
MO-100	465448	6577995	Amphibolite, schist	3	S2 foliation	77	41	Vergence just west of MO-099, indicates synform to west, locally. Later 5mm-spaced cleavage in local zones, similar to observed further north.
MO-100	465448	6577995	Amphibolite, schist	3	Cleavage	80	158	Vergence just west of MO-099, indicates synform to west, locally. Later 5mm-spaced cleavage in local zones, similar to observed further north.
MO-101	465327	6577939	Saprolite	2	Cleavage	84	30	Unidentified pale saprolite (sed?). Layering/S1 cut by quite strong cleavage/fracture in zones. Qz rubble to west.
MO-101	465327	6577939	Saprolite	2	Banding	46	252	Unidentified pale saprolite (sed?). Layering/S1 cut by quite strong cleavage/fracture in zones. Qz rubble to west.
MO-102	465402	6577796	Mafic schist	3	S1 foliation	78	71	Likely chloritic schist/MA.
MO-103	465394	6577855	Mafic schist	3	S1 foliation	82	66	Ferrug MA likely.
MO-104	465405	6577633	Biotite granitoid, chlorite-biotite schist	3	S1 foliation	69	61	Sump. Pre-foliated "greenstone" xenolith in bi GT. Xenolith strongly cooked, with very coarse biotite, no garnet/sillimanite - so this granite is not responsible for hg metamorphism! Granite is 5%bi, equigranular GT with occasional coarse qz eyes.
MO-104	465405	6577633	Biotite granitoid, chlorite-biotite schist	3	L1 stretching	18	341	Sump. Pre-foliated "greenstone" xenolith in bi GT. Xenolith strongly cooked, with very coarse biotite, no garnet/sillimanite - so this granite is not responsible for hg metamorphism! Granite is 5%bi, equigranular GT with occasional coarse qz eyes.
MO-104	465405	6577633	Biotite granitoid, chlorite-biotite schist	3	Dyke	57	271	Sump. Pre-foliated "greenstone" xenolith in bi GT. Xenolith strongly cooked, with very coarse biotite, no garnet/sillimanite - so this granite is not responsible for hg metamorphism! Granite is 5%bi, equigranular GT with occasional coarse qz eyes.
MO-104	465405	6577633	Biotite granitoid, chlorite-biotite schist	3	Contact	78	241	Sump. Pre-foliated "greenstone" xenolith in bi GT. Xenolith strongly cooked, with very coarse biotite, no garnet/sillimanite - so this granite is not responsible for hg metamorphism! Granite is 5%bi, equigranular GT with occasional coarse qz eyes.
MO-105	465452	6577613	Biotite granitoid, chlorite-biotite schist, pegmatite	3	S1 foliation	82	75	Sump. Mostly bi GT, but invaded by irregular PEG array. Pic of PEGs invading schist with cgsz biotite.
MO-106	465698	6577780	Amphibolite	2	S1 foliation	88	231	
MO-107	465818	6577730	Amphibolite?	2	S1 foliation	78	256	Leached sap, probable MA.
MO-108	465828	6577638	Amphibolite?	2	S1 foliation	78	243	Fairly uniform, likely chloritic MA sap beneath LAT.

MO-109	466236	6577623	Muscovite schist.	2	Bedding	75	253	Pic of definite compositional banding in sed (?) schist - leached, but looks micaceous. S1 is layer-parallel, and there are no later fabrics present.
MO-110	466218	6577511	Granitoid	1				Fine, hard, qz-rich sap - granite?
MO-111	465974	6577565	Quartz-mica schist	3	S1 foliation	62	274	F-m gsz qz-bearing schist, prob same rock as MO-110, but deformed. Pic 3615 just south of ferrug band with cgsz elongated white porphyroblasts or phenocrysts - prob former feldspar, andesite parent?
MO-111	465974	6577565	Quartz-mica schist	3	L1 stretching	45	337	F-m gsz qz-bearing schist, prob same rock as MO-110, but deformed. Pic 3615 just south of ferrug band with cgsz elongated white porphyroblasts or phenocrysts - prob former feldspar, andesite parent?
MO-112	465347	6577086	Biotite granitoid	1	Vein - biotite	61	75	Massive, 5-10% bi GT, equigranular, ~3mm gsz. Interesting coarse biotite alteration bands, folded, and with foliated biotite selvedges - poss min-related, and preserve stress field in selvedge? Flattish sweaty PEGs also - cut bi-rich zones?
MO-112	465347	6577086	Biotite granitoid	1	Fracture	82	38	Massive, 5-10% bi GT, equigranular, ~3mm gsz. Interesting coarse biotite alteration bands, folded, and with foliated biotite selvedges - poss min-related, and preserve stress field in selvedge? Flattish sweaty PEGs also - cut bi-rich zones?
MO-112	465347	6577086	Biotite granitoid	1	Foliation	70	67	Massive, 5-10% bi GT, equigranular, ~3mm gsz. Interesting coarse biotite alteration bands, folded, and with foliated biotite selvedges - poss min-related, and preserve stress field in selvedge? Flattish sweaty PEGs also - cut bi-rich zones?
MO-113	465360	6576975	Biotite granitoid	1	Vein - biotite	38	261	Pic of biotite vein with rex+kf halo. Common late fractures measured also.
MO-113	465360	6576975	Biotite granitoid	1	Fracture	73	41	Pic of biotite vein with rex+kf halo. Common late fractures measured also.
MO-114	465388	6576920	Biotite granitoid	1	Dyke	82	354	10cm prot dyke cuts GT, sinistrally offsets pegmatites. 3 dykes in vicinity. Main PEG ori measured.
MO-114	465388	6576920	Biotite granitoid	1	Pegmatite	70	51	10cm prot dyke cuts GT, sinistrally offsets pegmatites. 3 dykes in vicinity. Main PEG ori measured.
MO-115	465167	6577080	Biotite granitoid	1	Vein - chlorite	65	164	1m wide zone of anastomosing, chloritic fractures/veins.
MO-116	465140	6577177	Biotite granitoid	1	Fracture	65	225	Main spaced fracture set. West tip of this outcrop has freshish material - in case required for geochem/dating. Rock around 5%bi, 35% qz, 60% fl.
MO-117	465410	6577267	Biotite granitoid	1	Pegmatite	82	15	Coarser and kf-phyric bi GT, cut by several coarse, late GT dykes.
MO-117	465410	6577267	Biotite granitoid	1	Vein - biotite	42	71	Coarser and kf-phyric bi GT, cut by several coarse, late GT dykes.
MO-118	466470	6558756	Granitic gneiss	3	S1 foliation	52	9	Genuine high strain gneiss - very good. Affected by ~N-S cren??
MO-119	466317	6559148	Biotite granitoid	0				Undeformed 5-10% bi GT, 35% qz, equigranular.
MO-120	466361	6559217	Diorite	1				Qz-poor, pyroxene-phyric rock, diorite? Sample taken.
MO-121	466230	6559073	Granitic gneiss	4	S1 foliation	77	21	Strongly banded gneiss, with leucosomes sometimes cutting melanosome foliation.
MO-122	466196	6559043	Granitoid, granite-gneiss	3	S1 foliation	67	18	Lower strain version of MO-121, still with leucosome partial melts, but more recognisable as GT parent?
MO-123	466125	6559066	Granitic gneiss	4	S1 foliation	72	24	075-trending fold axis, one example only. High strain gneiss. Hints of 315-trending foln cutting banding in many areas (pic 3469). Possibly same fabric that weakly affects regional granites?

MO-123	466125	6559066	Granitic gneiss	4	S1 foliation	43	121	075-trending fold axis, one example only. High strain gneiss. Hints of 315-trending foln cutting banding in many areas (pic 3469). Possibly same fabric that weakly affects regional granites?
MO-123	466125	6559066	Granitic gneiss	4	Foliation	67	41	075-trending fold axis, one example only. High strain gneiss. Hints of 315-trending foln cutting banding in many areas (pic 3469). Possibly same fabric that weakly affects regional granites?
MO-124	465998	6559216	Doleritic amphibolite	2	Foliation	73	225	Thoroughly kf-ep altered doleritic amphibolite, highly foliated/fractured in measured ori - fault? Pic 3650 of px-phyric "diorite" to south.
MO-125	465991	6559186	Biotite granitoid	1	Foliation	56	26	Coarse bi GT cut by weak foln oblique to trend of rocks.
MO-126	466083	6558993	Biotite granitoid	1	Foliation	63	21	Coarse oldish GT again cut by weak foln going across lith trend.
MO-127	466108	6558943	Granitic gneiss	3	S1 foliation	57	24	Well-defined band in granitic gneiss, rare folds, but not clearly insitu.
MO-128	466274	6558907	Granitoid, granite-gneiss	2	S1 foliation	73	25	
MO-129	466240	6558835	Granitic gneiss	3	S1 foliation	66	15	
MO-130	465995	6558871	Granitic gneiss	3	S1 foliation	56	25	
MO-131	465771	6558964	Granitoid	1	S1 foliation	72	21	
MO-132	465729	6558923	Granitoid, granite-gneiss	3	S1 foliation	77	35	Likely kf-phyric precursor rock. Note that PD cuts foln thru this area.
MO-133	465627	6558830	Granitoid, granite-gneiss	3	S1 foliation	62	39	
MO-134	465714	6558682	Mica schist, saprolite	3	S1 foliation	65	31	Fm gsz weathered micaceous schist (saprolitic) - greenstone parent, sed?
MO-135	466300	6558697	Granitic gneiss	4	S1 foliation	53	19	Typical coarse gneiss.
MO-136	466183	6558756	Granitic gneiss	4	S1 foliation	68	19	
MO-137	465031	6559531	Granitic gneiss, saprolite	4	S1 foliation	72	9	Weathered, banded gneiss.
MO-138	468767	6560425	Granitoid	0				Sump. Massive granite.
MO-139	468821	6560538	Granitoid	0				Sump. Massive granite.
MO-140	468723	6560525	Granitoid	2	Vein	52	148	Sump. Foliated granite, with limonitic veins/fractures. Sump smells strongly of sulphur.
MO-140	468723	6560525	Granitoid	2	S1 foliation	46	349	Sump. Foliated granite, with limonitic veins/fractures. Sump smells strongly of sulphur.
MO-141	468807	6560688	Biotite granitoid	2	S1 foliation	46	14	Sump.
MO-150	468720	6560689	Granitic gneiss	3	S1 foliation	50	16	Sump. Gneissic banding measured, smells sulphidic in here.
MO-151	468633	6560687	Granitoid	1				Sump. Plain, fairly coarse GT.
MO-152	468616	6560525	Granitoid, granite-gneiss	2	Banding	66	30	Sump. Bi-rich band in coarse, low strain GT.
MO-153	468666	6560423	Granitoid	0				Sump. Coarse, massive granite, quite qz-rich.
MO-154	472522	6582577	Granitoid	0				Very coarse 5%bi-40%qz GT on edge of town, dated 2651Ma.
MO-155	460150	6570594	Granitoid	1	S1 foliation	77	276	Fine GT sap, clear fabric/layering.
MO-156	460266	6570188	Granitoid, quartz vein	4	Fault	72	317	Fracturing on edge of very thick qz blow.
MO-157	460384	6570195	Granitoid, quartz vein	4				Approx south edge of vein/fault zone, possibly even wider.
MO-158	459887	6569829	Granitoid, quartz vein	5	Fault	28	316	Strong fault/vein in granite, possible sinistral S-C?
MO-159	460503	6568922	Granitoid	2	Foliation	18	346	Dam. Mostly massive granite sap, but with shallow dipping fol (flatted qz) and veining at west edge - S1??
MO-160	460332	6568891	Granitoid	3	S1 foliation	64	285	Excellent likely F2 folds with shallow north plunge. 64/284 ori is likely long limb - antiform to east vergence.

MO-160	460332	6568891	Granitoid	3	S1 foliation	37	83	Excellent likely F2 folds with shallow north plunge. 64/284 ori is likely long limb - antiform to east vergence.
MO-160	460332	6568891	Granitoid	3	S2 foliation	86	116	Excellent likely F2 folds with shallow north plunge. 64/284 ori is likely long limb - antiform to east vergence.
MO-161	460147	6568834	Biotite granitoid	3	S1 foliation	42	8	Similar setup to MO-160, with clearly two S1 oris (folded). No hinges observable. Short limb cut by steep likely S2 (axial planar).
MO-161	460147	6568834	Biotite granitoid	3	S1 foliation	64	286	Similar setup to MO-160, with clearly two S1 oris (folded). No hinges observable. Short limb cut by steep likely S2 (axial planar).
MO-161	460147	6568834	Biotite granitoid	3	S2 foliation	72	273	Similar setup to MO-160, with clearly two S1 oris (folded). No hinges observable. Short limb cut by steep likely S2 (axial planar).
MO-162	460390	6568778	Granitoid, granite-gneiss	4	S1 foliation	53	251	Pic of short limb S1/S2 relations - note more NW-trending fractures/kink bands also (common, sinistral).
MO-162	460390	6568778	Granitoid, granite-gneiss	4	S1 foliation	37	355	Pic of short limb S1/S2 relations - note more NW-trending fractures/kink bands also (common, sinistral).
MO-162	460390	6568778	Granitoid, granite-gneiss	4	S2 foliation	75	96	Pic of short limb S1/S2 relations - note more NW-trending fractures/kink bands also (common, sinistral).
MO-163	460305	6571971	Coarse biotite granitoid	1	S1 foliation	70	236	Coarse bi GT, very weak S1 foln, cut by 40cm bi-rich (20%) GT dykes, all cut by WNW-trending PEGs. Some aplite dykes parallel to S1.
MO-163	460305	6571971	Coarse biotite granitoid	1	Dyke	34	327	Coarse bi GT, very weak S1 foln, cut by 40cm bi-rich (20%) GT dykes, all cut by WNW-trending PEGs. Some aplite dykes parallel to S1.
MO-164	460263	6573522	Granitoid	1	S1 foliation	70	285	Low strain GT sap, higher strain GT rubble lies east.
MO-165	459292	6569592	Granitoid	4	Fault	42	336	Thick high strain zone.
MO-166	459195	6568651	Granitoid	1				Med gsz massive bi GT, Pics of fine gsz mafic just north - lots of rubble. Looks like basalt, possibly even at greenschist facies??
MO-167	459023	6568841	Mica schist	3	S1 foliation	46	236	Good outcrop of red, fine-grained micaceous saprolite, likely chloritic mafic. Quite strong cleavage causes Z-vergent folds with shallow west plunges. Evidence of irregular folding/interference in rubbly pieces.
MO-167	459023	6568841	Mica schist	3	Cleavage	82	6	Good outcrop of red, fine-grained micaceous saprolite, likely chloritic mafic. Quite strong cleavage causes Z-vergent folds with shallow west plunges. Evidence of irregular folding/interference in rubbly pieces.
MO-168	459320	6569655	Ferruginous schist	4				Ferruginous fine gsz rubble with quartz veining (sampled).
MO-169	459242	6569623	Sedimentary schist	3				Rubble of fine sed (?) schist, some bits with altn and oxide Cu? (sampled).
MO-170	459888	6569526	Quartz-mica schist	3	S1 foliation	41	251	Very good outcrop of mica+qz schost with compositional banding. Note pervasive EW cleavage in pic, also note earlier folding of Vqz. Quite complexly deformed.
MO-170	459888	6569526	Quartz-mica schist	3	Cleavage	77	349	Very good outcrop of mica+qz schost with compositional banding. Note pervasive EW cleavage in pic, also note earlier folding of Vqz. Quite complexly deformed.
MO-171	463304	6566939	K-feldspar-phyric biotite monzogranite	1				Small patch west of Dasher, with abundant poikilitic kf phenos to 20 mm, megacrystic.
MO-172	470210	6575662	K-feldspar-phyric biotite monzogranite	2	Foliation	70	226	Bi-rich (20%), kf-phyric, moderate strain GT/GN, with thin sweaty PEGs (partial melts?). This is an "old" granite, and is dated at 3.0 Ga (crystallisation), with a 2.8 Ga component (migmatisation?). Big prot dyke hill to northeast.

Appendix 4 – Dasher pavement outcrop map

Pavement centred south of Dasher at ~6566260N/463980E (MGA Zone 50).

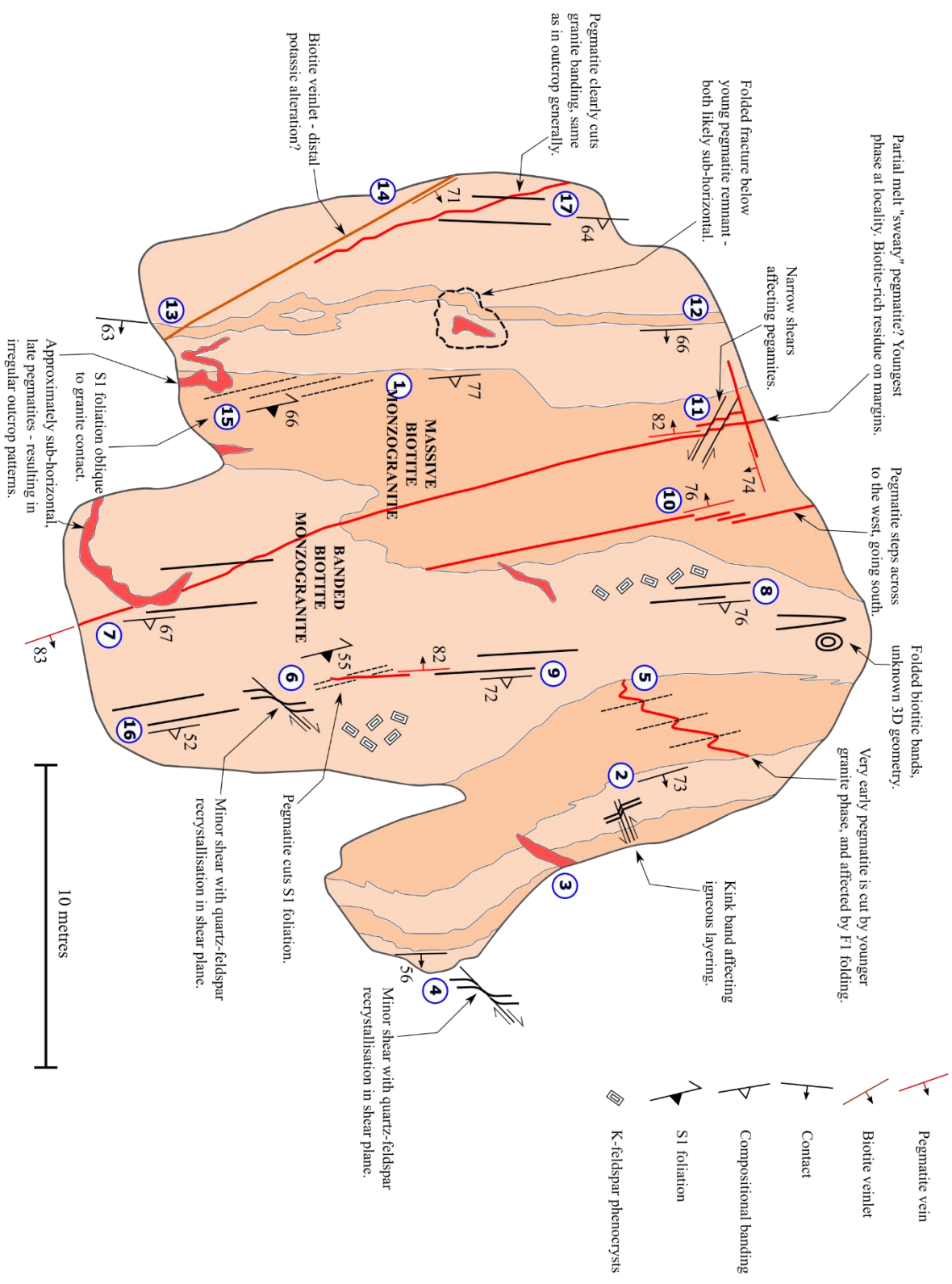

Appendix 5 – Drill core sample details

				Relevant structure measurements (dip/dip direction, or plunge-trend)		Orientation of thin-section with slide in drilled orientation (notch at top-of-hole)
Sample	Hole ID	From (m)	To (m)	Structure 1	Structure 2	
CAL004	12CADD002	36.26	36.36	S1 81/088	Vcppych 55/83	Looking north
CAL006	12CADD002	47.00	47.27	S1 54/062	Kf bands 51/096	Looking north
CAL007	12CADD002	48.60	48.85	S1 46/057		Looking north
CAL008	12CADD002	52.18	52.28	S1/Vcppoch 56/093		Looking north
CAL009	12CADD002	66.64	66.74	Vmo 67/031		N/A
CAL010	12CADD002	67.44	67.54	Vcppo 47/096		Looking north
CAL011	12CADD002	72.18	72.28	S1 gneissic 55/026	Vcpmtchpo 35/081	Looking east
CAL012	12CADD002	81.00	81.23	S1 26/022	L1 26-017	Looking east, perpendicular to lineation
CAL017	12CADD002	134.16	134.26	Banding 59/087		Looking north
CAL018	12CADD002	141.26	141.48	S1 gneissic 73/076		Looking north
CAL019	12CADD002	151.00	151.22	S1 57/067	S2 90/236	Looking north
CAL020	12CADD002	155.90	156.00			Looking north
CAL021	12CADD002	158.70	158.80	S1 71/070		Looking north
CAL022	12CADD001	68.28	68.38	S2 69/262	F2 10-176	Looking north
CAL023	12CADD001	130.75	130.85	S1 85/260		Looking north
CAL024	12CADD001	136.30	136.55	S1 73/076		Looking north
CAL025	12CADD001	149.30	149.40	S1 23/329	Vcppoch 18/043	Looking north
CAL026	12CADD001	154.09	154.34			Looking north
CAL027	12CADD001	195.00	195.10	Pegmatite vein 80/042		Looking north
CAL028	12CADD001	217.14	217.24	Vchgtmtcppypo 83/232		Looking north
CAL029	12CADD001	355.20	355.30	Breccia top 80/327	Breccia base 83/330	Looking north
CAL030	12CADD001	370.20	370.30	S1 82/052		Looking NW, right-angles to fabric
CAL031	12CADD001	520.40	520.50	Vqzgtcppopy 12/097		Looking north
CAL032	08WHDDH001	92.74	92.97	S1 39/298		Looking down to southwest, perpendicular to stretching lineation.
CAL034	08WHDDH001	132.23	132.43	S1 37/318		Looking down to southwest, perpendicular to stretching lineation.
CAL035	08WHDDH001	147.56	147.86	S1 29/302		Looking down to southwest, perpendicular to stretching lineation.
CAL038	08WHDDH001	198.20	198.46			Looking approximately south at very weak fabric.
CAL039	08WHDDH001	202.62	202.73	Shear 43/274		Looking down to southwest, perpendicular to stretching lineation.
CAL044	14CADD001	364.75	365.00			Looking north
CAL045	14CADD001	426.78	426.88	Vbint 52/086		Looking north
CAL046	14CADD001	437.29	437.39	Contact 57/083		Looking north
CAL047	14CADD001	451.70	451.80	Vqzflmocp 58/073		Looking east
CAL048	14CADD001	475.71	475.81	Vqzflcppo 46/059		Looking north
CAL050	14CADD001	488.84	488.94			Looking north
CAL052	14CADD001	514.50	514.75	S1 10/080		Looking north
CAL053	14CADD001	523.35	523.60	S1 74/067		Looking north
CAL054	14CADD001	527.21	527.31	Vcpchseqz 64/079		Looking north

CAL056	14CADD001	540.20	540.30	Contact 35/074		Looking north
CAL057	14CADD001	549.10	549.35	S1 48/029		TS looking east, best face for north-dipping foliation
CAL061	14CADD002	130.70	130.80			N/A
CAL062	14CADD002	149.60	149.85	S1 26/286		Looking north
CAL063	14CADD002	164.80	164.90	Vqzamcppygt 26/337		Looking north
CAL064	14CADD002	168.60	168.70	S1 35/343	S2 (sm) 26/293	Looking west
CAL065	DWN4	183.07	183.15			Unoriented, likely looking down to southwest, based on foliation ori
CAL066	DWN4	196.73	196.80			Unoriented, likely looking down to southwest, based on foliation ori
CAL067	DWN4	220.90	221.00			Unoriented, likely looking down to southwest, based on foliation ori

Appendix 6 – Drill core structural measurements

ab = albite		gt = garnet
am = amphibole		kf = K-feldspar
bi = biotite		mo = molybdenite
ca = calcite		mt = magnetite
ch = chlorite		mu = muscovite
cp = chalcopyrite		po = pyrrhotite
ep = epidote		py = pyrite
fl = feldspar		qz = quartz

Hole ID	Depth	Feature	Minerals	Dip	Direction	Plunge	Azimuth	Comments
12CADD002	19.7	S1 foliation		32	7			
12CADD002	20.1	S1 foliation		27	311			
12CADD002	22.75	Contact		72	177			Change from medium to coarse grainsize - possibly a rex front.
12CADD002	24.5	Banding		85	262			Rex banding in GT.
12CADD002	26.5	Vein	cppymo	85	82			1cm diffuse, parallel to S1.
12CADD002	28.75	S1 foliation		79	266			
12CADD002	29.95	Vein	cpmo	60	81			Dissem sulphide bands roughly follow S1.
12CADD002	34.8	Vein	kfmocp	71	110			1cm diffuse.
12CADD002	35.3	S1 foliation		81	76			Hint of moderate N-plunging bi-defined mineral lineation.
12CADD002	36.3	S1 foliation		81	88			Diffuse sulphide band cuts S1, causing local ch alteration, plus coarse, random bi (not in S1 ori).
12CADD002	36.3	Vein	cppych	55	83			Diffuse sulphide band cuts S1, causing local ch alteration, plus coarse, random bi (not in S1 ori).
12CADD002	38.9	Min pegmatite		89	76			Pegmatite contains mineralisation.
12CADD002	40.3	Pegmatite		37	137			Late peg cuts S1, which contains diffuse parallel cp-py bands.
12CADD002	40.3	S1 foliation		61	73			Late peg cuts S1, which contains diffuse parallel cp-py bands.
12CADD002	40.75	Vein	cppymomt	64	77			Parallel veinlets of hg cp-py-mt-mo aligned to S1. Magnetite clearly vein-related, not in host rock. Note bi-destructive nature of alteration.
12CADD002	43.4	Vein	cppymoch	89	234			Microfracture with ch-cp-py-po cuts kf-phyric rock - possibly later mineralisation than mt-cp-py-bi type?
12CADD002	45.1	Contact		80	59			Typical kf-phyric GT appears to intrude an earlier bi-rich unit which is highly mineralised. Xenolith (?) possibly contains earlier foliation?
12CADD002	47	S1 foliation		54	62			Narrow PEG bands/veins
12CADD002	47	Pegmatite		51	96			Narrow PEG bands/veins
12CADD002	48.2	Contact		60	81			Contact between kf-pyric GT and high strain, bi-rich mineralised zone, fairly sharp.
12CADD002	48.6	S1 foliation		46	57			
12CADD002	49.2	S1 foliation		25	46			Various mineralised veins cut S1, mostly acute, some high angle. Mo-bearing vein is pegmatitic, roughly parallel to S1. Coarse bi in selvedges is randomly oriented, associated with magnetite.
12CADD002	49.2	Vein	bipycpmt	56	91			Various mineralised veins cut S1, mostly acute, some high angle. Mo-bearing vein is pegmatitic, roughly parallel to S1. Coarse bi in selvedges is randomly oriented, associated with magnetite.
12CADD002	50.1	Contact		64	59			Lower contact of bi-rich (older?) mineralised zone. Coarse bi rex affects both rocks.
12CADD002	51.5	S1 foliation		56	77			Weak S2 bi alignment, folds S1.
12CADD002	51.5	S2 foliation		86	253			Weak S2 bi alignment, folds S1.

12CADD002	52.3	Vein	cppy	56	93			High-grade vein focuses at strain gradient in GT. But note that vein "breaches" into low strain domain - ie, vein pst-dates foliation.
12CADD002	59.4	S1 foliation		75	78			
12CADD002	61.4	S1 foliation		81	56			Vein parallel to weak S2 fabric, cuts S1. Sulphides mantle silicate grains.
12CADD002	61.4	Vein	cppy	75	249			Vein parallel to weak S2 fabric, cuts S1. Sulphides mantle silicate grains.
12CADD002	63.9	S1 foliation		44	27			
12CADD002	66.6	Vein	mo	67	31			High-grade mo distributed parallel to S1, but equigranular (later, rex?). Note spatial separation from high-grade cp.
12CADD002	67.5	Vein	cppo	47	96			Mantle type sulphide vein, definitely pyrrhotite.
12CADD002	71.35	Vein	cpmo	62	31			1cm almost pegmatitic vein parallel to S1, with coarse mo.
12CADD002	72.2	S1 foliation		55	26			High-grade vein cuts S1, and associated ch replaces existing bi.
12CADD002	72.2	Vein	cpmtch	35	81			High-grade vein cuts S1, and associated ch replaces existing bi.
12CADD002	74.2	S1 foliation		75	42			
12CADD002	75.2	Contact		55	60			GT-MA contact. Note high-grade cp-mo vein in GT, mantle type cp vein in MA, plus thin cp-ch stringer that cuts contact.
12CADD002	81.1	S1 foliation		26	22			Strong S1 zone where sm-ch have preferred linear ori with gentle north plunge. Photo shows "long" sections at core BOH line, and "end" sections near side.
12CADD002	81.1	L1 stretch				26	17	Strong S1 zone where sm-ch have preferred linear ori with gentle north plunge. Photo shows "long" sections at core BOH line, and "end" sections near side.
12CADD002	82.9	S1 foliation		46	9			Sm clearly defines low-alpha angle S2 fabric.
12CADD002	82.9	S2 foliation		75	7			Sm clearly defines low-alpha angle S2 fabric.
12CADD002	84.5	Dolerite dyke		46	65			
12CADD002	116.55	Dolerite dyke		87	80			
12CADD002	119.57	S1 foliation		52	59			
12CADD002	119.57	S2 foliation		82	49			
12CADD002	119.8	S1 foliation		73	50			High-grade vein cuts S1, and about parallel to sm-defined S2.
12CADD002	119.8	Vein	cpmoch	87	47			High-grade vein cuts S1, and about parallel to sm-defined S2.
12CADD002	120.2	Vein	epfl	88	21			Post-min narrow fracture.
12CADD002	123.55	Vein	cp	60	88			Up-hole edge of high-grade mantle style vein/swPEG.
12CADD002	125.5	Contact		85	73			Top contact of narrow late GT dyke, which cuts S1, but appear to entrain some mineralisation at margins.
12CADD002	125.5	S1 foliation		90	143			Top contact of narrow late GT dyke, which cuts S1, but appear to entrain some mineralisation at margins.
12CADD002	126	Banding		68	89			Diffuse grainsize banding.
12CADD002	126.65	Contact		61	81			Lower contact of narrow late GT dyke.
12CADD002	127.6	Vein	cpmoch	47	78			High-grade S1-parallel mantle type (rex) veins with thin chloritic selvedges.
12CADD002	128.6	Vein	qzfl	56	198			Coarse vein (with cordierite?) cuts S1 and high-grade cp bands, remobs some sulphide. Vein warps S1 in a "south-side-up" sense. Vein margin is diffuse, recrystallised.
12CADD002	128.6	S1 foliation		56	43			Coarse vein (with cordierite?) cuts S1 and high-grade cp bands, remobs some sulphide. Vein warps S1 in a "south-side-up" sense. Vein margin is diffuse, recrystallised.
12CADD002	129.65	Contact		60	102			Lower contact of thin late GT, cuts S1.
12CADD002	129.65	S1 foliation		55	78			Lower contact of thin late GT, cuts S1.

12CADD002	130.35	Vein	qzflmu	12	52			Late , coarse vein or PEG.
12CADD002	131.1	Pegmatite		41	81			20cm PEG.
12CADD002	131.4	Vein	abcp	80	151			Thin, late vein with hard selvedge (albite), remobs (?) some cp, cuts S1.
12CADD002	134.16	Pegmatite		59	87			swPEGs
12CADD002	134.2	Pegmatite		41	53			Mineralised PEGs parallel to S1, with some megacrystic GT visible on uphole side. Phenocrysts poikilitic and rex.
12CADD002	134.8	S1 foliation		61	69			Part of narrow, finer, high strain section about 1m wide. Several narrow PEGS slightly crosscut foln.
12CADD002	136.25	Vein	cppy	49	41			Mantle type vein of PEG or coarse rex GT.
12CADD002	138.6	Pegmatite		45	52			Coarse, random bi on PEG margins - rex, altn?
12CADD002	141.26	S1 foliation		73	76			
12CADD002	141.7	S1 foliation		78	95			High-grade cp-mt associated with early (?) bleached or kf-altd veins, some "rootless" - early? Note garnet not wrapped by foliation, includes cp in places.
12CADD002	147.4	S1 foliation		75	72			S2 high strain zone, only traces of S1, very strong ch-sm-gt altn.
12CADD002	147.4	S2 foliation		86	246			S2 high strain zone, only traces of S1, very strong ch-sm-gt altn.
12CADD002	149.2	S1 foliation		78	96			Very strong, sm-defined S2 zone.
12CADD002	149.2	S2 foliation		80	264			Very strong, sm-defined S2 zone.
12CADD002	151	S1 foliation		57	67			
12CADD002	151	S2 foliation		90	236			
12CADD002	154.9	S1 foliation		88	245			Vague banding defined by ch-mt-cp masses.
12CADD002	158.2	S1 foliation		41	51			Pale wisps (former bi/ch) of sericite (?) with patchy internal sm. Light qz-fl matrix, patchy gt. Mineralisation around faint rex PEG/vein. Prob still granite, just blitzed with altn, rex.
12CADD002	158.2	Vein	cpch	65	28			Pale wisps (former bi/ch) of sericite (?) with patchy internal sm. Light qz-fl matrix, patchy gt. Mineralisation around faint rex PEG/vein. Prob still granite, just blitzed with altn, rex.
12CADD002	158.7	Vein	cpbimt	56	55			Min vein with abundant coarse bi in selvedge, clearly overprints S1 and earlier, very strong altn.
12CADD002	158.75	S1 foliation		71	70			Weak fabric/banding.
12CADD001	14.95	S1 foliation		71	55			
12CADD001	17.4	Dolerite dyke		82	262			
12CADD001	48.6	Dolerite dyke		76	131			
12CADD001	50.9	S1 foliation		64	262			High strain zone.
12CADD001	54.8	S2 foliation		55	258			Shallow NNW-plunging fold of S1, PEG and sm?
12CADD001	54.8	F2 axis				5	171	Shallow NNW-plunging fold of S1, PEG and sm?
12CADD001	61.7	S1 foliation		76	80			
12CADD001	68.8	S2 foliation		69	262			Great F2 folds, weak bi alignment to S2.
12CADD001	68.8	F2 axis				10	176	Great F2 folds, weak bi alignment to S2.
12CADD001	70.6	Contact		78	244			High strain to low strain change - may not be lith boundary?
12CADD001	73.9	S1 foliation		75	68			Typical S1 in low strain domain.
12CADD001	74.8	S2 foliation		65	266			Folding of mineralised chloritic fractures.
12CADD001	85	Dolerite dyke		64	327			
12CADD001	86.3	Vein	chcppy	85	229			Ch-rich stockwork style veinlets - brittle, very different to usual.
12CADD001	93.2	S1 foliation		77	94			

12CADD001	93.2	Vein	cppychmt	64	232			
12CADD001	98.6	S1 foliation		9	187			Short limb S1.
12CADD001	107.2	S1 foliation		36	245			
12CADD001	121.7	Contact		62	279			GT-MA contact, parallel to S1.
12CADD001	130.9	S1 foliation		85	260			S1 folded through MA. Approx hinge area from here onwards.
12CADD001	133.5	Contact		57	259			MA-GT contact, distinctive bi-rich, relatively "old" GT.
12CADD001	134.5	S2 foliation		64	257			Nice folding in approx hinge zone. Weak but consistent S1 through this unit.
12CADD001	136.3	S1 foliation		73	76			
12CADD001	138.55	Contact		25	305			Very clear contact into younger(but mineralised) qz-rich GT.
12CADD001	141.8	Vein	cpchpo	17	215			Stockwork style vein in low strain domain, most common ori. Definite po.
12CADD001	146.1	Vein	cppoch	58	275			Stockwork style vein in low strain domain, both follow and cut S1.
12CADD001	146.1	Vein	cppoch	13	196			Stockwork style vein in low strain domain, both follow and cut S1.
12CADD001	146.55	Contact		83	221			Internal contact with younger, massive GT.
12CADD001	149.4	S1 foliation		23	329			Stockwork style vein cuts S1.
12CADD001	149.4	Vein	cppoch	18	43			Stockwork style vein cuts S1.
12CADD001	157.8	S1 foliation		62	81			Stockwork style vein cuts S1.
12CADD001	157.8	Vein	cppoch	47	6			Stockwork style vein cuts S1.
12CADD001	165.6	S1 foliation		55	9			Strong gneissic fabric.
12CADD001	169.2	Min pegmatite		58	9			Late PEG cuts mineralised swPEG.
12CADD001	169.2	Pegmatite		24	9			Late PEG cuts mineralised swPEG.
12CADD001	172.8	S1 foliation		38	12			Likely F1 fold of barren, rex qz vein.
12CADD001	172.8	F1 axis				12	298	Likely F1 fold of barren, rex qz vein.
12CADD001	174.45	Contact		80	221			Older granite contact into younger qz-rich GT.
12CADD001	180.3	S1 foliation		29	34			Highly variable foln and min ori through here, but dominantly "long limb".
12CADD001	184.5	S1 foliation		27	1			Localised short limb, very irregular S1 ori through this zone.
12CADD001	195.15	Min pegmatite		80	42			Excellent mineralised swPEGs, cp-py-mo, po also?
12CADD001	201.2	S1 foliation		58	219			Localised high strain domain.
12CADD001	210.2	S1 foliation		57	84			
12CADD001	217.05	Vein	chgtmtcppypo	83	232			Excellent 20cm, well defined vein with mt rims and cp-py-po-ch-am core. Mt-py-po intergrown.
12CADD001	222.3	S1 foliation		82	245			
12CADD001	223.1	Vein	chgtmtcppypo	81	81			Excellent 20 cm vein, as at 217.05m.
12CADD001	228.4	S1 foliation		78	55			
12CADD001	236.9	Vein	pycpbi	88	96			1cm vein parallel to S1.
12CADD001	241.3	S1 foliation		77	84			
12CADD001	243	Vein	cppy	84	67			Approx parallel to S1.
12CADD001	250.8	S1 foliation		89	237			Sm-defined.
12CADD001	258.9	S1 foliation		73	234			Sm-defined, with parallel veins and fractures.
12CADD001	262.9	Vein	qzcpypo	72	58			Irregular vein/PEG about 2m wide.
12CADD001	268	S1 foliation		45	22			
12CADD001	273.25	Contact		9	20			Narrow, late GT.

12CADD001	275.3	S1 foliation		46	54			
12CADD001	286.55	Contact		7	64			Narrow, late GT.
12CADD001	288.9	Vein	chmtgtcppy	42	360			Alteration zone/vein, marks change to much stronger alteration.
12CADD001	294.8	S1 foliation		37	39			Min veins generally parallel, pretty regular foln since 288.90.
12CADD001	298.5	S1 foliation		17	124			
12CADD001	305.9	S1 foliation		67	98			Vein with coarse bi flakes cuts, overprints S1 and strong early alteration.
12CADD001	305.9	Vein	bicp	61	327			Vein with coarse bi flakes cuts, overprints S1 and strong early alteration.
12CADD001	307.7	Vein	cppomt	75	74			Mantle type vein, running down core.
12CADD001	315	S1 foliation		35	37			
12CADD001	319.7	S2 foliation		59	284			
12CADD001	324.1	S1 foliation		53	28			
12CADD001	328.95	Contact		53	200			1.5m well defined PEG, marks start of distinctive megacrystic unit below.
12CADD001	334.3	S1 foliation		46	236			Minor short limb.
12CADD001	343.55	Contact		30	302			Megacrystic GT contact with "older" bi-rich GT, seems to cut old foliation.
12CADD001	345.55	Dolerite dyke		71	285			Top contact.
12CADD001	347.75	Dolerite dyke		77	261			Bottom contact.
12CADD001	348.7	Vein	cpchpobi	87	288			High-grade vein, assoc with coarse biotite, start of higher-grade section.
12CADD001	354.45	Breccia		80	327			Top contact of mineralised chloritic breccia, very distinctive.
12CADD001	357	Breccia		83	330			Bottom contact of mineralised chloritic breccia, very distinctive.
12CADD001	358.9	S1 foliation		29	251			
12CADD001	370.2	S1 foliation		82	52			Strong gneissic fabric, with with nice qz-fl lithons.
12CADD001	377.8	S1 foliation		46	69			Weak S2 crenulation.
12CADD001	377.8	S2 foliation		75	272			Weak S2 crenulation.
12CADD001	384.6	Vein	chcpmtgt	68	78			20cm vein.
12CADD001	389.4	S1 foliation		86	229			
12CADD001	391.8	Vein	chgt	7	127			Lower margin of strong altn zone, possibly unreliable, a bit hazy.
12CADD001	398.7	S1 foliation		58	76			
12CADD001	404.9	S1 foliation		59	68			Min veins dominantly parallel.
12CADD001	417.5	S1 foliation		69	56			
12CADD001	433.4	S2 foliation		65	274			
12CADD001	434.8	Vein	chgtcpmt	77	238			10cm vein.
12CADD001	449.45	Contact		85	83			Start of high strain zone - possibly MA?
12CADD001	451.6	S1 foliation		74	60			In high strain bit. Possibly some early veins folded by S1?
12CADD001	459.8	Contact		38	356			Bottom edge of high strain and altn zone.
12CADD001	470.3	S1 foliation		10	260			Sub-horizontal short limb now.
12CADD001	481.4	S1 foliation		13	344			
12CADD001	488.2	S1 foliation		35	82			Minor long limb.
12CADD001	492.7	S1 foliation		67	78			Minor long limb.
12CADD001	495.2	Vein	chgtmtcp	82	69			Sharp start of altn zone.
12CADD001	498.6	S1 foliation		87	254			Foliation internal to altn zone.

12CADD001	503.2	S1 foliation		7	267			
12CADD001	508.5	Vein	cppy	14	40			10cm, S1-parallel vein.
12CADD001	518.7	S1 foliation		7	184			
12CADD001	519.05	Vein	cppypomt	12	97			Thick, very sulphidic rex vein or swPEG.
12CADD001	528.85	Contact		15	54			
12CADD001	534.8	Contact		7	302			MA-GT contact.
12CADD001	537	S1 foliation		79	54			Hole ends on "long limb" of uncertain extent.
08WHDDH001	82.8	Contact		43	312			Contact between coarse schist (AN) and fine mafic (?). S1 and sulphide stringers are parallel.
08WHDDH001	85.8	S1 foliation		30	316			Typical bi-defined stretching lineation present throughout top of hole, about 30 to NW.
08WHDDH001	85.8	L1 stretch				29	308	Typical bi-defined stretching lineation present throughout top of hole, about 30 to NW.
08WHDDH001	88.35	Contact		41	310			Qz porphyry contact. Mineralised veins cut S1, but associated bi selvedge grows in S1 ori.
08WHDDH001	88.35	Vein	qzchbicp	53	278			Qz porphyry contact. Mineralised veins cut S1, but associated bi selvedge grows in S1 ori.
08WHDDH001	92.45	Contact		32	305			Qz porphyry contact.
08WHDDH001	92.74	S1 foliation		39	298			
08WHDDH001	95.3	Vein	qzambi	40	282			Veins both parallel to and cutting S1.
08WHDDH001	95.3	Vein	qzambi	39	325			Veins both parallel to and cutting S1.
08WHDDH001	96.55	Contact		31	347			Mafic dyke contact, oblique to S1, but affected by it.
08WHDDH001	97	S1 foliation		40	286			
08WHDDH001	97	L1 stretch				40	293	
08WHDDH001	100	Vein	qzbiab	40	309			3 vein types. Vqz and Vqzbi subtley cut S1, but bi grows parallel to it. Vqzabbi earliest vein type?
08WHDDH001	100	Vein	qz	37	299			3 vein types. Vqz and Vqzbi subtley cut S1, but bi grows parallel to it. Vqzabbi earliest vein type?
08WHDDH001	100	Vein	biqz	31	297			3 vein types. Vqz and Vqzbi subtley cut S1, but bi grows parallel to it. Vqzabbi earliest vein type?
08WHDDH001	101.6	Contact		40	321			Qz porphyry contact, parallel to S1.
08WHDDH001	102.75	Contact		36	297			Discrete ep-mt altered shear on porphyry contact - reactivated?
08WHDDH001	109	S1 foliation		39	299			Stretching lin about 30 to WNW.
08WHDDH001	109	L1 stretch				39	296	Stretching lin about 30 to WNW.
08WHDDH001	124.05	Contact		33	330			Late granite contact, post-dates S1 but approx parallel.
08WHDDH001	126.1	Vein	amepcppomtbi	38	316			S1-parallel "Dasher-style" mineralised vein, with coarse bi selvedge.
08WHDDH001	127.3	Contact		19	354			10cm GT dyke in albitic zone. Note that dykes cut albitic altn front, and include albitised xenoliths.
08WHDDH001	129.65	Contact		63	298			Pegmatite.
08WHDDH001	132.23	S1 foliation		37	318			Faint layering.
08WHDDH001	133.7	Vein	qzamab	39	321			Irregular, boudinaged (?) vein.
08WHDDH001	135	S1 foliation		32	317			About 20 to NW strecthing lineation. Photo shows "christmas tree" Vqzgtambi. Gt and am (ch?) clearly intergrown.
08WHDDH001	135	L1 stretch				31	322	About 20 to NW strecthing lineation. Photo shows "christmas tree" Vqzgtambi. Gt and am (ch?) clearly intergrown.
08WHDDH001	144	Shear		31	320			Core of approximate 2m wide bi-ch shear zone.
08WHDDH001	147.56	S1 foliation		29	302			
08WHDDH001	153.6	Bedding		38	301			Bedding/layering, coarse porphyryitic stuff to fine massive stuff, typical example.
08WHDDH001	156.55	Contact		40	302			Qz porphyry.

08WHDDH001	159.15	Contact		50	288			Granite.
08WHDDH001	160.45	Contact		37	318			Qz porphyry.
08WHDDH001	162.45	Contact		66	251			Granite contact. Foliated xenoliths at lower contact (ie. Post S1 dykes).
08WHDDH001	165.9	Vein	qzambicpab	35	306			Typical vein orientation.
08WHDDH001	177.7	S1 foliation		36	323			About 30 to NW stretch lin. Vqzambi vein folded in S1 (F1?). Also photo of grey qz veins both with and without selvedges - one exploiting an old one?
08WHDDH001	177.7	L1 stretch				32	290	About 30 to NW stretch lin. Vqzambi vein folded in S1 (F1?). Also photo of grey qz veins both with and without selvedges - one exploiting an old one?
08WHDDH001	179.1	Vein	cpch	38	284			Excellent pics of "Dasher style" min veins cutting S1 and Vqzambimt, which is folded into ~20 to NW F1 fold.
08WHDDH001	179.1	S1 foliation		47	289			Excellent pics of "Dasher style" min veins cutting S1 and Vqzambimt, which is folded into ~20 to NW F1 fold.
08WHDDH001	179.4	Vein	qzambipy	35	302			
08WHDDH001	184	Vein	cpch	34	298			Typical min vein ori. 20 to W F1 fold of grey qz vein, which itself cuts Vqzamab veins?
08WHDDH001	184	F1 axis				33	312	Typical min vein ori. 20 to W F1 fold of grey qz vein, which itself cuts Vqzamab veins?
08WHDDH001	186.5	Vein	cpch	44	273			Parallel to S1.
08WHDDH001	187.4	Vein	cppyammtab	40	282			
08WHDDH001	189.1	S1 foliation		42	302			Mineralised vein cuts S1 in albitised andesite.
08WHDDH001	189.1	Vein	cppyepmt	42	274			Mineralised vein cuts S1 in albitised andesite.
08WHDDH001	191.5	S1 foliation		30	335			Vein cuts S1, L1 dips plunges about 20 to NW.
08WHDDH001	191.5	L1 stretch				26	304	Vein cuts S1, L1 dips plunges about 20 to NW.
08WHDDH001	191.5	Vein	ammtcppy	55	346			Vein cuts S1, L1 dips plunges about 20 to NW.
08WHDDH001	196.6	Contact		44	1			Qz porphyry contact, a bit deformed.
08WHDDH001	197.2	Vein	ambicppopy	49	329			High-grade vein with 3 sulphides?
08WHDDH001	202.3	Shear		39	270			Strong shear, a bit off normal S1 - younger, I think.
08WHDDH001	202.62	Shear		43	274			
08WHDDH001	203.4	Shear		44	278			Strong biotite wraps garnet in shear zone, accumulate in shadow. Note strong sm/mu (?) increasing to RHS.
08WHDDH001	205.3	Shear		35	314			Strong cp-py min in shear, mixed with mu/sm (retrogression?).
08WHDDH001	205.95	Pegmatite		27	335			PEG marks end of SZ, contains some remob sulphide.
08WHDDH001	208.5	Vein	ampocpbimt	23	316			20cm high-grade vein. Note that thin GT is also mineralised, with mt-cp-po.
08WHDDH001	212.1	S1 foliation		45	298			
08WHDDH001	214	Contact		24	314			Granite.
08WHDDH001	216.3	Bedding		44	303			Layering/bedding in interpreted interflow chert.
08WHDDH001	221.4	S1 foliation		40	292			
08WHDDH001	226.1	Pegmatite		64	179			Irregular, brittle PEG contact, not exact.
08WHDDH001	227.2	S1 foliation		51	273			Very weak S1 in dolerite.
14CADD001	334.6	S1 foliation		63	85			
14CADD001	345.6	S1 foliation		33	92			
14CADD001	357.4	Vein	bi	28	111			10cm bi-defined foliation band.
14CADD001	360.65	Pegmatite		56	10			
14CADD001	363.2	Pegmatite		76	217			2cm PEG with coarse bi-mt masses.
14CADD001	365.1	S1 foliation		52	55			

14CADD001	368.6	Vein	qzkfchep	8	325			Very thin qz stringer with kf-ch-ep selvedge, late.
14CADD001	369.5	S1 foliation		38	354			Different S1 ori here, no clear point of change.
14CADD001	372	Dolerite dyke		85	122			
14CADD001	377.2	Dolerite dyke		90	116			
14CADD001	380.75	Pegmatite		74	38			Irregular PEG with coarse bi-mt masses.
14CADD001	384.2	S1 foliation		37	57			Coarse, random bi-mt vein cuts S1 foliation.
14CADD001	384.2	Vein	bimt	45	134			Coarse, random bi-mt vein cuts S1 foliation.
14CADD001	397.15	Pegmatite		56	301			
14CADD001	402.5	Vein	bimt	38	92			Series of bi-mt veins/fol zones 402.4-402.6 + recrystallisation zone. Cuts acute to very faint earlier foliation (S1?).
14CADD001	402.5	S1 foliation		38	53			Series of bi-mt veins/fol zones 402.4-402.6 + recrystallisation zone. Cuts acute to very faint earlier foliation (S1?).
14CADD001	409.4	Vein	bimt	8	195			Vein/foln/rex zone 409.3-410.3, similar to previous.
14CADD001	411.35	Pegmatite		65	298			
14CADD001	414.2	Pegmatite		58	290			
14CADD001	418.5	S1 foliation		54	9			South-side-up displacement of strongish foln across thin PEG. Foln poss not S1?
14CADD001	418.5	Pegmatite		53	192			South-side-up displacement of strongish foln across thin PEG. Foln poss not S1?
14CADD001	424.6	Banding		59	97			Acute relationship between grainsize banding and S1 foliation.
14CADD001	424.6	S1 foliation		61	66			Acute relationship between grainsize banding and S1 foliation.
14CADD001	426.7	Vein	bimt	52	86			
14CADD001	427.7	Banding		56	99			Same BAN/S1 relationship as at 424.60, suggests F1 synform to the west, NW-plunging.
14CADD001	427.7	S1 foliation		60	66			Same BAN/S1 relationship as at 424.60, suggests F1 synform to the west, NW-plunging.
14CADD001	430.5	Vein	cppymtch	56	95			Mineralised vein in hangingwall granite, cuts weak bi foln. Typical ch-type vein, wih definite pyrite.
14CADD001	430.5	S1 foliation		57	58			Mineralised vein in hangingwall granite, cuts weak bi foln. Typical ch-type vein, wih definite pyrite.
14CADD001	432.3	Banding		59	97			Excellent example of BAN/S1 vergence relationship.
14CADD001	432.3	S1 foliation		74	75			Excellent example of BAN/S1 vergence relationship.
14CADD001	437.2	Vein	bimtcp	46	86			Critical contact zone, clearly showing bi-cp-mt veinlets affecting hangingwall rock.
14CADD001	437.35	Contact		57	83			Critical contact zone, clearly showing bi-cp-mt veinlets affecting hangingwall rock.
14CADD001	437.6	Vein	flqzmtmo	61	70			Typical qzflmo vein, with mt also, approx parallel to S1.
14CADD001	438.1	Banding		46	86			Thin megacrystic band.
14CADD001	438.6	Vein	cppobiam	86	61			Vein cuts S1.
14CADD001	439.1	Banding		53	83			Two foliations? Gneissic banding, plus later "S1".
14CADD001	439.1	S1 foliation		50	54			Two foliations? Gneissic banding, plus later "S1".
14CADD001	440.2	Contact		54	56			
14CADD001	441.5	S1 foliation		51	59			Amphibole-defined foliation, no lineation on this fabric.
14CADD001	445.6	S1 foliation		36	88			Spaced S2 crenulation cleavage in S1 high-strain zone.
14CADD001	445.6	S2 foliation		58	286			Spaced S2 crenulation cleavage in S1 high-strain zone.
14CADD001	446.5	Vein	cpch	15	280			Late vein cuts mineralised, gt-bearing PEG, typical late/remob vein.
14CADD001	447.2	Vein	eppy	76	96			
14CADD001	447.9	S1 foliation		68	81			Foliation with parallel pegmatitic qz-fl veins.

14CADD001	448.75	Vein	qzflgtmocpmt	51	97			Unusual, banded 20cm vein.
14CADD001	449.4	S1 foliation		58	64			Photo of "F1" folding of Vqzflcpmo veins - can't measure plunge, but look moderate E-plunging, with no clear vergence.
14CADD001	451.7	Vein	qzflmocp	58	73			Typical mo-rich veins folded by S1 fabric, or else wobbling across it.
14CADD001	454	S2 foliation		77	264			Weak crenulation.
14CADD001	455.2	S1 foliation		78	84			
14CADD001	456.6	Vein	gtchcp	73	87			Rich vein approx parallel to S1. Note hazy F1-folded qzfl vein at left - Vgtchcp post-dates it.
14CADD001	459.2	S1 foliation		73	64			Highly contorted early qzfl vein, minimal sulphide. Fold plunging about 45 to SE.
14CADD001	459.2	F1 axis				41	139	Highly contorted early qzfl vein, minimal sulphide. Fold plunging about 45 to SE.
14CADD001	460.7	Contact		69	64			High strain contact.
14CADD001	464.55	Contact		72	80			
14CADD001	465.1	S1 foliation		60	59			Excellent F1-folded Vqzflmocp example, plunging about 60 to ENE.
14CADD001	465.1	F1 axis				60	63	Excellent F1-folded Vqzflmocp example, plunging about 60 to ENE.
14CADD001	466.3	S1 foliation		60	71			
14CADD001	468.5	Vein	qzgtcppymt	64	65			15cm mantle-type vein.
14CADD001	468.9	Vein	qzflgtmocpmt	50	64			15cm gt-rich, but su-poor vein.
14CADD001	472.6	Vein	capy	79	256			Very late, open-space calcite-pyrite vein with fe-carbinate selvedge.
14CADD001	475.2	S1 foliation		73	61			Folded Vqzflcp with no obvious moly. Plunge about 45 to E.
14CADD001	475.2	F1 axis				42	135	Folded Vqzflcp with no obvious moly. Plunge about 45 to E.
14CADD001	475.7	Vein	cpqzfl	46	59			Good cp min in S1-parallel qzfl veins or miniPEGs.
14CADD001	477.6	S2 foliation		62	267			
14CADD001	478.35	Contact		78	52			
14CADD001	480.25	Contact		41	177			
14CADD001	481.5	S1 foliation		5	311			Very irregular S1 through here. Vein cuts S1, but is also wobbly.
14CADD001	481.5	Vein	mtcp	42	36			Very irregular S1 through here. Vein cuts S1, but is also wobbly.
14CADD001	482.3	Vein	cpch	34	35			Late stringer, note mt-bi masses in pic also.
14CADD001	484.1	S1 foliation		58	53			Part of noticeable low alpha angle zone.
14CADD001	487.8	S1 foliation		45	39			Part of noticeable low alpha angle zone.
14CADD001	490	Vein	bimtcp	35	71			End of higher strain zone, series of stringers and foln. Note general low strain and alteration here.
14CADD001	492.2	S1 foliation		39	64			Narrow high strain band.
14CADD001	492.9	S1 foliation		32	69			
14CADD001	494.3	Banding		39	26			Grainsize/altn change.
14CADD001	494.6	Vein	cppybi	63	17			Rich 2cm vein.
14CADD001	496.7	S1 foliation		7	354			
14CADD001	498.45	Contact		32	357			Contact/banding.
14CADD001	500.3	S1 foliation		53	31			
14CADD001	502.8	S1 foliation		54	83			
14CADD001	503.1	Banding		50	36			Change to high strain zone - finer grainsize?
14CADD001	505.3	S1 foliation		32	357			
14CADD001	505.6	S1 foliation		35	31			Late (remob?) stringer cuts foln in otherwise barren unit.

14CADD001	505.6	Vein	qzcppych	20	157			Late (remob?) stringer cuts foln in otherwise barren unit.
14CADD001	510.5	Contact		74	66			
14CADD001	511.2	S1 foliation		54	32			
14CADD001	513.3	Contact		41	289			
14CADD001	514.6	S1 foliation		10	80			Variable foliation.
14CADD001	514.9	S1 foliation		36	71			
14CADD001	515.6	Contact		70	64			
14CADD001	517.1	S1 foliation		63	56			
14CADD001	517.95	Contact		41	101			Foln in high strain zone runs straight down core. Note first appearance of "S3" axial planar fabric.
14CADD001	517.95	Crenulation		29	133			Foln in high strain zone runs straight down core. Note first appearance of "S3" axial planar fabric.
14CADD001	519.8	Crenulation		31	66			Shallow east-dipping "S3" is axial planar to irregular folds.
14CADD001	520.55	Contact		56	74			Change into strong kf alteration zone - not necessarily a textural change.
14CADD001	521.8	Crenulation		34	113			S3 folding of existing foliation, likely S1, abundant feature through this zone. Ph3811 section veiw suggests F3 antiform uphole?
14CADD001	523.2	S1 foliation		68	54			Irregular S1 all throught this zone, but "trying" to be this ori (F2 long limb).
14CADD001	523.5	S1 foliation		74	67			
14CADD001	524.6	Contact		51	90			Alteration front.
14CADD001	525.3	Contact		54	42			Alteration front, note garnet in pic.
14CADD001	526.9	Contact		28	80			Alteration front.
14CADD001	527.1	Vein	cpchmuqz	64	79			Late stringers cut kf alteration - clearly qzmuchcp veins.
14CADD001	528.25	Contact		56	78			
14CADD001	529.8	Contact		51	52			
14CADD001	532.3	S1 foliation		14	303			
14CADD001	532.9	S2 foliation		54	274			Standard F2 setup.
14CADD001	532.9	F2 axis				24	345	Standard F2 setup.
14CADD001	535.7	S1 foliation		73	65			
14CADD001	536.35	Contact		34	89			
14CADD001	537.4	S1 foliation		22	66			
14CADD001	538.75	Contact		52	78			
14CADD001	539.6	Contact		15	111			
14CADD001	540.3	Contact		35	74			
14CADD001	547.3	S1 foliation		55	24			
14CADD001	547.9	S1 foliation		64	45			
14CADD001	548.3	Contact		80	60			Aplite dyke.
14CADD001	549.2	S1 foliation		48	29			Very weak fabric.
14CADD001	550.1	S1 foliation		45	21			
14CADD001	552.5	Vein	bimt	31	25			Foliation, veins.
14CADD001	552.9	Vein	bimt	14	173			
14CADD001	553.2	Vein	bimt	25	291			Foliation, veins.
14CADD001	559.9	S1 foliation		52	76			Weak bi-defined foln, with some bi-mt wisps.

14CADD001	561.2	S1 foliation		37	42			S1?
14CADD001	561.9	S1 foliation		61	45			S1? Garnet mass associated with qz in foln zone.
14CADD001	563.5	Vein	bimt	40	90			
14CADD001	565.2	S1 foliation		76	52			S1?
14CADD002	34.9	S1 foliation		33	303			
14CADD002	43.55	Contact		46	340			
14CADD002	65.5	Banding		34	291			Coarse-to-fine amphibolite banding, with parallel foliation.
14CADD002	68.3	S2 foliation		35	270			Local F2 folding, no clear vergence, gentle W plunge.
14CADD002	68.3	F2 axis				33	292	Local F2 folding, no clear vergence, gentle W plunge.
14CADD002	76.9	S1 foliation		37	349			
14CADD002	83	S1 foliation		43	331			
14CADD002	90.8	Banding		42	281			Fine banding in amphibolite near contact - interflow sed? Mafic-derived sed package?
14CADD002	96.2	S1 foliation		38	314			
14CADD002	100.2	Contact		35	278			
14CADD002	121.4	S2 foliation		41	269			Folded mineralised banding/S1 foliation, cut by epidote stringers.
14CADD002	121.4	F2 axis				40	282	Folded mineralised banding/S1 foliation, cut by epidote stringers.
14CADD002	123.7	S1 foliation		44	298			Typical mineralisation parallel to S1.
14CADD002	149.4	S1 foliation		39	307			
14CADD002	149.7	S1 foliation		26	286			Gneissic foln/banding.
14CADD002	152.9	Vein	chamcp	46	320			Mineralised veins follow S1, but likely post-date (unaligned amphiboles).
14CADD002	158.3	S1 foliation		52	302			
14CADD002	159.8	S2 foliation		37	228			F2 gentle west-plunge, approximately.
14CADD002	159.8	F2 axis				25	281	F2 gentle west-plunge, approximately.
14CADD002	164.8	Vein	qzamcppygt	26	337			Nice vein, note association of gt with min.
14CADD002	168.7	S1 foliation		35	343			Sm-defined folitation (S2?) overprints S1, garnet likely post-S1 also.
14CADD002	168.7	S2 foliation		26	293			Sm-defined folitation (S2?) overprints S1, garnet likely post-S1 also.
14CADD002	168.8	S2 foliation		34	247			Gentle west-plunging F2 folds.
14CADD002	168.8	F2 axis				33	262	Gentle west-plunging F2 folds.
14CADD002	172.8	S1 foliation		36	271			
14CADD002	177.2	S1 foliation		49	281			
14CADD002	198.7	S1 foliation		30	336			
14CADD002	203.4	S2 foliation		23	330			Axial plane, can't measure a solid gamma for plunge. Pic looking west at core - these are shallow W-plunging Z folds, pic looking approx down plunge.
14CADD002	207.8	Vein	qzcppych	37	308			Mantle-style (rex) vein with definite purple bornite, approx parallel to S1.
14CADD002	212	S2 foliation		40	291			Gentle W-plunging Z folds.
14CADD002	212	F2 axis				37	317	Gentle W-plunging Z folds.
14CADD002	213.7	S1 foliation		46	333			

Appendix 7 – Whole-rock geochemistry

	PUL-QC	ME-XRF26	ME-XRF26	ME-XRF26	ME-XRF26	ME-XRF26	ME-XRF26	ME-XRF26	ME-XRF26	ME-XRF26	ME-XRF26	ME-XRF26	ME-XRF26	ME-XRF26
SAMPLE	Pass75um	Al2O3	BaO	CaO	Cr2O3	Fe2O3	K2O	MgO	MnO	Na2O	P2O5	SiO2	SrO	
DESCRIPTION	%	%	%	%	%	%	%	%	%	%	%	%	%	
CAL006	94	15.24	0.11	2.24	<0.01	2.94	2.93	0.66	0.04	4.26	0.08	70.85	0.03	
CAL007		15	0.08	2.45	<0.01	5.71	1.87	0.89	0.26	4.12	0.06	68.68	0.01	
CAL012		14.18	0.09	0.67	<0.01	4.01	3.78	0.33	0.12	1.57	0.02	74.01	<0.01	
CAL018		15.62	0.04	3.99	<0.01	6.81	1.88	1.41	0.33	2.92	0.25	65.95	0.02	
CAL019		12.02	0.05	0.13	<0.01	4.36	2.63	0.2	0.23	0.47	0.01	78.64	<0.01	
CAL024		15.53	0.18	1.67	<0.01	5.55	5.28	1.11	0.08	3.28	0.11	66.99	0.02	
CAL026		13.54	0.17	1.1	<0.01	1.81	4.96	0.29	0.02	3.27	0.03	74	0.01	
CAL032		14.71	0.12	1.01	<0.01	3.98	2.94	0.77	0.04	5.46	0.07	70.21	0.01	
CAL034		15.04	0.03	3.05	0.02	12.7	2.74	2.7	0.25	2.77	0.16	58.99	0.01	
CAL035		15.24	0.05	2.07	<0.01	6.9	1.82	1.44	0.07	5.18	0.1	65.71	0.01	
CAL038		14.36	0.08	1.68	<0.01	1.29	3.45	0.19	0.02	4.43	0.02	73.27	0.02	
CAL044		14.62	0.1	1.76	<0.01	2.11	4.01	0.51	0.03	4.05	0.06	71.99	0.02	
CAL052		14.66	0.13	2.16	<0.01	3.93	3.52	0.79	0.06	3.7	0.08	69.48	0.02	
CAL053		13.94	0.21	1.1	<0.01	0.69	5.97	0.1	0.01	3.08	0.04	74.75	0.01	
CAL057		14.84	0.16	1.81	<0.01	2.11	4.24	0.55	0.04	3.87	0.08	71.38	0.03	
CAL062		14.08	0.09	1.33	<0.01	5.86	3.59	0.99	0.12	2.81	0.09	69.24	0.01	

	ME-XRF26	ME-GRA05	ME-XRF26	ME-MS81	ME-MS81	ME-MS81	ME-MS81	ME-MS81	ME-MS81	ME-MS81	ME-MS81	ME-MS81	ME-MS81	ME-MS81
SAMPLE	TiO2	LOI	Total	Ba	Ce	Cr	Cs	Dy	Er	Eu	Ga	Gd	Ge	
DESCRIPTION	%	%	%	ppm	ppm	ppm	ppm	ppm	ppm	ppm	ppm	ppm	ppm	
CAL006	0.28	0.25	99.97	880	87.1	20	1.62	1.92	0.97	0.95	21.3	2.57	<5	
CAL007	0.38	0.29	100.5	636	42.2	20	1.85	1.44	0.93	0.74	20.3	1.61	<5	
CAL012	0.16	0.74	100.4	781	22.4	20	1.38	0.77	0.59	0.46	23.8	1.14	<5	
CAL018	0.64	0.31	100.55	312	117	30	3.86	1.91	0.9	1.63	23.1	3.65	<5	
CAL019	0.11	0.18	99.18	397	48.6	10	1.68	0.99	0.68	0.4	19.2	1.37	<5	
CAL024	0.48	0.2	100.75	1525	69	20	4.27	1.13	0.66	0.74	25.1	1.91	<5	
CAL026	0.14	0.23	99.78	1525	29.9	10	2.64	0.93	0.5	0.52	19	1.17	<5	
CAL032	0.31	0.28	100.05	974	48.7	20	4.22	1.24	0.77	0.49	17.7	1.82	<5	
CAL034	0.78	0.72	100.15	189.5	56.8	110	8.08	3.74	2.37	1.44	19.8	3.97	<5	
CAL035	0.5	0.47	99.63	370	41.2	30	1.84	1.48	0.86	0.68	18	1.76	<5	
CAL038	0.08	0.27	99.26	>10000	42.7	10	7.71	4.92	3.88	0.69	23.6	3.73	<5	
CAL044	0.24	0.2	99.76	879	71.2	10	2.04	2.76	1.43	0.66	21.8	3.44	<5	
CAL052	0.33	0.24	100.25	1105	46	10	2.2	1.14	0.53	0.61	21.1	1.63	<5	
CAL053	0.04	0.12	100.35	1680	15.8	10	0.86	1.14	0.76	0.37	13.7	1.23	<5	
CAL057	0.26	0.24	99.67	1420	103	20	2.38	1.08	0.45	0.87	22.1	2.07	<5	
CAL062	0.44	1.36	100.2	690	68	20	1.36	1.47	0.79	0.78	18.5	2.16	<5	

	ME-MS81	ME-MS81	ME-MS81	ME-MS81	ME-MS81	ME-MS81	ME-MS81	ME-MS81	ME-MS81	ME-MS81	ME-MS81	ME-MS81	ME-MS81
SAMPLE	Hf	Ho	La	Lu	Nb	Nd	Pr	Rb	Sm	Sn	Sr	Ta	Tb
DESCRIPTION	ppm	ppm	ppm	ppm	ppm	ppm	ppm	ppm	ppm	ppm	ppm	ppm	ppm
CAL006	4.6	0.37	53.2	0.1	9.1	26.5	8.91	91.9	3.76	2	208	1.4	0.41
CAL007	3.8	0.27	26.6	0.14	4.6	13.3	4.34	75	1.99	2	94.6	0.4	0.23
CAL012	3.3	0.18	14.7	0.06	5.1	6.7	2.4	80.6	1.13	1	31.9	0.3	0.18
CAL018	4.8	0.33	63.5	0.12	7.1	40.5	13	97.4	5.62	4	116.5	0.5	0.43
CAL019	3.7	0.21	29.5	0.1	3.5	14.3	4.96	61.3	1.92	1	9	0.2	0.18
CAL024	4.7	0.25	41.6	0.08	5	21.5	7.32	166	2.8	2	118.5	0.3	0.25
CAL026	2.9	0.17	18.5	0.05	5.4	8.8	3	118	1.65	1	90.7	0.5	0.17
CAL032	3.8	0.28	30.7	0.1	6.5	14	4.73	71.1	2.07	2	46.6	0.7	0.23
CAL034	4.6	0.79	33.2	0.33	9.3	20.9	6.28	114	3.84	6	46.9	0.7	0.62
CAL035	3.4	0.34	26	0.12	5.1	13.8	4.25	44.5	2.24	2	42.9	0.5	0.3
CAL038	5.2	1.2	18.3	0.8	13.4	12.5	3.77	168	3.21	2	346	4	0.66
CAL044	4.6	0.57	41.5	0.24	8.9	23.2	7.49	135	3.95	2	184	1.3	0.52
CAL052	3.8	0.21	29.4	0.07	7.4	13.5	4.58	116.5	1.83	2	163	1.1	0.21
CAL053	2.1	0.25	9.7	0.08	1.1	5.4	1.67	115	1.28	<1	111	0.2	0.18
CAL057	6.1	0.21	65.5	0.05	6.4	28.6	10.05	129	3.76	1	212	0.4	0.22
CAL062	4.3	0.29	43.3	0.12	7.3	18.7	6.72	138.5	2.97	2	75	0.7	0.32

	ME-MS81	ME-MS81	ME-MS81	ME-MS81	ME-MS81	ME-MS81	ME-MS81	ME-MS81	ME-4ACD81	ME-4ACD81	ME-4ACD81	ME-4ACD81	ME-4ACD81
SAMPLE	Th	Tm	U	V	W	Y	Yb	Zr	Ag	Cd	Co	Cu	Li
DESCRIPTION	ppm	ppm	ppm	ppm	ppm	ppm	ppm	ppm	ppm	ppm	ppm	ppm	ppm
CAL006	17	0.11	12.95	30	<1	10.2	0.7	175	<0.5	<0.5	8	7	50
CAL007	11.15	0.13	1.47	48	1	8.4	0.92	149	<0.5	<0.5	22	429	40
CAL012	7.35	0.06	2.18	18	1	5.4	0.47	100	<0.5	<0.5	17	478	30
CAL018	8.71	0.12	2.86	74	1	9.6	0.78	184	<0.5	<0.5	13	666	60
CAL019	14.7	0.09	1.41	6	1	6	0.69	103	<0.5	<0.5	8	123	20
CAL024	10.95	0.09	1.99	54	1	6.4	0.58	182	<0.5	<0.5	15	193	60
CAL026	9.51	0.06	30.9	12	1	5.2	0.44	84	<0.5	<0.5	5	211	30
CAL032	15	0.11	3.78	34	1	7.9	0.74	146	<0.5	<0.5	8	232	30
CAL034	11.55	0.35	2.9	120	3	23.3	2.3	189	<0.5	<0.5	26	211	80
CAL035	10.45	0.13	2.73	70	2	8.7	0.81	138	<0.5	<0.5	14	25	40
CAL038	18.45	0.66	19.1	9	1	39.2	4.66	170	<0.5	<0.5	4	65	20
CAL044	21.8	0.21	7.64	25	<1	16.2	1.58	148	<0.5	<0.5	4	3	30
CAL052	8.91	0.06	2.63	34	1	6.5	0.39	148	0.5	<0.5	13	1580	40
CAL053	5.68	0.1	2.46	<5	<1	7.7	0.56	38	<0.5	<0.5	3	514	10
CAL057	27.4	0.05	2.62	23	<1	5.4	0.42	211	<0.5	<0.5	5	4	40
CAL062	13.15	0.1	2.89	45	4	8.5	0.74	172	<0.5	<0.5	47	269	10

	ME-4ACD81	ME-4ACD81	ME-4ACD81	ME-4ACD81	ME-4ACD81	ME-MS42	ME-MS42	ME-MS42	ME-MS42	ME-MS42	ME-MS42	ME-MS42	ME-MS42
SAMPLE	Mo	Ni	Pb	Sc	Zn	As	Bi	Hg	In	Re	Sb	Sc	Se
DESCRIPTION	ppm	ppm	ppm	ppm	ppm	ppm	ppm	ppm	ppm	ppm	ppm	ppm	ppm
CAL006	18	6	22	3	27	1.1	0.02	<0.005	0.015	0.014	0.7	3.2	0.3
CAL007	22	4	9	5	35	0.3	0.08	0.006	0.045	0.009	<0.05	3.3	0.5
CAL012	6	3	8	2	12	0.4	0.3	<0.005	0.009	0.001	<0.05	1.3	0.4
CAL018	7	14	7	6	23	0.6	0.49	<0.005	0.032	0.001	0.09	4.2	0.3
CAL019	1	4	3	2	8	0.3	0.1	<0.005	0.026	<0.001	<0.05	0.6	<0.2
CAL024	<1	5	9	5	21	0.1	0.08	<0.005	0.036	<0.001	<0.05	5.9	0.3
CAL026	93	1	20	2	9	0.2	0.11	<0.005	0.008	0.009	0.05	2	0.2
CAL032	1	9	6	4	8	0.5	0.24	<0.005	0.012	<0.001	<0.05	4.6	0.2
CAL034	6	61	6	12	16	0.3	0.05	<0.005	0.019	0.001	<0.05	9.6	0.5
CAL035	1	20	3	8	4	0.2	0.06	<0.005	0.02	<0.001	0.05	9.2	0.3
CAL038	1	2	29	2	6	0.4	0.05	<0.005	0.005	<0.001	<0.05	2.2	0.2
CAL044	<1	4	35	3	24	0.2	0.01	<0.005	0.011	<0.001	<0.05	3.5	0.2
CAL052	3	7	18	3	41	0.1	0.3	<0.005	0.063	<0.001	<0.05	4.5	0.5
CAL053	6	6	21	<1	11	<0.1	0.18	0.005	0.018	0.001	<0.05	0.5	<0.2
CAL057	<1	4	34	2	22	0.2	0.01	<0.005	0.008	<0.001	<0.05	2.4	<0.2
CAL062	115	12	10	5	81	0.2	0.35	<0.005	0.016	0.03	<0.05	3.2	0.3

	ME-MS42	ME-MS42	S-IR08	C-IR07
SAMPLE	Te	Tl	S	C
DESCRIPTION	ppm	ppm	%	%
CAL006	<0.01	0.22	0.01	<0.01
CAL007	0.09	0.24	0.19	<0.01
CAL012	0.11	0.05	0.2	<0.01
CAL018	0.06	0.29	0.08	<0.01
CAL019	0.03	0.05	0.03	<0.01
CAL024	0.03	0.4	0.08	<0.01
CAL026	0.03	0.12	0.06	0.01
CAL032	0.01	0.1	0.04	<0.01
CAL034	0.01	0.31	0.03	<0.01
CAL035	<0.01	0.06	<0.01	0.04
CAL038	0.01	0.17	0.02	0.05
CAL044	<0.01	0.26	<0.01	0.02
CAL052	0.3	0.31	0.34	<0.01
CAL053	0.07	0.04	0.07	<0.01
CAL057	<0.01	0.24	<0.01	0.02
CAL062	0.2	0.06	0.04	<0.01

Appendix 8 – Caravel Minerals Ltd four-acid digest geochemistry

Hole_ID	From	To	Garnet	Al	K	Na	Au	Ag	As	Bi	Cd	Cs	Cu	Mn	Mo	Pb	S	Sb	Se	Sn	Te	W	Zn
				%	%	ppm	ppb	ppm	ppm	ppm	ppm	ppm	ppm	%	ppm	ppm	%	ppm	ppm	ppm	ppm	ppm	ppm
12CADD001	324.2	325	Mod	7.19	2.23	22700	62	4.17	1.8	2.27	0.17	1.58	5780	0.196	86.6	20.8	0.79	1.2	2	2.2	0.56	3.1	50
12CADD001	325	326	Mod	7.04	2.41	22000	42	3.35	5.7	1.93	0.14	1.33	4690	0.199	25	24.7	0.59	4.1	1	1.9	0.51	0.4	44
12CADD001	326	327	Mod	7.29	1.92	26800	27	2.55	2.5	1.21	0.17	1.45	3850	0.081	114.5	26	0.5	1.49	1	1.8	0.44	1	53
12CADD001	327	328	Mod	6.94	1.68	25700	17	1.8	2.6	0.73	0.1	1.6	2490	0.051	48.9	16.5	0.31	0.69	1	2.3	0.29	0.3	28
12CADD001	328	329	Mod	7.18	1.43	27300	24	1.55	1.1	0.64	0.12	2.27	2130	0.062	152.5	17.3	0.27	0.51	1	2.8	0.21	1.5	41
12CADD001	329	330	Weak	4.91	2.58	15300	2.5	0.22	1.2	0.13	0.05	1.09	222	0.028	1.95	21.3	0.04	0.65	0.5	1.8	0.025	0.4	46
12CADD001	330	331	Weak	6.97	3.25	22400	7	0.63	0.8	0.47	0.06	2.98	836	0.027	10.2	22.7	0.1	0.47	0.5	2.2	0.09	2.1	30
12CADD001	331	332	Weak	8.14	2.89	28800	2.5	0.65	1.4	0.4	0.07	3.9	749	0.044	6.65	22.9	0.09	0.43	1	2.8	0.1	1.1	38
12CADD001	332	333	Weak	7.57	3.15	26300	2.5	0.19	0.6	0.61	0.01	2.35	174	0.031	7.97	17.8	0.03	0.44	0.5	1.8	0.025	2	22
12CADD001	333	334	Weak	7.5	3.5	24600	2.5	0.13	0.7	0.1	0.02	1.75	26.4	0.021	6.59	16.5	0.01	0.27	0.5	1.4	0.025	0.3	20
12CADD001	334	335	Weak	7.72	3.76	24700	2.5	0.68	1.2	0.36	0.04	1.68	757	0.026	7.65	18.4	0.11	0.39	0.5	1.4	0.1	0.9	19
12CADD001	335	336	Weak	9.07	3.39	32400	2.5	0.15	1.5	0.25	0.04	1.9	127	0.049	5.1	17.3	0.02	0.35	0.5	1.4	0.025	0.5	14
12CADD001	336	337	Weak	8.77	3.6	30000	5	0.5	1.4	0.28	0.03	1.76	572	0.05	10.95	17.1	0.09	0.84	1	1.5	0.07	1.2	20
12CADD001	337	338	Weak	6.61	3.9	18700	8	0.82	0.7	0.49	0.03	1.28	1140	0.069	51.4	16.3	0.24	0.43	1	1.3	0.16	0.3	16
12CADD001	338	339	Weak	6.19	3.72	17900	8	0.58	0.3	0.35	0.02	1.11	726	0.039	41.2	14.9	0.12	0.23	0.5	0.9	0.09	0.9	11
12CADD001	339	340	Weak	6.61	2.89	21800	24	1.85	1.4	1.17	0.07	1.36	2400	0.035	101.5	13.9	0.37	0.2	1	1.7	0.3	0.3	22
12CADD001	340	341	Weak	6.66	3.69	19000	9	0.86	0.1	0.45	0.03	1.73	1240	0.04	35.4	15.9	0.28	0.21	1	1.7	0.18	1.6	23
12CADD001	341	342	Weak	6.34	3.92	18200	30	2.25	0.4	1.55	0.09	1.47	3250	0.027	42	16.9	0.5	0.19	1	1.3	0.35	0.8	21
12CADD001	342	343	Weak	6.64	3.97	19200	26	2.2	1.6	1.24	0.08	1.48	2960	0.049	106.5	15.3	0.43	0.18	1	1.5	0.34	0.3	18
12CADD001	343	344	Weak	7.4	3.27	22400	20	1.14	1.8	0.74	0.05	2.09	1690	0.058	105	14.5	0.31	0.16	1	2	0.25	1.5	27
12CADD001	344	345	Mod	6.7	1.84	21700	39	2.81	0.8	1.47	0.21	2.3	5310	0.098	593	11.7	0.97	0.22	2	2.9	0.68	1.4	47
12CADD001	347.75	349	Weak	6.46	2.58	19200	90	3.94	0.4	2.72	0.25	1.38	8310	0.122	21.2	11.7	1.7	0.15	2	2.8	0.86	1	55
12CADD001	349	350	Weak	6.79	3.17	11500	157	4.68	1.4	4.89	0.27	3.63	9930	0.437	66.3	12.2	1.72	0.13	2	4.7	1.12	1.3	69
12CADD001	350	351	Weak	7.68	4.45	21300	2.5	0.12	0.5	0.11	0.01	2.08	123.5	0.032	1.64	19.1	0.02	0.13	1	1.5	0.025	1.3	15
12CADD001	351	352	Weak	6.87	1.91	22200	140	4.52	0.7	2.96	0.15	1.11	9540	0.09	31.3	12.2	1.24	0.11	2	2.7	0.77	0.6	45
12CADD001	352	353	Weak	7.2	1.94	27700	93	2.47	0.3	2.21	0.04	0.53	6180	0.047	68.1	13.2	0.75	0.09	1	2.6	0.58	0.8	25
12CADD001	353	354	Weak	7.3	2.03	29100	57	1.97	1.1	1.81	0.05	0.64	6370	0.039	54.3	16	0.71	0.16	1	2.5	0.52	0.5	24
12CADD001	354	355	Weak	5.76	2.03	19000	2.5	0.61	0.5	0.51	0.02	0.79	3480	0.053	24.4	8	0.36	0.11	1	1.4	0.18	1.3	25
12CADD001	355	356	None	4.01	0.92	2400	2.5	0.35	0.4	0.29	0.02	0.67	3110	0.07	15.45	5.1	0.38	0.21	1	1.3	0.1	0.5	34
12CADD001	356	357	None	6.56	1.39	14000	2.5	0.18	0.4	0.71	0.01	0.67	721	0.078	1.5	10.3	0.46	0.16	1	2.4	0.16	1	46
12CADD001	357	358	None	7.81	1.59	32700	35	1.86	0.9	1.71	0.05	0.51	6240	0.049	35.6	10.8	0.8	0.16	2	2.8	0.43	0.6	27
12CADD001	358	359	None	7.28	3.23	22800	37	2	0.2	1.37	0.06	1.3	3760	0.046	58.7	15.9	0.51	0.12	1	2.1	0.39	0.5	25
12CADD001	359	360	Mod	7.28	1.93	15200	44	0.73	0.4	0.43	0.05	1.96	1380	0.647	55.4	9.9	0.62	0.18	1	2.9	0.55	1.1	40
12CADD001	360	361	Mod	7.39	1.67	17800	27	0.72	1.1	0.5	0.05	1.56	1740	0.597	51.7	6.6	0.76	0.17	1	2	0.65	0.8	23
12CADD001	361	362	Mod	7.86	2.08	21200	19	0.41	0.4	0.4	0.02	1.25	841	0.335	6	5.5	0.33	0.11	1	1.7	0.26	1.2	28
12CADD001	362	363	Mod	7.18	1.32	22300	25	1.31	0.9	0.66	0.05	1.12	2540	0.175	50.1	8.8	0.7	0.15	1	1.8	0.42	0.6	25
12CADD001	363	364	Mod	8.05	2.36	24600	18	1.17	0.3	0.76	0.05	1.88	2030	0.111	41.3	8.5	0.57	0.11	1	1.5	0.34	0.6	21
12CADD001	364	365	Weak	8.08	2.27	26500	22	0.96	0.4	0.76	0.04	2.07	1510	0.098	8.1	7.1	0.24	0.09	1	1.3	0.18	0.4	18

12CADD001	365	366	Weak	7.94	2.71	24700	116	8.42	0.1	4.82	0.27	1.57	15700	0.062	76.9	8.3	1.84	0.1	3	2.7	1.36	0.6	57
12CADD001	366	367	Weak	7.76	2.38	24300	20	1.15	0.1	0.81	0.04	1.79	1720	0.092	4.09	5.1	0.23	0.08	1	1.5	0.21	0.6	15
12CADD001	367	368	Weak	7.72	2.42	23800	17	1.13	0.3	0.71	0.04	1.71	1690	0.099	9.97	5.2	0.26	0.09	1	1.5	0.21	0.6	14
12CADD001	368	369	Weak	7.51	1.54	22900	28	2.36	0.6	1.53	0.08	1.47	4170	0.239	54.6	9	0.69	0.11	1	2.3	0.34	1.3	20
12CADD001	369	370	Weak	8.29	2.81	24100	12	0.99	0.2	0.66	0.04	1.3	1660	0.197	10.5	5.5	0.29	0.07	1	2.1	0.16	1	15
12CADD001	370	371	Weak	7.83	1.9	24500	13	1.34	0.3	0.75	0.04	1.27	1830	0.118	4.24	5.4	0.25	0.12	1	2.4	0.15	0.5	20
12CADD001	371	372	Weak	7.72	2	23200	26	2.54	0.3	2.11	0.08	1.13	4200	0.139	20.6	5	0.57	0.13	1	1.9	0.35	0.4	19
12CADD001	372	373	Weak	7.29	1.47	20100	34	2.74	0.2	1.92	0.08	1.18	4660	0.174	26.5	4.8	0.8	0.1	1	2.1	0.36	1.3	21
12CADD001	373	374	Weak	7.33	1.99	19100	22	2.06	0.2	1.41	0.06	1.03	3650	0.162	27.8	5.8	0.85	0.13	1	1.9	0.39	1	17
12CADD001	374	375	Weak	7.77	1.53	18700	18	1.3	0.3	0.87	0.05	1.19	2480	0.3	14.2	5.5	0.71	0.13	1	2	0.28	1	16
12CADD001	375	376	Weak	7.48	2.35	19000	26	2.04	0.1	1.48	0.05	1.3	3160	0.157	44.4	5.4	0.61	0.14	1	1.7	0.31	0.9	15
12CADD001	376	377	Weak	7.52	2.33	19400	36	3.08	0.8	2.4	0.1	1.68	4950	0.122	21.4	5.1	0.71	0.09	1	2	0.49	1	20
12CADD001	377	378	Weak	7.74	2.46	19500	57	3.8	0.2	2.83	0.11	1.83	5730	0.133	12.25	7.1	0.87	0.08	1	2.1	0.53	1.1	19
12CADD001	378	379	Weak	7.62	2.14	19300	20	1.06	4.6	1.05	0.03	2.11	1560	0.22	6.89	6.5	0.25	0.05	1	2.2	0.13	1.4	15
12CADD001	379	380	Mod	7.6	1.75	19400	14	0.63	3.9	0.45	0.03	2.14	1070	0.276	23.8	5.4	0.25	0.025	1	2.3	0.14	1.5	16
12CADD001	380	381	Mod	7.51	1.38	18600	11	0.39	5.1	0.44	0.03	2.72	664	0.276	24.7	5	0.52	0.07	1	2.1	0.25	4.5	17
12CADD001	381	382	Mod	7.58	2.89	15800	18	0.89	4.1	0.55	0.04	2.1	1590	0.221	66	4.4	0.44	0.05	1	1.8	0.17	1.2	13
12CADD001	382	383	Mod	7.56	3.45	14000	18	0.75	1.3	0.62	0.03	1.98	1120	0.147	35.6	3.9	0.19	0.025	0.5	2.1	0.15	1.7	11
12CADD001	383	384	Strong	7.49	1.9	13000	30	1.41	1.2	1.02	0.04	1.84	2350	0.35	33.6	3.6	0.52	0.05	1	2.5	0.24	4	14
12CADD001	384	385	Strong	7.01	1.56	11200	37	2.08	1.2	1.36	0.08	1.79	3490	0.414	12.6	5.1	0.59	0.05	1	2.7	0.29	2.6	23
12CADD001	385	386	Strong	7.76	2.62	15500	32	2.58	0.9	1.51	0.08	1.38	3670	0.242	12.35	4.6	0.51	0.025	1	2.1	0.3	1.2	18
12CADD001	386	387	Strong	7.6	3.22	13400	18	1.25	0.6	0.87	0.04	1.37	1740	0.295	4.28	4.4	0.42	0.05	1	1.7	0.21	0.7	15
12CADD001	387	388	Strong	7.35	2.58	15100	27	1.51	0.6	0.78	0.06	1.27	2200	0.204	2.21	4.1	0.56	0.05	1	1.9	0.4	1.2	16
12CADD001	388	389	Strong	7.22	3.13	10700	10	0.79	1.3	0.26	0.05	1.55	2510	0.424	7.13	4.3	1.22	0.05	1	2.2	0.6	0.6	20
12CADD001	389	390	Strong	5.69	2.36	5000	65	1.97	0.8	1.12	0.09	2.59	4600	0.472	158	5.3	1.42	0.06	2	2.1	0.75	0.6	26
12CADD001	390	391	Strong	5.83	1.35	2500	19	0.66	1.3	0.57	0.07	2.63	1270	0.833	16.45	3.5	0.18	0.07	1	1.1	0.19	0.6	17
12CADD001	391	392	Strong	6.46	3.25	6500	35	0.91	1.6	0.88	0.09	3.49	1830	0.713	13.45	7.7	0.43	0.12	1	1.3	0.28	1.2	19
12CADD001	392	393	Weak	7.86	2.83	27100	2.5	0.03	0.8	0.08	0.02	4.5	26.1	0.028	5.06	12.5	0.01	0.09	0.5	1.5	0.025	1.8	14
12CADD001	393	394	Weak	7.31	2.86	20300	15	0.68	1	0.76	0.05	5.58	1310	0.285	90.2	11.9	0.38	0.09	1	1.6	0.28	2.2	19
12CADD001	394	395	Weak	7.4	3.9	19700	19	1.51	0.9	1.19	0.07	5.84	2590	0.092	63.9	18.9	0.45	0.1	1	1.8	0.28	2.6	24
12CADD001	395	396	Weak	7.82	2.64	25500	24	1.45	1.1	1.22	0.08	6.32	2600	0.073	37.7	14	0.45	0.12	1	2.4	0.37	2.5	29
12CADD001	396	397	Weak	7.57	2.16	26000	29	2.63	1.3	1.62	0.13	5.33	4400	0.071	36.2	10.8	0.66	0.12	1	2.6	0.43	1.8	35
12CADD001	397	398	Weak	7.54	2.8	25000	40	2.53	0.9	2.15	0.16	3.58	4460	0.038	42.6	10.1	0.62	0.08	1	1.9	0.46	0.7	28
12CADD001	398	399	Weak	7.27	1.91	26500	23	1.7	0.5	1.21	0.12	3.17	2900	0.036	18.9	7.3	0.44	0.08	1	1.6	0.3	0.5	28
12CADD001	399	400	Weak	7.32	2.99	23100	135	7.87	0.6	4.69	0.36	3.5	9330	0.051	179.5	8.4	1.51	0.09	2	2.2	1.29	0.6	49
12CADD001	400	401	Weak	7.72	2.18	27300	36	1.92	0.5	1.27	0.12	3.71	3130	0.069	78.9	9.5	0.45	0.1	1	1.5	0.39	0.8	29
12CADD001	401	402	Weak	7.75	2.38	28600	8	0.56	0.4	0.48	0.06	2.91	792	0.034	6.46	10.1	0.09	0.025	0.5	1.2	0.1	0.5	20
12CADD001	402	403	Weak	7.75	2.28	27300	22	1.37	0.9	1.15	0.12	4.75	2200	0.051	23.1	10	0.33	0.09	1	1.5	0.24	1.2	25
12CADD001	403	404	Weak	7.54	2.09	26400	51	3.16	0.5	2.31	0.17	3.35	5220	0.099	32.1	5.7	0.67	0.025	1	1.4	0.52	0.3	31

12CADD001	404	405	Weak	7.96	2.29	28500	34	2.43	0.2	1.69	0.13	3.33	4020	0.065	5.99	5.7	0.52	0.025	1	1.4	0.4	0.3	25
12CADD001	405	406	Weak	7.72	2.1	27500	15	1	0.5	0.69	0.09	3.46	1690	0.093	8.6	6.7	0.28	0.06	0.5	1.2	0.19	0.3	25
12CADD001	406	407	Weak	7.51	1.63	29300	35	1.93	0.3	1.54	0.12	3.08	2980	0.049	1.25	5.5	0.35	0.025	1	0.9	0.33	0.3	23
12CADD001	407	408	Weak	7.23	2.04	27000	34	1.64	0.4	1.3	0.1	3.04	2490	0.058	15.35	5.6	0.32	0.025	1	0.9	0.28	0.2	19
12CADD001	408	409	Weak	7.58	2.2	28500	24	1.39	0.3	1.14	0.04	2.91	2200	0.046	78.2	5.8	0.29	0.025	1	1	0.22	0.3	18
12CADD001	409	410	Weak	7.43	2.11	27400	48	3.32	0.5	2.4	0.11	2.5	5410	0.043	42.2	7.2	0.75	0.025	1	1.2	0.49	0.2	25
12CADD001	410	411	Weak	7.41	2.79	27100	12	0.81	0.5	0.66	0.03	2.32	1110	0.036	8.09	10.4	0.15	0.025	0.5	1.2	0.13	0.4	17
12CADD001	411	412	Weak	7.57	2.22	28700	19	1.53	0.3	1.12	0.05	2.08	2180	0.046	131.5	8.2	0.29	0.025	1	1.1	0.23	0.4	18
12CADD001	412	413	Weak	7.56	2.61	27000	26	2.22	0.3	1.6	0.07	2.28	3720	0.037	60.9	6.9	0.5	0.06	1	1.1	0.35	0.3	18
12CADD001	413	414	Weak	7.75	2.02	29200	40	1.64	0.6	1.54	0.05	4.35	2730	0.064	16.5	6.8	0.39	0.06	1	1.4	0.31	0.7	18
12CADD001	414	415	Weak	7.52	2.06	28200	16	1.11	0.4	0.84	0.04	2.05	1810	0.039	2.11	5.1	0.23	0.025	0.5	0.9	0.19	0.3	15
12CADD001	415	416	Weak	7.45	1.63	29000	12	0.79	0.4	1	0.03	1.38	1500	0.063	22.2	4.7	0.26	0.025	1	1	0.31	0.4	14
12CADD001	416	417	Weak	7.95	1.81	29200	2.5	0.27	0.4	0.23	0.02	1.51	559	0.114	40.3	5.2	0.18	0.025	0.5	1.2	0.14	0.4	14
12CADD001	417	418	Weak	7.32	2.34	24300	10	0.72	0.3	1.64	0.03	1.56	1300	0.151	62.1	5.2	0.5	0.025	1	1.4	0.35	0.3	15
12CADD001	418	419	Weak	7.13	1.52	25900	12	0.86	0.4	0.6	0.04	2.16	1240	0.15	4.87	5.6	0.27	0.025	1	1.5	0.16	0.5	16
12CADD001	419	420	Weak	7.16	1.55	27000	38	2.44	0.5	2.67	0.09	2.24	4120	0.067	31.7	8.7	0.57	0.05	1	2	0.55	0.7	21
12CADD001	420	421	Weak	7.28	1.84	27600	10	0.73	0.1	0.55	0.02	2.03	969	0.042	4.65	5.1	0.14	0.025	1	1	0.12	0.4	14
12CADD001	421	422	Weak	7.22	1.56	28300	23	1.7	0.1	1.37	0.06	2.08	2420	0.037	16.45	5.1	0.31	0.05	1	1	0.27	0.5	16
12CADD001	422	423	Weak	7.12	2.02	26500	35	2.07	0.1	1.63	0.08	1.92	3040	0.054	20.1	5.6	0.4	0.025	1	1.2	0.31	0.4	17
12CADD001	423	424	Weak	7.08	2.01	26000	25	1.45	0.2	1.15	0.05	1.85	2090	0.076	13.15	6.1	0.26	0.025	1	1.1	0.21	0.5	15
12CADD001	424	425	Weak	7.18	1.8	27200	31	2.11	0.1	1.64	0.08	2.06	3050	0.085	13.7	6.1	0.38	0.025	1	1.2	0.29	0.6	17
12CADD001	425	426	Weak	7.11	2.01	26600	31	2.42	0.2	1.91	0.07	1.89	3420	0.046	37.3	6.2	0.45	0.025	1	1.2	0.45	0.5	18
12CADD001	426	427	Weak	6.53	1.93	24100	86	4.3	0.3	3.86	0.13	1.39	7110	0.033	172.5	8.2	1.01	0.025	2	1.3	0.85	0.4	24
12CADD001	427	428	Weak	6.73	1.51	26900	15	1.17	0.4	1.17	0.02	1.08	1840	0.05	20.9	6.4	0.27	0.025	1	1.1	0.28	0.4	12
12CADD001	428	429	Weak	7	1.69	26800	58	2.42	0.2	1.93	0.07	1.25	3640	0.056	8.21	8.1	0.51	0.025	1	1.2	0.49	0.4	17
12CADD001	429	430	Weak	7.61	2.04	28900	40	2.13	0.3	1.75	0.06	1.2	3420	0.064	4.7	11.8	0.56	0.025	1	1.3	0.48	0.5	15
12CADD001	430	431	Weak	7.33	2.26	25900	12	0.86	0.2	0.63	0.03	1.56	1190	0.069	15.95	7.4	0.18	0.025	1	1.3	0.18	0.5	13
12CADD001	431	432	Weak	7.06	2.65	22800	16	1.03	0.3	0.83	0.02	2.03	1620	0.094	91.4	7.4	0.35	0.025	1	1.4	0.35	0.9	14
12CADD001	432	433	Mod	6.01	1.17	11100	16	0.6	0.4	0.51	0.04	1.45	1240	0.686	18.1	5.2	0.45	0.025	1	1.5	0.4	0.7	20
12CADD001	433	434	Mod	5.75	1.29	15500	88	1.79	0.4	1.17	0.06	1.14	3690	0.309	40.1	4.9	1.01	0.025	2	1.7	0.69	0.8	20
12CADD001	434	435	Mod	6.09	0.9	16600	26	1.08	0.9	1.45	0.03	2.06	2320	0.264	28.4	4.2	1.35	0.025	2	2.2	1.01	1.6	22
12CADD001	435	436	Weak	7.17	2.8	22900	26	1.73	0.2	1.21	0.04	1.64	2700	0.062	67.6	5.9	0.41	0.025	1	1.5	0.56	0.3	16
12CADD001	436	437	Weak	6.27	2.1	20800	27	1.92	0.9	1.68	0.06	1.27	2960	0.073	12.75	4.9	0.49	0.05	1	1.4	0.55	0.7	16
12CADD001	437	438	Weak	6.13	1.59	22300	28	1.35	0.8	1.12	0.03	1.94	2280	0.067	29.6	5.7	0.42	0.08	1	1.3	0.43	1.3	14
12CADD001	438	439	Weak	7.38	1.59	28700	17	0.97	0.3	0.88	0.03	1.97	1600	0.052	9.02	5.2	0.23	0.025	1	1.1	0.2	0.4	14
12CADD001	439	440	Weak	7.21	2.07	26800	19	1.21	0.3	1.15	0.04	1.67	1880	0.038	17.45	5.7	0.27	0.025	1	1	0.21	0.4	13
12CADD001	440	441	Weak	7.24	1.84	27900	11	0.76	0.4	0.69	0.04	1.9	1090	0.042	6.5	7.9	0.14	0.025	0.5	1	0.12	0.4	16
12CADD001	441	442	Weak	6.91	2.35	25400	32	1.63	0.6	1.45	0.05	1.75	2750	0.036	30.2	12	0.36	0.07	1	1.1	0.28	0.6	14
12CADD001	442	443	Weak	7.36	2.17	27100	62	3.89	0.4	3.87	0.07	1.7	4670	0.051	228	8.2	0.72	0.05	1	1.4	1.57	0.7	21

12CADD001	443	444	Weak	6.93	2.03	25500	37	1.62	0.3	1.82	0.04	1.37	2700	0.048	39.5	7.8	0.33	0.025	1	1.2	0.31	0.4	15
12CADD001	444	445	Weak	7.07	2.19	25800	22	1.2	0.4	1.19	0.04	1.19	1990	0.049	26	8.3	0.27	0.025	1	1.2	0.25	0.4	13
12CADD001	445	446	Weak	6.69	1.85	22800	56	2.47	0.2	2.42	0.09	0.97	4540	0.151	67.7	8	0.66	0.025	1	1.3	0.78	0.3	18
12CADD001	446	447	Weak	6.91	2.12	23600	41	1.56	0.3	1.33	0.05	0.93	2790	0.118	34.3	9	0.42	0.025	1	0.9	0.43	0.3	13
12CADD001	447	448	Weak	6.1	1.74	14700	35	0.65	0.5	0.7	0.04	0.54	1270	0.486	14.55	5.8	0.36	0.025	1	0.9	0.27	0.3	26
12CADD001	448	449	Weak	6.42	3.54	15400	36	0.99	0.5	1.06	0.11	2.19	1880	0.179	48.5	6.7	0.35	0.05	1	1.3	0.38	0.7	15
12CADD001	449	450	Weak	7.38	1.29	24000	25	1.83	0.2	2.08	0.11	2.12	3300	0.135	8.53	6.7	0.46	0.025	1	1.9	0.47	1	23
12CADD001	450	451	Mod	6.86	0.96	19300	47	1.64	0.1	2.38	0.11	1.82	3010	0.109	3	6.4	0.39	0.025	1	2.6	0.36	2.4	21
12CADD001	451	452	Mod	7.08	0.95	20900	57	1.96	0.3	2.7	0.21	1.86	3520	0.072	5.69	6.5	0.55	0.025	1	2.8	0.57	2.1	34
12CADD001	452	453	Mod	6.63	0.76	18600	120	2.78	0.2	7.16	0.3	2.05	5100	0.095	33.9	6.8	0.65	0.025	1	3.2	0.68	1.7	42
12CADD001	453	454	Mod	7.13	2.26	19900	32	1.26	0.4	1.73	0.09	2.23	2190	0.084	13.95	9.4	0.27	0.025	1	2	0.24	1.3	20
12CADD001	454	455	Mod	7.06	1.54	18000	48	1.24	0.3	1.82	0.11	3.05	2380	0.26	5.98	6.7	0.37	0.025	1	2.5	0.38	1.2	24
12CADD001	455	456	Mod	6.56	2.25	16700	35	1.84	0.7	1.39	0.09	2.9	3140	0.068	13.65	7.2	0.76	0.06	1	2.1	0.79	0.5	21
12CADD001	456	457	Mod	6.48	1.72	17200	75	2.33	0.2	2.09	0.13	2.28	4910	0.135	44.1	7.8	1.21	0.025	2	1.8	0.86	0.5	23
12CADD001	457	458	Mod	6.6	2.91	15800	26	0.61	0.5	0.89	0.06	2.8	1370	0.125	34	10.2	0.3	0.025	1	1.7	0.3	0.5	17
12CADD001	458	459	Mod	6.76	1.99	18300	30	1.17	1	1.52	0.07	3.13	2510	0.176	6.97	8.3	0.47	0.1	1	2.2	0.55	0.7	20
12CADD001	459	460.3	Mod	6.36	0.84	20200	59	1.92	0.3	2.19	0.12	2.54	3660	0.175	34.1	9	0.54	0.07	1	2	0.64	1.2	23
12CADD001	460.3	461.5	Weak	7.65	2.42	26200	2.5	0.15	0.3	0.18	0.01	2.42	209	0.023	116.5	11.1	0.03	0.025	0.5	1.6	0.025	1	15
12CADD001	461.5	462	Weak	6.14	1.61	17700	168	5.98	0.1	6.33	0.31	2.62	12200	0.194	22.6	9.9	1.67	0.025	2	3.8	1.9	1.4	58
12CADD001	462	463	Weak	7.44	1.6	25800	70	2.08	0.5	2.01	0.08	2.86	4050	0.103	52.8	10.5	0.51	0.06	1	2.6	0.59	1.3	32
12CADD001	463	464	Weak	7.07	3.31	22200	22	1.12	0.2	0.95	0.04	1.91	1950	0.03	15.05	12.3	0.23	0.025	1	1.2	0.26	0.6	18
12CADD001	464	465	Weak	8.1	1.65	33200	2.5	0.17	0.5	0.17	0.01	2.01	237	0.037	2.58	13.6	0.03	0.025	0.5	1.2	0.06	0.7	16
12CADD001	465	466	Weak	8.04	2.55	30900	15	0.7	0.6	0.47	0.05	1.52	1270	0.069	4.85	15.5	0.17	0.025	1	1	0.16	0.7	14
12CADD001	466	467	Weak	6.7	2.55	23900	12	0.65	0.2	0.53	0.03	1.11	1110	0.031	16.3	12.3	0.14	0.025	0.5	0.9	0.17	0.3	11
12CADD001	467	468	Mod	6.64	2.04	23300	42	1.73	0.2	1.64	0.06	0.93	3110	0.094	22.8	12.2	0.42	0.025	1	0.9	0.44	0.4	12
12CADD001	468	469	Mod	6.42	2.49	18300	23	1.01	0.2	0.88	0.04	0.83	1970	0.18	10.8	11.1	0.38	0.025	1	0.6	0.33	0.4	10
12CADD001	469	470	Mod	6.1	2.05	16900	59	1.55	0.6	1.61	0.05	1	3010	0.217	68	8	0.53	0.025	1	1	0.63	0.4	12
12CADD001	470	471	Mod	7.16	2.33	21600	49	1.02	0.2	1.47	0.05	1.37	1830	0.254	20.6	6.7	0.31	0.025	1	1.2	0.27	0.4	15
12CADD001	471	472	Mod	7.19	2.83	22100	11	0.52	0.3	0.48	0.03	1.76	863	0.128	9.49	7.6	0.13	0.025	0.5	1.1	0.15	0.4	13
12CADD001	472	473	Mod	7.41	2.52	24900	27	0.92	0.2	0.87	0.04	2.02	1480	0.042	9.12	6.2	0.19	0.025	0.5	1.3	0.2	0.5	15
12CADD001	473	474	Mod	7.06	2.09	24500	110	1.03	0.4	1.01	0.04	2.1	1650	0.057	6.1	6.1	0.24	0.025	1	1.4	0.21	0.7	15
12CADD001	474	475	Mod	7.24	1.98	25500	22	0.96	0.3	0.88	0.05	2.52	1630	0.06	4.25	5	0.22	0.025	1	1.4	0.18	1	16
12CADD001	475	476	Mod	6.85	2.1	24700	35	1.43	0.2	1.44	0.05	1.55	2500	0.026	3.9	4.9	0.36	0.025	1	1.1	0.37	0.4	13
12CADD001	476	477	Mod	7.35	2.65	23900	26	1.21	0.4	1.42	0.04	2.16	2200	0.089	46.8	5.8	0.39	0.06	1	1.4	0.29	1.1	14
12CADD001	477	478	Mod	7.34	2.2	22600	19	0.63	0.4	0.65	0.04	2.01	1270	0.179	30.9	5.2	0.37	0.025	1	1.4	0.27	0.7	14
12CADD001	478	479	Mod	7.4	2.18	25000	6	0.43	0.5	0.39	0.03	1.83	627	0.059	3.76	4.4	0.1	0.025	0.5	1.1	0.08	0.4	11
12CADD001	479	480	Mod	7.37	2.56	22200	64	1.96	0.2	2.42	0.08	2.19	3590	0.133	12.4	4.7	0.57	0.025	1	1.6	0.44	0.8	16
12CADD001	480	481	Mod	7.34	2.21	22000	13	0.7	0.3	0.71	0.01	2.21	1180	0.166	389	6.6	0.24	0.025	1	1.3	0.18	1	14
12CADD001	481	482	Mod	8.08	2.08	25400	40	1.51	0.1	1.36	0.1	2.6	2810	0.107	17.8	4.7	0.42	0.025	1	1.7	0.42	0.8	19

12CADD001	482	483	Mod	7.72	3.57	20700	41	1.2	0.1	1.15	0.05	2.3	2240	0.028	9.73	5	0.45	0.025	1	1.4	0.42	0.6	14
12CADD001	483	484	Mod	7.73	2.26	25300	29	0.62	0.1	0.64	0.02	1.88	987	0.063	29.8	4.2	0.14	0.025	0.5	1.4	0.14	0.6	13
12CADD001	484	485	Mod	8.53	3.27	23800	21	0.46	0.1	0.37	0.02	2.32	730	0.1	56.8	5.2	0.13	0.025	0.5	1.6	0.12	0.8	14
12CADD001	485	486	Mod	7.02	2.17	14200	45	1.27	0.6	1	0.06	1.89	3370	0.673	66.7	5.6	1.22	0.06	2	1.5	0.5	0.8	22
12CADD001	486	487	Mod	6.94	2.98	15900	19	0.63	0.2	0.65	0.02	2.54	1900	0.331	73.1	6.5	1.21	0.025	2	1.6	0.52	0.8	17
12CADD001	487	488	Mod	7.66	2.24	24900	17	1.07	0.1	0.9	0.05	2.26	1670	0.087	19.75	5.1	0.27	0.025	1	1.3	0.17	0.6	17
12CADD001	488	489	Mod	8.3	2.23	27100	19	1.14	0.1	0.97	0.05	2.22	1800	0.059	18.85	4.9	0.22	0.025	1	1.2	0.18	0.6	23
12CADD001	489	490	Mod	7.52	1.91	26700	24	1.15	0.1	0.91	0.05	1.91	1850	0.055	3.4	4.4	0.24	0.025	1	0.9	0.16	0.4	17
12CADD001	490	491	Mod	7.8	1.75	27600	6	0.49	0.1	0.33	0.03	1.9	613	0.075	1.37	4	0.08	0.025	0.5	0.8	0.06	0.4	16
12CADD001	491	492	Mod	8.18	1.79	28100	8	0.67	0.1	0.51	0.04	2.03	936	0.063	2.86	4.6	0.12	0.025	0.5	0.9	0.09	0.3	15
12CADD001	492	493	Mod	7.69	1.74	27000	25	1.39	0.3	1.11	0.06	2.24	2370	0.065	2.88	4.2	0.28	0.025	1	1	0.21	0.3	17
12CADD001	493	494	Mod	8.61	2.1	27200	33	0.67	0.2	0.54	0.04	3.38	1270	0.171	16.35	11.6	0.18	0.05	1	1.8	0.13	0.7	22
12CADD001	494	495	Mod	7.48	2.22	22600	29	1.11	0.2	0.96	0.04	2.15	2260	0.173	72.5	6.7	0.36	0.025	1	1.7	0.29	0.5	21
12CADD001	495	496	Mod	6.95	2.14	14200	128	4.17	0.6	3.01	0.17	1.39	8800	0.727	235	6.8	1.38	0.05	2	1.8	0.99	0.6	37
12CADD001	496	497	Mod	6.64	2.85	12400	120	4.77	0.1	3.73	0.21	1.43	9790	0.554	132	7	1.53	0.025	3	1.6	1.39	0.4	30
12CADD001	497	498	Mod	6.27	2.77	7100	162	3.85	0.3	3.22	0.16	1.44	7910	0.9	66.5	6	1.65	0.08	3	1.3	1.45	1.2	27
12CADD001	498	499	Mod	4.19	2.02	7100	301	12.65	0.3	11.45	0.54	0.95	28200	0.382	98.2	4.7	4.43	0.11	8	2.3	4.84	0.5	63
12CADD001	499	500	Mod	7.14	1.93	19200	38	1.11	0.1	1.07	0.03	1.32	2370	0.415	63.8	6.3	1.26	0.025	2	1	0.79	0.4	14
12CADD001	500	501	Mod	6.72	3.01	16300	48	1.07	0.2	0.76	0.02	1.85	2480	0.296	81.7	8	1.29	0.025	2	1	0.66	0.6	13
12CADD001	501	502	Mod	7.55	3.32	17500	62	1.34	0.4	1.12	0.06	1.98	2810	0.413	89.3	10.1	0.65	0.05	1	1.2	0.54	1	18
12CADD001	502	503	Mod	7.89	2.73	23000	24	1.11	0.1	0.89	0.04	2.34	1910	0.121	12.2	6.8	0.27	0.025	1	1.6	0.25	0.6	18
12CADD001	503	504	Mod	7.74	2.24	24700	12	0.68	0.1	0.51	0.03	2.3	1130	0.094	42.1	10.6	0.15	0.025	0.5	1.8	0.13	0.4	18
12CADD001	504	505	Mod	7.93	2.07	25300	27	1.64	0.1	1.09	0.07	2.37	2480	0.117	4.73	9.5	0.35	0.025	1	2.2	0.28	0.4	25
12CADD001	505	506	Mod	7.19	2	23100	22	1.07	0.1	0.88	0.02	2.23	1680	0.09	70	5.5	0.23	0.025	0.5	1.3	0.19	0.8	17
12CADD001	506	507	Mod	7.74	2.22	25100	36	1.84	0.1	1.63	0.05	2.05	3050	0.065	18.5	5.6	0.38	0.025	1	1.3	0.38	0.5	20
12CADD001	507	508	Mod	7.86	2.04	26600	22	1.18	0.1	0.84	0.03	2.3	1880	0.071	27.8	5.4	0.24	0.025	0.5	1.5	0.21	0.6	18
12CADD001	508	509	Mod	7.61	2.34	24600	64	3.3	0.1	2.68	0.12	2.42	5460	0.079	32.6	6.1	0.76	0.025	1	1.9	0.9	1	29
12CADD001	509	510	Mod	7.51	2.2	25600	17	1.11	0.1	0.83	0.03	2.12	1760	0.045	28.8	5.2	0.21	0.025	1	1.2	0.16	0.5	15
12CADD001	510	511	Mod	8.1	1.77	28100	17	1.07	0.1	0.79	0.04	2.19	1680	0.074	15.75	5.4	0.2	0.025	0.5	1.2	0.18	0.5	15
12CADD001	511	512	Mod	7.44	1.68	26900	65	2.58	0.2	2.39	0.08	1.77	4550	0.054	26.7	5.2	0.54	0.025	1	1.4	0.42	0.4	21
12CADD001	512	513	Mod	7.22	1.54	26300	35	1.77	0.4	1.46	0.06	1.75	2940	0.046	8.48	5.2	0.36	0.025	1	1.2	0.26	0.4	16
12CADD001	513	514	Mod	7.61	1.74	26600	23	1.2	0.1	0.93	0.05	2	1850	0.054	12.55	5.6	0.23	0.025	0.5	1.1	0.17	0.6	15
12CADD001	514	515	Mod	7.5	2.24	22100	36	1.26	0.1	0.81	0.04	2.45	2320	0.177	25.5	5.1	0.37	0.025	1	1.8	0.33	0.9	20
12CADD001	515	516	Strong	8	2.34	19500	16	0.69	0.1	0.37	0.03	2.93	1440	0.384	17.5	4.9	0.46	0.025	1	2.3	0.26	1	22
12CADD001	516	517	Strong	7.34	3.11	15000	26	0.58	0.5	0.4	0.03	2.71	1150	0.294	9.53	4.1	0.34	0.025	1	2.4	0.23	1	20
12CADD001	517	518	Strong	6.74	3.06	9300	34	1.4	0.2	0.69	0.05	2.67	3140	0.579	31.4	5.1	0.69	0.06	1	2.6	0.74	1.1	29
12CADD001	518	519	Strong	7.14	2.37	21500	72	0.97	0.1	0.63	0.05	2.26	1910	0.101	8.98	5	0.4	0.025	1	1.9	0.37	0.9	21
12CADD001	519	520	Strong	4.88	0.5	12600	55	2.81	0.1	2	0.08	1.11	7420	0.464	6.65	6.4	4.79	0.025	6	1.2	2.09	0.6	29
12CADD001	520	521	Strong	4.69	0.81	14000	248	6.18	1.1	5.73	0.39	0.48	16800	0.332	41.9	7.8	3.91	0.1	5	2	3.02	0.4	62

12CADD001	521	522	Strong	6.01	0.97	15600	235	8.57	0.3	6.39	0.47	2.62	19300	0.439	14.6	7	3.81	0.06	5	3.5	3.56	0.8	88
12CADD001	522	523	Mod	7.49	1.1	26700	34	1.09	0.3	1.13	0.07	2.42	2180	0.14	2.99	9.4	0.33	0.09	1	1.2	0.48	1.1	21
12CADD001	523	524	Mod	7.09	1.62	25200	6	0.21	0.4	0.21	0.03	2.18	451	0.074	2.8	7.9	0.09	0.06	0.5	0.8	0.1	0.8	11
12CADD001	524	525	Mod	7.59	2.09	22200	11	0.77	0.1	0.57	0.05	2.91	1680	0.269	7.88	9.2	0.87	0.025	1	1.7	0.37	0.8	25
12CADD001	525	526	Mod	8.11	1.7	26200	9	0.35	0.3	0.28	0.04	2.65	695	0.226	3.54	10.2	0.21	0.025	1	1.7	0.11	0.8	24
12CADD001	526	527	Mod	8.05	2.29	25600	22	1.19	0.1	1.02	0.07	2.5	2330	0.115	11.95	9.6	0.39	0.025	1	1.9	0.25	0.4	30
12CADD001	527	528	Mod	7.69	1.4	25700	25	1.03	0.3	0.78	0.05	3.05	1960	0.191	16.35	9.5	0.29	0.05	1	2	0.21	0.7	25
12CADD001	535	536	Weak	7.12	1.69	25200	43	2.28	0.4	1.49	0.17	2.38	4510	0.039	38.6	14.2	0.57	0.07	1	2.2	0.42	0.7	42
12CADD001	536	537.1	Weak	7.17	1.39	24900	55	2.54	0.4	1.81	0.17	2.63	4960	0.066	99.5	11.1	0.69	0.06	1	3.4	0.49	0.5	51
14CADD001	437	438	Weak	6.37	1.96	24100	53	0.57	0.4	0.2	0.01	2.43	1710	0.032	320	26.1	0.56	0.025	1	2	0.22	0.2	61
14CADD001	438	439	Weak	7.23	1.88	26300	24	0.99	0.7	0.52	0.06	3.49	1750	0.091	40.7	20.2	0.6	0.025	1	2.9	0.4	0.6	45
14CADD001	439	440	Weak	7.11	2.23	25000	65	2.59	0.4	1.45	0.14	2.92	4380	0.052	159.5	16.4	0.68	0.025	1	1.7	0.61	0.3	32
14CADD001	446	447	Weak	6.84	1.18	19900	52	2.66	0.2	2.77	0.12	5.04	4330	0.064	64.2	11.8	0.63	0.025	1	1.8	0.36	1	37
14CADD001	447	448	Mod	7.11	1.67	23700	39	1.43	0.3	2.07	0.28	1.71	2730	0.1	267	10.9	0.87	0.025	2	2.1	0.68	0.4	28
14CADD001	448	449	Mod	5.95	2.8	15200	6	0.61	0.6	0.64	0.01	2.02	1900	0.172	546	15.7	1.9	0.025	4	2	0.6	0.5	24
14CADD001	449	450	Mod	6.67	2.02	20100	17	1.24	0.4	0.62	0.05	2.03	3420	0.194	233	10.6	1.53	0.025	3	1.9	0.55	0.5	23
14CADD001	450	451	Mod	5.47	2.02	15100	20	2.19	1.2	1.47	0.05	2.3	6750	0.11	168	10.2	2.5	0.025	5	2.5	0.96	0.7	28
14CADD001	451	452	Mod	6.45	2.24	19300	23	0.98	0.5	0.72	0.01	2.84	2720	0.111	1480	13.3	1.24	0.05	2	2.3	0.73	0.8	24
14CADD001	452	453	Mod	7.48	2.4	25100	27	0.88	0.4	0.61	0.06	2.57	1620	0.05	113	21.8	0.29	0.06	1	2.4	0.23	0.6	28
14CADD001	453	454	Mod	7.14	2.47	24200	14	0.86	0.5	0.56	0.02	1.65	1510	0.03	27.9	26.5	0.21	0.025	1	2.3	0.15	0.3	24
14CADD001	454	455	Mod	6.72	1.73	22800	223	6.24	0.3	6.19	0.15	2.77	6690	0.059	277	13.3	1.1	0.025	2	3.3	2.44	0.6	43
14CADD001	455	456	Mod	7.16	1.84	24500	36	1.88	0.2	1.09	0.07	2.29	3090	0.083	59.2	8.7	0.49	0.025	1	2.2	0.45	0.3	26
14CADD001	456	457	Mod	7.18	2.25	21700	22	1.12	0.2	0.72	0.05	2.48	2000	0.183	73.9	6.5	0.52	0.025	1	2	0.36	0.3	21
14CADD001	457	458	Mod	6.6	2.15	21300	221	1.5	0.1	0.91	0.05	2.66	2340	0.087	225	12.6	0.45	0.025	1	1.8	0.35	0.4	23
14CADD001	458	459	Mod	5.74	1.67	19600	19	0.93	0.4	0.66	0.07	2.54	1670	0.064	51.2	13.5	0.39	0.025	1	2.4	0.23	0.6	24
14CADD001	459	460	Mod	7.23	1.89	26300	18	0.67	0.2	0.43	0.03	2.61	1220	0.062	94.7	18.1	0.35	0.025	1	3	0.21	0.4	29
14CADD001	460	461	Mod	7.08	2.3	23800	26	1.07	0.3	0.82	0.1	2.68	2150	0.085	169	28.3	0.89	0.025	2	3.3	0.44	0.7	36
14CADD001	461	462	Mod	5.73	1.82	21000	37	1.9	0.4	1.06	0.09	1.6	3530	0.032	64.7	17	0.85	0.025	2	2.3	0.53	0.4	26
14CADD001	462	463	Mod	6.48	2.52	21500	24	1.44	0.1	1.01	0.09	2.11	2400	0.063	109.5	17	0.37	0.025	1	2.6	0.31	0.5	28
14CADD001	463	464	Mod	6.37	2.35	22700	47	1.86	0.3	1.39	0.09	1.19	3000	0.068	77	16.1	0.47	0.025	1	1.5	0.53	0.3	18
14CADD001	464	465	Mod	6.45	2.04	23100	91	3.28	0.7	2.72	0.19	1.81	6340	0.061	89	14.6	0.89	0.025	2	2.5	0.66	0.4	28
14CADD001	465	466	Mod	7.16	1.52	24600	29	1.11	0.1	0.7	0.06	2.42	2370	0.122	128	8	0.82	0.025	2	1.8	0.46	0.8	22
14CADD001	466	467	Mod	7.38	2.42	24700	43	1.86	0.3	1.28	0.09	2.56	3330	0.091	50.8	10.3	0.44	0.025	1	2	0.35	0.4	22
14CADD001	467	468	Mod	7.09	1.71	25100	45	1.7	0.5	1	0.08	2.31	3170	0.097	9.73	8.6	0.5	0.025	1	2.2	0.34	0.4	23
14CADD001	468	469	Strong	6.53	1.54	17600	53	3.34	2	1.7	0.18	2.2	6610	0.588	57.5	5.6	1.91	0.025	3	2.3	1.23	0.6	31
14CADD001	469	470	Mod	7.17	1.69	24500	37	1.61	1.9	1.27	0.05	2.35	2690	0.1	73.4	5.8	0.4	0.025	1	1.7	0.41	0.5	20
14CADD001	470	471	Mod	6.99	1.72	23800	51	2.14	5.9	1.52	0.11	2.84	4110	0.066	76.9	6.8	0.58	0.025	1	2.2	0.42	0.6	29
14CADD001	471	472	Mod	5.7	1.16	18200	47	1.7	9.3	1.49	0.08	1.86	4880	0.226	270	9.4	1.81	0.025	3	2.4	1.83	0.5	32
14CADD001	472	473	Mod	6.01	2.83	17600	17	0.62	3.1	0.42	0.06	1.64	1400	0.064	135	23.9	0.54	0.025	1	1.4	0.29	0.3	19

14CADD001	473	474	Mod	6.81	2.17	22800	39	1.58	1.2	0.95	0.09	2.77	3420	0.052	179.5	22.2	0.56	0.025	1	2.5	0.39	0.4	36
14CADD001	474	475	Mod	7.13	2.37	22900	71	2.89	1.2	1.79	0.13	2.78	5830	0.086	37.9	11	0.92	0.025	2	2.2	0.52	0.4	31
14CADD001	475	476	Mod	6.5	1.97	20800	108	4.38	0.6	2.64	0.24	2.49	9100	0.098	105	12.4	1.35	0.025	2	3	0.82	0.7	44
14CADD001	476	477	Mod	6.59	1.86	21500	25	1	0.5	0.6	0.07	1.93	2170	0.178	130	9.8	0.72	0.025	1	1.8	0.5	0.6	22
14CADD001	477	478	Mod	7.04	2.02	25000	22	1.67	0.6	1	0.13	2.11	3380	0.068	101	15.9	0.58	0.025	1	2.2	0.59	0.4	33
14CADD001	478	479	Mod	6.3	2.12	20600	40	2.18	0.7	1.33	0.19	1.75	4990	0.106	43.5	16.9	0.95	0.025	1	2	0.81	0.3	41
14CADD001	479	480	Mod	5.47	2.45	17600	52	4.85	0.6	3.4	0.48	1.15	10100	0.027	34	19.2	2.12	0.05	3	2	1.84	0.2	72
14CADD001	480	481	Weak	6.95	2.81	23300	24	1.54	0.5	0.91	0.14	2.07	3140	0.033	30.8	24.9	0.45	0.025	1	2	0.52	0.3	38
14CADD001	481	482	Weak	5.92	3.96	16000	36	2.45	0.4	1.67	0.24	1.1	5460	0.034	43	23.1	0.75	0.025	1	1.3	0.69	0.1	35
14CADD001	482	483	Weak	6.58	3.18	21100	25	1.8	0.6	1.28	0.19	1.56	3800	0.048	49.8	18.7	0.54	0.025	1	1.6	0.45	0.3	37
14CADD001	483	484	Weak	7.34	2.38	26400	2.5	0.37	0.5	0.21	0.01	2.24	673	0.03	4.22	15.5	0.11	0.025	0.5	1.5	0.1	0.3	26
14CADD001	484	485	Strong	6.72	2.04	21400	17	1.48	0.6	1.05	0.16	1.96	3830	0.219	103.5	12.7	0.99	0.025	1	2.2	0.73	0.3	48
14CADD001	485	486	Strong	7.09	2.23	22500	7	0.76	0.6	0.57	0.07	1.61	2240	0.26	56.7	13.2	1.03	0.025	1	1.7	0.53	0.2	39
14CADD001	486	487	Weak	7.13	2.11	24800	16	1.33	0.5	0.91	0.13	1.96	3180	0.063	8.24	12.4	0.78	0.025	1	1.8	0.57	0.2	36
14CADD001	487	488	Weak	6.2	1.62	21400	38	4.54	0.4	2.5	0.32	1.59	10650	0.063	42.8	11.2	2.01	0.025	2	2	1.63	0.4	48
14CADD001	488	489	Weak	6.81	0.69	22600	48	2.67	0.3	2.42	0.26	1.53	6400	0.051	5.61	7.7	1.57	0.025	1	2.3	1.48	0.6	47
14CADD001	489	490	Weak	6.84	0.8	25100	41	2.02	0.3	1.64	0.18	1.56	4610	0.064	40.3	10.3	0.92	0.025	1	2	0.87	0.4	44
14CADD001	490	491	Weak	7.36	2.33	25400	8	0.72	0.1	0.53	0.07	2.48	1600	0.049	6.25	14.2	0.33	0.025	1	1.7	0.22	0.4	35
14CADD001	491	492	Weak	7.11	2.52	24400	13	1.05	0.3	0.73	0.14	2.13	2330	0.049	26.6	17.6	0.37	0.025	1	1.6	0.24	0.3	39
14CADD001	492	493	Weak	6.83	2.97	21600	21	1.75	0.2	1.21	0.23	2.14	3780	0.054	17.75	15.5	0.7	0.025	1	1.9	0.55	0.3	52
14CADD001	493	494	Weak	6.85	2.56	22600	23	1.53	0.5	1.26	0.23	2.05	3350	0.052	6.49	15.6	0.56	0.025	1	2	0.41	0.3	60
14CADD001	494	495	Weak	7.27	2.38	25500	7	0.97	0.3	0.47	0.14	2.15	3040	0.059	9.55	16.2	0.89	0.025	1	1.6	0.24	0.3	48
14CADD001	495	496	Weak	6.97	3.02	23700	2.5	0.18	0.5	0.13	0.04	1.89	245	0.028	2.94	18.6	0.03	0.025	0.5	1.1	0.025	0.3	23
14CADD001	496	497	Weak	6.82	2.51	24500	11	0.92	0.3	0.73	0.16	1.66	2020	0.035	2.35	16	0.26	0.025	0.5	1.4	0.16	0.4	35
14CADD001	497	498	Weak	7.39	2.8	25700	2.5	0.09	0.1	0.04	0.02	2.3	27.6	0.042	0.55	18.4	0.01	0.025	0.5	1.7	0.025	0.3	34
14CADD001	498	499	Weak	6.99	2.51	23600	11	0.94	0.3	0.85	0.13	2.02	2300	0.046	299	20	0.63	0.025	1	1.7	0.54	0.5	40
14CADD001	499	500	None	6.93	1.96	23500	2.5	0.18	0.1	0.11	0.04	1.8	395	0.043	5.61	11.9	0.14	0.025	0.5	1.2	0.11	0.4	30
14CADD001	500	501	None	7.16	2.16	22100	7	0.56	0.1	0.55	0.15	1.89	1380	0.043	7.46	9.1	0.26	0.025	0.5	1.2	0.3	0.5	36
14CADD001	501	502	None	7.05	1.53	24000	12	1.36	0.2	0.91	0.27	1.62	2700	0.042	26.4	10.8	0.34	0.025	1	1.6	0.37	9.9	46
14CADD001	502	503	None	7.33	2.3	23300	15	1.44	0.1	1.12	0.33	1.94	3090	0.044	28.1	11.9	0.41	0.025	1	1.4	0.36	0.3	60
14CADD001	503	504	None	7.21	1.46	24500	19	1.48	0.3	1.07	0.36	1.62	3220	0.046	39.8	10.6	0.45	0.025	1	1.6	0.34	0.5	70
14CADD001	504	504.6	None	6.73	0.91	20300	28	2.36	0.2	1.79	0.39	2.14	5230	0.046	497	9.2	1.2	0.025	1	2	0.91	1.5	90
14CADD001	504.6	505	None	7.87	1.79	29900	2.5	0.1	0.2	0.02	0.04	2.71	55.6	0.047	1.54	14.4	0.01	0.025	0.5	1.6	0.05	0.4	58
14CADD001	505	506	None	7.8	2.04	28700	2.5	0.19	0.1	0.04	0.03	2.79	150	0.038	0.57	14.5	0.02	0.025	0.5	1.3	0.025	0.4	47
14CADD001	506	507	None	7.7	2.05	28900	2.5	0.08	0.1	0.01	0.02	2.96	21.3	0.043	0.55	14.2	0.01	0.025	0.5	1.5	0.025	0.4	51
14CADD001	507	508	None	7.73	2.24	28200	2.5	0.23	0.2	0.09	0.04	2.73	289	0.043	2.84	18.9	0.04	0.025	1	2.1	0.025	0.2	51
14CADD001	508	509	None	7.59	2.05	27200	2.5	0.09	0.1	0.01	0.03	2.85	6	0.044	0.32	13.5	0.01	0.025	0.5	1.6	0.025	0.4	50
14CADD001	509	510	None	7.65	2.2	28200	2.5	0.08	0.1	0.005	0.02	2.84	3.7	0.044	0.26	14.8	0.005	0.025	0.5	1.4	0.025	0.3	44
14CADD001	510	511	None	7.09	2.28	25200	2.5	0.61	0.1	0.39	0.11	2.68	1130	0.041	2.09	13.4	0.15	0.025	0.5	1.5	0.14	0.3	48

14CADD001	511	512	None	7.39	2.56	26000	14	1.45	0.4	0.72	0.21	2.71	2880	0.04	3.82	19.3	0.37	0.025	1	2.3	0.32	0.3	55
14CADD001	512	513	None	7.19	2.51	26300	11	0.89	0.4	0.49	0.15	2.65	1850	0.035	9.8	23.6	0.25	0.025	1	1.9	0.19	0.4	39
14CADD001	513	514	None	6.75	2.17	25100	5	0.77	0.3	0.48	0.1	2.3	1240	0.038	61.2	18.4	0.17	0.025	0.5	2.1	0.25	0.2	42
14CADD001	514	515	None	7.03	2.58	26200	10	1	0.1	0.31	0.14	2.23	1970	0.043	40.4	16.9	0.32	0.025	1	2.2	0.24	0.1	48
14CADD001	515	516	None	6.73	2.69	24600	22	1.42	0.1	0.6	0.2	2.58	2930	0.041	47.4	18.2	0.41	0.05	1	2.6	0.31	0.2	51
14CADD001	516	517	None	6.85	4.1	20000	15	1.25	0.3	0.54	0.18	2.83	2650	0.044	11.3	25.9	0.38	0.07	1	2.5	0.24	0.5	49
14CADD001	517	518	None	7.06	2.7	26000	17	1.46	0.2	0.7	0.21	2.72	2960	0.048	10.65	12.2	0.41	0.025	1	2.4	0.38	0.2	52
14CADD001	518	519	None	7.16	3.07	26400	11	1.31	0.1	0.55	0.17	2.28	2460	0.037	2.12	14.1	0.36	0.05	1	1.7	0.27	0.2	41
14CADD001	519	520	None	7.14	2.56	27300	9	1.06	0.1	0.47	0.12	2.41	1770	0.048	15.15	10.7	0.28	0.025	1	1.7	0.27	0.2	41
14CADD001	520	521	None	6.37	3.68	22100	14	1.48	0.1	0.73	0.29	2	3080	0.026	41.8	14.5	0.51	0.05	1	1.2	0.35	0.2	37
14CADD001	521	522	None	6.09	3.75	21400	13	1.3	0.5	0.57	0.21	1.66	2350	0.015	38.8	18.5	0.39	0.07	1	0.8	0.26	0.4	28
14CADD001	522	523	None	6.42	4.55	20900	16	1.67	0.3	1.15	0.25	1.74	3510	0.011	15.9	18.8	0.49	0.05	1	1	0.54	0.5	26
14CADD001	523	524	None	6.65	4.07	22900	7	0.82	0.1	0.45	0.13	1.69	1600	0.016	23.9	17.7	0.24	0.05	0.5	0.9	0.2	0.1	21
14CADD001	524	525	None	6.78	3.49	23900	11	1.1	0.2	0.54	0.17	2.48	2130	0.028	26.8	17.8	0.37	0.025	0.5	1.6	0.26	0.2	39
14CADD001	525	526	None	6.81	3.53	24000	11	1.13	0.2	0.7	0.2	2.06	2140	0.024	68.8	20.2	0.39	0.025	1	1.4	0.3	0.2	35
14CADD001	526	527	None	6.62	3.66	23500	10	0.78	0.1	0.39	0.16	2.24	1610	0.027	7.16	17.8	0.27	0.06	1	1.2	0.21	0.4	29
14CADD001	527	528	None	6.14	3.25	23400	11	0.79	0.2	0.46	0.28	0.98	1580	0.014	96.1	18	0.28	0.05	0.5	0.6	0.24	0.1	23
14CADD001	528	529	None	6.89	3.1	25300	12	1.18	0.1	0.51	0.22	2.39	2080	0.025	24.7	16.3	0.3	0.025	1	1.7	0.23	0.2	38
14CADD001	529	530	Weak	7.43	2.98	28200	11	0.88	0.3	0.51	0.15	2.29	1700	0.039	40.3	17.8	0.24	0.025	0.5	1.6	0.18	0.3	34
14CADD001	530	531	Weak	6.69	3.65	23500	41	2.67	0.3	1.12	0.42	1.76	4750	0.023	17.8	17	0.66	0.05	1	1.4	0.43	0.2	50
14CADD001	531	532	Weak	6.85	2.36	26200	12	1.02	0.1	0.54	0.15	2.46	2030	0.039	7.55	13.9	0.33	0.025	1	1.7	0.21	0.2	41
14CADD001	532	533	Weak	7.01	2.39	27000	6	0.48	0.1	0.25	0.07	2.34	904	0.036	1.34	14.1	0.14	0.025	0.5	1.7	0.1	0.1	35
14CADD001	533	534	Weak	7.09	1.89	28200	13	0.9	0.4	0.49	0.17	2.18	2400	0.061	24.5	13.3	0.48	0.025	1	1.8	0.27	0.2	47
14CADD001	534	535	Weak	6.41	2.24	24200	14	0.69	0.6	0.38	0.12	2.62	1580	0.045	30.8	13.8	0.21	0.07	0.5	1.6	0.16	0.4	34
14CADD001	535	536	Weak	6.73	2.76	24500	94	1.38	0.4	0.75	0.14	2.58	2790	0.048	52.9	16.8	0.42	0.05	1	2	0.29	0.3	36
14CADD001	536	537	Weak	5.52	2.46	18700	167	8.46	0.6	4.99	0.88	2.8	20800	0.07	395	19.4	2.74	0.08	5	4.7	2.33	0.6	118
14CADD001	537	538	Weak	5.89	1.97	23700	44	3.12	0.2	1.71	0.37	1.35	7880	0.075	126	19.2	1.06	0.08	2	1.9	0.85	0.3	49
14CADD001	538	539	Weak	6.46	2.37	24800	35	1.61	0.4	0.93	0.19	1.34	3480	0.092	90	22.8	0.52	0.05	1	1.5	0.47	0.2	35
14CADD001	539	540.3	Weak	6.68	2.95	24600	14	0.9	0.2	0.45	0.14	1.97	1790	0.034	27.2	25.5	0.25	0.025	0.5	1.7	0.17	0.2	46

Appendix 9 – SEM data

Note: limited SEM data was collected, seeking to establish the suitability of the samples for garnet-biotite thermometry and/or garnet-aluminosilicate-silica-plagioclase barometry (GASP). However due to uncertainty over the applicability of those methods to rocks with igneous and secondary biotite, metamorphosed hydrothermal alteration zones, and rocks containing significant sulfide and/or magnetite, this work was not continued.

CAL022 igneous/metamorphic biotite			**Average FeO/(FeO+MgO) = 0.82**		**Average TiO2 = 1.90**	
CAL009 hydrothermal alteration biotite			**Average FeO/(FeO+MgO) = 0.92**		**Average TiO2 = 3.48**	
Garnet calculated to 12 oxygens, plagioclase to 8 oxygens, biotite to 24 oxygens						
Not certain that 24 oxygens is correct for biotite.						
Sample_site	Analysis No.	Mineral	Oxide	Oxide %	Oxide % Sigma	Number of Ions
STANDARD	78	Garnet	MgO	10.11	0.11	1.18
			Al2O3	21.86	0.16	2.02
			SiO2	36.93	0.21	2.9
			CaO	1.1	0.06	0.09
			MnO	1.2	0.1	0.08
			FeO	27.44	0.28	1.8
			SUMS	98.63		8.09
Sample_site	Analysis No.	Mineral	Oxide	Oxide %	Oxide % Sigma	Number of Ions
STANDARD	79	Garnet	MgO	10.15	0.11	1.18
			Al2O3	21.96	0.16	2.02
			SiO2	37.2	0.21	2.91
			CaO	1.06	0.06	0.09
			MnO	1.27	0.1	0.08
			FeO	27.36	0.29	1.79
			SUMS	99.01		8.08
Sample_site	Analysis No.	Mineral	Oxide	Oxide %	Oxide % Sigma	Number of Ions
CAL022-site3	80	Garnet	MgO	1.19	0.07	0.15
			Al2O3	20.09	0.15	1.99
			SiO2	34.43	0.2	2.9
			CaO	1.05	0.06	0.09
			MnO	8.84	0.17	0.63
			FeO	33.21	0.31	2.34
			SUMS	98.81		8.1
Sample_site	Analysis No.	Mineral	Oxide	Oxide %	Oxide % Sigma	Number of Ions
CAL022-site3	81	Garnet	MgO	1.22	0.07	0.15
			Al2O3	20.07	0.15	2
			SiO2	34.08	0.2	2.88
			CaO	0.98	0.06	0.09
			MnO	8.68	0.17	0.62
			FeO	33.56	0.31	2.37
			SUMS	98.6		8.12
Sample_site	Analysis No.	Mineral	Oxide	Oxide %	Oxide % Sigma	Number of Ions
CAL022-site3	82	Garnet	MgO	1.22	0.07	0.15
			Al2O3	20.26	0.15	2.01
			SiO2	34.25	0.2	2.89
			CaO	0.99	0.06	0.09
			MnO	8.43	0.17	0.6
			FeO	33.43	0.31	2.36
			SUMS	98.57		8.1

Sample_site	Analysis No.	Mineral	Oxide	Oxide %	Oxide % Sigma	Number of Ions
CAL022-site3	83	Garnet	MgO	1.19	0.06	0.15
			Al2O3	20.3	0.15	2.02
			SiO2	34.07	0.2	2.88
			CaO	0.96	0.06	0.09
			MnO	9.27	0.17	0.66
			FeO	32.86	0.31	2.32
			SUMS	98.65		8.11

Sample_site	Analysis No.	Mineral	Oxide	Oxide %	Oxide % Sigma	Number of Ions
CAL022-site3	84	Biotite	MgO	5.42	0.09	1.44
			Al2O3	18.72	0.14	3.94
			SiO2	31.3	0.19	5.59
			K2O	8.42	0.09	1.92
			CaO	0.75	0.06	0.14
			TiO2	1.74	0.1	0.23
			MnO	0.52	0.09	0.08
			FeO	25.5	0.28	3.81
			SUMS	92.36		17.16

Sample_site	Analysis No.	Mineral	Oxide	Oxide %	Oxide % Sigma	Number of Ions
CAL022-site3	85	Biotite	MgO	5.31	0.09	1.41
			Al2O3	18.41	0.14	3.86
			SiO2	31.66	0.19	5.63
				0	0.03	0.03
			K2O	9.37	0.09	2.13
			TiO2	2.14	0.1	0.29
			MnO	0.29	0.09	0.04
			FeO	25.72	0.28	3.83
			SUMS	92.91		17.18

Sample_site	Analysis No.	Mineral	Oxide	Oxide %	Oxide % Sigma	Number of Ions
CAL022-site3	86	Biotite	MgO	5.9	0.09	1.57
			Al2O3	18.9	0.15	3.98
			SiO2	30.83	0.19	5.51
				0	0.03	0.03
			K2O	8.22	0.09	1.87
			TiO2	1.67	0.09	0.22
			MnO	0.36	0.09	0.05
			FeO	26.68	0.28	3.98
			SUMS	92.55		17.19

Sample_site	Analysis No.	Mineral	Oxide	Oxide %	Oxide % Sigma	Number of Ions
CAL022-site3	87	Biotite	MgO	5.49	0.09	1.46
			Al2O3	18.51	0.14	3.9
			SiO2	31.22	0.19	5.58
			K2O	8.77	0.09	2
			TiO2	2.07	0.1	0.28
			MnO	0.31	0.09	0.05
			FeO	25.68	0.28	3.84
			CoO	0.49	0.16	0.07
			SUMS	92.53		17.19

Sample_site	Analysis No.	Mineral	Oxide	Oxide %	Oxide % Sigma	Number of Ions
CAL022-site3	88	Plagioclase	Na2O	8.93	0.1	0.8
			Al2O3	23.55	0.15	1.28
			SiO2	58.65	0.24	2.7
			K2O	0.18	0.04	0.01
			CaO	5.21	0.09	0.26
			FeO	0.69	0.1	0.03
			SUMS	97.21		5.07

Sample_site	Analysis No.	Mineral	Oxide	Oxide %	Oxide % Sigma	Number of Ions
CAL022-site3	89	Plagioclase	Na2O	8.81	0.1	0.79
			Al2O3	23.42	0.15	1.28
			SiO2	58.44	0.24	2.7
			K2O	0.17	0.04	0.01
			CaO	5.13	0.09	0.25
			FeO	0.54	0.1	0.02
			SUMS	96.51		5.06

Sample_site	Analysis No.	Mineral	Oxide	Oxide %	Oxide % Sigma	Number of Ions
CAL022-site3	90	Plagioclase	Na2O	8.83	0.1	0.8
			Al2O3	23.5	0.15	1.29
			SiO2	57.95	0.24	2.69
			K2O	0.17	0.04	0.01
			CaO	5.22	0.09	0.26
			FeO	0.52	0.1	0.02
			SUMS	96.19		5.07

Sample_site	Analysis No.	Mineral	Oxide	Oxide %	Oxide % Sigma	Number of Ions
CAL022-site3	91	Plagioclase	Na2O	8.56	0.09	0.77
			Al2O3	23.48	0.15	1.29
			SiO2	58.15	0.24	2.7
			K2O	0.2	0.04	0.01
			CaO	5.16	0.09	0.26
			FeO	0.59	0.1	0.02
			SUMS	96.15		5.05

Sample_site	Analysis No.	Mineral	Oxide	Oxide %	Oxide % Sigma	No. of Ions
CAL009 alteration	36	Biotite	MgO	2.35	0.14	0.61
			Al2O3	18.7	0.27	3.87
			SiO2	32.52	0.36	5.7
			K2O	8.94	0.17	2
			TiO2	3.35	0.2	0.44
			FeO	29.28	0.53	4.29
			SUMS	95.14		16.92

Sample_site	Analysis No.	Mineral	Oxide	Oxide %	Oxide % Sigma	No. of Ions
CAL009 alteration	37	Biotite	MgO	2.35	0.14	0.61
			Al2O3	18.7	0.27	3.87
			SiO2	32.52	0.36	5.7
			K2O	8.94	0.17	2
			TiO2	3.35	0.2	0.44
			FeO	29.28	0.53	4.29
			SUMS	95.14		16.92

Sample_site	Analysis No.	Mineral	Oxide	Oxide %	Oxide % Sigma	No. of Ions
CAL009 alteration	38	Biotite	MgO	2.53	0.14	0.66
			Al2O3	18.79	0.27	3.86
			SiO2	32.53	0.36	5.67
			K2O	8.96	0.17	1.99
			TiO2	3.64	0.21	0.48
			FeO	29.19	0.53	4.26
			SUMS	95.64		16.92

Sample_site	Analysis No.	Mineral	Oxide	Oxide %	Oxide % Sigma	No. of Ions
CAL009 alteration	39	Biotite	MgO	2.57	0.14	0.69
			Al2O3	18.09	0.27	3.82
			SiO2	31.8	0.36	5.69
			K2O	9	0.16	2.06
			TiO2	3.43	0.2	0.46
			FeO	28.38	0.52	4.25
			SUMS	93.27		16.96

Sample_site	Analysis No.	Mineral	Oxide	Oxide %	Oxide % Sigma	No. of Ions
CAL009 alteration	40	Biotite	MgO	2.57	0.14	0.68
			Al2O3	18.2	0.27	3.79
			SiO2	32.27	0.36	5.7
				0	0.06	0.06
			K2O	8.72	0.17	1.96
			TiO2	3.54	0.21	0.47
			FeO	28.97	0.53	4.28
			SUMS	94.27		16.87

Sample_site	Analysis No.	Mineral	Oxide	Oxide %	Oxide % Sigma	No. of Ions
CAL009 alteration	41	Biotite	MgO	2.61	0.14	0.69
			Al2O3	18.62	0.27	3.9
			SiO2	31.66	0.36	5.62
			K2O	8.81	0.17	1.99
			TiO2	3.58	0.2	0.48
			FeO	28.74	0.53	4.27
			SUMS	94.02		16.95

Appendix 10 – SHRIMP U-Pb zircon geochronology data

Unpublished Wingate and Lu (2016) report is included here, followed by the SHRIMP analytical data provided by those authors. In the "Group ID" field of that data: I = igneous, X = xenocrystic, D = discordance >5% and P = radiogenic Pb-loss.

Geological Survey of Western Australia

PRELIMINARY REPORTS
ON
U-Pb GEOCHRONOLOGY SAMPLES

GSWA ID	rock type	details
205930	metamonzogranite	DDH 12CADD001, 136.55 – 137.55 m, Dasher prospect (Caravel Minerals), sample CAL024
205931	metasyenogranite	DDH 12CADD001, 154.34 – 155.34 m, Dasher prospect (Caravel Minerals), sample CAL026
205932	metamonzogranite	DDH 14CADD001, 365.00 – 366.00 m, Dasher prospect (Caravel Minerals), sample CAL044
205933	metamonzogranite	DDH 08WHDD001, 199.70 – 200.20 m, Ninan prospect (Caravel Minerals), sample CAL038

by
MTD Wingate & Y Lu

Monday, 27 June 2016

Citable final versions of these results will be published through the Geochronology Record Series available online at http://www.dmp.wa.gov.au/geochron

205930 (OUTHWAITE; metamonzogranite, GOOMALLING):
17 analyses of 17 zircons

DDH 12CADD001, 136.55 – 137.55 m, Dasher prospect (Caravel Minerals)
South West Terrane, Yilgarn Craton

- Zircons from this sample are colourless to pale brown, and subhedral to euhedral. Concentric zoning is ubiquitous, and a few crystals appear to contain older cores
- One analysis >5% discordant (Group D) is not considered further
- Fourteen analyses of 13 zircons (Group I) yield a weighted mean $^{207}Pb^*/^{206}Pb^*$ date of **3010 ± 4 Ma** (MSWD = 1.4), interpreted as the magmatic crystallization age of the monzogranite
- One analysis of a zircon core (Group X) yields a $^{207}Pb^*/^{206}Pb^*$ date of 3105 ± 13 Ma (1σ), interpreted as the age of an inherited component
- One analysis (Group P) yields a $^{207}Pb^*/^{206}Pb^*$ date of 2995 ± 4 Ma (1σ), interpreted to reflect minor loss of radiogenic Pb

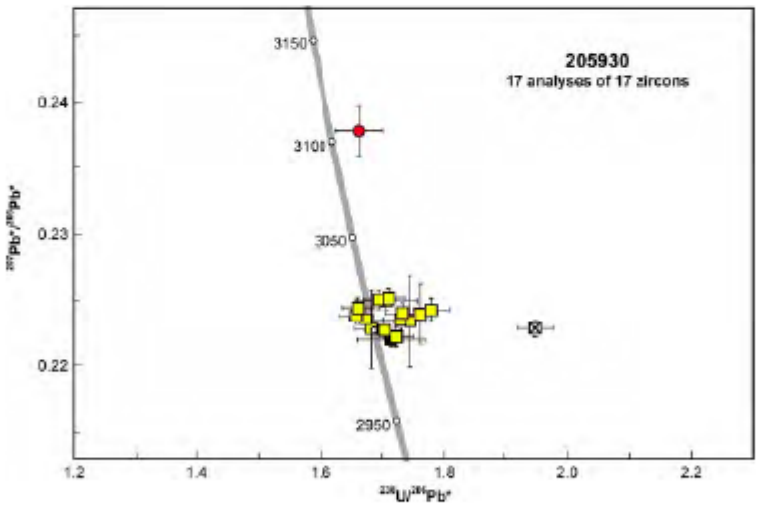

Figure 1. U–Pb analytical data for zircons from sample 205930: metamonzogranite, GOOMALLING. Yellow squares indicate Group I (magmatic zircons); red circle indicates Group X (xenocrystic zircon core); black square indicates Group P (radiogenic-Pb loss); crossed square indicates Group D (discordance >5%).

205931 (OUTHWAITE; metasyenogranite, GOOMALLING):
28 analyses of 28 zircons

DDH 12CADD001, 154.34 – 155.34 m, Dasher prospect (Caravel Minerals)
South West Terrane, Yilgarn Craton

- Zircons from this sample are colourless to dark brown, and subhedral to euhedral. Most crystals exhibit concentric zoning
- Eight analyses >5% discordant (Group D) are not considered further
- Twenty analyses (Group I) yield a concordia age of **3010 ± 4 Ma** (MSWD = 1.5), interpreted as the magmatic crystallization age of the syenogranite

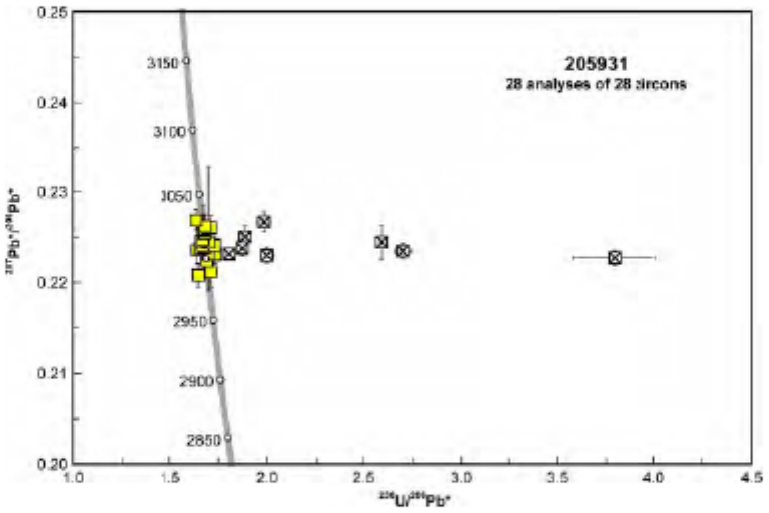

Figure 1. U–Pb analytical data for zircons from sample 205931: metasyenogranite, GOOMALLING. Yellow squares indicate Group I (magmatic zircons); crossed squares indicate Group D (discordance >5%).

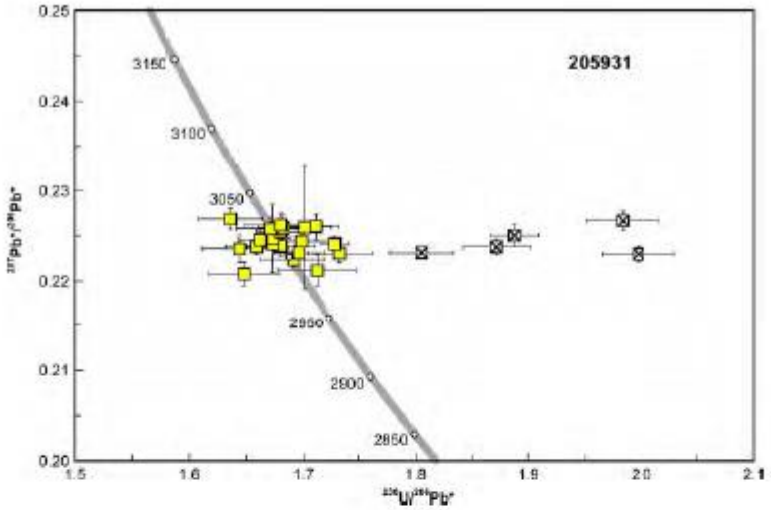

Figure 2. Expanded view of U–Pb analytical data for zircons from sample 205931: metasyenogranite, GOOMALLING. Symbols as in Figure 1.

205932 (OUTHWAITE; metamonzogranite, GOOMALLING):
45 analyses of 37 zircons

DDH 14CADD001, 365.00 – 366.00 m, Dasher prospect (Caravel Minerals)
South West Terrane, Yilgarn Craton

- Zircons from this sample are colourless to dark brown, and subhedral to euhedral. Most crystals exhibit concentric zoning, and many appear to contain older cores
- Two analyses are >5% discordant, and one analysis indicates high within-run variation of isotope ratios. These three analyses (Group D) are not considered further
- Nine analyses of seven zircons (Group I) yield a weighted mean $^{207}Pb^*/^{206}Pb^*$ date of **2673 ± 5 Ma** (MSWD = 2.4), interpreted as the magmatic crystallization age of the monzogranite
- Thirty analyses of 29 zircon cores (Group X) yield $^{207}Pb^*/^{206}Pb^*$ dates of 3282–2782 Ma, including age groups at c. 3011 and 2810 Ma, interpreted as the ages of inherited components
- Three analyses of two high-U zircons (Group P) yield $^{207}Pb^*/^{206}Pb^*$ dates of 2634–2627 Ma, interpreted to reflect minor loss of radiogenic Pb

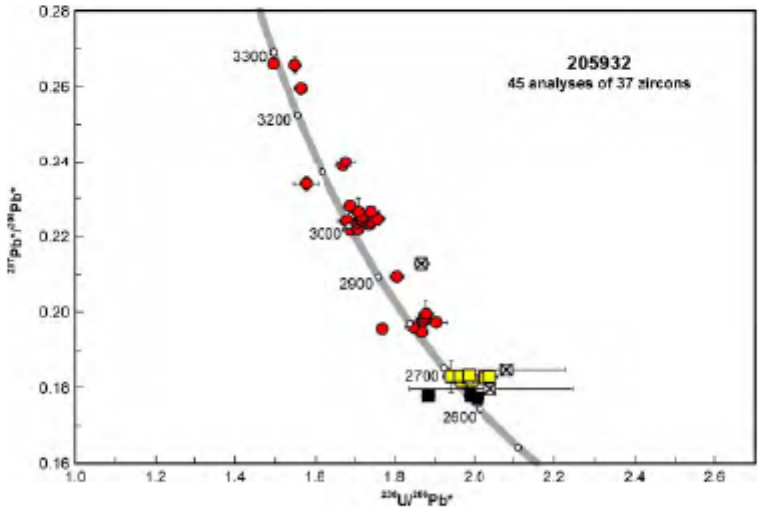

Figure 1. U–Pb analytical data for zircons from sample 205932: metamonzogranite, GOOMALLING. Yellow squares indicate Group I (magmatic zircons); red circles indicate Group X (xenocrystic zircon cores); black squares indicate Group P (radiogenic-Pb loss); crossed squares indicate Group D (discordance >5% or high within-run variation).

205933 (OUTHWAITE; metamonzogranite, WONGAN):
34 analyses of 34 zircons

DDH 08WHDD001, 199.70 – 200.20 m, Ninan prospect (Caravel Minerals)
South West Terrane, Yilgarn Craton

- Zircons from this sample are colourless to dark brown, and subhedral to euhedral. Most crystals exhibit concentric zoning, and many appear to contain older cores
- Four analyses >5% discordant (Group D) are not considered further
- Nine analyses (Group I) yield a weighted mean $^{207}Pb^*/^{206}Pb^*$ date of **2670 ± 7 Ma** (MSWD = 1.8), interpreted as the magmatic crystallization age of the monzogranite
- Twenty analyses of zircon cores (Group X) yield $^{207}Pb^*/^{206}Pb^*$ dates of 3219–2785 Ma, including age groups at c. 3012 and 2977 Ma, interpreted as the ages of inherited components
- One analysis (Group P) yields a $^{207}Pb^*/^{206}Pb^*$ date of 2653 ± 5 Ma (1σ), interpreted to reflect minor loss of radiogenic Pb

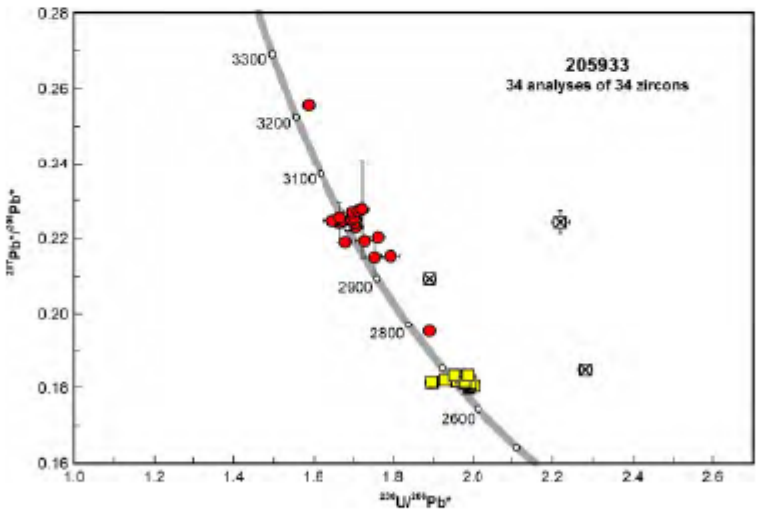

Figure 1. **U–Pb analytical data for zircons from sample 205933: metamonzogranite, WONGAN. Yellow squares indicate Group I (magmatic zircons); red circles indicate Group X (xenocrystic zircon cores); black square indicates Group P (radiogenic-Pb loss); crossed squares indicate Group D (discordance >5%).**

Group ID	Spot no.	Grain .spot	^{238}U (ppm)	^{232}Th (ppm)	$^{232}Th/^{238}U$	f_{204} (%)	$^{238}U/^{206}Pb$ ±1 σ	$^{207}Pb/^{206}Pb_{FC}$ ±1 σ	$^{238}U/^{206}Pb^*$ ±1 σ	$^{207}Pb^*/^{206}Pb^*_{FC}$ ±1 σ	$^{238}U/^{206}Pb^*$ date (Ma) ±1 σ	$^{207}Pb^*/^{206}Pb^*_{FC}$ Age	$^{207}Pb^*/^{206}Pb^*_{FC}$ Error	Disc (%)
X	9	930-9.1	33	24	0.73	-0.092	1.664	0.038	0.23702	0.00186	1.663	0.038	0.23782	0.00191	3036	56	3105	13	2.2
P	17	930-17.1	687	348	0.52	0.008	1.714	0.054	0.22198	0.00054	1.715	0.054	0.22191	0.00054	2962	77	2995	4	1.1
–	10	930-10.1	246	114	0.48	0.025	1.722	0.027	0.22238	0.00077	1.723	0.027	0.22215	0.00078	2951	38	2996	6	1.5
–	11	930-11.1	272	190	0.72	0.025	1.704	0.027	0.22287	0.00071	1.704	0.027	0.22265	0.00071	2976	38	3000	5	0.8
–	8	930-8.1	186	54	0.30	0.045	1.682	0.027	0.22318	0.00303	1.683	0.027	0.22278	0.00303	3006	39	3001	22	-0.2
–	5	930-5.1	404	207	0.53	0.072	1.743	0.027	0.22400	0.00349	1.745	0.027	0.22337	0.00349	2921	36	3005	25	2.8
–	7	930-7.1	266	190	0.74	0.022	1.729	0.027	0.22367	0.00081	1.730	0.027	0.22347	0.00082	2941	38	3006	6	2.2
–	14	930-14.1	178	74	0.43	0.028	1.673	0.027	0.22376	0.00088	1.674	0.027	0.22352	0.00089	3019	40	3006	6	-0.4
–	15	930-15.1	316	147	0.48	0.007	1.659	0.026	0.22386	0.00067	1.659	0.026	0.22380	0.00068	3042	38	3008	5	-1.1
–	16	930-13.2	487	238	0.50	0.021	1.762	0.027	0.22412	0.00232	1.762	0.027	0.22394	0.00233	2897	36	3009	17	3.7
–	2	930-2.1	262	89	0.35	0.062	1.732	0.027	0.22456	0.00077	1.733	0.027	0.22402	0.00079	2936	38	3010	6	2.4
–	4	930-4.1	165	88	0.55	0.013	1.779	0.029	0.22438	0.00088	1.779	0.029	0.22427	0.00088	2875	38	3012	6	4.5
–	13	930-13.1	241	152	0.65	-0.005	1.662	0.026	0.22436	0.00076	1.662	0.026	0.22441	0.00076	3037	39	3013	5	-0.8
–	3	930-3.1	307	102	0.34	0.004	1.707	0.050	0.22498	0.00067	1.707	0.050	0.22495	0.00067	2972	71	3016	5	1.5
–	1	930-1.1	297	108	0.38	0.022	1.694	0.026	0.22526	0.00074	1.695	0.026	0.22506	0.00074	2990	38	3017	5	0.9
–	12	930-12.1	378	277	0.76	0.131	1.708	0.026	0.22634	0.00065	1.711	0.026	0.22518	0.00068	2968	37	3018	5	1.7
D	6	930-6.1	401	195	0.50	0.085	1.948	0.029	0.22356	0.00066	1.949	0.029	0.22281	0.00068	2670	33	3001	5	11.0

GSWA ID 205931, CAL026, 12CADD001 154.34-15.34 m

Group ID	Spot no.	Grain .spot	^{238}U (ppm)	^{232}Th (ppm)	$^{232}Th/^{238}U$	f_{204} (%)	$^{238}U/^{206}Pb$ ±1 σ		$^{207}Pb/^{206}Pb_{FC}$ ±1 σ		$^{238}U/^{206}Pb^*$ ±1 σ		$^{207}Pb^*/^{206}Pb^*_{FC}$ ±1 σ		$^{238}U/^{206}Pb^*$ date (Ma) ±1 σ		$^{207}Pb^*/^{206}Pb^*_{FC}$ Age	Error	Disc (%)
I	13	931-13.1	86	28	0.34	0.078	1.647	0.031	0.22150	0.00127	1.648	0.031	0.22081	0.00131	3057	46	2987	10	-2.4
I	6	931-6.1	51	20	0.41	0.105	1.710	0.035	0.22211	0.00165	1.712	0.035	0.22118	0.00171	2966	50	2989	12	0.8
I	11	931-11.1	166	118	0.74	0.000	1.691	0.028	0.22240	0.00089	1.691	0.028	0.22240	0.00089	2994	40	2998	6	0.1
I	4	931-4.1	122	67	0.57	0.009	1.733	0.029	0.22314	0.00101	1.733	0.029	0.22306	0.00101	2937	41	3003	7	2.2
I	23	931-23.1	116	54	0.49	0.017	1.696	0.022	0.22325	0.00139	1.696	0.022	0.22310	0.00140	2987	32	3003	10	0.5
I	12	931-12.1	56	20	0.38	-0.043	1.645	0.033	0.22318	0.00149	1.644	0.033	0.22356	0.00151	3063	50	3007	11	-1.9
I	15	931-15.1	159	71	0.46	0.000	1.659	0.027	0.22377	0.00087	1.659	0.027	0.22377	0.00087	3041	40	3008	6	-1.1
I	9	931-9.1	97	46	0.50	-0.012	1.680	0.030	0.22377	0.00113	1.680	0.030	0.22387	0.00113	3011	43	3009	8	-0.1
I	28	931-28.1	1236	464	0.39	0.002	1.673	0.011	0.22409	0.00064	1.673	0.011	0.22408	0.00064	3021	17	3010	5	-0.4
I	19	931-19.1	737	578	0.81	0.031	1.728	0.013	0.22437	0.00072	1.729	0.013	0.22410	0.00072	2943	18	3010	5	2.2
I	8	931-8.1	157	76	0.50	0.006	1.698	0.028	0.22445	0.00085	1.698	0.028	0.22440	0.00085	2985	39	3013	6	0.9
I	18	931-18.1	174	71	0.42	0.000	1.662	0.019	0.22456	0.00118	1.662	0.019	0.22456	0.00118	3036	27	3014	8	-0.7
I	22	931-22.1	348	302	0.90	0.060	1.672	0.015	0.22526	0.00373	1.673	0.015	0.22473	0.00373	3020	21	3015	27	-0.2
I	27	931-27.1	130	52	0.41	-0.030	1.681	0.021	0.22514	0.00134	1.680	0.021	0.22541	0.00135	3010	30	3020	10	0.3
I	14	931-14.1	90	34	0.39	0.028	1.671	0.030	0.22602	0.00123	1.671	0.030	0.22577	0.00124	3023	44	3022	9	0.0
I	21	931-21.1	118	44	0.38	-0.017	1.682	0.022	0.22572	0.00141	1.682	0.022	0.22587	0.00142	3008	32	3023	10	0.5
I	25	931-25.1	90	39	0.45	0.124	1.699	0.025	0.22704	0.00676	1.701	0.025	0.22594	0.00679	2981	36	3024	48	1.4
I	20	931-20.1	120	76	0.65	-0.018	1.711	0.022	0.22587	0.00144	1.711	0.022	0.22603	0.00144	2967	31	3024	10	1.9
I	7	931-7.1	75	28	0.39	-0.162	1.683	0.031	0.22475	0.00125	1.680	0.031	0.22618	0.00132	3010	45	3025	9	0.5
I	1	931-1.1	117	48	0.42	-0.055	1.637	0.028	0.22638	0.00110	1.636	0.028	0.22686	0.00113	3074	43	3030	8	-1.5
D	2	931-2.1	384	231	0.62	0.065	3.791	0.213	0.22328	0.00080	3.793	0.213	0.22271	0.00082	1508	80	3000	6	49.7
D	5	931-5.1	192	127	0.68	0.012	1.997	0.032	0.22308	0.00083	1.997	0.032	0.22297	0.00083	2617	35	3002	6	12.8
D	16	931-16.1	493	368	0.77	0.038	1.805	0.028	0.22346	0.00062	1.805	0.028	0.22312	0.00063	2841	36	3003	5	5.4
D	3	931-3.1	232	161	0.72	0.034	2.702	0.042	0.22375	0.00081	2.703	0.042	0.22345	0.00082	2029	27	3006	6	32.5
D	10	931-10.1	243	136	0.58	0.096	1.870	0.030	0.22460	0.00083	1.872	0.030	0.22375	0.00085	2759	36	3008	6	8.3
D	26	931-26.1	156	100	0.66	0.606	2.579	0.030	0.22982	0.00148	2.594	0.030	0.22443	0.00185	2102	21	3013	13	30.2
D	24	931-24.1	180	84	0.48	0.112	1.886	0.021	0.22603	0.00124	1.888	0.021	0.22503	0.00128	2740	25	3017	9	9.2
D	17	931-17.1	166	128	0.79	0.031	1.982	0.032	0.22690	0.00106	1.983	0.032	0.22663	0.00107	2632	36	3028	8	13.1

Group ID	Spot no.	Grain .spot	^{238}U (ppm)	^{232}Th (ppm)	$^{232}Th/^{238}U$	f_{204} (%)	$^{238}U/^{206}Pb$ ±1 σ	$^{207}Pb/^{206}Pb$ ±1 σ	$^{238}U/^{206}Pb^*$ ±1 σ	$^{207}Pb^*/^{206}Pb^*$ ±1 σ	$^{238}U/^{206}Pb^*$ date (Ma) ±1 σ	$^{207}Pb^*/^{206}Pb^*$ date (Ma) ±1 σ	Disc (%)
X	21	932-18.1	1542	141	0.09	0.000	1.868 0.016	0.19469 0.00034	1.868 0.016	0.19469 0.00034	2763 20	2782 3	0.7
X	10	932-10.1	3427	971	0.29	0.000	1.771 0.015	0.19556 0.00023	1.771 0.015	0.19556 0.00023	2886 20	2789 2	-3.5
X	4	932-4.1	213	49	0.24	-0.044	1.848 0.022	0.19567 0.00093	1.847 0.022	0.19606 0.00095	2789 27	2794 8	0.2
X	12	932-12.1	159	121	0.79	-0.017	1.904 0.029	0.19705 0.00116	1.904 0.029	0.19720 0.00117	2721 35	2803 10	2.9
X	26	932-23.1	567	317	0.58	0.004	1.874 0.018	0.19765 0.00058	1.874 0.018	0.19762 0.00058	2757 22	2807 5	1.8
X	28	932-25.1	419	232	0.57	0.006	1.873 0.017	0.19769 0.00071	1.873 0.017	0.19763 0.00071	2758 21	2807 6	1.7
X	34	932-31.1	157	46	0.30	-0.081	1.878 0.023	0.19761 0.00456	1.877 0.023	0.19834 0.00457	2753 28	2813 38	2.1
X	7	932-7.1	672	37	0.06	0.029	1.879 0.018	0.19964 0.00052	1.879 0.018	0.19939 0.00053	2750 21	2821 4	2.5
X	5	932-5.1	630	36	0.06	0.007	1.806 0.017	0.20935 0.00058	1.806 0.017	0.20929 0.00058	2840 22	2900 4	2.1
X	23	932-20.1	325	221	0.70	-0.021	1.692 0.019	0.22142 0.00084	1.692 0.019	0.22161 0.00084	2994 26	2992 6	-0.1
X	25	932-22.1	110	64	0.61	0.121	1.708 0.025	0.22298 0.00142	1.710 0.025	0.22191 0.00148	2968 36	2995 11	0.9
X	6	932-6.1	160	162	1.05	0.013	1.740 0.022	0.22329 0.00116	1.740 0.022	0.22318 0.00117	2927 30	3004 8	2.6
X	18	932-16.1	336	202	0.62	0.012	1.709 0.018	0.22358 0.00077	1.709 0.018	0.22348 0.00077	2970 25	3006 6	1.2
X	13	932-13.1	183	91	0.51	0.048	1.742 0.022	0.22414 0.00111	1.743 0.022	0.22372 0.00113	2923 30	3008 8	2.8
X	30	932-27.1	275	175	0.66	0.026	1.682 0.017	0.22412 0.00100	1.683 0.017	0.22389 0.00101	3007 25	3009 7	0.1
X	17	932-15.1	162	55	0.35	0.076	1.682 0.022	0.22467 0.00114	1.683 0.022	0.22400 0.00117	3006 31	3010 8	0.1
X	1	932-1.1	134	71	0.55	-0.014	1.723 0.023	0.22394 0.00120	1.723 0.023	0.22406 0.00120	2951 32	3010 9	2.0
X	31	932-28.1	331	271	0.85	-0.013	1.714 0.016	0.22414 0.00082	1.714 0.016	0.22426 0.00082	2962 23	3011 6	1.6
X	29	932-26.1	663	798	1.24	-0.007	1.719 0.014	0.22429 0.00061	1.719 0.014	0.22436 0.00061	2956 20	3012 4	1.9
X	8	932-8.1	283	145	0.53	0.023	1.757 0.019	0.22471 0.00105	1.758 0.019	0.22451 0.00106	2903 26	3013 8	3.6
X	27	932-24.1	226	71	0.33	0.031	1.720 0.019	0.22545 0.00104	1.720 0.019	0.22517 0.00105	2954 26	3018 7	2.1
X	43	932-36.2	292	221	0.78	0.059	1.710 0.022	0.22684 0.00362	1.711 0.022	0.22632 0.00363	2966 31	3026 26	2.0
X	11	932-11.1	160	98	0.63	0.098	1.740 0.022	0.22725 0.00113	1.742 0.022	0.22638 0.00117	2925 30	3027 8	3.4
X	38	932-33.1	830	17	0.02	0.017	1.690 0.016	0.22808 0.00044	1.690 0.016	0.22793 0.00045	2996 23	3038 3	1.4
X	2	932-2.1	53	75	1.48	0.000	1.578 0.031	0.23382 0.00200	1.578 0.031	0.23382 0.00200	3164 50	3078 14	-2.8
X	24	932-21.1	324	223	0.71	0.013	1.673 0.018	0.23887 0.00084	1.673 0.018	0.23876 0.00084	3020 26	3112 6	2.9
X	39	932-33.2	210	129	0.63	-0.007	1.679 0.021	0.23975 0.00091	1.679 0.021	0.23982 0.00091	3012 30	3119 6	3.4
X	32	932-29.1	288	355	1.27	0.026	1.564 0.016	0.25970 0.00093	1.564 0.016	0.25947 0.00094	3186 26	3244 6	1.8
X	41	932-35.1	931	335	0.37	0.013	1.549 0.015	0.26571 0.00227	1.549 0.015	0.26560 0.00227	3211 24	3280 13	2.1
X	3	932-3.1	765	366	0.49	0.009	1.496 0.014	0.26604 0.00055	1.496 0.014	0.26597 0.00055	3300 24	3282 3	-0.5

Group ID	Spot no.	Grain .spot	^{238}U (ppm)	^{232}Th (ppm)	$^{232}Th/^{238}U$	f_{204} (%)	$^{238}U/^{206}Pb$ ±1 σ	$^{207}Pb/^{206}Pb$ ±1 σ	$^{238}U/^{206}Pb^*$ ±1 σ	$^{207}Pb^*/^{206}Pb^*$ ±1 σ	$^{238}U/^{206}Pb^*$ date (Ma) ±1 σ	$^{207}Pb^*/^{206}Pb^*$ date (Ma) ±1 σ	Disc (%)
P	14	932-13.2	2278	38	0.02	0.007	2.009 0.017	0.17733 0.00029	2.009 0.017	0.17727 0.00029	2604 18	2627 3	0.9
P	19	932-13.3	1688	38	0.02	0.001	1.989 0.017	0.17786 0.00031	1.989 0.017	0.17785 0.00031	2626 19	2633 3	0.3
P	35	932-2.2	4153	159	0.04	0.009	1.884 0.016	0.17801 0.00017	1.884 0.016	0.17792 0.00017	2745 19	2634 2	-4.2
I	15	932-9.2	116	85	0.76	0.000	1.983 0.028	0.18124 0.00121	1.983 0.028	0.18124 0.00121	2632 31	2664 11	1.2
I	45	932-37.1	2478	116	0.05	0.035	1.967 0.017	0.18190 0.00024	1.967 0.017	0.18158 0.00025	2649 19	2667 2	0.7
I	44	932-36.3	2038	337	0.17	0.059	1.991 0.018	0.18243 0.00027	1.992 0.018	0.18190 0.00029	2622 19	2670 3	1.8
I	20	932-17.1	549	42	0.08	0.026	1.981 0.019	0.18294 0.00056	1.982 0.019	0.18271 0.00057	2634 21	2678 5	1.6
I	40	932-34.1	1579	98	0.06	-0.007	2.025 0.018	0.18266 0.00031	2.025 0.018	0.18272 0.00031	2587 19	2678 3	3.4
I	36	932-17.2	770	105	0.14	0.036	2.040 0.020	0.18322 0.00044	2.040 0.020	0.18291 0.00045	2571 21	2679 4	4.0
I	16	932-14.1	351	38	0.11	0.015	1.941 0.021	0.18312 0.00423	1.941 0.021	0.18299 0.00423	2679 24	2680 38	0.0
I	9	932-9.1	76	61	0.82	0.100	1.959 0.032	0.18393 0.00155	1.961 0.032	0.18303 0.00163	2657 36	2681 15	0.9
I	37	932-32.1	618	88	0.15	0.013	1.984 0.020	0.18340 0.00048	1.984 0.020	0.18328 0.00049	2631 22	2683 4	1.9
D	42	932-36.1	2352	106	0.05	0.027	2.040 0.204	0.17991 0.00126	2.041 0.204	0.17967 0.00127	2571 231	2650 12	3.0
D	33	932-30.1	181	55	0.31	-0.101	2.084 0.146	0.18384 0.00110	2.082 0.146	0.18474 0.00116	2528 156	2696 10	6.2
D	22	932-19.1	571	85	0.15	0.073	1.865 0.018	0.21335 0.00066	1.867 0.018	0.21271 0.00067	2766 22	2926 5	5.5

Group ID	Spot no.	Grain .spot	^{238}U (ppm)	^{232}Th (ppm)	$^{232}Th/^{238}U$	f_{204} (%)	$^{238}U/^{206}Pb$ ±1 σ	$^{207}Pb/^{206}Pb$ ±1 σ	$^{238}U/^{206}Pb^*$ ±1 σ	$^{207}Pb^*/^{206}Pb^*$ ±1 σ	$^{238}U/^{206}Pb^*$ date (Ma) ±1 σ	$^{207}Pb^*/^{206}Pb^*$ date (Ma) ±1 σ	Disc (%)
P	21	933-21.1	710	326	0.48	0.015	1.987 0.019	0.18018 0.00051	1.988 0.019	0.18005 0.00051	2627 21	2653 5	1.0
I	25	933-25.1	500	286	0.59	0.078	1.999 0.020	0.18122 0.00061	2.001 0.020	0.18053 0.00063	2613 22	2658 6	1.7
I	28	933-28.1	554	320	0.60	0.070	1.992 0.017	0.18168 0.00060	1.993 0.017	0.18106 0.00062	2621 19	2663 6	1.6
I	29	933-29.1	146	70	0.50	-0.018	1.979 0.025	0.18129 0.00113	1.978 0.025	0.18145 0.00114	2637 28	2666 10	1.1
I	30	933-30.1	444	294	0.69	0.364	1.890 0.017	0.18470 0.00069	1.897 0.017	0.18145 0.00083	2729 20	2666 8	-2.4
I	5	933-5.1	458	289	0.65	0.005	1.959 0.020	0.18172 0.00062	1.959 0.020	0.18168 0.00063	2658 22	2668 6	0.4
I	16	933-16.1	442	258	0.60	0.439	1.921 0.019	0.18606 0.00062	1.929 0.020	0.18215 0.00081	2692 22	2673 7	-0.7
I	18	933-18.1	464	259	0.58	0.006	1.970 0.020	0.18273 0.00067	1.970 0.020	0.18268 0.00068	2646 22	2677 6	1.2
I	10	933-10.1	242	111	0.47	-0.010	1.952 0.022	0.18316 0.00104	1.952 0.022	0.18325 0.00104	2666 25	2683 9	0.6
I	22	933-22.1	397	206	0.54	0.025	1.985 0.020	0.18353 0.00068	1.985 0.020	0.18330 0.00069	2630 22	2683 6	2.0
X	19	933-19.1	1155	47	0.04	0.025	1.891 0.017	0.19520 0.00042	1.891 0.017	0.19498 0.00042	2736 20	2785 4	1.7
X	9	933-9.1	154	89	0.60	0.075	1.753 0.022	0.21552 0.00523	1.755 0.022	0.21486 0.00524	2907 30	2943 39	1.2
X	8	933-8.1	162	66	0.42	0.053	1.794 0.023	0.21565 0.00112	1.795 0.023	0.21518 0.00114	2854 30	2945 9	3.1
X	31	933-31.1	485	428	0.91	0.644	1.671 0.015	0.22464 0.00066	1.682 0.015	0.21892 0.00084	3007 21	2973 6	-1.2
X	6	933-6.1	155	60	0.40	0.029	1.730 0.023	0.21950 0.00119	1.730 0.023	0.21925 0.00120	2941 31	2975 9	1.2
X	12	933-12.1	324	228	0.73	0.196	1.759 0.019	0.22188 0.00081	1.763 0.019	0.22014 0.00087	2897 25	2982 6	2.8
X	20	933-20.1	224	98	0.45	0.216	1.704 0.020	0.22478 0.00102	1.707 0.020	0.22287 0.00111	2972 29	3002 8	1.0
X	14	933-14.1	829	318	0.40	0.026	1.708 0.016	0.22311 0.00052	1.708 0.016	0.22287 0.00053	2970 22	3002 4	1.0
X	17	933-17.1	750	282	0.39	0.022	1.704 0.016	0.22395 0.00053	1.704 0.016	0.22376 0.00053	2976 22	3008 4	1.0
X	3	933-3.1	133	87	0.68	0.077	1.666 0.023	0.22464 0.00532	1.667 0.023	0.22396 0.00533	3030 33	3009 38	-0.7
X	1	933-1.1	357	545	1.58	0.047	1.657 0.017	0.22496 0.00074	1.657 0.017	0.22454 0.00075	3043 26	3014 5	-1.0
X	11	933-11.1	151	75	0.51	0.041	1.649 0.022	0.22493 0.00117	1.650 0.022	0.22457 0.00119	3055 32	3014 8	-1.4
X	4	933-4.1	175	84	0.50	0.034	1.675 0.021	0.22497 0.00108	1.675 0.021	0.22467 0.00109	3018 30	3014 8	-0.1
X	34	933-34.1	123	54	0.45	0.039	1.697 0.024	0.22513 0.00140	1.698 0.024	0.22478 0.00143	2985 34	3015 10	1.0
X	13	933-13.1	657	288	0.45	0.014	1.704 0.016	0.22544 0.00060	1.704 0.016	0.22531 0.00060	2977 23	3019 4	1.4
X	32	933-32.1	436	337	0.80	0.000	1.668 0.015	0.22540 0.00072	1.668 0.015	0.22540 0.00072	3028 22	3020 5	-0.3
X	7	933-7.1	139	87	0.64	-0.031	1.700 0.023	0.22651 0.00127	1.700 0.023	0.22679 0.00129	2983 33	3030 9	1.5
X	33	933-33.1	95	53	0.57	-0.088	1.714 0.025	0.22637 0.00151	1.713 0.025	0.22715 0.00156	2965 35	3032 11	2.2
X	15	933-15.1	376	280	0.77	0.000	1.724 0.018	0.22765 0.01299	1.724 0.018	0.22765 0.01299	2948 25	3036 91	2.9
X	23	933-23.1	706	174	0.26	0.011	1.587 0.015	0.25563 0.00062	1.587 0.015	0.25553 0.00062	3149 24	3219 4	2.2
D	26	933-26.1	729	257	0.36	0.469	6.601 0.063	0.09717 0.00060	6.632 0.063	0.09315 0.00100	905 8	1491 20	39.3
D	27	933-27.1	1069	107	0.10	0.046	2.281 0.017	0.18514 0.00044	2.282 0.017	0.18473 0.00045	2342 15	2696 4	13.1
D	24	933-24.1	1043	460	0.46	0.028	1.891 0.017	0.20948 0.00044	1.891 0.017	0.20923 0.00045	2736 20	2900 3	5.6
D	2	933-2.1	476	212	0.46	0.039	2.219 0.022	0.22453 0.00306	2.220 0.022	0.22418 0.00307	2397 20	3011 22	20.4

Appendix 11 – Re-Os geochronology data

Report with methods and results is from Dr. Svetlana Tessalina (JDLC, Curtin University).

Isotope Research for the Earth and Environment

GEOLOGICAL SURVEY WESTERN AUSTRALIA

THE UNIVERSITY OF WESTERN AUSTRALIA

CSIRO

Curtin University

JOHN DE LAETER CENTRE FOR ISOTOPE RESEARCH
Department of Imaging & Applied Physics, Curtin University
GPO Box U 1987, Perth, Western Australia 6845
Phone: +61 8 9266 2108
E-mail: b.mcinnes@curtin.edu.au
Web: jdlc.curtin.edu.au

Report: Re-Os dating of molybdenite (Samples ID: 14CA00001 [451.7 – 451.8] and 12CA00002 [66.64 – 66.74])

Methods

Sample material and preparation

Sample was crushed using hydraulic press and then molybdenite grains have been picked up using binocular microscope.

12CA00002 [66.64 – 66.74]	14CA00001 [451.7 – 451.8]
	

Analytical methods

Chemistry

Molybdenite separate was precisely weighed (roughly 20 mg) and transferred via funnels into Carius tubes resting in liquid nitrogen, followed by a weighed amount of the spikes (mixed ^{188}Os-^{190}Os and Re spikes). To this is added 1 ml concentrated, Teflon-distilled HCl and 3 ml concentrated, distilled HNO_3. The sealed tubes were placed in oven at 220° and reacted for 48 hours. After sample digestion, the tubes are refrozen and opened. Os is separated by solvent extraction, with a final purification of the Os by microdistillation. Rhenium was separated from a portion of the residuum liquid using anion exchange chromatography.

Mass spectrometry

Isotopic measurements were made by Thermo-Ionization Mass-Spectrometer (TIMS) Triton™ instrument for both Os and Re. All Re and most Os measurements were made using the Faraday cup collectors. Re and Os aliquots were loaded onto Pt filaments and covered with the $Ba(OH)_2$/NaOH activator. The multiple measurements of natural Re was within uncertainty of $^{185}Re/^{187}Re = 0.59$; therefore, no fractionation correction was applied. Measured Os isotope ratios are first corrected for contributions from natural Os (based on preliminary isotope dilution calculations), then corrected for mass fractionation based on the $^{190}Os/^{188}Os$ ratio of the spike. ^{187}Os is determined from the $^{187}Os/^{188}Os$ of the mixture and corrected for minor contributions from total common Os (blank plus sample).

Data reduction

Rhenium and osmium concentrations are determined by isotope dilution using measured isotopic ratios for Os and spikes weight. Concentrations of common Os and radiogenic ^{187}Os are then calculated using the isotope dilution equations. Note the nil concentrations of common Os relative to that of radiogenic Os in this molybdenite.

Error propagation on individual analyses includes the uncertainties on the spike calibrations, the uncertainty on the mass spectrometric measurements, an error magnification factor, uncertainties on blank corrections and, for the age determination, uncertainty in the decay constant for ^{187}Re. Analytical blanks are essentially insignificant for the age calculations, given the Re and ^{187}Os concentrations of the studied molybdenites and the sample size used in the analyses. Blank values were 10 pg for Re and 0.5 pg for Os with $^{187}Os/^{188}Os$ of 0.23±0.01.

Because of the essentially mono-isotopic nature of Os in molybdenite (nearly all ^{187}Os), the error magnification is insignificant for the determination of ^{187}Os concentration for molybdenites. Essentially, most of the quoted error in both the Re and Os concentrations is from the uncertainty in the Re and Os spike calibrations, and weighing errors for spikes and sample. The weighing error of the sample does not contribute to the uncertainty on the ages.

Data quality

Data quality was verified by the measurement of international reference material of Henderson molybdenite with known age (see the Table). The age returned for molybdenite standard material is within the error of certified value.

Results

For Re-Os age determination in molybdenite, there is no need in isochron because the initial ^{187}Os is nil. The results are presented in the Table.

Table. Re-Os age and abundance results for analyse of studied molybdenite samples and Henderson molybdenite Reference Material (RM) using ^{188}Os-^{190}Os double spike. The age of Reference Material molybdenite (RM) is within the error of the certified age of 27.66±0.02 Ma.

Sample	Re (ppm) ±2σ	^{187}Re (ppm) ±2σ	^{187}Os (ppb) ±2σ	Model Age (Ma) ±2σ
Reference Material	*11.18±0.07*	*7.02±0.04*	*3.23±0.01*	*27.65±0.02*
Cal 12CA	277.9±0.7	174.7±0.4	8838.1±0.6	2963±12
Cal 14CA	27.0±0.3	17.0±0.1	862.6±0.1	2977±20
Cal 14CA repeat	25.4±0.2	16.0±0.1	810.7±0.1	2975±27

Appendix 12 – Thin-section descriptions

Sample ID: CAL004

Hole ID: 12CADD002

Depth: 32.26-36.36 m

Reason for sample: Nature of common stringer style mineralisation. Two biotite types – foliated and unoriented.

Transmitted Light

Parent rock is typical biotite monzogranite, as described in CAL006.

Widespread chloritisation of biotite, mainly replacing igneous form but also replacing salmon-pink unaligned alteration biotite. Chloritisation inevitably associated with sulphide patches.

Pale yellow feldspar patches in hand specimen are slightly oxidised granoblastic plagioclase (85%), quartz (10%) and biotite (5%), with irregular grain boundaries.

Widespread sericite dusting of feldspars, along with selective chloritisation.

Some replacement of plagioclase by coarser sericite/muscovite.

Coarse, unaligned biotite in "veins" is associated with rounded high-relief mineral, likely monazite.

Reflected Light

Cleavage planes in large magnetite grains replaced by chlorite.

Subhedral cubic pyrite the dominant sulphide, with lesser chalcopyrite – no pyrrhotite. Chalcopyrite is pitted, intergrown with magnetite in places, and as fine inclusions within sericitised feldspars, especially around biotite vein.

Very little sulphide in granoblastic plagioclase domains.

Summary and comments

No quartz vein associated with mineralised biotite vein.

No clear evidence of S2 biotite alignment.

Sample ID: CAL006

Hole ID: 12CADD002

Depth: 47.00-47.27 m

Reason for sample: Type example of K-feldspar-phyric biotite monzogranite.

Transmitted Light

Biotite (10%) is subhedral to euhedral, with abundant zircons.

Quarts (25%) is irregular and anhedral, with poikilitic inclusions of biotite and plagioclase. Sub-grains are common in larger grain, and have undulose extinction.

Plagioclase (50%) An24-27, some polysynthetic twinning, and definite areas of 120-degree triple junctions (polygonal granoblastic texture).

Microcline (15%) as large anhedral phenocrysts that are poikilitic with biotite and quartz inclusions. Also occurs as anhedral grains in groundmass.

Traces of fine sillimanite, in random orientations inside feldspar grains.

Usual retrogression of biotite to chlorite-sericite-magnetite and sericite-chlorite-epidote overprint of feldspars.

Reflected Light

Trace opaques. Subhedral magnetite within and adjacent to retrogressed biotite. Tiny trace of subhedral chalcopyrite associated with unaligned biotite clump, causes localised retrogression to chlorite, both within biotite and in adjacent microcline.

Summary and comments

Rock is a microcline-phyric biotite monzogranite with granoblastic recrystallisation textures and chlorite-sericite-epidote retrogression.

Sample ID: CAL007

Hole ID: 12CADD002

Depth: 48.60-48.85 m

Reason for sample: High-strain variant of CAL006. Timing between garnet and foliation.

Transmitted Light

Rock is porphyritic, but phenocrysts now recrystallised into poikilitic feldspar-garnet masses (pale patches in hand specimen).

Biotite (10%) in two forms: (1) Finer, subhedral light-dark brown igneous grains in groundmass; (2) Masses of decussate (?) larger subhedral to euhedral grains, light to dark brown. Zircons in both forms.

Garnet (2%) is light pink, relatively clean and of consistent grainsize. Not affected by the foliation, clearly overgrows and is distributed throughout the rock.

Plagioclase (58%) An27, coarse recrystallised phenocrysts (poikilitic with quartz and biotite), and abundant in groundmass. Anhedral in both settings.

Microcline (5%) is anhedral, rare in groundmass, more common as recrystallised phenocrysts. No association with mineralised vein.

Quartz (25%) in groundmass only, hard to pick from plagioclase. Lack of sericite dusting used to identify.

Biotite to chlorite retrogression is focused around sulphides, and dusting of sericite is ubiquitous. Coarser masses of sericite and chlorite are focused around mineralised vein.

Reflected Light

Opaques are 1% overall.

Chalcopyrite (50%) in disseminated form is subhedral, weakly pitted and intergrown with pyrite and pyrrhotite. Clusters occupy grain boundaries, wholly included in quartz or feldspar, and also replace biotite lamellae.

Pyrite (35%) generally cleaner and more euhedral than other sulphides. One diffuse vein of intergrown, pitted chalcopyrite-pyrrhotite-magnetite is overgrown by cleaner pyrite. Vein is a focus for very localised muscovite-chlorite retrogression, but adjacent silicates are no more affected by retrogression that elsewhere in the rock.

Pyrrhotite (15%) is pitted and euhedral, intergrown with chalcopyrite.

Magnetite in pitted subhedral grain grains is disseminated through the rock, usually associated with biotite.

Summary and comments

Formerly K-feldspar-phyric biotite monzogranite, now recrystallised to poikilitic plagioclase-microcline blotches. Disseminated chalcopyrite-pyrite clusters and diffuse vein have no obvious silicate alteration, but are a focus for localised retrogression.

Within reason that this is the same rock as CAL006 least-altered variant.

Garnet post-dates S1 foliation.

Weak secondary alignment of biotite in S2 orientation (moderate west dip).

Sample ID: CAL008

Hole ID: 12CADD002

Depth: 52.18-52.28 m

Reason for sample: Effects of strain gradient on textures. Sulphide-rich stringer cuts foliation.

Transmitted Light

Parent rock is CAL006 biotite monzogranite.

Only about 10% retrogression of biotite to chlorite (<< than CAL004), focused around sulphide patches and vein that "breaches" foliation. Weak to moderate sericitisation, but with no spatial relationship to mineralisation.

One patch of garnet associated with mantle-style mineralised vein – no retrogression in garnet, but >sericite in adjacent feldspar.

Portion of mineralised vein that "breaches" foliation is clearly associated with very localised chlorite-sericite retrograde alteration (1-2 times vein width).

Foliation-parallel mineralised zones are associated with thin quartz veins.

Reflected Light

Breaching vein is chalcopyrite-rich (90%), with lesser pyrrhotite, and there is also fine pyrrhotite-chalcopyrite in the retrograde selvedge.

Remaining mineralisation (bulk) is anhedral chalcopyrite-pyrrhotite interstitial to silicate grains (mantling them). Both sulphides are pitted and dirty, with minor euhedral pyrite overgrowth. Minor tabular molybdenite in the mantle-style veins.

Chalcopyrite-pyrrhotite also invade cracks in the garnet – i.e. remobilised post garnet formation? Minor sulphide inclusions within garnets.

Notably very little magnetite in this sample.

Summary and comments

Likely example of remobilised type of mineralisation in breaching vein, associated with retrogression, remobilised into grain boundaries and cracks.

Sample ID: CAL009

Hole ID: 12CADD002

Depth: 66.64-66.74 m

Reason for sample: Alteration associated with high-grade molybdenite, possible Re-Os age.

Transmitted Light

Quartz (30%) to 3 mm in anhedral, irregular cuspate-lobate crystals with lots of sub-grain boundaries (recrystallised?)

Plagioclase (45%) to 3 mm in anhedral, irregular cuspate-lobate texture with quartz and K-feldspar, little primary texture. Most twinned examples are ~An23.

Microcline (10%) mainly in large masses to 4 mm that may be relict phenocrysts. Patchy retrogression to sericite, and also replaced by fine sillimanite in places.

Garnet (5%) to 7 mm, larger grains have inclusions of pale brown-green biotite, quartz-feldspar, and sulphides. Minor retrogression to chlorite. Some inclusions also of coarse, clean white mica.

Sillimanite (2%) in two forms: (1) Fibrolitic foliation-parallel bands pseudomorphing biotite, but not necessarily aligned with biotite; (2) Prismatic needles inside feldspar crystals (pervasive through sample).

Biotite (3%) is very minor, little remaining. Vast majority is deep red-brown alteration-related form, associated with foliation bands containing magnetite and sillimanite. Some green-brown primary biotite remains, including within and around large garnets.

There is weak sericite-chlorite retrogression throughout.

Reflected Light

Molybdenite, magnetite, chalcopyrite, pyrite and pyrrhotite all present. Large aggregates of molybdenite (to 3 mm) comprise subhedral laths, with intimately intergrown chalcopyrite-pyrrhotite (all cogenetic). Chalcopyrite-pyrrhotite aggregates are also coarsely associated with molybdenite chunks. Coarse garnet contains inclusions of molybdenite-chalcopyrite-pyrrhotite, including well away from cracks – mineralisation cannot be post garnet growth. Magnetite and minor chalcopyrite-pyrrhotite are associated with foliation-parallel red-brown biotite-sillimanite streaks, as observed in normal Cu-rich mineralisation. Rare euhedral pyrite overgrowths of pyrrhotite are observed.

No silicate “vein” controls high-grade molybdenite, and it is not clear why the coarse molybdenite is concentrated in this band.

Summary and comments

High-grade dated Mo-rich mineralisation also contains chalcopyrite-pyrrhotite – i.e. is part of the overall Cu event, not separate. This mineralisation event must pre-date garnet growth (all sulphides observed as inclusions in garnet).

Biotite-magnetite-chalcopyrite-pyrrhotite vein/streak seems to pre-date sillimanite growth also – i.e. sillimanite replaces alteration. Sillimanite also replaces feldspars and quartz in isolated occurrences.

Sample ID: CAL010

Hole ID: 12CADD002

Depth: 67.44-67.54 m

Reason for sample: Characterise “mantle” textured veins. Why is garnet associated with mineralisation?

Transmitted Light

Parent rock is CAL006 biotite monzogranite.

Pale uphole end is granoblastic microcline (85%) with minor plagioclase, quartz and biotite. Likely K alteration zone, recrystallised. Pale downhole end granoblastic also, but plagioclase dominated (low An) with 20% quartz and trace biotite, but no microcline. Vein through the centre is dominantly untwinned feldspar with faint perthitic texture (K-feldspar), with minor clean quartz.

Clumps of unaligned biotite are distinctly reddish brown, as usually observed.

Feldspar is very weakly sericitised. Pervasive weakish sericitisation is clear greater around sulphide grains, and weakish chlorite throughout affects biotite and feldspars.

Reflected Light

Main vein opaques are chalcopyrite (50%), pyrrhotite (40%), magnetite (10%) molybdenite (trace) and euhedral pyrite (trace). Sulphides are anhedral, dirty and mantled around silicate grains.

Remnants of cubic to octohedral magnetite are evident, but eaten away by fine chlorite (?) and chalcopyrite. Outside of the vein, magnetite is more abundant than chalcopyrite-pyrhhotite, but disseminated sulphides are still evident.

Chalcopyrite and pyrrhotite have two relations with garnet: (1) Fine inclusions; (2) More commonly, along cracks in grains

Summary and comments

Vein is quartz-K-feldspar, with chalcopyrite-pyrrhotite-magnetite equilibrium assemblage. Garnet likely post-dates mineralisation, evidenced by fine sulphide inclusions in it.

Sample ID: CAL011

Hole ID: 12CADD002

Depth: 72.18-72.28 m

Reason for sample: Characterise increasing gneissic fabric.

Transmitted Light

Parent rock is CAL006 biotite monzogranite.

Fibrolitic sillimanite is focused in foliation-parallel biotite bands at the top of hole end. One biotite streak at the uphole end has fibrolitic sillimanite growing at an acute angle (~40 degrees) to the streak, consistent with the S2 fabric orientation.

Brighter white patches at downhole end are highly sericitised plagioclase, while more translucent parts are untwinned, weakly perthitic K-feldspar and microcline, as seen in CAL010. These feldspars are in a granoblastic texture.

Yellowish uphole end is 80% granoblastic K-feldspar, with lesser quartz, biotite and rare plagioclase.

The centre of the slide is a vein of mainly coarse quartz, plus opaques as described below.

Reflected Light

Central vein is chalcopyrite (90%), pyrrhotite (3%), pyrite (3%), magnetite (3%) and molybdenite (1%) in usual habits (pyrite clean, euhedral)

Magnetite in wallrock clearly was euhedral/octohedral, but is now corroded and replaced, including by needle-like ilmenite lamellae, in cleavage orientations.

Summary and comments

Clearly significant K added to this rock in relation to CAL006 parent, based on the much greater amount of K feldspar.

Sillimanite grows both parallel to (pseudomorphing) and acute to biotite streaks, with the latter form here in the s2 orientation.

Sample ID: CAL012

Hole ID: 12CADD002

Depth: 81.00-81.23 m

Reason for sample: Characterise garnet-sillimanite gneiss – same parent as other rocks?

Transmitted Light

Biotite (5%) in irregular anhedral-subhedral grains aligned to the foliation, with margins eaten away by sillimanite and chlorite-sericite retrogression. Traces of zircons. There was probably much more biotite in the original rock.

Sillimanite (20%) as clumpy fibrolitic masses, with brownish tinge due to remnants of the biotite it has replaced. Second form is clear to pale green prismatic crystals with microcline (most commonly) or quartz.

Quartz (40%) and microcline (35%) form weakly granoblastic leucosomes. Microcline is variously clean, partly replaced by randomly oriented sillimanite needles (most strongly near fibrolite bands), and in places completely altered to sericite.

Trace garnet mainly in a large light pink grain that is moderately cracked and poikiloblastic with inclusions of biotite, quartz, microcline, and sillimanite-bearing quartz.

Retrograde sericitisation is common and nearly wholly replaces some microcline. Usual biotite to chlorite retrogression is most common adjacent to sulphides.

No clear shear sense on foliation. Most sillimanite aligned with biotite (pseudomorphs), but is random when in microcline.

Reflected Light

Magnetite looks old – skeletal remnants restricted to mica/sillimanite bands.

Pyrite, pyrrhotite and chalcopyrite restricted to leucosomes, and in usual forms. Fine chalcopyrite sometimes enclosed in coarse silicates (mainly quartz), but mostly interstitial, dirty, pitted intergrowths with pyrrhotite. Pyrite cleaner and more subhedral. All sulphides associated with chlorite retrogression of biotite.

Summary and comments

Rock is a microcline-quartz-sillimanite-garnet-biotite gneiss with well defined leucosomes and melanosomes, with strong sericite retrogression. Garnet and biotite in textural equilibrium. K-enriched parent rock (all microcline). Sillimanite replaces existing biotite melanosomes. Magnetite looks old, eaten away.

Sample ID: CAL017

Hole ID: 12CADD002

Depth: 134.16-134.26 m

Reason for sample: Study mineralised pegmatite vein and margin.

Transmitted Light

White zones of pegmatite vein are granoblastic microcline (85%) with lesser quartz, plagioclase and biotite.

Mineralised band of pegmatite is similar, but microcline (30%)-quartz(50%)-plagioclase(20%). Plagioclase preferentially sericitised and also contains abundant fine sulphide inclusions (much greater than quartz and microcline, which basically have none).

Residuum zone on margin are very poor in microcline (none), roughly plagioclase (30%)-biotite(15%)-quartz(55%) in even grained granoblastic texture. Much weaker retrogression than inside pegmatite vein.

Reflected Light

In residuum domain very fine chalcopyrite-pyrrhotite inside silicate grains (plagioclase and biotite), plus lesser magnetite with relict subhedral outlines (resorbed/altered).

Pegmatoidal mineralisation is chalcopyrite-pyrrhotite dominant, with minor molybdenite. Chalcopyrite-pyrrhotite is in two forms: (1) Larger interstitial anhedral masses; and (2) Very fine inclusions within heavily retrogressed plagioclase (but not quartz of K-feldspar).

No mineralisation in microcline band – why?

Summary and comments

Sulphide inside plagioclase in pegmatite has possibly been trapped inside in during crystallisation of the vein, followed by barren quartz and K-feldspar.

Sample ID: CAL018

Hole ID: 12CADD002

Depth: 141.26-141.48

Reason for sample: Study higher-strain, biotite-rich granite-gneiss, and relationship of garnet to foliation?

Transmitted Light

Biotite (15%) as small subhedral flakes in groundmass (dark brown), plus as coarser, subhedral decussate masses with random orientations (lighter orange-brown). Zircons with rad damage are common in both forms.

Garnet (1%) irregular light pink, weakly cracked and generally not retrogressed, fairly clean. Larger grain poikiloblastic (feldspar and quartz).

Plagioclase in two forms: (1) An25 phenocrysts, large white patches poikilitic with plagioclase, quartz, garnet and biotite. Generally quite retrogressed to sericite; (2) An40 in groundmass, weakly developed granoblastic texture, generally equant, anhedral.

Quartz (10%), but not much convincing, mostly plagioclase in groundmass. Large anhedral grains in vein.

Pale green sillimanite needles in minor amounts?

Weakly pegmatoidal vein of quartz and plagioclase is difficult to follow, but very large, irregular quartz grains and lack of biotite mark its location. Minor garnet in there, including with chalcopyrite inclusions.

Sericite retrogression pervasive but weak, except for phenocrysts, where noticeably stronger. Biotite to chlorite is focused around sulphide.

S2 biotite ori running down length of thin section.

Reflected Light

Chalcopyrite(70%)-pyrite(20%)-pyrrhotite(10%), with negligible magnetite. Two mineralisation forms: (1) Patches of fine, anhedral chalcopyrite and very minor pyrite, at or around grain boundaries, sometimes internal or replacing lamellae in biotite; (2) Pegmatoidal vein, dirty, pitted chalcopyrite-pyrrhotite interstitial to silicates, overgrown in places but clean sub-euhedral pyrite.

Summary and comments

Formerly K-feldspar phyric biotite monzogranite, now distinctly poor in quartz and K-feldspar.

Garnet not wrapped by S1.

Biotite in poikilitic silicates is randomly oriented, suggesting likely igneous phenocrysts (not post-S1 porphyroblasts).

Sample ID: CAL019

Hole ID: 12CADD002

Depth: 151.00-151.22

Reason for sample: Understand origin of garnet-sillimanite rocks. S1 and S2 fabric relationships.

Transmitted Light

Sillimanite (15%) as fibrolitic masses after biotite, and finer needles marginal to fibrolite clumps, replacing both microcline and quartz.

Biotite (3%) is rare, mostly pseudomorphed by sillimanite. Generally light-dark brown but distinctly pale to moderate green in proximity to garnets, including as inclusions in garnet.

Microcline (35%) and quartz (45%) form moderately granoblastic bands between sillimanite-biotite melanosomes, with both anhedral. Quartz has quite irregular shapes and typically coarser than microcline. Rare larger microcline grain are poikilitic and may be ex-phenocrysts.

Garnet (2%) as light pink grains with inclusions of chlorite/green biotite and quartz. Not affected by S1 or S2 in any way.

Chlorite-sericite retrogression focused in biotite adjacent to mineralisation blebs.

Weak S2 biotite alignment. Sillimanite mimics S1 and S2-aligned biotite, but is can be random within those bands – i.e. post D2?

Reflected Light

Magnetite as scattered, heavily pitted, subhedral grains in between silicates. Chalcopyrite and pyrite intergrown in dirty, pitted masses, with pyrite generally cleaner and subhedral. Can be internal to garnet and on cracks, interstitial to silicates, or replacing biotite lamellae.

Summary and comments

Quartz-microcline-sillimanite-biotite-garnet gneiss with sillimanite-biotite melanosomes and mineralised quartz-microcline-garnet leucosomes. Likely after K-feldspar-phyric granitoid.

Sample ID: CAL020

Hole ID: 12CADD002

Depth: 155.90-156.00 m

Reason for sample: Characterise intense magnetite-chalcopyrite-garnet-hornblende(?) veins.

Transmitted Light

Uphole end is quartz(55%)-magnetite(40%)-green biotite(5%) with trace high relief, colourless elongate crystals with low biref and retrogression to sericite – sillimanite?

Downhole end is garnet (45%)-quartz(35%)-biotite(5%)-plagioclase(2%)-opaques(18%).

No silicate retrogression associated with chalcopyrite-pyrite remob veinlet.

Some garnets have magnetite inclusions.

Reflected Light

In uphole half, opaques are ~38% magnetite and 20% chalcopyrite-pyrrhotite with clear pyrite overgrowth, with magnetite-chalcopyrite-pyrrhotite appearing in equilibrium.

Downhole half is all magnetite, apart from thin remobilised chalcopyrite-pyrite veinlet.

Summary and comments

Vein as described. Green colour is green biotite, not hornblende.

Sample ID: CAL021

Hole ID: 12CADD002

Depth: 158.70-158.80 m

Reason for sample: Characterise intense feldspar-garnet alteration.

Transmitted Light

About 50:50 granoblastic mix between plagioclase and quartz, with essentially no K-feldspar. Very nice triple junctions between plagioclase grains.

Traces of biotite with minor chlorite retrogression. Sericite retrogression also minor.

One large garnet grain appears to overgrow coarse chlorite.

Reflected Light

Weak chalcopyrite-pyrrhotite-pyrite interstitial to silicates and fine within plagioclase. Subhedral interstitial magnetite to 1%.

Summary and comments

Where has all the K gone in this rock? Alteration is plagioclase dominated? Good evidence also of garnet replacing earlier chlorite.

Sample ID: CAL022

Hole ID: 12CADD001

Depth: 68.28-68.38 m

Reason for sample: Microstructure of F2 folding, relationship to garnet development.

Transmitted Light

Biotite monzogranite parent rock, here in gneissic form.

Melanosomes dominated by dark brown biotite, pretty much no retrogression. Leucosomes are biotite (5%)-plagioclase(10%)-quartz(40%)-microcline(55%) and are equigranular and slightly granoblastic.

Clear second biotite orientation axial planar to folds, most evident in leucosome domain. Difficult to say much about garnet relationship to S2.

Quite a lot of granular, high-relief monazite. Fine sillimanite in feldspars and rare coarser fibrolitic replacement of biotite, with no clear preferred ori.

Reflected Light

Around 1% disseminated subhedral magnetite. Trace chalcopyrite in fine disseminations.

Summary and comments

S2 alignment of biotite, garnet relationship to this fabric unclear.

Quite high microcline to presumed parent – alteration?

Sample ID: CAL023

Hole ID: 12CADD001

Depth: 130.75-130.85 m

Reason for sample: Type-example of amphibolite, with weak biotite alteration.

Transmitted Light

Hornblende(50%) is dark green, stubby and aligned to fabric. Plagioclase (45%) the same grainsize, in interlocking texture.

Biotite (5%) mostly aligned to foliation in elongate sheets, mostly at uphole end (i.e. alteration). Odd patch of muscovite – after biotite? Biotite appears to replace hornblende in many places, likely post foliation. Hints of a second biotite orientation, but poorly developed.

Very little retrogression.

Reflected Light

Trace sub- to euhedral magnetite, and a few specks of chalcopyrite.

Summary and comments

Definitely mafic amphibolite. Biotite post-dates amphibolite formation.

Sample ID: CAL024

Hole ID: 12CADD001

Depth: 136.30-136.55 m

Reason for sample: Type-example of biotite-rich granite-gneiss, older relative to CAL024.

Transmitted Light

Biotite (15%) is dark khaki brown and subhedral, with abundant zircons associated with rad damage. Chlorite retrogression completely absent. Clear preferred alignment of grains.

Microcline (35%) is poikilitic, tends to form larger granoblastic masses, possibly former phenocrysts. Anhedral to subhedral.

Plagioclase (30%) is ~An23, poikilitic (biotite), anhedral and even grained. Untwinned feldspar is also likely plagioclase, sometimes has albite (?) rims against microcline.

Quartz (20%) is anhedral, even grained and poikilitic (biotite).

Zircons in and outside of biotite. Monazite also common.

Rare retrogression tightly focused around sulphide grains.

Reflected Light

Magnetite as dirty, pitted grains, commonly overgrown by clean pyrite. Pyrite as distinctly clean grains overgrowing dirty magnetite-chalcopyrite in a variety of settings. Some clean pyrite cores with dirty pyrite rims. Chalcopyrite as isolated, anhedral, dirty grains.

Summary and comments

Weakly K-feldspar-phyric biotite monzogranite with biotite foliation and weak retrogression.

Sample ID: CAL025

Hole ID: 12CADD001

Depth: 149.30-149.40 m

Reason for sample: Typical stockwork-style veining in syenogranite.

Transmitted Light

Unaltered parent is CAL026.

Compositionally very similar to CAL026, but perhaps more microcline (~50%). Minor chloritisation of biotite outside vein area, plus weak sericite dusting.

Vein is a poorly defined band of coarse quartz, microcline and minor muscovite (possibly primary vein mineral?). Distinctly more quartz (and coarser) than host rocks, but vein margin is not sharp.

Reflected Light

Vein sulphides are chalcopyrite(60%)-pyrrhotite(40%) with trace molybdenite and pyrite. Most sulphide is sub- to anhedral and interstitial to silicates, but some is very fine-grained in and around degraded feldspar to muscovite aggregates. Basically no magnetite, and very little sulphide outside of vein area.

Summary and comments

No major compositional variation from unaltered version.

Why no magnetite in rock here?

Sample ID: CAL026

Hole ID: 12CADD001

Depth: 154.09-154.34 m

Reason for sample: Type-example of syenogranite, "younger" relative to CAL024.

Transmitted Light

Biotite (5%) is subhedral, isolated or within clumps with muscovite, dark brown, and patchily altered to chlorite-magnetite-ilmenite(? Needles). Weak preferred alignment parallel to thin section.

Muscovite (1%) as subhedral, rare grains intergrown with biotite, appearing primary? Largeish, optically continuous grains.

Quartz (30%) as several large anhedral poikilitic phenocrysts (microcline inclusions), plus in groundmass.

Microcline (45%) is rarely perthitic. Grain boundaries between microcline, plagioclase are commonly hazy. Microcline possibly replaced plagioclase in places – possibly mixed igneous and hydrothermal origin?

Plagioclase (19%) ~An20, rare anhedral grains with albite twinning, and some with no twinning at all.

Some alteration of primary (?) muscovite to K-feldspar?

Zircons fairly rare in biotite.

Sericite-chlorite retrogression of biotite and feldspars is widespread, weak to moderate strength.

Reflected Light

Trace overall. Magnetite as subhedral, pitted grains associated with retrogressed biotite. Chalcopyrite as subhedral inclusions in untwinned feldspar, with pyrite, localises retrogression. Magnetite-pyrite rarely as lamellae within chloritised biotite. Pyrite also occurs as fine lamellae in muscovite and biotite, and filling grain boundaries.

Summary and comments

Quartz-phyric, biotite syenogranite, granoblastic, with some K-feldspar possibly of alteration origin. Possibly traces of primary muscovite.

Sample ID: CAL027

Hole ID: 12CADD001

Depth: 195.00-195.10 m

Reason for sample: Type-example of mineralised pegmatoidal vein.

Transmitted Light

Parent is ~CAL024 biotite monzogranite.

Residual monzogranite is ~10% biotite, 2% microcline, 30% plagioclase and 58% quartz, with biotite proportion increasing to pegmatite margin. Quartz and feldspars are anhedral, with irregular grain boundaries and hints of granoblastic texture. Microcline-poor in relation to parent rock.

Coarsest pegmatite areas are 70% quartz, with microcline, plagioclase and sulphide interstitial and moderately sericitised. Some coarse sericite/muscovite may be primary. Margins of pegmatite (and other patches) that are milkier white are ~90% feldspar (70plag/30kspar) with much less quartz, and lack significant sulphide. These may be earlier crystallised rims of the vein. Minor biotite in pegmatite zones.

Reflected Light

Residual monzogranite has ~1% disseminated chalcopyrite with rare clean pyrite overgrowths, plus <1% magnetite.

Pegmatite mineralisation is chalcopyrite-dominant, with pyrrhotite occurring as lamellar intergrowth. Chalcopyrite is dominantly anhedral and interstitial to coarse silicates, rarely as intergrowths with biotite. Traces of magnetite in pegmatite sulphide.

Some lamellar pyrrhotite-chalcopyrite inside plagioclase twin planes.

Summary and comments

Pegmatoidal vein is zoned, with much more sulphide is last-crystallised (?) quartz-rich part?

Sample ID: CAL028

Hole ID: 12CADD001

Depth: 217.14-217.24 m

Reason for sample: Type-example of magnetite-garnet related high-grade mineralisation.

Transmitted Light

Whole slide is a ~50-50 split between quartz and distinctly green biotite (pale brown to blue-green pleochroism), with biotite being more abundant in dark green, sulphide-poor downhole end.

Coarseish, granular apatite is common, and zircon is abundant in biotite.

Large quartz crystal at downhole end is actually several large grains, with one clear garnet inclusion and weakly poikilitic with biotite.

Some remnant colour banding in biotite may indicate pseudomorphing of an earlier phase? Some fine, hair-like sillimanite wisps in biotite.

Reflected Light

Pyrrhotite dominant sulphide, in anhedral interstitial masses with chalcopyrite, with pyrite as clean subhedral overgrowths. Pyrrhotite-chalcopyrite-magnetite in textural equilibrium. Magnetite has extensive exsolution of ilmenite along cleavage planes.

Summary and comments

Origin as a potassic quartz vein? Why green (low Ti?) biotites? Has titanium gone into magnetite instead?

Sample ID: CAL029

Hole ID: 12CADD001

Depth: 355.20-355.30 m

Reason for sample: Characterise late, retrograde breccia mineralisation.

Transmitted Light

Clasts of quartz-microcline-plagioclase-biotite granitoid with total biotite to chlorite retrogression and extensive sericite-chlorite-epidote retrogression of feldspars.

All silicate grains show strong deformation effects: internal grain boundaries, bent grains, fracturing etc.

Clasts are separated by up to 5 mm wide fine-grained breccia zones with chlorite-calcite-epidote cement, with angular grains and rock fragments of all sizes.

Reflected Light

Opaques are 100% chalcopyrite, and focused within breccia fragments at all scales, rather than in cement – i.e. this is brecciated mineralisation, rather than a young event.

Summary and comments

Brecciated mineralisation – not a younger min event. Deformation and retrograde alteration clearly linked.

Sample ID: CAL030

Hole ID: 12CADD001

Depth: 370.20-370.30 m

Reason for sample: Characterise proto-gneiss formation, with leucosome-melanosome banding.

Transmitted Light

Generally a weakly granoblastic quartz(45%)-plagioclase(45%-biotite(10%) rock, with An content greater than typical? One band of microcline, but otherwise quite poor in that mineral. 10 mm white patch at uphole end is coarse quartz and heavily sericitised K-feldspar.

Biotite streaks/clumps are same composition as remainder (dark brown), with abundant zircons and rad damage.

Weak to mod localised chlorite-sericite retrogression.

Garnet clearly post-dates biotite foliation, not wrapped by it at all.

Reflected Light

No mineralisation. Traces of subhedral magnetite.

Summary and comments

Garnet clearly post-S1. Poor in microcline and >An than usual – why?

Sample ID: CAL031

Hole ID: 12CADD001

Depth: 520.40-520.50 m

Reason for sample: Characterise wide “mantle-style” high-grade quartz-garnet vein.

Transmitted Light

Rock is a quartz-garnet-microcline-biotite/chlorite vein with fine retrograde needles (?) and some epidote and tourmaline (?).

Microcline heavily retrogressed to sericite.

Garnet seems to overgrow coarse, earlier chlorite, and contain fine chlorite grains. But chlorite also occurs as retrogression of biotite.

Reflected Light

Chalcopyrite-pyrrhotite dominant, between quartz and garnet grains, with some clean pyrite. Fine sulphide inclusions in garnet grains, especially where marked, but also inside coarse quartz.

No significant magnetite.

Summary and comments

Mineralisation clearly pre- or syn-garnet. Likely origin as a recrystallised vein.

Sample ID: CAL032

Hole ID: 08WHDDH001

Depth: 92.74-92.97 m

Reason for sample: Type-example of early quartz-feldspar porphyry sills.

Transmitted Light

Biotite (10%) subhedral dark green-brown, focused into well defined foliation, bands of coarse crystals, with much finer grains intervening. ~20% of grains altered to chlorite.

Quartz (45%) as phenocrysts to 7 mm, now recrystallised into aggregates with varying extinction directions.

Feldspars ~45% overall split between plagioclase (~5% convincing) and microcline (15% convincing). Overall texture is likely quartz- and feldspar-phyric igneous rock. Phenocrysts now highly strung out into granoblastic quartz and mixed feldspar aggregates, the latter cloudy with sericite.

Zircons common inside and outside of biotite.

Retrograde sericitisation of feldspars is pervasive, and ~20% of biotite is chloritised.

Structurally, biotite deflects around quartz phenocrysts. Top to the west sense of movement suggested by sigma-type deformed quartz phenocrysts. Retrograde sericite in feldspars aligned in flatter foliation than main foliation (~subhorizontal).

Reflected Light

Magnetite as subhedral equigranular crystals, likely grown post foliation (?) – foliation doesn't deflect around or rotate them. Some larger grains appear to have have euhedral biotite growth in their strain shadows?

Summary and comments

Quartz-feldspar porphyry, now highly flattened and stretched.

Sample ID: CAL034

Hole ID: 08WHDDH001

Depth: 132.23-132.43 m

Reason for sample: Characterise more mafic variant of Ninan volcanic sequence.

Transmitted Light

Biotite (25%) as ragged subhedral crystals strongly aligned in foliation, likely pre-dates more variable amphibole.

Actinolite (20%) as subhedral ragged grains mostly aligned to foliation, but variable end-sections visible and some end-sections visible, likely grew post-foliation?

Hornblende (1%) as ragged blue-green crystals altered to biotite or actinolite. Probably an earlier metamorphic mineral?

Plagioclase (50%) as laths aligned to foliation, rare twinning, strongly interlocking with biotite-actinolite. Possibly some is quartz?

Quartz (1%) as constituent of foliation-parallel veins with actinolite, which are at core of actinolite-rich band in slide centre.

Garnet 1% as one large strongly poikiloblastic (biotite, plagioclase, actinolite) grain. Abundant cracks are retrogressed to chlorite.

Possible tourmaline spatially associated with large garnet grain.

Reflected Light

Opaques ~2% overall. Magnetite as cubic, pale crystals clearly more abundant in actinolite-rich layers and veins. Largest grains seem to deflect biotite foliation, remainder not really. Disseminated form most common, but also as lamellar inclusions in garnet. Largest grain has exsolved ilmenite on cleavages.

Chalcopyrite in fine masses associated with quartz-actinolite veins.

Summary and comments

Biotite-plagioclase-hornblende schist of likely mafic-intermediate parent, altered to actinolite around quartz-actinolite-magnetite-chalcopyrite veinlets, all overgrown by garnet.

Amphibole seems to post-date biotite – biotite alteration, amphibole metamorphic?

Sample ID: CAL035

Hole ID: 08WHDDH001

Depth: 147.56-147.86 m

Reason for sample: Type-example of andesite-dacite host rock at Ninan.

Transmitted Light

Biotite (25%) as dark green-brown subhedral grains strongly aligned to foliation, though some grains are oblique.

Plagioclase (75%) is ~An25. Possible some other feldspar or quartz, but most grains seem to show twinning and sericitisation. Two forms: (1) Phenocrysts are white spots in the rock, elongate masses of plagioclase that is recrystallised/granoblastic, with laths broadly aligned in foliation, though some is oblique. Biotite foliation deflects around these, no sense of asymmetry; (2) Groundmass, weakly granoblastic, even grained, likely some quartz in here also?

Retrogression of biotite to chlorite-magnetite/ilmentite, all feldspars to sericite. Retrograde minerals have no preferred ori, except where pseudomorphing other minerals.

Minor epidote.

Reflected Light

Magnetite as weakly pitted subhedral grains.

Chalcopyrite-pyrite together as pitted, interstitial, anhedral grains (trace). Straight edges defined by bounding biotite/chlorite. No associated vein/crack or alteration, though retrograde chlorite generally focused around sulphides.

Summary and comments

Feldspar-phyric intermediate volcanic rocks, strongly flattened, with chlorite-sericite retrogression. Biotite probably not primary. Probably more quartz than recognised here.

Sample ID: CAL038

Hole ID: 08WHDDH001

Depth: 198.20-198.46 m

Reason for sample: Type-example of Ninan post-S1 monzogranite dykes, with sulphide blebs.

Transmitted Light

Biotite (5%) as subhedral, dark brown grains with rare small zircons. ~25% of grains show retrogression to chlorite-magnetite/ilmenite.

Quartz (40%) is anhedral in groundmass, no phenocrysts.

Plagioclase (35%) is ~An25, compositionally zoned to Na-rich rims? Ubiquitously sericitised, strongly favouring cores. Poikilitic with biotite, quartz, opaques.

K-feldspar (20%) generally unzoned, untwinned, but rare simple twinning and microcline hatching.

In main mineralised area, opaques are internal to silicate minerals, not controlled by any clear fracture or vein (i.e. a bleb). Muscovite very localised around sulphides (retrograde), but adjacent feldspars are not any more altered than distal examples. Chunky monazite crystals in mineralised patch also.

Trace epidote and very fine sillimanite?

Reflected Light

Chalcopyrite in disconnected patches of dirty, pitted grains, interstitial to and internal to silicate grains. Pyrite in the same setting, but some cleaner subhedral grains may be later overgrowths. Magnetite is minor, but in the same setting.

Summary and comments

Plagioclase-phyric biotite monzogranite with extensive sericite retrogression of plagioclase cores. Sulphide likely entrained during intrusion, trapped in silicate grains.

Sample ID: CAL039

Hole ID: 08WHDDH001

Depth: 202.62-202.73 m

Reason for sample: Establish timing of garnet to S1 fabric development.

Transmitted Light

Rock is quartz(50%)-biotite(30%)-muscovite(10%)-garnet(10%)-sillimanite schist, after intermediate rock?

Biotite is light brown to dark green pleochroic. Garnets clearly wrapped by pervasive biotite-muscovite defined foliation. Muscovite in granular masses, possibly after feldspars seen in parent rock?

Garnets are messy, irregular, poikilitic and a bit retrogressed to chlorite.

Sillimanite in rare ribbons within biotite bands.

Some coarse epidote, likely retrograde.

Reflected Light

Abundant fine magnetite aligned to foliation.

Negligible sulphide.

Summary and comments

Foliation definitely post-dates this garnet phase, which is altered/retrogressed since formation (i.e. likely early phase).

Sample ID: CAL044

Hole ID: 14CADD001

Depth: 364.75-365.00 m

Reason for sample: Type-example of Dasher hangingwall granite.

Transmitted Light

Biotite (8%) as subhedral primary flakes with rare zircons with dark brown rad damage.

Quartz (25%) is anhedral, has irregular grain boundaries, and is common in groundmass, but also as large poikilitic (biotite microcline) phenocrysts. Some phenocrysts have very irregular intergrowths with plagioclase. Some recrystallisation into aggregates of smaller grains.

Plagioclase (32%) is ~An20, anhedral, only in groundmass, other than intergrowths with large quartz grains.

Microcline (35%) can be weakly perthitic (orthoclase), anhedral to subhedral, common in groundmass, but also several large poikilitic phenocrysts (biotite, quartz and plagioclase inclusions). Some perthitic bands are wavy/kinked.

No signs of alteration, deformation, or peak met phases.

Widespread retrogression of biotite to chlorite-sericite-magnetite/ilmenite. Sericitisation of feldspars throughout, focused on cleavage and twin planes.

Reflected Light

Magnetite lamellae in retrogressed biotite, and also as subhedral disseminated grains interstitial to silicates, commonly adjacent to biotite grains.

Trace chalcopyrite in one interstitial crack extending from biotite.

Summary and comments

K-feldspar and quartz-phyric biotite granite with retrograde chlorite-sericite.

Sample ID: CAL045

Hole ID: 14CADD001

Depth: 426.78-426.88 m

Reason for sample: Typical biotite-magnetite veins affecting hangingwall granite.

Transmitted Light

Parent rock is CAL044 granite. Mineralogy as per parent rock, but fine sillimanite is present.

Vein biotite is same colour/composition as igneous biotite.

Pale garnet or apatite (?) in vein?

Reflected Light

Trace subhedral magnetite focused around the vein, but no sulphide.

Summary and comments

Sillimanite in this rock appears to confirm peak metamorphism post-dates this granite.

Sample ID: CAL046

Hole ID: 14CADD001

Depth: 439.29-437.39

Reason for sample: Precise contact between hangingwall granite and granite-gneiss.

Transmitted Light

Granite is as per CAL044 type example (microcline-rich), with no distinguishing differences. Lots of zircons and apatite (?).

In contrast old granite-gneiss is plagioclase-rich, with 5-10% microcline.

Vein biotite is distinctly more red-brown than dark green-brown igneous biotite present in both ages of granite. Narrow vein in hangingwall granite is the colour of igneous biotite, perhaps therefore schlieren, rather than vein?

Reflected Light

Vein at contact is associated with magnetite-chalcopyrite-pyrite.

No mineralisation in young granite.

Weak chalcopyrite-magnetite in old granite.

Summary and comments

No mineralisation in hangingwall granite. No contact metamorphic effects of young granite, and no strain increase on contact.

Sample ID: CAL047

Hole ID: 14CADD001

Depth: 451.70-451.80 m

Reason for sample: Type-example pre-S1 high-grade molybdenite veining.

Transmitted Light

Three components of thin-section:

(1) Late pegmatite is microcline-quartz and possibly primary muscovite, with fairly straight contact with granite-gneiss.

(2) White vein is trace green-brown biotite in quartz(30%)-microcline(70%) mixture. Some quartz optically continuous to 5 mm, microcline variable to 1 mm, weakly to moderately granoblastic. Trace very fine sillimanite throughout vein. Sericite retrogression pervasive at weak-mod intensity.

(3) Wallrock has green-brown biotite (15%), subhedral, with zircons and rad damage, in quartz(40%)-plagioclase(45%) matrix, with basically no K-feldspar – i.e. vein is definitely different composition. Strong preferred ori of biotite, with limited chlorite retrogression.

Noteably, coarse moly is associated with coarse biotite that has limited zircons or rad damage (alteration origin?).

Reflected Light

In vein, fine sulphide patches throughout, strongly dominated by chalcopyrite, with trace pyrite, no pyrrhotite. Coarse molybdenite at both margins of mineralised vein but little internally. Molybdenite has fine chalcopyrite inclusions, but is also associated with adjacent pyrite and magnetite (minor).

Summary and comments

Vein pre-dates peak metamorphism, because sillimanite overprints it.

Sample ID: CAL048

Hole ID: 14CADD001

Depth: 475.71-475.81 m

Reason for sample: Typical high-strain zone mineralisation.

Transmitted Light

Parent rock is typical microcline-poor granitoid with 20% biotite, 30% quartz and 50% plagioclase.

Veins are moderately granoblastic microcline(40%)-plagioclase(30%)-quartz(30%) with trace biotite. Either K is higher or K now in K-feldspar.

Garnet in wallrock on vein margin, none in veins.

Nothing of note in accessory minerals.

Weak S2 biotite alignment.

Reflected Light

Main vein is chalcopyrite-pyrrhotite-pyrite-magnetite-molybdenite, in usual forms.

Fine, lamellar intergrowths of chalcopyrite-pyrrhotite are widely developed, in places overgrown by clean pyrite.

Summary and comments

Molybdenite definitely in these veins.

K added to create veins? Or biotite just broken down?

Sample ID: CAL050

Hole ID: 14CADD001

Depth: 488.84-488.94 m

Reason for sample: Characterise greenish alteration associated with strong chalcopyrite.

Transmitted Light

Parent is CAL052.

Light to dark green-brown biotite (10%)-garnet(2%) in strongly granoblastic groundmass of plagioclase(58%)-quartz(20%)-Kspar(10%) groundmass. Plagioclase distinctly Ca-rich.

Roundish, high relief apatite (?) is abundant.

A ~2 mm quartz vein persists across the slide, composed of a few very large grains – late style, not recrystallised?

Little retrogression.

Reflected Light

About 50:50 pyrrhotite-chalcopyrite split in sulphides, spatially associated with quartz veins, plus as anhedral disseminations. Lamellar intergrowths of the two are common.

Disseminated subhedral magnetite with some ilmenite exsolution on cleavage planes.

Summary and comments

Not sure why this appears as a “sick” green colour – alteration hard to recognise.

Very calcic rock though – more plagioclase and greater Ca content than typical.

Sample ID: CAL052

Hole ID: 14CADD001

Depth: 514.50-514.75 m

Reason for sample: Type-example of least-altered granite-gneiss parent from this hole.

Transmitted Light

Biotite (5%) is a mix of primary fine-grained dark brown biotite, and masses of distinctly lighter brown euhedral biotite, intimately associated with opaques. Some very coarse zircons associated with primary type, but also in other type.

Quartz (10%) as irregular anhedral grains, hard to pick from untwinned feldspar.

Microcline (25%) with tartan cross-hatching sometimes evident.

Plagioclase (60%?) is ~An27 and anhedral grains of varying size. Larger ones can be poikilitic (biotite). Have included here ~50% untwinned to vaguely twinned feldspar that s granoblastic with abundant 120-triple junctions.

Some largeish apatite grains associated with radiation damage?

Biotite to chlorite-magnetite/ilmenite retrogression is present, but rare.

Reflected Light

Magnetite mostly as anhedral, pitted grains intimately associated with clumps of light brown biotite, with or without sulphides.

Chalcopyrite as some discrete, subhedral grains, some small grains intergrown with magnetite, traces intergrown with pyrrhotite.

Pyrite sub- to euhedral cubic forms, usually together with chalcopyrite, possibly overgrowing magnetite? Distinctly clean and euhedral cf. other opaques.

Summary and comments

Granoblastic plagioclase-K-feldspar-quartz-biotite granitoid. Though may have overestimated plagioclase content.

Sample ID: CAL053

Hole ID: 14CADD001

Depth: 523.35-523.60 m

Reason for sample: Characterise intense white feldspar alteration zone.

Transmitted Light

Biotite (2%) is dark brown-red, some lighter brown in masses. Subhedral normally, nearly euhedral in masses, as seen in CAL052. No clear preferred alignment. Zircons pretty rare.

Microcline (35%) anhedral with textbook granoblastic texture. Seems to overgrow plagioclase in places.

Plagioclase (43%) is vaguely twined to untwinned – close to An20, so more sodic than usual?

Quartz (20%) anhedral, part of granoblastic texture.

Possibly some fine sillimanite. Trace zircon, monazite, apatite also.

Chlorite-sericite retrogression is weak, concentrated next to opaque masses.

Reflected Light

Chalcopyrite and pyrrhotite intergrown and texturally similar: dirty, anhedral, pitted, and interstitial to well-formed silicates, which seem to impose their outlines on sulphide.

No pyrite or magnetite – very unusual.

No silicate alteration immediately evident with sulphides.

Summary and comments

Granoblastic K-feldspar-plagioclase-quartz-biotite rock of likely granitic origin.

Lack of magnetite and biotite is highly distinctive.

Sample ID: CAL054

Hole ID: 14CADD001

Depth: 527.21-527.31 m

Reason for sample: Characterise typical mineralised vein through white feldspar alteration.

Transmitted Light

CAL053 is weaker mineralised parent example.

As for CAL053, essentially a granoblastic K-feldspar(65%)-quartz(30%)-biotite(5%) rock of recrystallised origin. More than 90% of feldspar is microcline, possibly some other types, but minor.

Same albitic reaction rims as observed in CAL053, but less developed.

Moderate chlorite-sericite retrogression throughout.

Mineralised vein is vague corridor of greater quartz content, plus coarse, optically continuous muscovite flakes that are strongly replaced by quartz-microcline.

Trace sillimanite, no garnet.

Reflected Light

Mineralised vein is anhedral chalcopyrite-pyrrhotite (50:50) with clean pyrite overgrowth.

Basically no magnetite in sample – either stripped or sulphidised.

Summary and comments

Coarse muscovite good evidence of early white mica assemblage.

Where is all Fe gone? Low biotite, no magnetite, as for CAL053.

Sample ID: CAL056

Hole ID: 14CADD001

Depth: 540.20-540.30 m

Reason for sample: Study exact lower contact of granite-gneiss with footwall granite.

Transmitted Light

Far uphole end is coarse quartz-microcline (white band in gneiss).

Biotite is brown-green throughout the remainder, including vein area. Some very coarse monazite in central vein areas, with radiation damage of biotite.

Main difference between old granite and young granite is >microcline:plagioclase ration in the latter – this is quite clear.

Weak chlorite-sericite retrogression.

Traces of very fine sillimanite in young granite.

Reflected Light

Vein is chalcopyrite-pyrrhotite with lamellar intergrowths and minor magnetite, minor clean pyrite overgrowth. No mineralisation is young rock, weak disseminated mineralisation in old rock.

Summary and comments

Contact low strain, marked by clearly >microcline in granite dike.

Definite sillimanite in young granite.

Sample ID: CAL057

Hole ID: 14CADD001

Depth: 549.10-549.35 m

Reason for sample: Type-example of footwall granite.

Transmitted Light

Biotite (8%) is subhedral to euhedral, uniform grainsize, with some zircon inclusions, light to dark brown with pretty clear preferred alignment.

Quartz (42%) as abundant anhedral grains in groundmass, traces of undulose extinction and granoblastic texture.

Plagioclase (15%) is ~An20, anhedral in groundmass, with much less twinning and less abundant overall that in CAL044.

Microcline (35%) is anhedral, common in groundmass, more rarely as large poikilitic phenocrysts (biotite, quartz). Very rare perthitic K-feldspar.

Trace zircon associated with biotite, some apatite.

Retrogression of biotite to chlorite-sericite-magnetite/ilmenite is common, as is sericitisation of feldspars (usual forms).

Reflected Light

Trace magnetite as lamellae in retrogressed biotite and coarser subhedral form still spatially associated with biotite. Some tiny pyrite inclusions.

Summary and comments

Weakly microcline-phyric biotite granite.

Same rock as CAL044 though that example is more porphyritic and has >plagioclase and <quartz.

Sample ID: CAL061

Hole ID: 14CADD002

Depth: 137.70-130.80 m

Reason for sample: Characterise multiple phases of brecciation in hangingwall fault.

Transmitted Light

Quartz-microcline-plagioclase-biotite granitoid, with near complete biotite retrogression to chlorite.

All minerals show strong deformation effects: very undulose extinction, bent/cracked grains, fracturing of rock, grains and grain boundaries.

Early brecciation accompanied by chlorite-sericite-epidote-carbonate retrogression especially around central quartz vein.

Retrograde sericite focused around fractures, but in detail is randomly oriented within individual grains.

Reflected Light

Trace chalcopyrite inclusions in quartz grains. A little bit of hematite?

Summary and comments

Likely multiple deformation phases. No association of mineralisation with late breccia zones.

Sample ID: CAL062

Hole ID: 14CADD002

Depth: 149.60-149.85 m

Reason for sample: Type-example of Bindi West host granite-gneiss.

Transmitted Light

Chlorite (10%) as anhedral to subhedral grains aligned to S1 fabric, likely replacing biotite (full of zircons with rad damage)

Amphibole (actinolite?) (7%) randomly oriented (i.e. post-S1) colourless high relief crystals with some elongate grains showing inclined extinction.

Garnet (1%) as round grains partially to wholly replaced by chlorite and/or actinolite. Some actinolite clumps have rounded garnet-like outlines. Garnet not wrapped by S1.

Quartz (35%)-microcline(20%)-plagioclase(27%) form mosaic of irregular anhedral grains, quartz with undulose extinction, feldspars cloudy with extensive sericite-chlorite retrogression.

Some quite calcic (?) plagioclase phenocrysts are large white patches in rock, and have crossing plag twins. They are extensively replaced by actinolite blades, and also heavily retrogressed to sericite.

Trace fine sillimanite, and also carbonate associated with vein.

Weak secondary alignment of chlorite/biotite in S2 ori, antiform east vergence. Actinolite unaligned, must be retrograde.

Reflected Light

Chalcopyrite in fine downhole end is in typical form but lacks pyrrhotite or pyrite. Irregular, anhedral, pitted and interstitial, rarely within silicates., including in actinolite. Mineralisation vaguely aligned in concentrations parallel to S1, but no vein or alteration associated, besides usual retrogressive alteration around blebs.

At uphole end, coarse pegmatoidal vein has near-pure chalcopyrite interstitial to quartz, including some enclosed within a single large grain. Very rare pyrite and magnetite in the same setting. One small molybdenite grain in this vein also.

Summary and comments

Plagioclase-microcline-quartz-chlorite/biotite-sillimanite gneiss after biotite equivalent, with retrograde unaligned chlorite-actinolite.

Sample ID: CAL063

Hole ID: 14CADD002

Depth: 164.80-164.90 m

Reason for sample: Characterise typical Bindi West mineralisation.

Transmitted Light

Quartz-microcline-plagioclase-biotite(chlorite)-garnet gneiss.

Strong retrogression by chlorite-sericite-epidote: biotite to chlorite and coarse muscovite, feldspars to sericite-chlorite-epidote, garnet to chlorite. The only clean garnets are isolated inside larger silicate grains.

Strong deformation effects evident in some quartz grains, undulose extinction, some kinked mics also.

Some K-feldpsar is hazy microcline/orthoclase mix?

Some amphibole was possibly present, now retrogressed to chlorite masses.

Reflected Light

No pyrrhotite. Chalcopyrite-pyrite veins associated with retrograde assemblage but chalcopyrite also observed in large garnet grain, suggesting low-temp mineralisation is remobilisation of earlier high-temp assemblage.

Summary and comments

Likely remob of earlier mineralisation, strongly retrogressed.

Garnets overgrow foliation, then all retrogressed.

Sample ID: CAL064

Hole ID: 14CADD002

Depth: 168.60-168.70 m

Reason for sample: Study relationship of garnet and sillimanite to main foliation.

Transmitted Light

Moderately granoblastic quartz-microcline-plagioclase-biotite-garnet-sillimanite gneiss.

Intense sericite-chlorite-epidote retrogression of biotite-garnet-sillimanite assemblage, intense pervasive sericitisation of feldspars.

Sillimanite in foliation bands near-totally retrogressed to fine sericite mess, but fine sillimanite internal to silicates (quartz-feldspar) is well preserved as small needles, in random oris.

Retrograde sericite is in random oris unless pseudomorphing biotite/chlorite.

Main foliation clearly kinked/folded, by S2.

Some clean garnet, some retrogressed.

Reflected Light

Trace chalcopyrite in clean silicates, with or without clean pyrite.

No pyrrhotite.

Summary and comments

Sillimanite either pseudomorphs S1-aligned micas, or is occasionally in S2-aligned masses. My feeling is it actually post-dates both fabrics.

Sample ID: CAL065

Hole ID: DWN4

Depth: 183.07-183.15 m

Reason for sample: Typical higher-grade mineralised vein and garnet-biotite selvedge.

Transmitted Light

Proximal vein/selvedge is grunerite (and other amphibole?), with some retrogression to chlorite (30%).

Sharp change moving away into quartz-plagioclase-biotite-garnet domain. Quartz as polygonal interlocking matrix to coarse light brown to dark green-brown biotite and pink garnet.

Garnet shows clear evidence of multiple growth and retrogression events: newest outer garnet overgrows chlorite pseudomorph of earlier garnet, but that original garnet still present in the core.

All garnets overgrow/include biotite, and become finer and cleaner away from the vein. Uphole end is same assemblage as near vein, but just much finer.

Biotite foliation deflects around garnets.

Late veinlet of stilpnomelane.

Reflected Light

Vast bulk is grunerite zone. Euhedral magnetite is dominant, finely disseminated. Sulphide is pyrite and just a little bit of chalcopyrite, mostly fine disseminations, with larger grains aligned to foliation.

Summary and comments

Vein is alteration-derived grunerite.

Potassic altn (biotite) pre-garnet – includes biotites. But foliation at vein margin is also deflected around garnets.

Sample ID: CAL066

Hole ID: DWN4

Depth: 196.73-196.80 m

Reason for sample: Characterise mineralogy of typical high-strain zone, with garnet-sillimanite alteration.

Transmitted Light

Rock structure is very coarse microcline crystals (greater than thin section width, likely metamorphic origin) full of fine biotite and quartz that preserved S1 foliation. This is full of fine sillimanite in a variety of orientations. Between microcline grains are bands of quartz-biotite-chlorite-sillimanite-andalusite and streaks/clumps of fibrolitic sillimanite, mostly after biotite, but also after diamond shaped staurolite in places.

Reflected Light

Trace disseminated ilmenite, associated with biotite-sillimanite bands.

Summary and comments

Microcline-quartz-biotite-sillimanite-andalusite-staurolite schist. Very coarse microcline is certainly of metamorphic origin, probably from quartz+muscovite origin, to produce sillimanite also.

Probably a ~sericite-chlorite shear zone, metamorphosed.

Sample ID: CAL067

Hole ID: DWN4

Depth: 220.90-221.0 m

Reason for sample: Characterise mineralogy of late (post-S1) sulphide-rich veinlets.

Transmitted Light

Quartz-plagioclase-biotite-grunerite schist. Grunerite is light brown, moderate to high relief, variable extinction and int colours dur to different grain orientations.

Reflected Light

Very fine magnetite throughout. Pyrrhotite-chalcopyrite in places, most strongly developed around a clearly retrogressive chlorite stringer – total chloritisation around narrow selvedge.

Summary and comments

Grunerite of alteration-metamorphic origin. Vein is late/retrograde.

Appendix 13 – Drill core graphic log sheets

A3 graphic log sheets for 12CADD001, 12CADD002, 14CADD001, 14CADD002, 08WHDDH001 and DWN 4. Structural readings are in alpha/beta/gamma format. Structural features are drawn as though looking north at an east-west cross-section, with the hole aligned at its drilled dip – i.e. for 12CADD001 (drilled to 090), bottom of hole is the left hand side.

Calingiri Project

Graphic Log

HOLE ID: 12CADD001 (537.10m)	**COORDINATES:** 463720 E 6566899 N	**ORIENTATION:** -55 → 090	**PAGE:** 1 of 7
PROSPECT: Dasher	**LOGGED BY:** Outhwaite	**DATE:** 10/2/2015	1 tick = 2 metres

DEPTH | LITHOLOGY | STRUCTURE | ALTERATION 1 % | ALTERATION 2 % | MINERALISATION | CA int

LITHOLOGY NOTES

1.0 – 17.40 ksp-phyric bi monzogranite, weathered & moderately @ top, joint oxidation @ lower contact. Phenos quite rare. Pegmatites common, ~15% of rock.

17.40 – 48.6 chilled MD, variable margins, chloritised por fl megacrysts ~25-44m.

48.60 – 82.15 bi monzogranite, ksp-phyric, strain strongly increases to sharp low ε domain @ 70.60m – very nice transition in ε intensity.

(52.8m – 53.0m pMD dyke.
56.55 – 56.75 "

Ph 3390 @ 70.60m high ε to low ε gt transition marked by strong ch-mt zone. No reason to think these are different rocks?

STRUCTURE NOTES

14.95m S_1 – 10/327

17.40 – CON – 42/350

48.60 CON 12/041

50.90 S_1 high ε 60/346

54.80 S_2 – 68/333
F_2 – 70 → 087 (Y/d) (~10° NNW plunge)
Ph 3412 → 3415 Folded S_1, PEG + sill?

61.70 S_1 70/350

68.80 S_2 55/347
F_2 86 → 276 (~10° S plunge?)
Ph 3416, 3417 Great F_2 folds, weak bi alignment to S_1? (TS ok)

70.6 CON(?) 42/325
high ε to low ε sharp change.

73.90 – S_1 18/338 typical in low ε zone

74.80 – S_2 60/353
Ph 3418, 3419 Folding of min. chlorite fractures (F_2)

ALTERATION/MINERALISATION NOTES

Chl predom frac-controlled around min veins...

py-cpy-ch veins, mostly // to S_1

76.8
Str grt-sill + fracture-controlled ch. Ph 3411 @ 74.9m of ch-act(?)-cp fractures.

OTHER

Calingiri Project
Graphic Log

HOLE ID: 12CADD001	COORDINATES:	ORIENTATION:	PAGE: 2 of 7
PROSPECT:	LOGGED BY:	DATE:	

DEPTH | LITHOLOGY | STRUCTURE | ALTERATION 1 | ALTERATION 2 | MINERALISATION | CA int

LITHOLOGY NOTES

82.15 – 85.00 strongly chilled pMB

85.00 – 115.10 typical ksp-phyric bi monzoGT, w poikilitic ksp megacrysts preserved in v low ε zone domains

96.5 – Ph (3391, 3392) poikilitic, zoned ksp megacrysts @ 96.80m

115.10 – 116.30 highly chloritic & biotitic MA.
Ph (3393) of upper CON @ 115.10 – note faint ksp pxts right up to MA margin.
Orientations suggest MA partly flat-lying.

116.30 – 121.70 bi monzoGT, wobbly, abundant PEGs (~25%). Ph (3394) @ 121.70 at contact zone.

121.70 – 133.50 MA, variably chloritised, biotised, and intruded by abundant PEGs – ~25% of interval. PEGs are irregular, and likely folded, along w MA.
Both CONs suggest moderate dip to WEST.

133.50 – 138.55 distinctive bi-rich ksp-phyric monzogranite. Ph (3395) @ 138.55 shows this unit in sharp contact w monzoGT & <biotite (younger from contact relationship, but also mineralised, and also suffers S_1 fold
Ph (3396) @ 135.50m of typical "old" bi monzoGT

138.55 – 164.75 "younger" unit well mineralised, true granite (?) w ~50% qz, ~5% bi, remainder feldspars.
(146.55 – 147.25 = narrow, later bi monzoGT)

Ph (3397) @ 151.50m of typical qz-rich, bi-poor "young" granite.

STRUCTURE NOTES

α/β taken w HQ3 post for this sheet ✗

85.00 CON 40/076 79

86.30 Vch ± cpy pyp 30/308 310
Ph (3420) Church stockwork-type fractures/veinlets.

97.40 F_2 85 → 040 (~10° → NW) LH 39

93.20 S_1 – 22/004 4
Vcppych mt – 50/298 300 SL

98.60 S_1 – 55/190 (short limb nav) 196

100.80 F_2 – 83 → 070 (~10 → NNW) 67
Ph (3421) short-limb vergence...

107.20 S_1 – 75/260 264

121.70 CON – 63/015 16
(see Photo)

130.90 – S_1 40/344 345
S_1 folded thru MA... ~ hinge area from here onwards...
Bi-rich, but low S_1 ε...

133.50 CON – 67/332 333
✗ clear contact.

134.50 S_2 – 60/332 333
· Ph (3422) Nice folding ~ hinge zone.
Weak but consistent S_1 fabric thru this unit.

138.55 CON – 70/143 137

141.80 Vcpchpo (stock) – 60/206 210
most common ori in low ε domain

146.10 S_1 + Vcppach – 68/008 (stockwork)
Vcppach – 55/195 202 SL
Ph (3423) VNs follow & cut wk S_1

146.55 CON – 28/297 299
Internal contact w younger, massive GT Ph (3424).

149.40 S_1 – 60/138
Vcppach – 40/162 (stock)

157.80 S_1 – 8/350
Vcppach – 31/121

ALTERATION/MINERALISATION NOTES

Cnt focused in patchy higher ε zones.

Strongly frac-controlled ch-act (?) stockworks

93.7

96.2

102.6

Last ksp? Just weathering effect??

Both in MA units – not sure percentages...

Distinct v low cnt domain, restricted to traces in some min selvedges. ✗
Frac-controlled, v. localised ch alt'n.

OTHER

Calingiri Project
Graphic Log

HOLE ID: 12CADD001	COORDINATES:	ORIENTATION:	PAGE: 3 of 7
PROSPECT:	LOGGED BY:	DATE:	

DEPTH | LITHOLOGY | STRUCTURE | ALTERATION 1 | ALTERATION 2 | MINERALISATION | Chl int

LITHOLOGY NOTES

164.75 – 174.45 "Old", bi-rich, high ε granitoid, w abundant pegmatites, incl mineralised ones, cut by young ones. Hole drilled ~straight down S_1, strat pass repeats across it?

Ph 3398 @ 164.75m – upper cont of "old" bi-rich GT

Ph 3399/3400 @ 167.20m – 3 rock phases: ① old bi GT, ② qz-rich, bi-poor GT w// to S_1 in ①, but also w weak fabric, and ③ garnet-bearing PEG – ie. pre metamorphic...

Ph 3401 @ 168.50m * STAR PIC * cut bearing (old) PEG both cuts & follows S_1 fabric, and contains mineralisation

Ph 3402 @ 169.20m "young" PEG cuts S_1 + "mineralised" old PEGs.

Ph 3403 @ 172.00m (as above) – subhor 'contact' young PEG.

174.45 – 179.50 "young" fairly qz-rich GT, as above old bit

179.50 – 180.70 "Old" bi-rich GT (?) w thin, mineralised PEGs // to S_1.

180.70 – 193.20 as for 174.95 – 179.50

193.20 – 195.85 – more "old" bi-rich stuff

195.85 – 262.90m cgsl ksp-plag-qz (mk) bi monzo GT, 10-15% bi – prob not the distinctive qz-rich one now? Various ε & alt changes.

} low ε domain 200-201 – poss younger GT?

212.3 – 212.8 poss "old" bi-rich domain.

STRUCTURE NOTES

165.60 S_1 – 24/117
strong gneissic fabric.

169.20 S_1/swPEG – 24/115
late PEG – 45/145
Ph(3402) – see lith notes...

172.80 S_1 – 35/132
F_1 – 71 → 196 (~10° → E)
Ph(3425) Likely F_1 of barren rex. qz vn.

174.45 CON – 30/296

180.30 S_1 – 33/150
Highly variable fol'n – min ori thru here, but dominantly long limb...

184.50 S_1 – 46/139
Local start limb...

V. irreg foln ori all thru here.

195.15 S_1/swPEG – 14/308
Ph(3427) Excellent mineralised PEGs, incl some moly. Sulphides are cp-py-mo +po?

195.85-236.20 Patchy ε, in & out of mod "3" zones, drilled down foln...

201.20 S_1 – 46/276 – localised high ε domain.

210.20 S_1 – 4/352.

~70cm
217.05 V ch gnt mt cp(py)po 34/308
Ph(3428) Brilliant vein w mt rims & cpppy-po-ch-act(?) core. Mt-py-po intergrown on rims. One of the few measurable veins of the kind.

222.30 – S_1 40/321

20cm
223.10 V ch gnt mt cp py po 28/346
(another vein as above)

228.40 – S_1 18/320

236.90 V py cp bi – 36/002
~// to S_1, 1cm.

ALTERATION/MINERALISATION NOTES

Trace chl, v. localised on min fractures – poss not even chl...

Gnt in qz-rich GT clearly assoc w min selvedges.

Ph(3426) @ 183.40 – cgsz, "min-stage" bi (potassic alt'n), w cpy-po masses. V. irregular patches, no pref ori thru here.

Variable S_1 & min oris

Several narrow chl-mt-gnt-cp zones (hg).

Variable, messy veining, folded w S_1, irregular

OTHER

Calingiri Project
Graphic Log

HOLE ID: 12CADD001	COORDINATES:	ORIENTATION:	PAGE: 4 of 7
PROSPECT:	LOGGED BY:	DATE:	

Columns: DEPTH | LITHOLOGY | STRUCTURE (Ducti) | ALTERATION 1 (Bi%) | ALTERATION 2 (Gnt%) | MINERALISATION (Sill%) | Chl int | LITHOLOGY NOTES | STRUCTURE NOTES | ALTERATION/MINERALISATION NOTES | OTHER

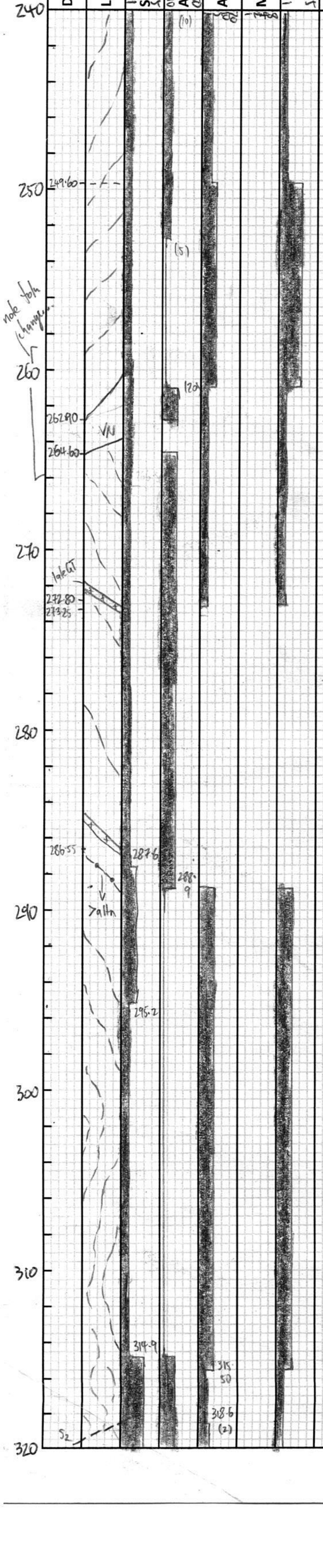

LITHOLOGY NOTES

From 249.60m strong altn makes lith ID difficult, but no clear change

262.90 – 264.60 (Dominantly) Qz-cpy-po vein / PEGMATITE, quite irregular? Contains GT sections.

264.60–272.80 Bi monzoGT ~20% bi (quite high)

272.80–273.25 Narrow, late, rel. qz rich (50) & bi-poor monzoGT, seems post-S1.
Ph (3404) @ 273.25 – lower CON, cuts S1

273.25 – 328.95 bi monzoGT, poss qz-rich variant from ~289m but maybe just > altn... In pristine uppr bits ~15% bi, 30% qz.

(286.55 - 286.85) Narrow, late, bi-poor (5), qz-rich (40) GT, subhoriz
Photo (3405) @ 286.55 ...

STRUCTURE NOTES

241.30 S1 – 25/349

243.00 Vcppy – 28/329
~ // to S1

250.80 – S1 – 31/315
sillimanite-defined

258.90 - S1 43/302
Sill-defined, // vns & fracs.

262.90 Vqz-cpy-po/PEG – 14/324

268.00 - S1 25/132

273.25 CON - 48/167

275.30 S1 – 12/151

286.55 CON 45/175

288.90 "VN" chl-mt gnt cpy py 38/122
change (sharp) to >>altn, marked by typical ch-mt zone.. -

294.80 S1 24/147
min veins ~//, fairly regular foln since 288.90...

298.50 S1 35/190

305.90 S1 ~ – 17/002
Vbicp – 46/081
Ph. (3429) vn w cg bi flakes, cuts overprints S1 & strong early foln...

307.70 Vcppomt "mantle" – 22/337
drilled straight down vein here...

@ 314.9 v. clear E increase, same lith.

315.0 S1 – 26/147.

319.70 S2 – 70/021

Since ~ 295m v. clearly drilled straight down S1 & open F2 fold variations – but all roughly long limb...

ALTERATION/MINERALISATION NOTES

241.0

Strong altn, chl-gnt-sill. Still primary bi tho.

* Strong altn zone coincides w S1 ori change *

259.0

Pristine primary bi t'out

Strong early bleaching/stripping (?) w garnet overprint...
Primary bi remains, some localised chl – oprinted by gnt?

293.20

312.00

Calingiri Project
Graphic Log

HOLE ID: 12 CADD001	COORDINATES:	ORIENTATION:	PAGE: 5 of 7
PROSPECT:	LOGGED BY:	DATE:	

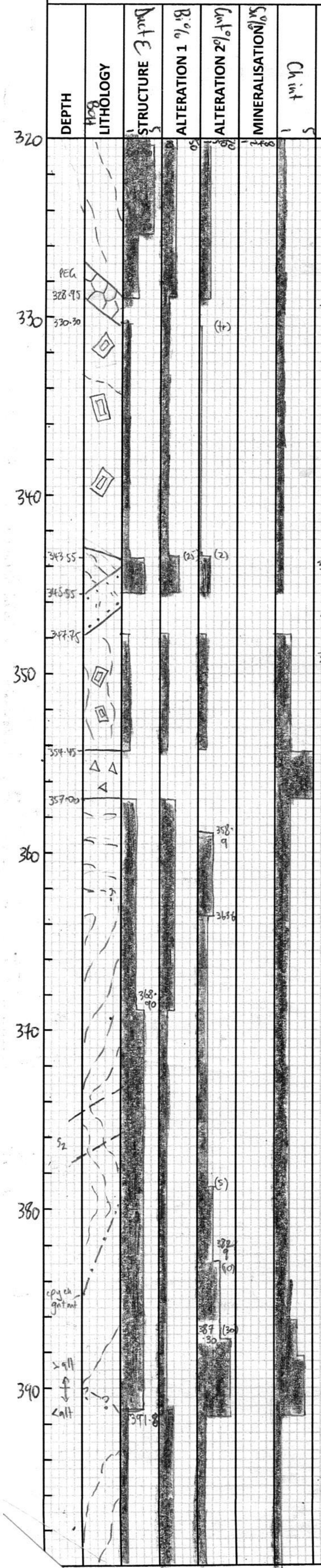

LITHOLOGY NOTES

328.95 – 330.30m Largish, well defined PEG, marks start of distinctive unit below.

330.30 – 343.55m V distinct kspar-megacrystic bi monzoGT – otherwise ~ similar composition to "normal"
Ph (3406) @ 330.8m – megacrystic monzoGT

Late-ish intrusive? Seems to cut/deform S1, but def. mineralised also

343.55 – 345.45 High E, more bi-rich monzoGT, older than above unit?
345.45 – 347.75 pMD

347.75 – 354.45 bi monzo GT, traces of ksp megacrysts to 20mm – prob that unit same as 330.30 – 343.55m

354.45 – 357.00 Chloritic flt breccia – ~ E-W, steep North dip.

357.00 – 519.05 Bi monzogranite, hints of mod ksp-pxsts. ~~Quite~~ Mod E increases to high E, high altn variant @ to 391.80m, where change is to low E variant @ ~15% bi, 30% qz – poss different rocks, but no definitive change...
Beyond that area, many changes in E intensity + altn + S1 ori, but all same rock.

STRUCTURE NOTES

324.10 – S1 – 15/130
Very variable S1 throughout to 400 mainly long limb ↓

328.95 · CON 36/253

334.30 S1 62/267
minor short limb

Fairly massive unit thru here...

343.55 CON – 72/133
megacrystic stuff con w "older" stuff. seems to cut/deform "old" S1 fabric?

345.55 CON 58/017 pMD (t)
347.75 CON 51/336 pMD (b).
348.70 Vcpy ch po bi 42/016
assoc w cg bi, hg vein, start of hg section.
354.45 BX (t) 32/065
Ph (3432) @ 355.20m ↗ str chl breccia w hg cpy + broken GT fragments
357.00 BX (b) 28/066
358.90 S1 – 72/220
LL ↑ small SL ↓ LL

368.90 – 391.20 – micas really "clustering" into gneissic foln...
370.20 S1 – ~~2~~ 21/313
Strong gneissic fabric – note low E qz-fl domains. Ph (3434 3435)

377.80 S1 – 7/161
S2 – 55/353
Ph (3436) weaker S2 cren

384.60 – Vchcpmtgnt – 18/342 (20cm)

389.40 S1 – 30/302

391.8 Con/Vchgnt (~~on~~ margin of strong altn zone) – 42/185
~~not~~ A bit hazy ↗

398.70 S1 8/343

ALTERATION/MINERALISATION NOTES

Chl. very localised @ selvedges.

Gnt focused on str ch-mt-cpy patches...
Ph (3430 3431) @ 351.40m – hg cp-ch veins w rex/mantle texture.

Extreme chl altn in breccia

Ph (3433) @ 365.50 – hg cpy+ch min, typical of this interval, overprints gneissic fabric.

Lower bi thn higher E zone – chloritised/sericitised?

388.30 – 391.20
Ch in selvedges only.

OTHER

Calingiri Project
Graphic Log

HOLE ID: 12 CADD001	COORDINATES:	ORIENTATION:	PAGE: 6 of 7
PROSPECT:	LOGGED BY:	DATE:	

DEPTH	LITHOLOGY	STRUCTURE	ALTERATION 1	ALTERATION 2	MINERALISATION	Ch int	LITHOLOGY NOTES	STRUCTURE NOTES	ALTERATION/MINERALISATION NOTES	OTHER

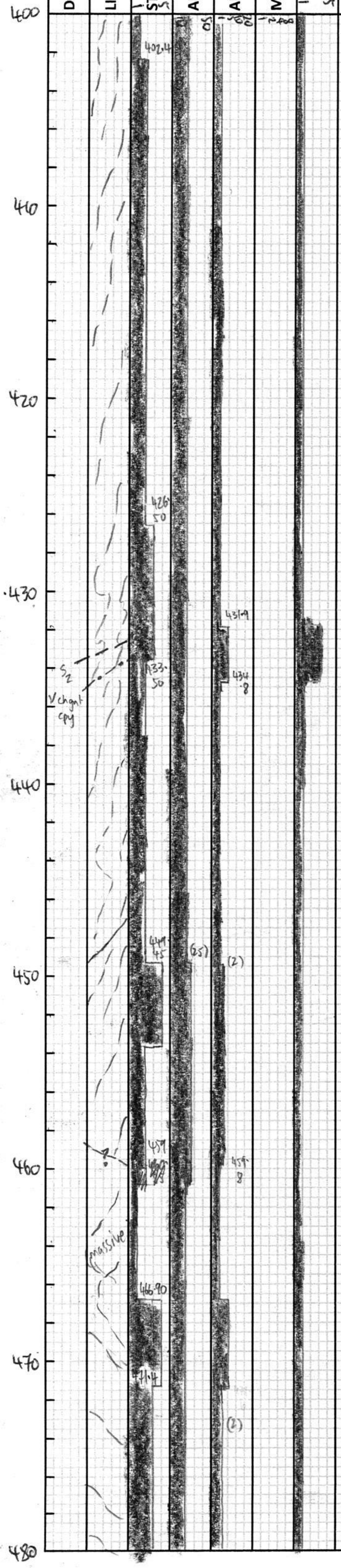

Structure notes

LL ↓

Consistent mod foln, some higher & lower ε bits...

404.9 S1 7/336
min veins dominantly //

417.50 S1 13/322

433.40 S2 – 67/356

434.80 Vchgnt cp mt 10cm – 45/305

449.45 CON(?) 35/342
Start of high ε zone – poss MA??

451.60 S1 18 /322
in high ε bit. Poss some early veins folded by S1?

459.80 CON/VN(?) 42 /126
edge of high ε + altn zone

460-468m – v. clear fold hinge zone, from steep E-dipping limb to sub-horiz "short limb".

LL ↕ SL

Discrete high ε, altn zone – sericite?

470.30 S1 58 /186
sub-horiz. short limb.

468.20
469.30

Alteration/mineralisation notes

Patch str ch-mt-cp-gnt. zones.

Ch selvedges only.

Slightly more bi in high ε zone?

Calingiri Project
Graphic Log

HOLE ID: 12CADD001	COORDINATES:	ORIENTATION:	PAGE: 7 of 7
PROSPECT:	LOGGED BY:	DATE:	

DEPTH | LITHOLOGY | STRUCTURE | ALTERATION 1 % | ALTERATION 2 % | MINERALISATION % | Cu int | LITHOLOGY NOTES | STRUCTURE NOTES | ALTERATION/MINERALISATION NOTES | OTHER

480
490
500
510
520
530
540

STRUCTURE NOTES

481.40 – S_1 52/160

S_1 ori change corresponds to ch-gnt zone.

488.20 S_1 14/172 — minor LL

492.70 S_1 16/343

495.20 VN ch gnt mt cp 28/329
start of altn zone, sharp.

498.60 S_1 41/331
internal to altn zone.

503.20 S_1 56/182

508.50 S_1 + Vcppy (10cm) 40/165

518.70 S_1 48/191

519.05 VN/PEG cpy py po mt – 37/180

528.85 CON 37/167

534.80 CON 55/175

537.00 S_1 19/315

ALTERATION/MINERALISATION NOTES

Small ch-gnt cp section.

Strong altn in hinge zone

* No garnet in MA – not regional, pervasive metamorphism, localised in altn zones.

LITHOLOGY NOTES

519.05 – 521.60 "messy" cp-po-py-gnt-PEG vein, high-grade sulphide, def pyrrhotite.
PH (3407 – 3410) @ 520.50m * STAR PIC *
3 sulphides together, w gnt in "PEG/mantle-type" vein. Sulphides clearly are interstitial to silicates, incl. garnet (2) – These vhg "mantle/PEG" features are prob partial melt/remob features...

521.60 – 528.85 – bi monzo GT, nothing distinctive, as w long prev. interval to 519.05m

528.85 – 534.80 ch-bi altd MA w largish magnetite clots to 5mm, w pale halos. Some small internal pegmatites.
Lower CON ~ subhoriz, or shallow W dip.

534.80 – 537.10 bi monzo GT as above, some PEGs, as usual...

Calingiri Project

Graphic Log

HOLE ID: 12CADD002 (159.80m)	COORDINATES: 463812 E 6566797 N	ORIENTATION: -64 → 270	PAGE: 1 of 4
PROSPECT: Dasher	LOGGED BY: Outhwaite	DATE: 4/2/2015	1 tick = 1 metre

• ~~peg%~~
• sillimanite
• chlorite
• magnetite.

Column headings: DEPTH | LITHOLOGY / mc, peg. struct. | STRUCTURE ductE (1 2 3 4) | ALTERATION 1 %Bi (~~1 5 10 20~~ 10 20 30 40 50) | ALTERATION 2 %Gnt (1 5 10 20 50) | MINERALISATION Sulf% (colour by species??) (1 2 4 8) | ~~...~~ ch (~~1 2 3 4 5~~ 1 2 3 4) | LITHOLOGY NOTES | STRUCTURE NOTES | ALTERATION/MINERALISATION NOTES (ksp ... ch sill) | OTHER (gneiss?, mt, ...)

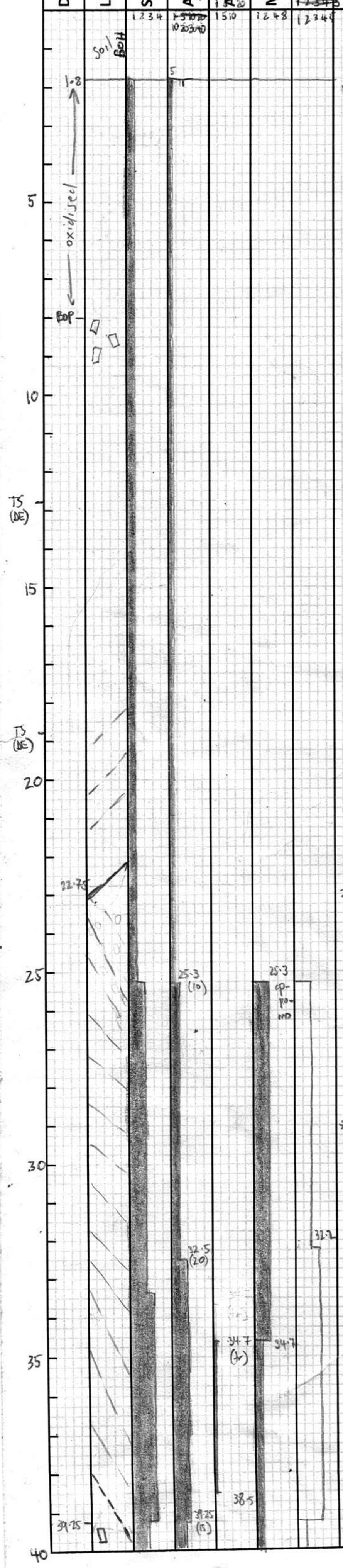

Lithology notes

1.8 – Biotite monzogranite, ~5% 1-2mm bi, 30% qz, remainder feldspar. Poikilitic kspar to 8mm common, one megacrystic section

8.0-9.0 poikilitic kspar phenocrysts to 30mm, appear recrystallised into aggregates. Photo (3315) @ 8.90m

sharpish change → (see Photo 3328)

22.75 start of more abundant cg. leucosomes. Photo (3316) contact mg→cg monzogranite.

22.75 – 39.25 ~5% total irregular leucosomes in more bi-rich host (?). No clear compositional difference from previous interval, no clear contact.

27.10m Ph (3330) swPEG cuts (but drags) S1, also cuts & remobs min veins.

~~29.9~~

39.25 → PTO see next page...

Structure notes

20.1m S1 40/200 wk bi foln, shallow WNW dip.

22.75m CON 20/~~80~~090 Photo (3328) mg-cg con – rext. or primary gsz change?

24.5 BAN 20/345 REX banding in GT, subvert.

26.5 Vcppymo 30/344 1cm diffuse, ~// to S1 Ph (3329)

29.95 S1 + Vcpmo 55/338 diss sulphide bands roughly follow S1

34.80 Vksp mo cp 1cm diffuse ~~45/016~~ 45/016 Ph (3332)

35.30 S1 bi 33/334 subvert, hint of mod (~45) N-plunging lin, based on bi elongation.

36.30 S1 bi 35/348
Vcppych 60/335
Ph (3333) diffuse Sn band (3334) cuts S1 causing local ch altn, plus crystallising coarse bi that is not in S1 ori (2nd photo).

38.90 S1/swPEG 25/336 Ph (3337) contains min, // to vein.

Alteration/mineralisation notes

25.7

32.2

25.3 clear bi increase – lithological?

~~...~~

30.90 Ph (3331) cgsz bi-py±cpy overprints (?) hg cp-py-mt – neither has pref ori, both cut ~~...~~ swPEG

34.70-38.50 scattered gnt, poss assoc w/ ksp altn selvedges?

36.50 Ph (3335) (3336) py-~~...~~-cp-ch-bi vein cuts peg margin (gnt-bearing peg). Cg bi is random oriented, not aligned to S1

Calingiri Project
Graphic Log

HOLE ID: 12CADD002	COORDINATES:	ORIENTATION:	PAGE: 2 of 4
PROSPECT:	LOGGED BY:	DATE:	

DEPTH | LITHOLOGY / struct | STRUCTURE dust ε | ALTERATION 1 Bi% | ALTERATION 2 Cpy% | MINERALISATION Py% | Ch | LITHOLOGY NOTES | STRUCTURE NOTES | ALTERATION/MINERALISATION NOTES (Ksp, ch, sill) | OTHER (Mb)

40 | 45 | 50 | 55 | 60 | 65 | 70 | 75 | 80

PEG

late min

41.1

48.2 (30) (2)

50.1 (15)

51.8

S2 S1 S2

S2/Vn

61.0 (5)

61.2

65.4 (2)

67.2

68.0 (10) (1)

77.5

78.5 (5)

LITHOLOGY NOTES

39.25 – 51.80 clearly a kspar-phyric rock thru here, probably beyond into higher ε domain also

43.2 Ph 3338 Remnant Ksp phenocrysts in bimanzoGT these are poikilitic (primary), but also appear recrystallised, ie diffuse margins and numerous internal grain boundaries visible.

45.10 – strong fol, mineralised xenolith (?) in this rock – could ksp-phyric rock be bracketed min??

50.1 CON 45/308 back from high ε, bi-rich, min-rich zone into ksp-phyric bimanzoGT. Cg bi re-xtal affects both rocks, min. far stronger in bi-rich zone, but remob(?) locally into manzoGT ✱Ph 3352

still def ksp-px manzoGT to 52.3, prob beyond.

77.60 S_1 33/350
Ph 3364 S_1 foln, note high angle sill. (S_2 ori), note cp-mt-ch patches, ie pref gnt growth.

STRUCTURE NOTES

49.30 PEG – 67/080
S_1 – 52/324
Ph 3339 late PEG clearly cuts S_1 foln, which contains diffuse ∥ cp-py bands.

50.75 S_1 // Vcp-py-mo-mt S0/331
Parallel veinlets of hg cp-py-mt-mo aligned to S_1. Magnetite clearly vein-related, mt in host rock. Note bi-destructive nature of altn!
Ph 3340 ✱STAR PHOTO✱

45.10 Ph 3341 3342 Ksp-phyric, cg "background" rock appears to intrude earlier, highly mineralised, bi-rich unit – but ksp-phyric rock also ~~for~~ mineralised.
CON 30/315
Xenolith (?) pass contains earlier fols.

48.2 CON 55/335
Ph 3344 3345 CON zone between low ε Ksp manzoGT & high ε high min zone – fairly sharp!

49.2m S_1 68/244 Ph 3350
Vbipycpmt 60/348
Ph 3346 – 3350 Various min veins cut S_1 foln, mostly acute, some high angle. Hg-mo vein is weakly pegmatitic, roughly // to S_1. Cg bi in V selvedges ie random, & assoc w magnetite.

51.5 S_1 58/326 S_2 20/334
Ph 3353 weak bi alignment in steep S_2

52.30 Vcp-py 60/353
Ph 3356 hg vein formed e strain gradient within ksp-phyric manzoGT – note vein "breaches" into low ε rocks.

59.40 S_1 40/335

61.40 S_1 – 30/317
Vcppy (S_2?) – 10/336
Ph 3357 Remob(?) vein // to weak S_2 alignment (ch-bi-sill), cuts S_1. Sulphide "mantles" silicate grains, not true veins.

63.90 S_1 50/263

66.60 Vmo 33/284
Ph 3360 hg, cg Mo distributed // to S_1, but equigranular. Note spatial separation from hg Cu.

67.50 Veppo // 70/005
Ph 3361 "mantling" type su vein, def. pyrrhotite...

71.35 Vcpmo/peg 37/282
1cm almost pegmatitic vn // to S_1, ie cg Sz Mo.

72.20m S_1 – 41/272
Vcpmtch – 80/318
Ph 3362 hg vein cuts S_1. Vn. def assoc w ch altn of biotite (existing)

74.2 S_1 30/300

75.2 CON/S_1 55/308

Ph 3363 GT-MA(?) contact. Note hg cp-mo vn in GT, "mantle"-type hg cp in MA, plus thin cp-ch stringer that cuts CON!

ALTERATION/MINERALISATION NOTES

Vcpqmoch 18/313
43.40 Ph 3343 Microfracture w Ech-cp-py-mo (min) cuts ksp-phyric rock – pos a later stage min than mt-cp-py-bi-ksp type?

57.5

Stronger mt tends to be assoc w stronger chl ± su...

Ph 3358 @ 62.90m – hg cp-py-bi-mt-ch(?) mass cuts S_1, is unaligned (micas), post-dates S_1 for sure.

Calingiri Project
Graphic Log

HOLE ID: 12CADD002	COORDINATES:	ORIENTATION:	PAGE: 3 of 4
PROSPECT:	LOGGED BY:	DATE:	

DEPTH | LITHOLOGY/struc | STRUCTURE dveste | ALTERATION 1 Bi % | ALTERATION 2 Gnt % | MINERALISATION Sulf % | CH | LITHOLOGY NOTES | STRUCTURE NOTES | ALTERATION/MINERALISATION NOTES (kp, ch, sill) | OTHER (NO)

80 — S_2

81.10 S_1 – 60/236
L_1 < ~~δ~~ – 63 δ – 290
~N plunge, @ ~15°

Ph 3365 – Strong S_1 zone, clear sill + ch(?) have pref linear ori; ~ gentle N-plunge. Photo shows "long" sections @ ~core Bot, & "end" sections near side. Quite clear pref. ori.

Ph 3366/3367 Note flows E qz-fl domains, between ch-sill + bands (white).

82.9 S_1 – 41/251
S_2 – 15/266
Ph 3368 Sill defines low α S_2.

84.50 CON 65/306
GT – MD

85

84.5 — 116.55 Thick prot(?) MD with strongly chilled margins, progressively coarsening to centre. Scattered plag phenocrysts ↑ out (<1%) to ~25mm size, all partly chloritised from "inside out". ~5% bi & trace py ↑ out – bi prob a regional metamorphic product? Phenocrysts tend to be larger in centre, but persist to chilled margins, indicating early (pre-)initial formation.

NB Bi + MT seem to occupy centre, but not chilled margins – both poss primary, and products of subtle differentiation?

90

95

Photo 3319 @ 96.1m – prot dolerite w zoned plag phenocrysts (poikilitic?) w cores replaced by chlorite (?)

100

105

110

Photo 3320 @ 91.30m – ep vein w ch selv. cuts prot MD – ie. ep. v. late!

115

Photo 3322 @ 116.55m – late fe-cb(?) vein cuts earlier strong ch "chunks" @ dyke margin – paragenesis = ch fault → dyke → fe-cb vein.

116.55 CON 30/345

119.80 S_1 – 36/307
Vegmach – 22/310
Ph 3369 Hy vein cuts S_1, ~// to sill-defined S_2

120

Calingiri Project

Graphic Log

HOLE ID: 12 CADD002	COORDINATES:	ORIENTATION:	PAGE: 4 of 4
PROSPECT:	LOGGED BY:	DATE:	

Columns: DEPTH | LITHOLOGY/struct | STRUCTURE ductile | ALTERATION 1 Bi% | ALTERATION 2 Cht% | MINERALISATION Su% | CH | LITHOLOGY NOTES | STRUCTURE NOTES | ALTERATION/MINERALISATION NOTES (ksp, ch, sill) | OTHER (mo)

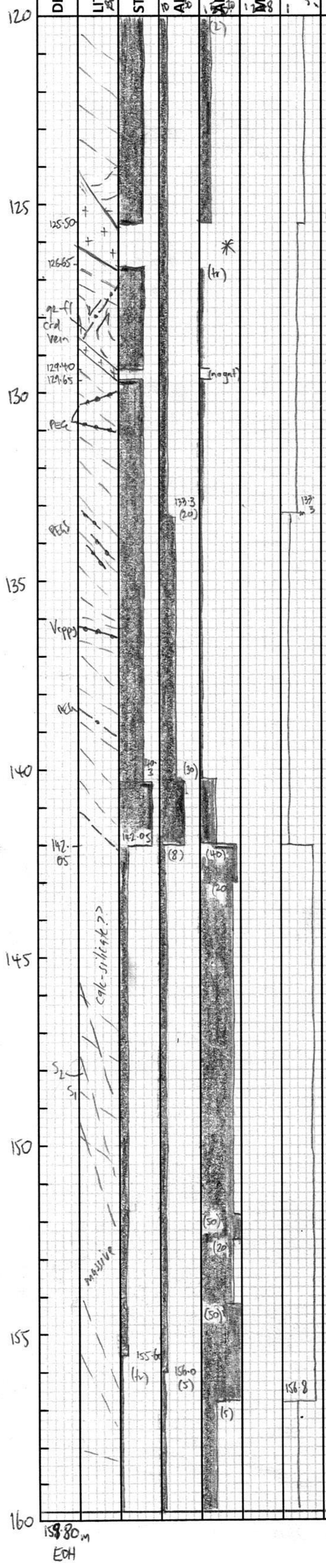

LITHOLOGY NOTES

125.50 – 126.65 Equigranular bi monzoGT (~40% qz 10% bi), clearly cuts strong S1 foln @ upper contact – Photo 3323 @ 125.50m. Appears post-S1 & post-min, but has some remob su @ both margins.

Photo 3235 | 3236 @ 129.65 Late equigran bi monzoGT, as above, post-S1 but clearly chloritised (pre-ch alth).

142.05 – 159.80 (EOH): quartz + feldspar (?) + garnet + chlorite ± sillimanite ± chalcopyrite rock. Not recognisable as granitoid, coarse-gsz tho. Possibly calc-silicate rock? Poss also intense altn subject to metamorphism… Chl-bi patches perhaps just thoroughly replaced (see description below…).

– S_2 high ε zone.

Photo 3327 @ 158.20m typical example of final tray. pale yellow wisps (of former bi/ch?) – sericite? – w patchy internal sillimanite. Light qz+fl matrix, patchy garnet, mineralisation around faint, rexstallised peg vein?
Poss still GT, just blitzed by altn, recrystallised?

STRUCTURE NOTES

120.2 Vepfl (postmin) 8/280
Ph 3370.

123.55 Vcp 58/343 (mantle)
beginning of hg mantle vein/peg zone.
Ph 3371/3372 mantle-type hg CPY, prob remob into swPEG.

125.50 CON 30/330
S_1 20/048

126.65 CON 55/332

127.60 S_1 + Vcpmach 68/317
Ph 3373 Hg S_1 ll "mantle" or "rext" veins w thin ch selvedges.

128.60 Vqzfl crd(?) – ~~25~~ 15/115
S_1 – 45/282
Ph 3374 Cgsz vein cuts S_1 + hg cpy bands, remob some su. Vn warps S_1 in a "S-side-up" sense. NOTE diffuse "rex" margin on vein – very neat, gradational gsz increase.

129.15 CON 58/005
S_1 60/324

130.35 – 68/203 PEG/Vqzflmucrd(?)
Ph 3375 late cg peg/qzflmucrd(?) vein

131.10 ~~CON~~ PEG 74/313 (20cm)

131.40 Valb-cpy(?) 26/060
thin, v. late vein (alb selvedge? hard…) remobs cpy, cuts S_1. Ph 3376

134.20 S_1 + PEG 62/276
Ph 3378 "Mineralised" PEGS // to S_1, w small section of megacrystic GT on uphole side. Pxsb poikilitic + rext.

134.80 S_1 52/316 – part of narrow, finer, higher ε section ~1m wide, several narrow pegs slightly x-cut S_1

136.25 Veppy "mantle" 50/274
Ph 3379 cp-py rich "vein" mantling PEG or cgsz GT (rex)

138.60 ~~S1~~ PEG/GT – 58/280
Ph 3380 cg bi (unoriented) on PEG/GT margins – rex/altn?

141.70 S_1 40/355
Ph 3381 hg cp±mt assoc w early(?) bleached/ksp veins, ~~[illegible]~~ some "rootless" – early? remob? Note gnt not wrapped by foln, includes cpy in places.

147.40 S_1 40/325
S_2 20/325
Ph 3385 S_2 high ε, only trace S_1, v. str ch-sill-gnt altn.

149.20 S_1 – 40/356
S_2 – 17/345
Ph 3386/3387 V. str. sill-defined S_2 zone

154.90 S_1? 24/332 (ch-mt)
vague banding defined by ch-mt ± cpy masses.

158.20 S_1 – 65/282
Vepch – 35/282

158.70 Vcpbimt 55/304
Ph 3388 vein w abundant cgsz bi, unoriented, cuts across earlier blitzed altn, then gnt grows over all –

✱ critical observation ✱ Bi (potassic altn) is added, after S_1 + some earlier strong altn

ALTERATION/MINERALISATION NOTES

ksp: 120.5 – 139.50; ch: 133.3 – 156.8; sill: 144.2, 146.8, 151.7

Photo 3324 @ 125.70 = late monzoGT affected by retrograde altn. Clear conversion of bi → ch (right to left)
NO GARNET IN THIS ROCK ✱

Ph 3382/3383 @ 142.70m
garnet overgrows (?) v. str ch-mt ± cpy altn zone (later).

Calingiri Project
Graphic Log

HOLE ID: 14CADD001	**COORDINATES:** 464 269 E / 6566599 N	**ORIENTATION:** -64 -> 270	**PAGE:** ~~4 of 10~~ 1 of 7
PROSPECT: Daster	**LOGGED BY:** M. Outhwaite	**DATE:** 23/3/2015	1 tick = 1 metre.

DEPTH	LITHOLOGY BDH	STRUCTURE dust E	ALTERATION 1 %Bi	ALTERATION 2 %Gt	MINERALISATION	1 < ch int	LITHOLOGY NOTES	STRUCTURE NOTES	ALTERATION/MINERALISATION NOTES	OTHER
320										
325										
~~330~~ 335										
~~340~~ 340										
~~345~~ 345										
~~350~~ 350										
~~355~~ 355										
360										

334.40 (start of core)

334.40 | (Ar) | (5) | (0) | (0) | 334.40 – 437.35 m (w minor PEGs + PB, as detailed) Thick interval of bimzGT – ~5% bi, 45% qz, 50% fl, spotted w kspar prots to ~15mm, approx 1 per metre avg. Typical qz/fl grain = 2-4mm, biotite = 1-3mm. No garnets noted. Several PEGs, as described. Rare bandings in the rock, as described

Undoubtedly fines to lower contact (weak chill against mineralised zone.

334.60 – S_1 weak bi fabric 47/342

345.60 S_1 – 77/344

(359.75 – 360.65) irregular, diffuse, vc qtz PEG

357.40 foln, 10cm bi-defined – 81/041 thin shear band.

359.35

Calingiri Project

Graphic Log

HOLE ID: 14CADD001	COORDINATES:	ORIENTATION:	PAGE: ~~5 of 10~~ 2 of 7
PROSPECT:	LOGGED BY:	DATE:	

Column headings: DEPTH | LITHOLOGY (BOH) | STRUCTURE (Z Bi/ct) | ALTERATION 1 % Bi | ALTERATION 2 % Ct | MINERALISATION | Ch int | LITHOLOGY NOTES | STRUCTURE NOTES | ALTERATION/MINERALISATION NOTES | OTHER

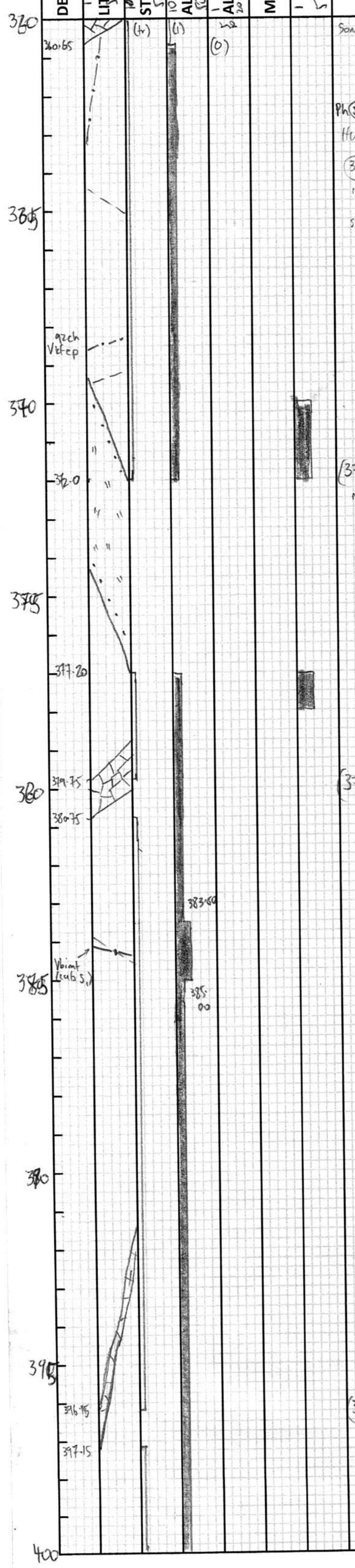

LITHOLOGY NOTES

Some cgsz bi+mt clots in PEG *

Ph (3719) @ 364.60 m – typical texture of cgsz HW bi mzGT, note kspar pxst.

(3720) @ 364.60 + 436.30 m – comparison of "centre" & "margin" of HW granite, note significant gsz change.

(372.00 – 377.20) fgsz, PD, vfgsz @ chilled margins. No effect on surrounding rocks.

(379.75 – 380.75) cgsz PEG, coarse bi clots

(396.15 – 397.15) vcgsz PEG, thin but v. low α angle

STRUCTURE NOTES

360.65 PEG – 32/258

363.20 PEG 2cm w cg bi-mt – 4/122

365.10 S_1 – 51/300

368.60 Vqzkfchep, 1cm – 63/193

Ph (3768) V. thin qz stringer w kf-cht ep selvedge.

369.50 S_1 – 43/235

Different S_1 ori here, no clear point of change.

372.00 CON/PD – 24/026

377.20 CON/PD – 20/019

380.75 PEG w cg bi-mt – 25/292 a bit irregular.

384.20 S_1 – 65/289

384.20 Vbimt – 60/056

Ph (3769) Coarse, random bi-mt vein cuts S_1 foln.

397.15 PEG 14/199

ALTERATION/MINERALISATION NOTES

Ch surrounds PD.

~383.80 start of bi veins/bands?

Bi vein/band zone.

Calingiri Project

Graphic Log

HOLE ID: 14CADD001	COORDINATES:	ORIENTATION:	PAGE: ~~6 of 10~~ 3 of 7
PROSPECT:	LOGGED BY: \	DATE:	* ~~NOTE CHANGE TO 1 tick = 40m~~ *

DEPTH	LITHOLOGY BoH	STRUCTURE bnct &	ALTERATION 1 % Bi	ALTERATION 2 % Gt	MINERALISATION	ch int	LITHOLOGY NOTES	STRUCTURE NOTES	ALTERATION/MINERALISATION NOTES	OTHER

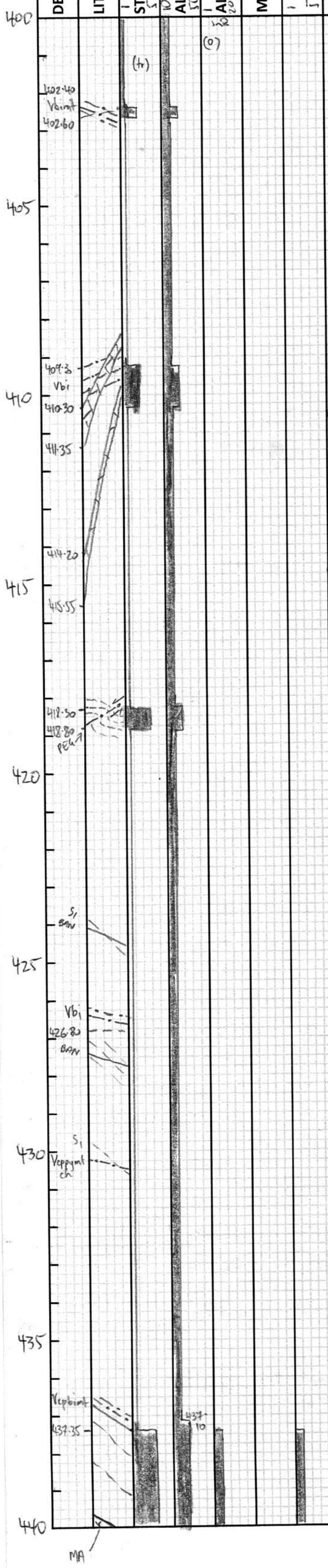

LITHOLOGY NOTES

(410.30–411.35) PEG. Ph (3721) @ 410.80m – cgsz bi+mt masses, typical of PEGs of this style further up hole also. Mt typically surrounded by cgsz mt.

(414.20 – 415.55) PEG, v. low α, ~5-10cm thick.

@ 426.80 – change from generally coarser (uphole) to generally finer (downhole), part of broader chilled margin.

Ph (3722) @ 426.80, showing downhole change.

(3723) @ 427.40m, banding internal to chill zone, evidence of initial chill being intruded (by itself).

Ph (3724, 3725) Major contact, chemical & textural change, w critical observation that mineralised veins affect the granite, at least the chilled section.

437.35 – 440.20m

undistinctive bi mzGT – Ph (3726) @ 439.80m of typical rock. No distinctive features.

STRUCTURE NOTES

402.50 foln/Vbimt – 73/347 (zone 402.40 – 402.60)
S1 (?) – 63/286

Ph (3770) Series of bi+mt veins/fol zones + rex zone. Cuts acute to very faint foln (S1), earlier.

409.40 Vbimt – 67/160

Ph (3771), similar zone to above, 409.30 – 410.30, incl. rex texture.

411.35 PEG – 5/198

414.20 PEG 11/190

418.50 S1/fol – 34/256
PEG – 11/108

South-side up displacement of strong foln across thin PEG. Photo (3772).

424.60 BAN – 52/355
S1 – 46/315

Ph (3773) acute relationship betw gsz banding & weak foln.

426.70 Vbimt – 58/339

427.70 BAN – 55/358
S1 – 47/315

Ph (3774) Same relationship as at 424.60, suggests F1 synform to west, NW-plunging.

430.50 Veppymtch – 55/352
S1 – 47/304

Ph (3775) min vein in the GT, cuts wk bi foln – typical "ch-type" vein, dct py.

432.30 BAN – 52/356
S1 – 35/330

Ph (3776) excellent example of BAN/S1 relationship.

437.20 Vbimtcp – 64/336

437.35 CON – 53/336

Ph (3777, 3778, 3780) Critical contact zone, clearly showing bi-cp-mt veinlets affecting the rock.

437.60 Vflqzmtmo – 47/320

Ph (3781) typical qzflmo vein w mt also ~|| S1.

438.10 BAN/CON – 64/336 Ph (3782) Thin megaxstic section in CON w the mzGT-style rock – note cg mt alt affects!

ALTERATION/MINERALISATION NOTES

Note: increased bi (veins + min) occurs within "the rock", over last 25cm.

438.60 Veppobiam(?) 20/318 cuts S1

439.10 BAN/GNfol – 57/335
S1 – 52/295

Ph (3783) 2 foliations?

Calingiri Project
Graphic Log

HOLE ID: 14CADD001	COORDINATES:	ORIENTATION:	PAGE: ~~7 of 10~~ 4 of 7
PROSPECT:	LOGGED BY:	DATE:	

DEPTH	LITHOLOGY	STRUCTURE	ALTERATION 1 % Bi	ALTERATION 2 % Ht	MINERALISATION	Ch int	LITHOLOGY NOTES	STRUCTURE NOTES	ALTERATION/MINERALISATION NOTES	OTHER

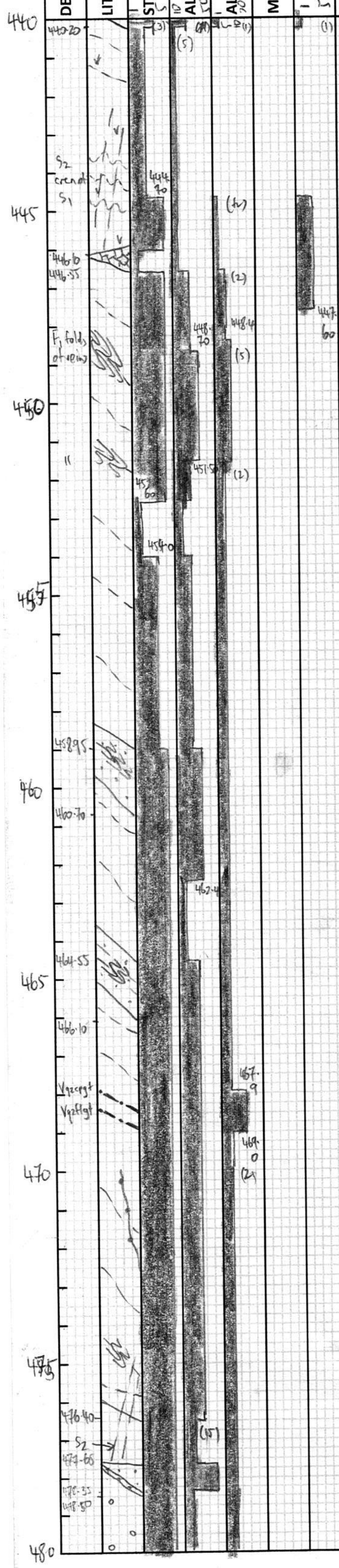

LITHOLOGY NOTES

440.20 – 446.10 m med gsz amphibolite, clear hbl-defined foln, patchily overprinted by cgsz bi altn (not aligned) – ie. potassically alted "post – S_1".
Ph (3727, 3728) of typical texture @ 442.00 m

Lower contact occupied by PEG… not reliable ori.

Ph (3729, 3730) MA-PEG contact. PEG look syn to post S_1. PEG contains mt + cp + gt (rel early, part of PEG "juice"), but cut/oprinted by v.pale green retrogressive (?) cp + se + ch (?) veinlets/zones.

446.10 – 446.55 mineralised PEG, as described above.

446.10 – 458.95 unremarkable bi mz GT, coarseish, typical "background" mineralised rock (see ph below)
Ph (3731) @ 453.40 m of low ε domain in interval, showing scattered kf phenos to 6mm – likely precursor to higher ε rocks.

458.95 – 460.70 higher ε, darker zone, poss diff lith. Ph (3723) @ 459.20 m of typical rock – bi + ksp + qz? Altn zone/shear zone?
Ph (3722) @ 460.70 m of lower "contact" into more recognisable, more equigranular monzogranite.

460.70 – 464.55 monzogranite, mostly intensely altered, but coarseish & unremarkable in low ε/altn areas. Some bi-rich bands

464.55 – 466.10 high ε, dark zone as prev, w Fl-qz-mo-cp veins folded in S_1?

466.10 – 476.40 coarse, equigranular bi mz GT, highly strained in parts, becoming comparable to "dark, high ε" intervals in parts, but gradational
Ph (3734) @ 466.60, 468.10, 469.20 (t to b) of effect of increasing strain on rock – even "low ε" rock quite deformed…

476.40 – 477.65 low ε bi mz GT, nothing distinctive, def mineralised.
477.65 – 478.35 narrow, dark high ε zone, appears older than surrounding mz GT units.
Ph (3735) @ 478.35 showing mineralised lower contact
478.35 – 478.50 thin, post S_1 (?) bi mz GT
478.50 – 480.25 distinct bi-poor, qz rich GT, as seen in 12CADD001, well mineralised (see next interval for pic)

STRUCTURE NOTES

440.20 con 49/300
441.50 S_1 (am-defined) 53/302 no lineation on this fabric.
445.60 S_2 cren – 11/185 Ph (3784)
S_1 – 74/332
446.50 Vepch – 54/180 Ph (3785)
late vein cuts min PEG (incl. gt) – remob vein.
447.20 Vep py – 35/355
447.90 S_1 – 42/336 w // pegm qzfl veins
448.75 Vqzfl gt mocp mt (20cm) 60/355 unusual banded vein Ph (3786)
449.40 S_1 – 48/312
Ph (3788, 3789) of "F_1" folding of Vqzflcpmo veins. – cant measure, but look ~ mod E plunging, no clear vergence.
451.70 Vqzflmocp // S_1 – 50/318
Ph (3790) typical mo-rich veins folded by S_1 fabric, or "wobbling across it".
454.00 S_2 8/341 weak cren.
455.20 S_1 32/337
456.60 Vgtchcp – 38/340
Ph (3791) Rich vein ~// to S_1 – note hazy F_1 folded qzfl vein @ left – Vgtchcp post-dates.

459.20 S_1 – 33/314
F_1 – " + (L) 63 → (~45 → SE)
Ph (3792) highly contorted early qzfl vein – minimal sulphide.
460.70 Con/S_1 – 37/312 high ε con.

464.55 con 38/331
465.10 S_1 – 44/303
F_1 – " + (L23) ~60 → ENE
Ph (3793) Folded Vqzflmocp, excellent example.
466.30 S_1 – 47/317
468.50 Vqz gt cp py mt (15cm) – 42/312 mantle type.
468.90 Vqzfl gt – (15cm) 55/303
Ph (3794) V. gt-rich, but su-poor vein
472.60 Vcapy – 9/333
V. late, open space calcite-py vein, w feeb selvedge. Ph (3795)
475.20 S_1 – 32/310
F_1 – " + (L) 63 (~45 → E)
Ph (3796) Folded Vqzfl + cp, no obvious mo
475.70 S_1/Vcpqzfl – 57/294
Ph (3797) Good cpy min in S_1// qzfl veins/mini PEGs.
477.60 S_2 – 7/166
478.35 con – 25/303

ALTERATION/MINERALISATION NOTES

Some altn bi in MA.

High ε + ch + gt @ lower MA contact, S_2 cren also.

V. high ε

Bi wiped out by ksp?

Calingiri Project

Graphic Log

HOLE ID: 14CADD001	COORDINATES:	ORIENTATION:	PAGE: ~~8 of 10~~ 5 of 7
PROSPECT:	LOGGED BY:	DATE:	

DEPTH	LITHOLOGY	STRUCTURE	ALTERATION 1 %Bi	ALTERATION 2 %Gt	MINERALISATION	Ch int

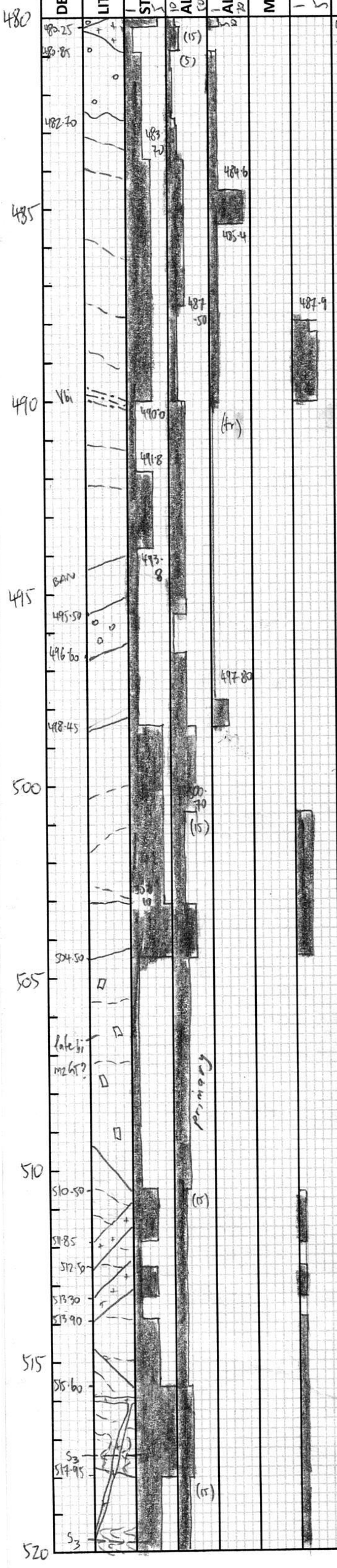

LITHOLOGY NOTES

480.25 – 480.85 Late-ish, poorly mineralised bi mzGT, as for interval 478.35 – ~~478.50~~, post-S_1, poss post min. Irregular ori.

490.85 – 482.70 Qz-rich, cgsz GT, w little bi, as in 12CADD001. Well mineralised. Ph (3737) @ 481.80m of typical rock.

482.70 – 498.45 equigran to wk ksp-phyric bi mzGT w highly variable ε & altn expressions.

Ph (3738, 3739) @ 482.70, 483.70, 487.80, 488.70 of effects of > ε + altn on same lith. 482.70 peice contains upper CON, 483.70 contains marked >> in ε (but both "sides" are mineralised).

Ph (3740) @ (490.90) Local effects of min on texture, foln intensity.

Ph (3741) @ 490.60 of irregular, mineralised qz-rich GT within locally unmineralised bi mzGT – poss xenolith?

(495.50 – 496.60) qz-rich GT band?

498.45 – 504.50 highly strained bimzGT zone, prob cgsz precursor rock.

Ph (3742) @ 503.10 of lower to higher ε transition zone – poss diff lith, but no clear reason to think so.

Lower CON invaded by vein/PEG. Ph (3743) @ 504.50m showing CON zone.

504.50 – 510.50m largely unmineralised and weakly deformed, bi-rich mzGT, weakly kf-por. Seems to cut v. highly strained rocks.

Ph (3744) @ 506.70m of typical texture

Ph (3745) @ 505.60m of planar cp-py-ch-se vein cutting this rock – late min/remob?

Ph (3746) @ 510.50m of lower CON, ~∥ to S_1, young rock also has weak fabric.

510.50 – 515.60 cgsz bi mzGT, same as 498.50 – 504.50, but < ε + altn, generally. Similar texturally to "qz-rich GT" unit. Ph (3747) @ 514.40m, typical rock.

(511.85 – 512.50) } late bi mzGT dykes, wk fol, unmineralised
(513.30 – 513.90) }

This interval (+ 498.50 – 504.50) is like the long interval near end of 12CADD001.

515.60 – 517.95 high ε rock, after kf-phyric, cgsz precursor (?)

Ph (3750) @ 516.90, typical...

Ph (3748, 3749) @ 516.0m late bi mzGT dyke cuts S_1 & mineralised qz-fl veins. Dyke itself contains some min also (remob?).

Ph (3751) (3752) @ 517.95 of lower CON, high ε stuff seems oldest? Hard to say for sure.

STRUCTURE NOTES

480.25 CON – 50/100

481.50 S_1 63/186 Vmt cpy – 53/270
V. irreg S_1 thru here. Ph (3798) – vein cuts foln, but also wobbly.

482.30 Vcpch – 59/260 (late stringer)
Ph (3799) note mt + bi masses also.

484.10 S_1 – 46/299 Noticeable low α zone

487.80 S_1 – 52/274

490.00 ~~[illegible]~~ – 72/298 – Vbi mtcp
^ end of higher ε zone, series of stringers + foln. Ph (3801) – note general low ε/altn.

492.20 S_1/shear – Narrow high ε band, 66/295 Ph (3800)

492.90 S_1 – 73/290

494.30 BAN – 52/258 gsz/altn change?

494.60 Vcppybi – 28/266 rich 2cm vn.

496.70 – S_1 65/195

498.45 CON/BAN – 48/230

500.30 S_1 – 42/273

502.80 S_1 – 57/335 "odd" S_1 zone

← ~ change of S_1 ori

503.10 BAN/S_1 – 46/276 Ph (3802) change to high ε zone – finer gsz?

505.60 S_1/fol – 57/257
Vqzcppych – 70/124
Ph (3803) late (remob?) stringer cuts fol in otherwise barren unit.

510.50 CON 34/320

511.20 S_1 41/275

513.30 CON – 26/186

514.90 S_1 – 71/298

515.60 CON – 38/315

517.10 S_1 – 42/303

517.95 CON – 72/002
"S_3" 75/083

Ph (3804) foln in high ε zone runs straight down core into contact – note first appearance of "S_3"

519.80 "S_3" (ax pl) 73/280

Ph (3805, 3806) (3807) shallow E-dipping "S_3" axial planes to irregular folds.

ALTERATION/MINERALISATION NOTES

Gt-rich ksp-qz-gt "vein" zone

Str ch alt controlled by su-rich stringer running down core?

* Local end of garnet * one or two tiny patches before ~529.5m... – why?

High primary bi in late intrusion.

Stringer-controlled ch altn, weak, localised.

OTHER

Calingiri Project
Graphic Log

HOLE ID: 14CADD001	COORDINATES:	ORIENTATION:	PAGE: ~~9 of 10~~ 6 of 7
PROSPECT:	LOGGED BY:	DATE:	

DEPTH | LITHOLOGY (both) | STRUCTURE (ductile) | ALTERATION 1 %Bi (10–50) | ALTERATION 2 %Gt (25–50) | MINERALISATION | Ch int (1–5)

LITHOLOGY NOTES

517.95 – 520.55 cgqz mod E bi mzGT, same as 510.5 – 515.60 interval
Ph(3753) @ 518.80m of typical rock.
Ph(3754) @ 520.55m of sharp change to "altn rock".
520.55 – 528.25 – thick zone of (?) qz-ksp-bi± gt "altn rock", likely after GT/mzGT. Faint banding preserved, rarely texture. Enclaves of cgbi mzGT as depicted.
Ph(3755) @ 523.80 } textures of pervv. altn eating
Ph(3756) @ 524.80 } up S_1 + biotite – note S_1 vaguely preserved.
Ph(3757) @ 527.50 of typical fgqz texture, note v. little biotite, lots of v. fine pink garnet.

528.25 – 529.80 m-cgqz bi mzGT ± generally low E, but some foln + min + garnet (ie not post-min).
Ph(3758+3759) @ 528.40m – excellent pics of E-gradient effects – here >E = >min, clearly.
529.80 – 530.70 more qz-ksp-bi "altn rock", retains vague fabric + coarsish qqz, some folded min veins.
Ph(3760) @ 530.70m of irregular altn front @ lower contact
530.70 – 535.65 cgqz bi mzGT, as previous, variable strain, some evidence of F_2 folding.

535.65 – 536.35 high E zone after kf-phyric rock? More bi-rich
Ph(3761) @ 535.65 of CON ± above rock. Possib look to be wrapped/rotated by foln, pass^normal sense on fabric. (E block down).

536.35 – 540.30 Mostly cgqz bi mzGT, but ± intervals of "FW rock" as depicted.
(536.40 – 537.05?) Ph(3762) – texturally identical to FW rock, but mineralised + garnet!
(538.75 – 539.00) Ph(3763) Det FW GT, rex upper CON?
(539.35 – 539.60) Ph(3764) "
Ph(3765) @ 540.30 – right @ "CON" ± last of mineralisation. Pretty sure this rock is not post-min – this looks like the same rock – no real textural or mineralogical change.
The interval 536.35 – 540.30 looks like altn transition zone betw cgqz bi mzGT ± FW rock, likely "primary interleaving" (intrusive), prob post-dating gneiss formation (D_1), but pre-min.

540.30 – 565.40 fw bi mzGT, qqz fw qz-ff-bi all ~2mm, egg. to rwk kf-phyric. Exceptions as depicted, various pegs, wk fol zones, rex zones (see structure log also).
(542.00 – 542.30) Irregular bit (xeno?) of coarser bi mzGT, unaltd, unmineralised. Relation betw rocks unclear.
(552.20 – 553.40) coarsish, recrystallised section ¾.
Ph(3766) @ 552.20m of diffuse start.

STRUCTURE NOTES

520.55 CON/BAN – S4 /321
Ph(3808) change into str. altn. zone. Note not necessarily a texture change...
521.80 S_3 – 78/035
Ph(3810) S_3 folding of existing foln, likely S_1 – this is abundant through this zone.
Ph(3811) section view – F_3 aform uphole.
523.20 S_1 36/303 – irreg all through this zone, but "trying" to be this (long lim)
524.60 CON/altn change – 61/343
525.30 " – 45/283
Ph(3812) note garnet.
526.90 " – 80/288
527.10 Vpeg/mqz – 47/331
Ph(3813) late stringers ext kaltn – clearly qz+ms+ch+sp.
528.25 CON – 55/327
529.80 CON – 51/291
530.30 Ph(3814) @ of folded sp-rich veins – no measurements, but approx 45°→NE plunges.
532.30 S_1 – 54/189
532.90 S_2 – 13/175
F_2 – " + (57)
Ph(3815) Standard F_2 setup.
(536.35) CON/S_1 – 78/329
537.40 S_1 77/249
538.75 – CON 58/325
539.60 CON 81/163
540.30 CON ~ 73/300
547.30 S_1 – 37/266
547.90 S_1 – 37/291
548.30 CON/Aplite – 27/314
550.10 S_1 – 44/257
552.50 fol/Vbimt – 57/245
552.90 Vbimt – 67/145
553.20 fol – 42/186
559.90 fol/S_1 – 58/322 weak bi-defined foln some bi+mt wisps.

ALTERATION/MINERALISATION NOTES

more abundant stringers ± ch selvedges.
* gt starts again, weak.
Still stringer-controlled ch altn
* 538.75 – 539.00 "FW dyke" contains gt.
* 539.9 – local end of gt – but see 561.90m.

OTHER

Calingiri Project
Graphic Log

HOLE ID: 14CASD001	COORDINATES:	ORIENTATION:	PAGE: ~~10 of 10~~ 7 of 7
PROSPECT:	LOGGED BY:	DATE:	

DEPTH	LITHOLOGY	STRUCTURE	ALTERATION 1 % Bi	ALTERATION 2 % Gt	MINERALISATION	chl int	LITHOLOGY NOTES	STRUCTURE NOTES	ALTERATION/MINERALISATION NOTES	OTHER
560							Ph (3767) @ 560.30 – typical texture, some ksp to 4mm now, bit coarser overall than upper contact.	561.20 fol/S_1 – 59/267 561.90 " – 40/290 Ph (3816) gt mass assoc w qz/rex in fol zone. 563.50 Vbimt – 73/337 565.~~30~~ 20 – S_1 – 28/304	sill	
	Vbimt			speck of gt						
565	565.4									

"F_3" vergence

L_1?

matic - ~53- ~85 . gt. ✓
higher sc/v ~ 85 - 105 . sm.
matic ~115-120 also. . bleaching.
. ch stringers?

Calingiri Project

Graphic Log

HOLE ID: 14CADD002	**COORDINATES:** 462051E / 6572596N	**ORIENTATION:** -58→110	**PAGE:** 1of 6
PROSPECT: Bindi West.	**LOGGED BY:** M. Cuthwaite	**DATE:** 27/3/2015	1 tick = 1 metre.

DEPTH	LITHOLOGY (Hos)	STRUCTURE (Acute)	ALTERATION 1 (Grey)	ALTERATION 2 (Bleach)	MINERALISATION (Sm)	Ch stringers	LITHOLOGY NOTES	STRUCTURE NOTES	ALTERATION/MINERALISATION NOTES	OTHER
		1 5	1 5 10 20			1 5				

0
5
10
15
20
25
30
35
40

31.30 – 33.50 – white, cgsz, wthd GT, leached/bleached. – same as 37.70 – 53.80 unit

33.50 – 34.30 rubble, sand, core loss – FLT?

34.30 – 37.70 ch-qz-bi-fl ~~rock~~ gneiss ± matic pre cursor? V. similar to mineralised rock

34.90 S_1 82/8-062

37.70 – 53.80 V. coarse, white, near pegmatoidal granite, highly bleached?, with irregular intervals of a finer, older granitoid, as marked.

Calingiri Project
Graphic Log

HOLE ID: 14CADD002	COORDINATES:	ORIENTATION:	PAGE: 2 of 6
PROSPECT:	LOGGED BY:	DATE:	

DEPTH	LITHOLOGY (HOg)	STRUCTURE (Ductile)	ALTERATION 1 (Cnt)	ALTERATION 2 (Bleach)	MINERALISATION (Sm)	Ch sting	LITHOLOGY NOTES	STRUCTURE NOTES	ALTERATION/MINERALISATION NOTES	OTHER
40										
41.20							(41.20 – 41.70 + 43.55 – 46.30) qz40 bi10 fl50 equigranular bi mzGT, similar to "Ninan adamellite" texturally. ~2mm qtz, rarely 3mm. Ph (3819) @ 44.60m of typical rock. Older than surrounding cgqz unit, intruded by it.	43.55 CON 58/080		
41.70										
43.55										
45							Ph (3820) @ 40.70 & Ph (3821) @ 45.30m show bleaching effects on this rock, poss alt^n transition into coarser rock			
46.30							(47.70) Ph (3818) typical, white, cgqz, bleached GT.			
50							ok irregular patches of "older" rock thru here, small.			
53.80							53.80 – 73.40 + 80.00 – 84.70 + 86.15 – 90.85 + 92.55 – 98.80 + 100.20 – 103.30 Fine to med qtz, gt-ch altered amphibolite, variably intruded by granite sills, as described below. Significant granite-bearing amphibolite intervals are indicated.			
55										
60							53.80 – 61.40 ~ 50% irregular granitic zones (highly "contaminated")			
60.0										
61.40				61.60			61.40 – 73.40 ~ 15% contam w GT			
65							Ph (3822) @ 64.70 of typical fgqz MA with GT band @ left Note pale garnets – lots of fine, pale gt disseminated.	65.50 BAN. 85/346 Ph (3838) cg/fg MA banding. ~// foln.		
65.0										
66.30										
S_3								68.30 "S_3" 76/286 (FAP) "f_3" + 252(a) Ph (3839) "F3" folding, no clear vergence. (gentle w plunge).		
70										
73.40							73.40 – 80.00 + 84.70 – 86.15 + 90.85 – 92.55 + 98.80 – 100.20 + 103.30 – 106.70 Intervals of kf ± qp-phyric bi mzGT generally "contaminated" with MA bands. Generally ~50% fl, 15% bi (ch+ep alld), 35% qz. Ph (3824) @ 76.80m – typical kf ± qz-phyric bi monzogranite, in least altered/contaminated state. Note large qz eye.			
75								76.90 S_1 60/100		
80										
80.00										

Calingiri Project
Graphic Log

HOLE ID: 14CADD002	COORDINATES:	ORIENTATION:	PAGE: 3 of 6
PROSPECT:	LOGGED BY:	DATE:	

DEPTH	LITHOLOGY (109)	STRUCTURE (Dvein)	ALTERATION 1 (Cont)	ALTERATION 2 (Bleach)	MINERALISATION (Sm)	Ch stringer	LITHOLOGY NOTES	STRUCTURE NOTES	ALTERATION/MINERALISATION NOTES	OTHER
80			5/10 20 80-0				80.00 – 84.70 · ~10% QT			
			82-0					83.00 S_1 64/074		
85 84.70										
86.15							Ph (3823) @ 88.60m – typical coarser MA			
90 90.85								90.80 BAN/S_0 – 75/325		
92.55								Ph (3840) Fine banding in "MA" near con. – interflow seal?		
95								96.20 S_1 ~~085~~ 76/062		
98.80										
100 100.20								100.20 CON 80/294		
103.30							Ph (3825) of altered mcHT, 103.70, 105.60, 106.50m approaching FLT. Fe ch (2/3) orange, light green ; ch+ep(?) microfractures.			
105 106.70							106.70 – 113.50			
							Cloudy, silica-flooded, veined breccia zone			
110							Ph (3826) @ 110.50m of typical example. Intense fault, silica-dominant alteration (over existing chlorite?).			
113.50							113.50 – 117.30 more recognisable fm gsz MA, though with elements of silicification/bx.			
115										
117.30							117.30 – 119.10 chlorite cemented "older" breccia of dominantly granitic precursor. Ph (3828), (3829) of earlier breccia over-printed by siliceous veins.			
119.10 120 120.00							119.10 – 120.00 thin mafic band.			

Calingiri Project
Graphic Log

HOLE ID: 14CADD002	COORDINATES:	ORIENTATION:	PAGE: 4 of 6
PROSPECT:	LOGGED BY:	DATE:	

DEPTH	LITHOLOGY	STRUCTURE	ALTERATION 1	ALTERATION 2	MINERALISATION	LITHOLOGY NOTES	STRUCTURE NOTES	ALTERATION/MINERALISATION NOTES	OTHER

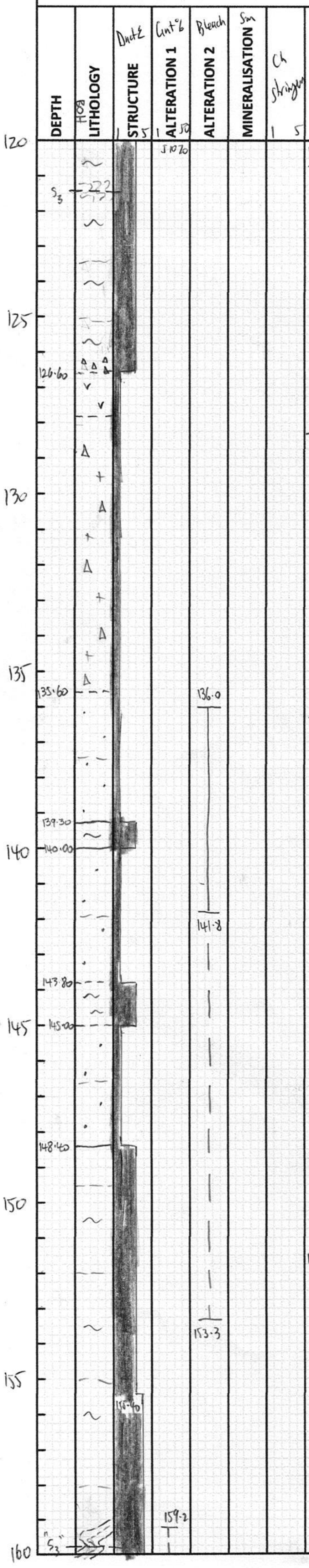

Lithology notes

120.00 – 126.60 ch-qz-fl "gneiss", as described further down – poss granitic parent?
Ph (3830) @ 123.90m, typical, mineralised

126.60 – 127.80 thin mafic?

127.80 – 135.60 Brecciated granite, as per 117.3-119.1.
Ph (3831) @ 133.20m – high ε breccia, paragenesis same as Ph 3829: dark ch breccia → light ch-ep (?) veinlets → silica (late).

135.60 – 148.40 fgr ch-qz(?)bi(?) rock,, looks mafic, but lots of fine qz, poss metased? Ch-qz-fl 'gneiss" intervals, as marked,,.
Ph (3832) @ 143.00m of typical rock, in least altd part.

148.40 – 184.30

Long interval of regularly banded ch-qz-fl± gt±ep "gneiss", of unknown parentage.
Ph (3833) @ 163.70 / (3834) 168.30 of typical examples.
Conceivably a high D_1 strain zone in GT?

Structure notes

121.40 "S_3" – 72/297
"F_3" – " + 52 (L)
Ph (3841) folded mineralised banding/ S_1 foln, cut by ep (?) stringers.

123.70 S_1 75/010
Ph (3842) typical min ~// to S_1

124.20 Ph (3843) typical min, variably folded in "F_3" folds.

Ph (3837) @ 138.20m – strong "bleach" altn – here greenish ≈ ep? cf. photo 3836 @ 191.80m. →

149.40 S_1 78/043

152.90 S_1 + // min veins – 67/056
Ph (3844) @ ch-act-py veins following S_1 foln, but likely post-dating – unaligned amphiboles.

158.30 S_1 – 68/016

159.80 Ph (3846) S_3 54/251
F_3 " + 278 (L)

(gentle W plunge approx)

Calingiri Project
Graphic Log

HOLE ID: 14CADD002	COORDINATES:	ORIENTATION:	PAGE: 5 of 6
PROSPECT:	LOGGED BY:	DATE:	

DEPTH | LITHOLOGY (Hog) | STRUCTURE (Ductile) | ALTERATION 1 (Cnt%) | ALTERATION 2 (Bleach) | MINERALISATION (Sm) | Ch stringers | LITHOLOGY NOTES | STRUCTURE NOTES | ALTERATION/MINERALISATION NOTES | OTHER

LITHOLOGY NOTES

— —"SOFT BOUNDARY"— — —
184.30 – 219.70
Very similar rock, but with more massive sections, less well-defined/common qzt fl banding – likely just lower E equivalent.

STRUCTURE NOTES

164.80 Vgz amoppy gt – 70/120
Ph (3847) nice vein, note assoc of gt with min.
168.70 S_1 – 64/101; sm fol – 86/190] Ph (3848) Sm+ gt post-date S_1 fabric.
168.80 "S_3" – 65/257
"F_3" – " + 255(G)
gentle W-plunging folds.
172.80 – S_1 76/286
177.20 S_1 – 69/330
Ph (3836) @ 191.80m – strong "bleach" alteration – prob retrogressive event.
198.70 S_1 70/111

Calingiri Project
Graphic Log

HOLE ID: 14CADD002	COORDINATES:	ORIENTATION:	PAGE: 6 of 6
PROSPECT:	LOGGED BY:	DATE:	

DEPTH	LITHOLOGY (HCB)	STRUCTURE (Ductile)	ALTERATION 1 (Gnt°B)	ALTERATION 2 (Bleach)	MINERALISATION (Sm)	Ch stringers	LITHOLOGY NOTES	STRUCTURE NOTES	ALTERATION/MINERALISATION NOTES	OTHER
200			2 5 10			i 5				
			203.0					203.40 Ph 3849 "S_3" – 73/130 (AP) "F_3" – Can't measure a good gamma...		
205				208.20			Ph 3835 @ 207.80 atypical rock, w faint banding.	Ph 3850 looking West @ core – these are shallow W-plunging "Z" folds, pic looking ~down plunge.		
				210.6				207.80 Vqz cpBn pgch 81/055		
210			211.2					Ph 3851 "mantle" (rock) vein w dk. purple bornite, ~// S_1.		
			212.0					212.00 "S_3" –80/340 "F_3" – " + 36 (G)		
215								Ph 3853 gentle W-plunging Z folds.		
								213.70 S_1 63/073		
			219.70							
220										

Calingiri Project

Graphic Log

HOLE ID: 08WHDDH001	COORDINATES:	ORIENTATION: ~ -60 → 090	PAGE: 1 of 3
PROSPECT: Ninan	LOGGED BY: Outhwaite	DATE: 18/2/2015	

Columns: DEPTH | LITHOLOGY | STRUCTURE (Ductile) | ALTERATION 1 (Bi %) | ALTERATION 2 (Grt %) | MINERALISATION (Mt %) | Albite | LITHOLOGY NOTES | STRUCTURE NOTES | ALTERATION/MINERALISATION NOTES | OTHER

Depth scale: 40, 50, 60, 70, 80, 90, 100, 110, 120

Lithology column: HQ; 55.60; sap; 61.0; 63.8; sap; 68.70; 73.50; 82.80; 87.00; 88.35; 92.45; 96.10; 96.55; 97.60; 101.60; 102.75

Depth margin: slightly wthd ↑ | wx ↓ | 80 fresh

Structure/alteration columns: NOT LOGGED (wthd) ↑; 86.00; 103.20; 114.4; 107.20; 77.0; (selvedges)

LITHOLOGY NOTES

Pre-collar ↑

55.60 – 61.00 – mod oxidised sap, banded.

61.00 – 63.80 mfol mg-cg granitoid w ~20% qz m – bi content not clear (wthd).

63.80 – 68.70 mod ox. banded sap, likely qz-fl-bi schist rock, as below + mafic voles?

68.70 – 73.50 less wthd, likely mafic-derived biotitic schist? fine gsz, gets distinctly coarser across vein interval below. → (AN-derived ✱)

73.50 – 74.00 Bucky qz vein

74.00 – 82.80 bi-fl-qz ~~rock~~ schist (AN) w bi retrogression to chlorite tlout. % qz vs. fl unclear – poss. dacitic MA.

Ph (3437/3438) @ 82.00m of typical rock – note former fl pxst? + ch stringer. Coarser grained than units above & below – primary?

Ph (3439) @ 82.80m – contact (diffuse?) w below unit.

82.80 – 87.00 – Dark, vfgsz likely mafic rock, strongly flatted, lineated & now amphibolite. Numerous v. thin granitic (?) lenses w cgsz texture – mini intrusions, flattened clasts? Hints of porphyritic texture in places (fl pxsts).

Ph (3440) @ 85.00 of typical textures – light patches are granitic (?) bands, dark patches are more bi-rich/coarser bands w pale haloes.

87.00 – 88.35 Distinctive qz-fl-bi "porphyry", poss after felsic/dacitic volcanic or subvolc. intrusion – cg qz diagnostic (~5%), plus cg fl (~30%). Remainder bi wisps (~1%) + veg matrix (qz-fl-bi?)

Ph (3441/3442) of typical rock – note v. strong linear fabric (L-tectonite) @ 87.50m.

88.35 – 92.45 bi-fl-qz schist (AN) as for 74.00 – 82.00, poss a bit finer gsz. After AN?

92.45 – 96.10 qz-fl-bi "porphyry", as per 87.00 interval.

96.10 – 96.55 Distinctive thin MB(?)-dyke? ep-py-qz filled amygdales – "cooked" @ both margins??

Ph (3443/3444) First of CON MB-porphyry @ 96.55 (note 'cooked margin'), 2nd of MB texture – note poss MB fragment??

96.55 – 97.60 – "porphyry" as above...

97.60 – 101.60 bi-fl-qz schist as above (AN), mgsz.

Ph (3445) @ 101.60 – "cooked" schist @ porphyry margin – porphyry likely early intrusion... Note extr. stretched qz pxst in porphyry also. "COOKED" ZONE Bi-enriched (potassic altn?).

101.60 – 102.75 porphyry, as prev.

102.75 – 117.45 dominantly fgsz mafic interval (MA), as per 82.80 – 87.00, looks bedded/banded, some porphyritic or amygdaloidal zones. Some thin intervals of bi-fl-qz schist & several thin, late GT dykes.

STRUCTURE NOTES

Strongly lineated.

82.80 CON/S1 – 62/080
Betw mg schist (AN?) & fg MB, fol + su stringers //

85.80 S1 – 68/108
L1 min lin – 72/034
~30° → NW
Typical bi-defined L1 lin. (stretching) t/out top of hole.

88.35 CON/S1 – 65/080
Vqzchbicpy – 66/014
Ph (3458 – 3460) min qzcpy veins w bi-ch selvedges, cut S1 fabric – but note bi growing // to S1 in selvedge (close ups)

92.45 – CON/S1 – 73/097

95.30 – Vqzhblbi ① – 78/036 (//S1)
② – 59/097 (cuts)
Ph (3461) qzhblbi veins both following & cutting S1 ie. post S1.

96.55 CON 54/122 – oblique to S1, but rock affected by S1 – early dyke?

str. magnetic

100.0m – Vqzbi±alb (L) – 66/080
Vqz (C) – 73/074
Vbiqz (R) – 77/094
Ph (3462) 3 vein types. Vqz & Vbiqz subtly cut S1, but bi grows // to it. Vqzbialb earliest?

101.60 CON 61/092 (S1 //)

102.75 – CON/shear 75/077
Discrete ep-mt shear on porphyry CON – reactivated zone?

109.00 S1 – 72/071
L1 – 74/021 (β γ)
~30 → WNW

ALTERATION/MINERALISATION NOTES

- garnet ✓
- albite
- ~~epidote~~
- sillimanite ✓
- biotite (cg) ✓

Epidote; ~~Albite~~; Fe; S1 //

Not LOGGED (wthd) ↑

Higher E bi-ch altd shear @ porphyry top contact, similar to other features down hole.

113.40 – 114.40

OTHER

GS2?

Calingiri Project

Graphic Log

HOLE ID: 08WHDDH001	COORDINATES:	ORIENTATION:	PAGE: 2 of 3
PROSPECT:	LOGGED BY:	DATE:	

DEPTH	LITHOLOGY	STRUCTURE	ALTERATION 1	ALTERATION 2	MINERALISATION	Albite	LITHOLOGY NOTES	STRUCTURE NOTES	ALTERATION/MINERALISATION NOTES	OTHER

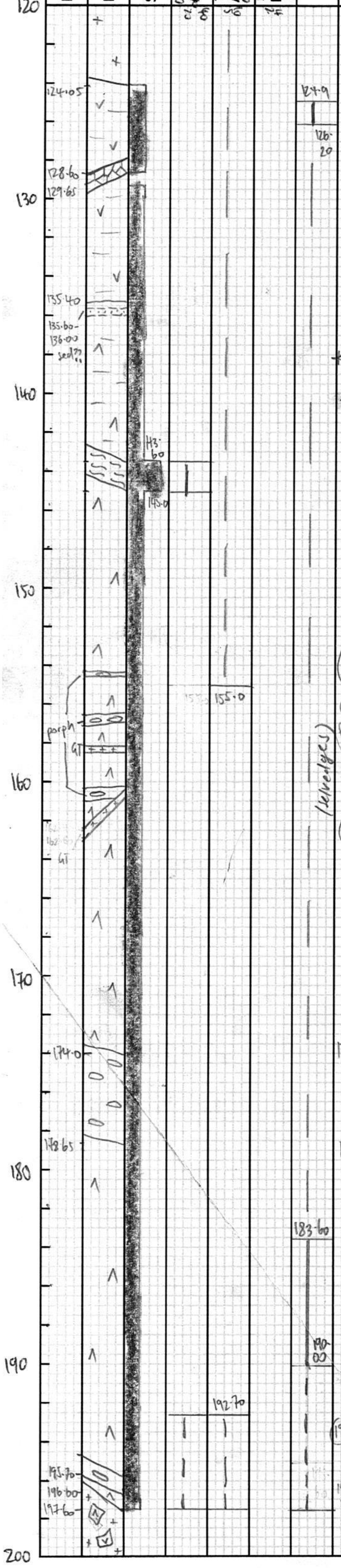

LITHOLOGY NOTES

117.45 – 124.05 – equigranular, mgsz (~2mm) qz(45)-bi(5)-fl GT. Only v.v. weak hints of preferred alignment, def post "D₁" fol/lin event. Sharp contacts ū narrow chills. Some pegmatitic sections.

124.05 – 128.60 mix of fg mafic & bi-fl-qz schist rocks, as described above. V str. "bleached" zones in here possibly include aphanitic "porphyries", but looks like just v. strong altn to me.

128.60 – 129.65 Odd mt-cpy-py-bearing pegmatite Mt + cpy intergrown.

129.65 – 135.40 – "Basaltic" fg mafic rock, as prev.

CHANGE TO AN-dominant sequence here

135.40 – 174.0 Thick AN-dominated sequence, ū minor porphyry & mafic bits, several narrow GT dykes & PEGs.

Ph (3446) @ 135.90m – rapid gsz/texture changes in "AN" sequence. Poss interflow seds? 135.60–136.00

Ph (3447/3448) @ 141.30m – typical porphyritic texture in lower E domain – note much lower degree of foln/stretching than likely equivalent rocks up-hole. In detail, plag(?) phsts look poikilitic & recrystallised.

(154.30 – 154.60, 156.55 – 157.10, 160.45 – 161.00) – thin qz-fl "porphyry" dykes.

(159.15 – 159.50) – fmgsz GT ū bi ~15% earlyish?

Ph (3449) @ 158.90m – thin "basaltic" (?) unit contains clasts of AN rock? AN older, basalt intrudes pile?

Ph (3450) @ 162.60m – late (post fol/lin) GT contains foliated AN xenos.

(162.45 – 162.80) – bi GT ↑ bi ~5% – late feature.

174.00 – 178.65 Typical "porphyry", perhaps < qz than prev, bit weaker foln/lin.

178.65 – 197.60 AN as prev. finer, coarser, some porphyritic, some more basaltic bits. Quite heavily altered than middle, significantly lighter colour.

(195.70 – 196.60) Thin, hazy "porphyry"

197.60 – 200.70 bi(5) monzo GT ū some clear ksp xtals, plus intriguing "blotchy" cpy mineralisation. Ph (3451 – 3453) @ 199.0m of granite ū blotchy, discontinuous cpy-py+ch(?) mineralisation. v. irreg geometry, several foliated xenoliths also.

STRUCTURE NOTES

124.05 CON – 61/109 ~// to S₁ locally, but post dates

126.10 Vhblepcp(po)mtbi – 65/090 (~S₁//) Dasler-style hg vein Ph (3464). (qz, random bi. Ep is new...

127.30 CON 58/142 10 cm GT dyke in albitic zone Ph (3465/3466) Note both dykes slightly cut S₁ AND RH dyke cuts across albitic zone "edge". Note albitised xeno in LH dyke.

129.65 CON (PEG) – 32/038

133.70 Vqzhblalb – 62/091 Ph (3467) boudinaged/irregular vein.

135.0 S₁ – 68/104
L₁ – 76/043 (~20°→NW)

Ph (3468) Xmas-tree style Vqzgnthblbi Gnt & hbl(ch?) clearly intergrown.

Discrete post-D₁ shear zone.

Ph (3469) @ 136.80m deformed qzbihbl+gnt veins, assymetry suggesting normal reactivation of zone?

144.00 Shear Zone 67/107

Ph (3470) Core of str chl-bi altd shear. Roughly // to S₁ ori?

153.60 Layer/BED – 74/070 Ph (3471) Typical cgPOR → fg transition in this sequence.

156.55 CON – 72/067 (porphyry)

159.15 CON – 68/026 (GT)

160.45 CON – 66/090 (porphyry)

162.45 CON – 50/324 (GT)

Ph (3472) @ 162.80 Foliated xenoliths @ lower contact.

165.90 Vqzhblbicpy(weak)alb – 73/086 Typical ori. Ph (3473)

Ph (3474) @ 170.50 – irregular GT cuts S₁ + Vqzhblgntalb. V. fine gnt t'out Vn + selvedge.

177.70 S₁ – 65/097
L₁ – 74/011 (~30→NW)

Ph (3475) of likely folded (F₁) Vqzhblbi (3476) of grey vq both creating a selvedge (L) & exploiting (but transgressing) an old one (R).

179.10 Vepch – 82/029
S₁ – 72/072
F₁ ~ – ~20° → NW (approx)

Ph (3477/3478) ✱ STAR PIC ✱ Hg "Dasler-style cp-ch veins cut S₁ & F₁ folded Vqzhblbimt (barren).

184.0 Vcpych – 79/082 (common ~//S₁)
F₁ – α – 86 γ – 209 (~20°→W)

Ph (3479) F₁ fold of grey qz vein, which itself cuts qzhblalb veins?

186.50 Vcpych – 76/348 (~//S₁)

187.40 Vcppyhblmtalb – 80/017 Very weak ... GT? (Ph 3480)

189.10 S₁ – 72/063
Vcppyepmt – 78/347

Ph (3481) Vn cuts S₁ in albitised (?) AN.

ALTERATION/MINERALISATION NOTES

Gnt focused in chloritic / strained zones?

• V str. Alb zone bound by Vhblepcppomt bi veins.

135.60 – 137.80 Sill in possible post-D₁ reactivation zone?

Ch-bi altn directly assoc ū shear zone.

Ph. (3494) of tray. 185.20 – 190.50m

• V str alb zone 183.60 – 190.00 (~20→NW)

191.50 L₁ α – 83 γ – 023
S₁ – 62/117
Vhblmtcpypy – 40/092

Ph (3482) Vn cuts S₁

196.60 CON – 41/113 (porphyry) A bit deformed.

197.20 Vhblbicpypopy – 54/083 Ph (3483) Hg vein ū 3 sulphides?

structure contd.

Calingiri Project
Graphic Log

HOLE ID: 08WHDDH001	COORDINATES:	ORIENTATION:	PAGE: 3 of 3
PROSPECT:	LOGGED BY:	DATE:	

DEPTH	LITHOLOGY	STRUCTURE	ALTERATION 1	ALTERATION 2	MINERALISATION	LITHOLOGY NOTES	STRUCTURE NOTES	ALTERATION/MINERALISATION NOTES	OTHER
200							Note: Sz has no clear lineation – post-dates D_1?		
200.70						200.70 – 214.00 – AN-dominated sequence, as prev. Poss > basaltic, fgnz stuff? Several thin GT dykes, poss thin "porphyry" zones in high ε zone. Interval contains strong ε – see structure log. Thin PEG (containing py-cpy) marks clear end to high ε zone.	202.30 Shear – 81/330 (S_1?) Ph(3484) Margins of Sz, ⊥ GT dyke cutting foln. Note gnt masses wrapped by foln. Ph(3485) @ 202.60m – v.str ch-bi shear wraps gnt porphyroblasts. Dn as above. Ph(3486) @ 203.00m – cpy masses in gnt pressure shadows. Str. cpy assoc w v.str bi altn.	203.10 Bi altn in v.str streaks + veins, tails off either side of Sz. Chlorite also assoc in high ε area	
205.80							205.40 Shear – 76/002 Ph(3487) Str bi wraps gnt, accumulates in pressure shadow. Note strong Sill (musc?) development, increasing to RHS. Ph(3488) @ 205.00m – gnt ⊃ Sn min in pressure shadow	·No altbile below Sz (trace selvedges) Sill? Or muscovite?	
210							205.30 Shear 70/093 Ph(3489) Str. cpy-py min in shear, mixed w musc (sill?) retrogression?	Bi retrogressed (?) to chl in GT	
214.00						214.00 – 216.00 Equigran (2mm) to v.fg ksp-phyric bi(10) monzoGT ⊃ ~25% qz. Seems to post-date foln. Some bi	205.95 PEG – 43/123 Marks end of Sz – contains some cgSz py-cpy – remob?		
216.00						216.00 – 216.30 – Thin AN interval.	208.50 V hbl po cpy bi mt – 71/130 Ph(3490/3491) – 20cm hg vein, note that thin GT is also mineralized ⊃ mt-cpy-po.		
216.30						216.30 – 216.55 – Thin likely interflow sed – silt/chert. Ph(3454/3455) @ 216.45m. Some sillimanite, plus bands of a sparkly mineral, grey-white, hard ∮(?).	212.10 S_1 71/052		
216.55						216.55 – 224.10 – Fine, dark, dominantly more basaltic rock (?). More homogenous bits are a bit fl or qz (?) rock – if qz, this is prob meta sed, if fl, amphibolite affected by bi altn.	214.00 con – 72/127 (GT)		
224.10						224.10 – 226.10 cg PEG ⊃ irreg margins & xenoliths of wallrock.	216.30 S_0/layering 70/063 In fg sed unit...		
226.10						226.10 – 235.65 mg-cg doleritic Amphibolite (?) Ph(3456) @ 233.50m of typical rock. Contains a lot of epidote. Not affected by fol/lin event (ie. oblish)	219.30 F_1 (?) ∂ – 80 ∀ – 005 (rough) ~ 30 → WNW? Isoclinally folded clear qz vein in high ε shear band Ph(3492/3493) Note dark bi-mt bands seem to pre-date clear vein (contains frags of altn) – late reactivated Sz?		
235.65						235.65 – 257.05 cg, irreg textured PEG Ph(3457) @ 239.00–244.50 of typical trocy. cgqz qz-ksp-plag(?) + some tourmaline needles. No signs of deformation, likely late.	221.40 S_1 78/051		
240							226.10 con 18/249 (PEG) irregular, brittle...		
250						251.05 – 251.74 plag-phyric, fol/finealed AN, typical of uphole sequence.	227.20 S_1 70/350 V. weak		
251.74						EOH	(No ori past ~228m)		
260									

100% core...

Calingiri Project
Graphic Log

HOLE ID: DWN4	**COORDINATES:**	**ORIENTATION:** ~-55→090	**PAGE:** 1 of 4
PROSPECT: Ninan	**LOGGED BY:** M. Outhwaite	**DATE:** 15/4/2015	

DEPTH	LITHOLOGY	STRUCTURE (ductile)	ALTERATION 1 (gt)	ALTERATION 2 (sm)	MINERALISATION	LITHOLOGY NOTES	STRUCTURE NOTES	ALTERATION/MINERALISATION NOTES	OTHER
60						START of HOLE = 59.60m			
						59.60 – 80.80 fmgbz, equigranular IV (in least altd areas) bi ch qz fl rock	Ph 2590 → 2613 trays 1-24 2614 → 2638 trays 25-49		
70		69.3	72			(74.60 – 75.10 egg Nin-style GT dyke, low E)			
			76.5	78		(79.60 – 80.60 PEG)			
80		80.80				80.80 – 85.00 fmgbz more chloritic, matic section.			
		85.00				85.00 – 111.60 fmgbz equigran IV, ch bi qz fl.			
90		88.0		95.5					
100		101.70						Ph 3910 e 98.80m gt-sm-ch-bi assemblage.	
110		111.60				111.60 – 114.60 fmgbz more matic section, some PEG + GT + altn.			
		113.60				114.60 – 115.20 LAMPROPHYRE DYKE (?) Ph 3907 @ 114.60 at lower con. Nole egbz ch/am masses, rock also has abundant diss cpy.		v. str sm zone.	
		115.20		115.70		115.20 – 134.50 fmgbz equigran IV.			
120		118.0							
		121.0							
130						134.50 – 136.40 fmgbz matic section, incl. thin LAMP dykl. (Ph 3908 e 135.30m – both LAMP margins w > cp).			
		134.50							
		136.40				136.40 – 139.10 vcgbz tourmaline-bearing PEG cf. end DWHD4001.			
140		139.10		139.70					

Calingiri Project
Graphic Log

HOLE ID: DWN4	COORDINATES:	ORIENTATION:	PAGE: 2 of 4
PROSPECT:	LOGGED BY:	DATE:	

DEPTH | LITHOLOGY | STRUCTURE (Discrete) | ALTERATION 1 (qt) | ALTERATION 2 (sm) | MINERALISATION

LITHOLOGY NOTES

139.10 – 159.10 fmgsz egg to wk po IV, w several narrow to-bearing PEGs.

(142.00–142.30 Small, "dusky" qz-ch breccia w assoc cpy min – Ph (3911) e 142.30m).

159.10 – 167.50 clear fl-phyric interval of IV unit – Ph (3909) e 159.80m of texture.

161.50 – 185.60 Long zone of fine gsz, dark rock, prob still IV, poss mafic sections.

185.60 – 188.70 Distinctly coarser & wk fl-phyric IV zone. Late, to-bearing PEGs in 188.00–188.50.

188.70 – 204.30 Continuation of fine → fm gsz IV, w poss mafic sections.

204.30 – 209.95 coarser, fl-phyric IV w internal gsz variation, bedded, likely reworked volcanic. Ph (3915) e 205.50 of gsz variation.

209.95 – 210.60 "adamellite", typical Ninan intrusive.

210.60 – 223.60 dark fmgsz matic/IV, small fl-phyric intervals.

STRUCTURE NOTES

Distinct higher ξ zone / shear ~ 139.10–156.20 = some folding/wobbling of shear fabric.

~~142.0~~

ALTERATION/MINERALISATION NOTES

Discrete strong sm

Ph (3912) e 183.20m ch/ac-cp-mt vein w strong gt+bi selvedges.

coarse garnets thru this interval

Ph (3913) e 194.50m – hg cp veinlet cuts coarse gt. ← Discrete strong sm.

+ Ph (3914) in sm, mafic > bi around gt masses.

OTHER

Calingiri Project
Graphic Log

HOLE ID: DWN 4	COORDINATES:	ORIENTATION:	PAGE: 3 of 4
PROSPECT:	LOGGED BY:	DATE:	

DEPTH | LITHOLOGY | STRUCTURE (brittle) | ALTERATION 1 (gt) | ALTERATION 2 (sm) | MINERALISATION

LITHOLOGY NOTES

223.60 – 225.50 massive, fg, internally homogenous mt-ch(?)± cpy rock, as seen in outcrop. Skarn origin? replacement of sed unit?

225.50 – 343.10 generally massive and eqg fine to fine-med gz andesitic/mafic volcanic rock w highly variable altn overprint, and internal granites/PEGs/veins, as described.
Ph 3916 e ~310m of typical rock e low ε, low altn - Looks like a bi-altd amphibolite, tho qz vs fl content unclear, as in 08WHDD1T001.

(237.90 – 240.10) "adamellite"

(265.10 – 270.40) mix adamellite ~~&~~ and PEG zones. Coarser than usual kind, poss more felsic/granite.

(280.00 – 281.20) mix adamellite + PEG

(286.40 – 289.00) adamellite, cut by PEGs. – clear timing relationship.

STRUCTURE NOTES

poss some arsenopyrite?
also, diss su looks interesting w fine garnet.

Clear high ε zone.

? Likely mod W-dipping axial plane to wobbly folding, based on "known" S_1/L_1 ori ??

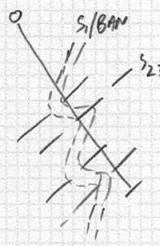

← clear drop in ε, altn, sillimanite.

ALTERATION/MINERALISATION NOTES

Ph 3922 e 320.90m typical late (post-S_1) hy cp assoc w vqz±cpy in chloritic matic/int w
Long interval of strong to very strong garnet development, assoc w bi, within ch/ac zones, incl vein selvedges.

Ph 3923 e 328.70m inter-banded ch-ac-gt + "albitised" zones (prob not albite) - typical.

Ph 3920 260.00m } early sm in S_1 foln is folded ↑.
3921 261.70m } Sm also is in L_1 ori ↑out hole.

Clear drop in garnet and ~~&~~ more sillimanite after granite dyke.

Abrupt end to sm coming out of high ε zone, no more in remainder of hole.

Trace gt 291.50 → 308.00

OTHER

350.80

Calingiri Project
Graphic Log

HOLE ID: DWN4	COORDINATES:	ORIENTATION:	PAGE: 4 of 4
PROSPECT:	LOGGED BY:	DATE:	

DEPTH	LITHOLOGY	STRUCTURE (ductile)	ALTERATION 1 (gt)	ALTERATION 2 (chl)	MINERALISATION	LITHOLOGY NOTES	STRUCTURE NOTES	ALTERATION/MINERALISATION NOTES	OTHER
300									
301.50						(301.50 – 302.30) adamellite, a few other thin ones from 299.80 → 301.50.			
302.30									
303.80						(303.80 – 304.50) vag, bucky.			
304.50									
306 -30			308.0						
310									
316.00						(316.00 – 316.60) massive epidote vein.			
316.60									
317.70						(317.70 – 388.60) adamellite, quite altd.			
320									
330.00						(330.00 – 332.90) coarser adamellite w coarse chloritic "clots" – Ph (3917) @ 331.40m.			
332.90									
335.90						(335.90 – 336.90 adamellite)			
336.90									
340			337.40					Stronger gt w chl/act veins/masses.	
341.7									
343.10						343.10 – 347.30 distinctive ft-phyric IV, reasonably clear contacts based on texture, plus internal variations. eg. Ph (3918) @ 346.00m.			
347.30						347.30 – 350.80 fm-gz mafic/IV, rare pxsts.			
348.20						(348.20 – 348.70 adamellite) Ph (3919) @ 348.20 – adamellite clearly cuts S1 fabric.			
348.70									
350						END OF HOLE			
350.80									
360									

The Calingiri Cu–Mo–Ag deposits are located in the South West Terrane of the Archean Yilgarn Craton, about 120 km northeast of Perth. Mineralization formed at about 2997–2957 Ma (Re–Os molybdenite), during early deformation of the high-Ca, granite–gneiss host rocks, which are dated at 3010 ± 4 Ma (SHRIMP U–Pb zircon). East–west compression at c. 2670 Ma was accompanied by additional granite magmatism, dated at 2673 ± 5 Ma (SHRIMP U–Pb zircon), and upper amphibolite facies metamorphism. The Cu–Mo–Ag mineralization was deformed during the c. 2670 Ma event, and proximal hydrothermally altered rocks were recrystallized into garnet- and sillimanite-bearing assemblages. Calingiri is an Archean example of metamorphosed porphyry-style mineralization.

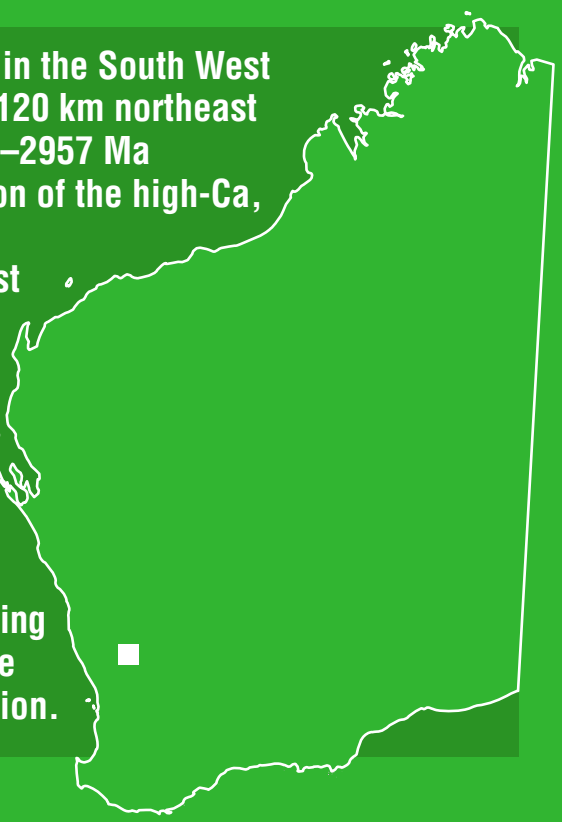

OUTHWAITE

METAMORPHOSED MESOARCHEAN Cu–Mo–Ag MINERALIZATION: EVIDENCE FROM THE CALINGIRI DEPOSITS, SOUTHWEST YILGARN CRATON

REPORT 183

Further details of geological products and maps produced by the Geological Survey of Western Australia are available from:

Information Centre
Department of Mines, Industry Regulation and Safety
100 Plain Street
EAST PERTH WA 6004
Phone: (08) 9222 3459 Fax: (08) 9222 3444

www.dmp.wa.gov.au/GSWApublications